



Université  
de Lille

THESE DE DOCTORAT  
PRESENTEE PAR

**Dan WU**

POUR L'OBTENTION DU TITRE DE  
DOCTEUR DE L'UNIVERSITE DE LILLE

Ecole Doctorale: Sciences de la Matière, du Rayonnement et de l'Environnement

Spécialité: Molécules et Matière Condensée

---

*Synergie d'effets stériques, électroniques et bifonctionnels  
pour la conception de catalyseurs métalliques hautement  
sélectifs promus par des éléments non métalliques*

---

Soutenue le 17<sup>th</sup> Décembre 2020

Composition du Jury:

Rapporteurs	Prof. Laurent Bonneviot, ENS Lyon (France) Prof. Francois Jérôme, Université de Poitiers (France)
Examineurs	Prof. Franck Dumeignil, Université de Lille (Président, France) Prof. Carine Michel, ENS Lyon (France)
Invité	Dr. Stéphane Streiff, Solvay E2P2L (Chine) Dr. Yesid Hernandez Enciso, Cardiff University (UK)
Directeurs	Prof. Vitaly Ordonsky, Université de Lille (France) Prof. Andrei Khodakov, Université de Lille (France)





THESE DE DOCTORAT  
PRESENTEE PAR

**Dan WU**

POUR L'OBTENTION DU TITRE DE  
DOCTEUR DE L'UNIVERSITE DE LILLE

Ecole Doctorale: Sciences de la Matière, du Rayonnement et de l'Environnement

Spécialité: Molécules et Matière Condensée

---

***Synergy of Steric, Electronic, and Bifunctional  
Effects for the Design of Highly Selective Metal  
Catalysts Promoted by Non-metallic Elements***

---

Soutenue le 17<sup>th</sup> Décembre 2020

Composition du Jury:

Rapporteurs	Prof. Laurent Bonneviot, ENS Lyon (France) Prof. Francois Jérôme, Université de Poitiers (France)
Examineurs	Prof. Franck Dumeignil, Université de Lille (President, France) Prof. Carine Michel, ENS Lyon (France)
Invité	Dr. Stéphane Streiff, Solvay E2P2L (China) Dr. Yesid Hernandez Enciso, Cardiff University (UK)
Directeurs	Prof. Vitaly Ordonsky, Université de Lille (France) Prof. Andrei Khodakov, Université de Lille (France)



## **Acknowledgements**

First and foremost, I would like to give my sincere acknowledge to CNRS, Solvay, and Lille University, for offering me the stipend for my Ph. D. researches. I am fortunate to have been able to work at two different laboratories in two different countries: E2P2L, shanghai, China, and UCCS, Lille, France. I learned a lot in both laboratories. Especially, I would like to express my sincerest appreciation to E2P2L director Dr. Stéphane Streiff and UCCS director Prof. Franck Dumeignil, for providing me with the safe and friendly research circumstance.

I would like to give my deepest gratitude to my supervisors, Prof. Vitaly Ordonsky, and Prof. Andrei Khodakov, for their excellent supervision in the last three years. They are not only my thesis director but also my life mentor. They often discussed experimental results with me and encourage me to think independently. I learned a lot from them, these knowledge help both my scientific and personal growth.

Next, I would like to thank the jury members Prof. Laurent Bonneviot, Prof. Francois Jérôme, Prof. Franck Dumeignil, Prof. Carine Michel, Dr. Stéphane Streiff, Dr. Yesid Hernandez Enciso, and Dr. Wenjuan Zhou. Thank you so much for the review and examination of my Ph.D. thesis.

Then, I would like to acknowledge Prof. Ovidiu Ersen, Prof. Maya Marinova, Prof. Bruno Grandidier, Dr. Evgeny I. Vovk, and Prof. Yong Yang, for their excellent collaboration works.

Furthermore, I would like to say thanks to all the members of E2P2L and UCCS, especially Dr. Zhen Yan, Dr. Wenjuan Zhou, Dr. Raphael Wischert, Prof. Mirella Virginie, Olivier Gardoll, Pardis Simon, Stéphane Chambrey, and so on. Thanks for their help and suggestion for my experiments. And also, I would like to send my thanks to my colleagues Dr. Bang Gu, Dr. Xiang Yu, Dr. Feng Niu, Dr. Jingpeng Zhao, Dr. Shuo Chen, Dr. Deizi Vanessa Peron, Yuanshuang Zheng, Qiyan Wang, Songwei Zhang, Alan Barrios, Di Hu, Ana Katiuce Fellenberg, Aleksandra Peregudova, Melissa de la Rocha, and so on. Thank them for their support. Wish they have a bright future.

Finally, I am greatly indebted to my family. Thanks for their understanding and support.

Dan WU

October, 2020

Lille

## **ABSTRACT.**

The depletion of fossil resources and increasing environmental concerns encourage the production of sustainable chemicals and fuels from biomass resources. Selectivity is the primary parameter for heterogeneous catalytic processes, especially for the catalytic conversion of biomass-based molecules, containing a lot of functional groups with the generation of various products. Recently, rational modification of the surface chemistry of metal catalysts has attracted intensive attention to tune the activity and selectivity. In this thesis, the modification of noble metal catalysts such as Pd and Ru with various non-metallic promoters such as iodine, bromine, and amines has been developed. These modifications lead to various effects like in-situ acidity generation, selective deactivation, electronic effect, and molecular imprinting. Important industrial reactions such as reductive etherification, hydrodeoxygenation, cleavage of lignin model compounds, and aromatics hydrogenation were investigated. The thesis consists of 7 chapters and 217 pages.

In Chapter 1, a literature review of the recent progress in tuning catalytic properties of metal catalysts with non-metallic modifiers will be introduced. Different modification strategies will be clarified. And a general analysis will be proposed about the effects imposed by non-metallic modifiers of metal catalysts. Various industrial important reactions with the selectivity problems are discussed to elucidate the promotion effects of the non-metallic modifiers in catalysis.

Chapter 2 introduces the experimental details about the preparation, characterization, and catalytic evaluation of the catalysts.

Modification of Pd catalyst with iodine and bromine was investigated in Chapter 3 ~ 4.

The structure-performance relationships were studied by catalytic reactions and various in-situ and ex-situ characterizations. We found that iodine and bromine withdraw electrons from Pd, leading to negative charged iodine and bromine atoms on the Pd surface. Heterolytic dissociation of hydrogen on the Pd-I and Pd-Br bifunctional sites leads to the in-situ generation of Brønsted acidity. The acid-metal bifunctional Pd-I and Pd-Br catalysts exhibited high efficiency for the reductive etherification of aldehydes with alcohol and hydrodeoxygenation of 5-hydroxymethylfurfural to dimethylfuran, respectively.

In Chapter 5, the modification of metal catalysts with halogens was extended to Ru catalysts. The Ru-Br catalyst has been developed and demonstrated high selectivity for the cleavage of lignin model compound diphenyl ether to mono aromatics. Further investigations indicate that the terrace sites on Ru nanoparticles, which are responsible for aromatic-rings hydrogenation, can be selectively deactivated by Br atoms. Moreover, Br as a strongly electronegative element withdraws electrons from Ru, leading to positively charged Ru nanoparticles. The electron-deficient Ru nanoparticles exhibited enhanced activity for hydrogenolysis of electron-rich C-O bonds. The synergy of selective deactivation and electronic effect made the Ru-Br catalyst high efficiency for the production of phenol and benzene from diphenyl ether with high selectivity.



Based on the deep understanding of the multifunctional effects of non-metallic modifiers of metal catalysts, a molecular imprinting strategy has been proposed in Chapter 6. Molecular imprinting for the preparation of imprinted heterogeneous catalyst involves adsorption of a template molecule, deactivation with poisoners, creation of non-poisoned active islands with pre-determined shape and size for selective transformation of the molecules corresponding to templates. We demonstrate the viability of this strategy for selective hydrogenation of aromatic molecules with different alkyl radicals by using preliminary deposition of these molecules as a template over Pd catalyst and deactivation using dimethylaminopropylamine (DMAPA). The elaborated strategy enables a practical application relevant to selective hydrogenation and removal of cancerogenic benzene from the mixture of aromatics and can be extended for selectivity enhancement of numerous catalytic reactions.

**Keywords:** Surface modification; Metal catalysts; Halogen-metal; Bifunctional catalysts; Selective poisoning; Molecular imprinting.



## Résumé

L'épuisement des ressources fossiles et les préoccupations environnementales croissantes encouragent la production de produits chimiques et de combustibles durables à partir des ressources de la biomasse. La sélectivité est le paramètre principal pour les processus catalytiques hétérogènes, en particulier pour la conversion catalytique de molécules à base de biomasse, contenant beaucoup de groupes fonctionnels avec la génération de divers produits. Récemment, une modification rationnelle de la chimie de surface des catalyseurs métalliques a attiré une attention intensive pour régler l'activité et la sélectivité. Dans cette thèse, la modification de catalyseurs de métaux nobles tels que Pd et Ru avec divers promoteurs non métalliques tels que l'iode, le brome et les amines a été développée. Ces modifications conduisent à divers effets tels que la génération d'acidité in situ, la désactivation sélective, l'effet électronique et l'empreinte moléculaire. Des réactions industrielles importantes telles que l'éthérisation réductrice, l'hydrodésoxygénation, le clivage des composés modèles de la lignine et l'hydrogénation des aromatiques ont été étudiées. La thèse comprend 7 chapitres et 217 pages.

Dans le chapitre 1, une revue de la littérature des progrès récents dans le réglage des propriétés catalytiques des catalyseurs métalliques avec des modificateurs non métalliques sera présentée. Différentes stratégies de modification seront clarifiées. Et une analyse générale sera proposée sur les effets imposés par les modificateurs non métalliques des catalyseurs métalliques. Diverses réactions industrielles importantes

avec les problèmes de sélectivité sont discutées pour élucider les effets de promotion des modificateurs non métalliques en catalyse.

Le chapitre 2 présente les détails expérimentaux sur la préparation, la caractérisation et l'évaluation catalytique des catalyseurs.

La modification du catalyseur Pd avec de l'iode et du brome a été étudiée au chapitre 3 ~ 4. Les relations structure-performance ont été étudiées par des réactions catalytiques et diverses caractérisations in-situ et ex-situ. Nous avons constaté que l'iode et le brome retirent des électrons du Pd, conduisant à des atomes d'iode et de brome chargés négativement sur la surface du Pd. La dissociation hétérolytique de l'hydrogène sur les sites bifonctionnels Pd-I et Pd-Br conduit à la génération in situ de l'acidité de Brønsted.

Les catalyseurs bifonctionnels acide-métal Pd-I et Pd-Br ont présenté une efficacité élevée pour l'éthérisation réductrice d'aldéhydes avec de l'alcool et l'hydrodésoxygénation du 5-hydroxyméthylfurfural en diméthylfurane, respectivement.

Au chapitre 5, la modification des catalyseurs métalliques avec des halogènes a été étendue aux catalyseurs Ru. Le catalyseur Ru-Br a été développé et a démontré une sélectivité élevée pour le clivage du composé modèle de lignine diphenyléther en mono-aromatiques. Des recherches plus poussées indiquent que les sites de terrasse sur les nanoparticules de Ru, qui sont responsables de l'hydrogénation des cycles aromatiques, peuvent être sélectivement désactivés par des atomes de Br. De plus, Br en tant qu'élément fortement électronégatif retire des électrons de Ru, conduisant à des nanoparticules de Ru chargées positivement. Les nanoparticules de Ru déficientes en électrons ont présenté une activité améliorée pour l'hydrogénolyse des liaisons C-O

riches en électrons. La synergie de la désactivation sélective et de l'effet électronique a rendu le catalyseur Ru-Br très efficace pour la production de phénol et de benzène à partir d'éther diphénylique avec une sélectivité élevée.

Sur la base de la compréhension approfondie des effets multifonctionnels des modificateurs non métalliques des catalyseurs métalliques, une stratégie d'impression moléculaire a été proposée au chapitre 6. L'empreinte moléculaire pour la préparation d'un catalyseur hétérogène imprimé implique l'adsorption d'une molécule modèle, la désactivation avec des empoisonneurs, la création d'îlots actifs non empoisonnés de forme et de taille prédéterminées pour la transformation sélective des molécules correspondant aux modèles. Nous démontrons la viabilité de cette stratégie d'hydrogénation sélective de molécules aromatiques avec différents radicaux alkyles en utilisant le dépôt préliminaire de ces molécules comme modèle sur le catalyseur Pd et la désactivation à l'aide de diméthylaminopropylamine (DMAPA). La stratégie élaborée permet une application pratique pertinente à l'hydrogénation sélective et à l'élimination du benzène cancérigène du mélange d'aromatiques et peut être étendue pour l'amélioration de la sélectivité de nombreuses réactions catalytiques.

**Mots-clés:** Modification de surface; Catalyseurs métalliques; Halogène-métal; Catalyseurs bifonctionnels; Empoisonnement sélectif; Impression moléculaire.



# Table of content

Acknowledgements.....	1
ABSTRACT.....	3
Résumé.....	7
1. Literature Review.....	15
ABSTRACT.....	15
1.1. Introduction.....	15
1.1.1. General introduction .....	15
1.1.2. Different promoters.....	18
1.1.3. Stability of modifiers on metal surfaces .....	20
1.1.4. Characterizations toolbox .....	20
1.2. Modification strategies.....	22
1.2.1. Direct preparation .....	22
1.2.2. Post-modifications .....	28
1.3. Identification of the role of promoters .....	34
1.3.1. Steric effects.....	35
1.3.2. Electronic effects .....	49
1.3.3. Bifunctionality .....	58
1.4. Catalytic hydrogenation over modified metal catalysts.....	60
1.4.1. Partial hydrogenation of alkynes to alkenes .....	62
1.4.2. Selective hydrogenation of unsaturated aldehydes to unsaturated alcohols .....	65
1.4.3. Hydrogenation of nitroarenes to N-hydroxylanilines .....	67
1.4.4. Hydrogen peroxide production .....	69
1.5. Goals and strategies of the thesis .....	72
1.6. Thesis structure .....	73
Reference .....	75
2. Experiment Section.....	87
2.1. Catalyst preparation .....	87
2.1.1. Chemicals.....	87
2.1.2. Preparation of I modified Pd catalyst.....	87
2.1.3. Preparation of Br modified Pd catalyst.....	89
2.1.4. Preparation of Br modified Ru catalyst .....	89
2.1.5. Preparation of Pd/SiO <sub>2</sub> catalyst.....	89
2.1.6. Preparation of imprinted Pd/SiO <sub>2</sub> catalyst.....	89
2.2. Catalyst Characterization .....	90
2.2.1. X-ray diffraction (XRD) .....	91

2.2.2.	Transmission electron microscopy (TEM) .....	91
2.2.3.	Chemisorption.....	91
2.2.4.	Thermogravimetric analysis (TGA).....	92
2.2.5.	X-ray photoelectron spectrometry (XPS) .....	92
2.2.6.	Fourier transform Infrared spectroscopy (IR).....	93
2.2.7.	X-ray florescence analysis (XRF).....	93
2.3.	Evaluation of catalytic reactions .....	94
2.3.1.	Reductive etherification .....	94
2.3.2.	Hydrodeoxygenation.....	95
2.3.3.	Hydrogenolysis of diphenyl ether .....	96
2.3.4.	Aromatics hydrogenation.....	97
2.3.5.	Selective benzene removal.....	97
3.	Modification of Pd Catalyst with Iodide: In-situ Generation of Brønsted Acidity for Selective Reductive Etherification.....	99
	ABSTRACT.....	99
3.1.	Introduction.....	101
3.2.	Results and discussion .....	103
3.2.1.	Etherification over the Pd-I catalysts .....	103
3.2.2.	Characterization of the catalyst.....	113
3.2.3.	Mechanism of the reaction.....	118
3.2.4.	Other substrates.....	123
3.3.	Conclusion .....	125
	Reference .....	126
4.	Dual Metal-Acid Pd-Br Catalyst for Selective Hydrodeoxygenation of 5-Hydroxymethylfurfural (HMF) to 2, 5-Dimethylfuran at Ambient Temperature.....	131
	ABSTRACT.....	131
4.1.	Introduction.....	133
4.2.	Results and discussions.....	135
4.2.1.	HMF deoxygenation over the Pd-Br catalyst at 60°C .....	135
4.2.2.	HMF deoxygenation at ambient temperature .....	139
4.2.3.	Other promoting agents.....	139
4.3.	Characterization of the Pd-Br catalysts.....	143
4.4.	Model reactions.....	149
4.5.	Discussion .....	151
4.6.	Conclusion .....	155
	Reference .....	156



5. Cleavage of Diphenyl Ether Lignin Model Compounds to Single-ring Aromatics over Ru-Br Catalyst .....	161
ABSTRACT.....	161
5.1. Introduction.....	163
5.2. Results and discussions.....	166
5.2.1. Catalytic conversion of DPE.....	166
5.2.2. Characterizations.....	173
5.2.3. Model reactions.....	177
5.3. Conclusion .....	178
Reference .....	180
6. Molecular Imprinting on the Supported Metal Catalysts for Size-dependent Selective Hydrogenation Reactions .....	185
ABSTRACT.....	185
6.1. Introductions .....	186
6.2. Results and discussion .....	189
6.2.1. Poisoning of supported Pd/SiO <sub>2</sub> catalysts by DMAPA.....	189
6.2.2. Investigations for imprinting process.....	194
6.2.3. Model reactions over imprinted Pd/SiO <sub>2</sub> catalyst.....	197
6.2.4. Selective removal of benzene from the mixture .....	203
6.3. Conclusions.....	205
Reference .....	207
7. General Conclusions and Perspectives .....	213
7.1. General Conclusion.....	213
7.1.1. In-situ generation of acid sites over metal nanoparticles.....	213
7.1.2. Selective blocking active sites .....	214
7.1.3. Molecular imprinting over heterogeneous catalyst.....	215
7.2. Perspective .....	217



# **1. Literature Review**

## **ABSTRACT.**

Molecular adsorption, reaction, and desorption occurring at the metal-substrates interface are the key steps for the catalytic process. Regardless of the intrinsic properties such as the active phase, particle size, and morphology, recently, the modification of metal nanoparticles with non-metallic modifiers has attracted intensive attention to tune the interfacial environment for smart catalysis. In this part, we will give a literature review about the recent progress in tuning catalytic properties of metal catalysts with non-metallic modifiers. A general analysis will be proposed about the effects imposed by non-metallic modifiers of metal catalysts. The most popular effects are steric and electronic effects. The electronic effects change the adsorption and activation energy of substrates. The steric effects change the access of the substrate molecules approaching the metal surface. Moreover, the demand for multifunctional catalysts for biomass conversion includes the development of the metal-acid/base functionalities. Various industrial important reactions with the selectivity problems including alkyne semi-hydrogenation,  $\alpha$ ,  $\beta$ -unsaturated aldehyde selective hydrogenation, and hydrogen peroxide production are discussed to elucidate the promotion effects of the non-metallic modifiers in catalysis.

## **1.1. Introduction**

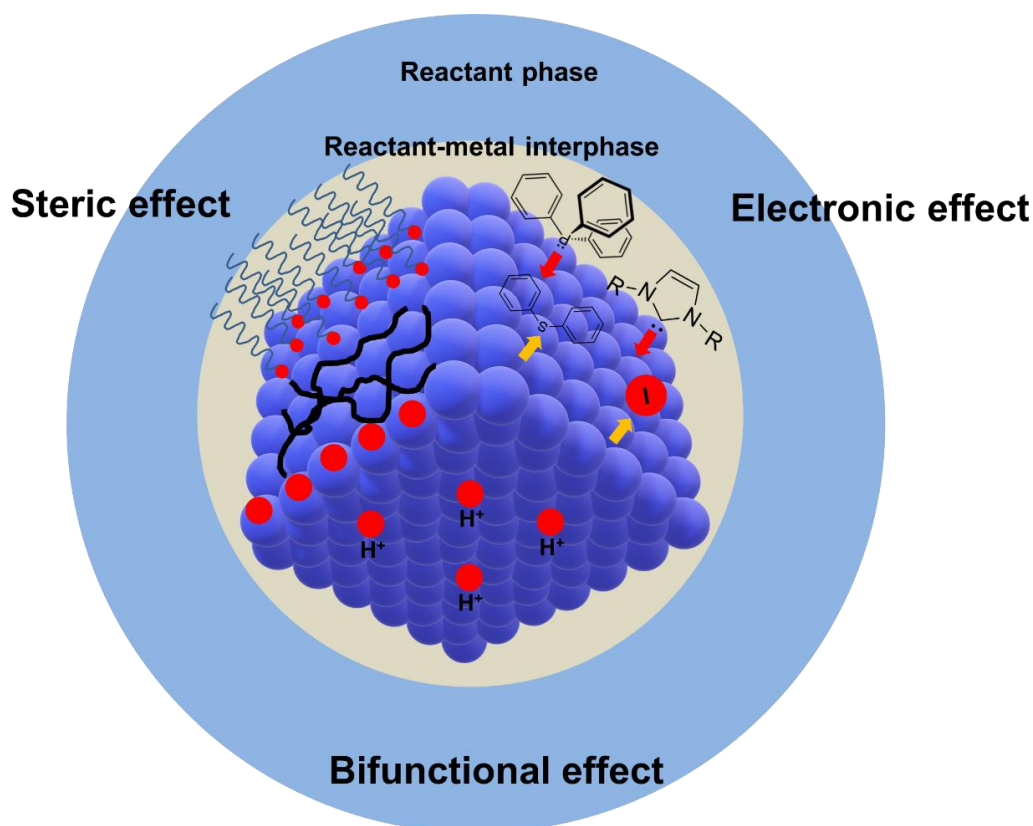
### **1.1.1. General introduction**

Catalytic processes are a fundamental part of fine chemicals synthesis, environmental protection, and energy generation. Due to the high stability, high activity, and long durability, metal catalysts are widely used in industrial processes such as hydrogenation, oxidation, and cascade reactions [1-5]. Recently, due to the depletion of fossil resources and increasing environmental concerns, biofuels and chemicals derived from renewable biomass resources have attracted intensive attention [6-8]. Metal catalysts with high activity and predictable selectivity are playing a more and more important role in biomass upgrading such as depolymerization and deoxygenation reaction [9-19].

The industrial processes require the uniform and standard properties of the catalysts, especially for fine chemical manufacturers. However, various reactions towards different products proceed on the surface of metal nanoparticles with different environments [20-24]. The parameters that affect the catalytic properties of metal nanoparticles include electronic structure, surface geography, metal-support interaction, size and morphology, and so on. Normally, these parameters are stable and well-optimized for commercial catalysts. From the viewpoint of industrial chemical processes, the usage of commercial catalysts is an attractive and economic-benefit way for new process development. However, in most cases, the screening of the industrial catalysts with various metals, loadings, and supports does not give a satisfactory result in terms of high selectivity and activity.

Inspired by enzymatic and homogeneous organometallics catalysis, tuning the electronic and steric effects of metal nanoparticles by organic ligands has attracted a lot of attention [25-32]. Surface modification of the metal catalysts is a promising way for

selective transformations of chemicals because it avoids the complex catalyst synthesis procedures and could be easily adapted in industry.



**Schema 1.1.** Illustration of the multifunctional effects of surface modification in the design of metal catalysts.

It is well known that metal catalysis involves the molecule adsorption, reaction, and desorption occurring at the reactant-metal interface (As shown in [Schema 1.1](#)). The reactant molecules firstly diffuse from the reactant phase to the reactant-metal interface. In this case, a steric effect might be introduced by the modifiers to tune the configuration and orientation of the molecules approaching the metal surface. Moreover, the molecular affinity between the catalyst surface and reactant molecules will dominate the concentration of reactant molecules in the reactant-metal interface. For example, hydrophobic modifiers endow quick diffusion and enhanced adsorption of hydrophobic

reactants, while hydrophilic modifiers favor the diffusion and adsorption of hydrophilic reactant molecules <sup>[33]</sup>. When the reactant molecules successfully pass through the reactant-metal interface with pre-adjusted orientations, they can readily adsorb on the metal surface. In this case, the nature of active sites will determine the activation and transformation of the reactant molecules. The electronic effects and bifunctional active sites introduced by modifiers will play an important role in tuning the activity and selectivity. However, usually, these effects are strongly interconnected with each other and several additional effects play different roles in catalysis.

### **1.1.2. Different promoters**

Numerous modification procedures of the metal nanoparticles with the utilization of various non-metallic modifiers have been reported. As summarized in *Figure 1.1*, these modifiers include (1) polymers, e.g. PVP, PVA <sup>[33-45]</sup>; (2) N-based compounds, e.g. alkanolamines, ethylenediamine, quinoline, N-heterocyclic carbenes <sup>[44-66]</sup>; (3) P-base compounds, e.g. triphenylphosphine <sup>[9, 48, 67-75]</sup>; (4) S-base compounds, e.g. alkanethiols, diphenyl sulfide, H<sub>2</sub>S <sup>[76-102]</sup>; (5) halogens-based compounds, e.g. ethyl iodide, dichloromethane, bromobenzene <sup>[60, 103-116]</sup>. In some cases, these modifiers not only act as electronic or steric promoters but also as capping agents for the synthesis of small metal nanoparticles <sup>[117]</sup>. These modifiers strongly adsorb over metal nanoparticles.

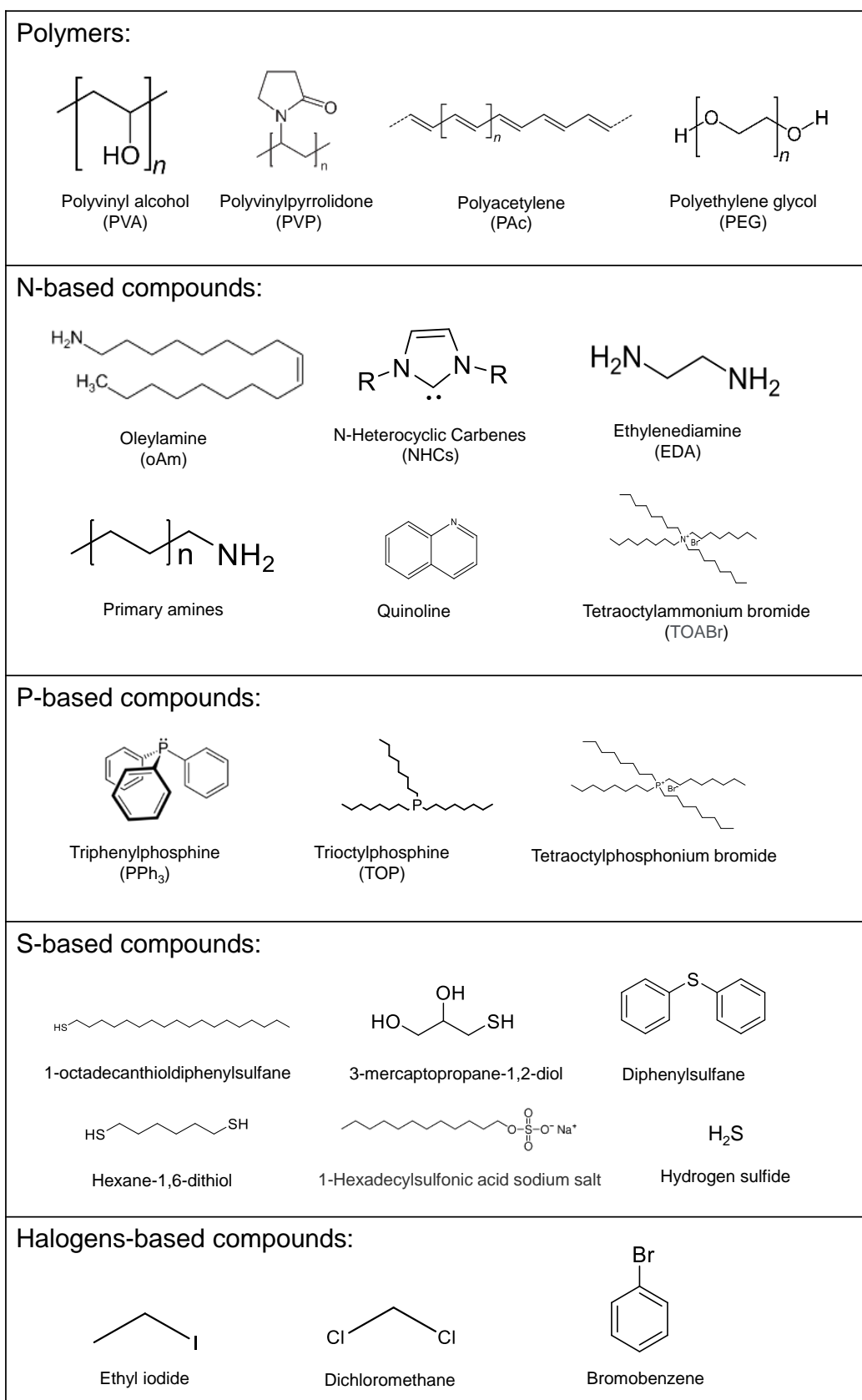


*Figure 1.1. Representative structures of different modifiers*

### **1.1.3. Stability of modifiers on metal surfaces**

The coordination of modifiers on the metal surface creates steric, electronic, and bifunctional effects, which could promote the catalytic properties of metal nanoparticles. The stability of modifiers which prevent them from being detached during catalysis [3, 118]. is particularly important for practical applications. However, in some cases, the interaction between modifiers and metal nanoparticles are relatively weak. In this case, a weak interaction of the modifier with the active sites which occurs often in competition with the reacting molecules, allows tuning the catalytic properties. Normally, the non-metallic modifiers containing heteroatoms such as oxygen, nitrogen, sulfur, phosphorus, and halogens are grafted on the metal surface through coordination bonds [22]. The interface of surface metal and modifiers could be considered as a layer of coordination compounds. The stability of modifiers on the metal surface is an important issue for the catalyst reusability, and also related to the separation problem. The stability of the modified metal catalysts is affected strongly by the reaction conditions. Some modifiers like N-based ionic or non-ionic surfactants suffer from leaching problems and loss of selectivity in liquid-phase reaction, however, they could be more stable in low-temperature gas-phase reactions. Thus, the use of surface modifiers bearing strong coordination to the catalyst surface or even chelating groups (e.g. thiolates, diamines) is preferred.

### **1.1.4. Characterizations toolbox**



Suitable characterization of the modifiers and modified metal surface is fundamental to understand the structure-performance relationship. However, it is also a challenge, because of the lack of direct tools to see the molecular-level interactions on the metal surface [22]. A lot of characterizations have been used to identify the amount, position, chemical bonds, and electronic effect of modifiers [23, 96]. The most frequently used characterizations in this area include temperature programmed analysis like TGA, TPD, transmission electron microscopy (TEM), infrared spectroscopy (IR), Raman spectroscopy, X-ray photoelectron spectroscopy (XPS), X-ray absorption spectroscopy (XAS), electrochemistry. Elemental analysis gives information about stoichiometry and stability of the modifiers. IR and Raman spectroscopies provide the molecular information of the modifiers. IR also gives specific signatures about the interaction of the modifier with metal by using probe molecules such as CO or pyridine. X-ray absorption near edge spectroscopy (XANES) and extended X-ray absorption fine structure spectroscopy (EXAFS) provide information about the oxidation state, geometry, and distances between the metal and close neighbors. Computational chemistry is a complementary tool to obtain energetic profiles that can relate to structural preferences and particular spectroscopic signatures of surface species that may relate to catalytic activity. The computational methods can confirm or rule out possible structures and allow a deeper understanding of the relation between structure and reactivity. The information obtained by combining complementary techniques in the characterization toolbox allows an atomic-level description of surface sites. This is

an essential step toward building structure-activity relationships of the modified metal catalysts.

## **1.2. Modification strategies**

There are diverse strategies to anchor non-metallic modifiers on the surface of metal nanoparticles. Generally speaking, the preparation strategies could be summarized in two ways. The first one is direct-preparation, in which the non-metallic modifiers are mixed with the metal precursors in a typical solvent and then after reduction of the metal precursors, the modifiers are grafted directly on the surface of metal nanoparticle [35, 36, 38, 41]. The second strategy is post-modification. The non-modified metal catalysts are prepared in advance. Then, the non-metallic modifiers are anchored on the metal surface by post-treatment [33, 42, 82, 98, 101].

### **1.2.1. Direct preparation**

Direct-preparation is applied usually for the preparation of ligand-protected colloidal metal nanocrystals (MNCs), where the modifiers normally act as capping or protecting agents to confine the over-growth and aggregation of MNCs. Generally, MNCs with capping agents exhibit lower activity than the bare metal nanoparticles. This phenomenon is mainly due to the partial blockage of active sites by capping agents. However, it was recently found that the capping agent endowed some abnormally catalytic properties to metal NPs [34, 43]. Thus, the role of the capping agent on the catalytic properties of MNCs is more complex. Direct preparation of MNCs with different capping agents have been intensively reported and reviewed. Some of them

were focused on the influence of removal and utilization of capping agents in heterogeneous catalysis.

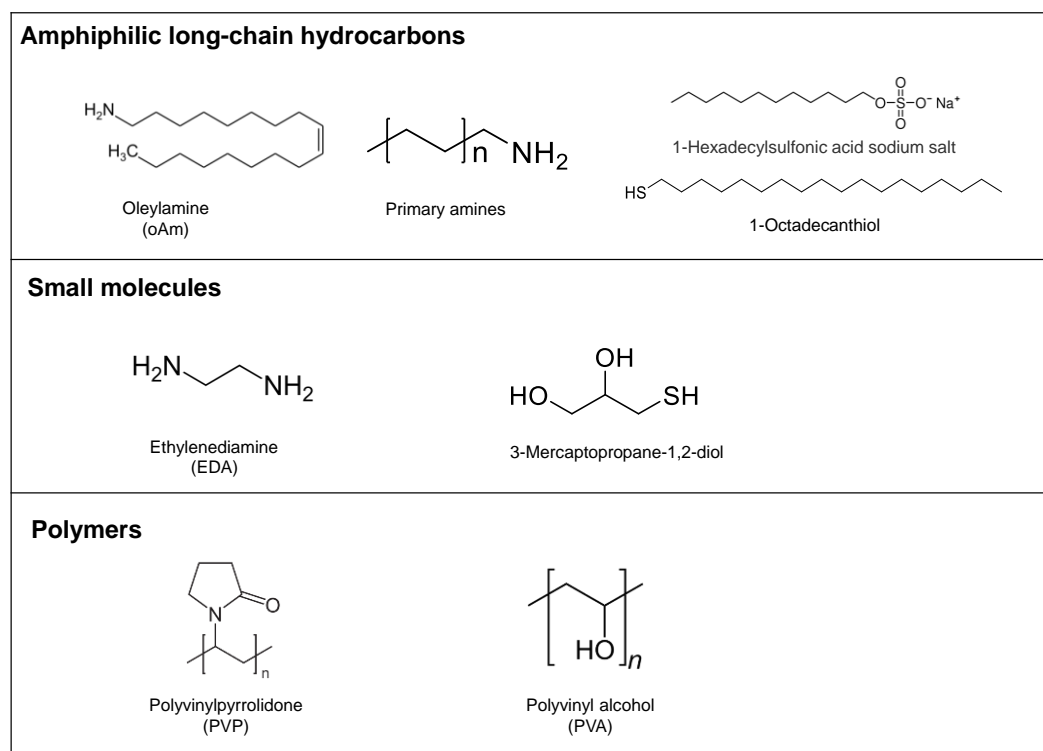


**Figure 1.2.** Structure of non-metallic modifiers for direct preparation

Direct preparation of ligand-capping MNCs normally involves the reduction of metal precursors in the reaction mixture along with the capping ligands to initiate and control the nanocrystal growth. The reduction of metal precursors could be performed by reducing agents such as  $\text{NaBH}_4$ , CO, citrate, alcohols<sup>[33, 36]</sup>, polyols<sup>[42]</sup>, and thermal decomposition of metal ions<sup>[63]</sup>. As shown in **Figure 1.2**, the used capping agents are mainly amphiphilic long-chain hydrocarbons (e.g. oAm), strong coordinated small molecules (e.g. EDA), and polymers (e.g. PVP, PVA).

For example, oAm-capped  $\text{Pt}_3\text{Co}$  bimetallic nanocrystals were prepared by thermal decomposition of  $\text{Pt}(\text{acac})_2$  and  $\text{Co}(\text{acac})_2$  in the oAm<sup>[63]</sup>. The mixture was kept stirring at 240 °C with CO flow for 40 min, followed by precipitation and washing with the

cyclohexane/ethanol solvent. As shown in [Figure 1.3](#), the as-synthesized oAm-capped  $\text{Pt}_3\text{Co}$  NCs were uniform in size and nearly all have a truncated octahedral shape with a particle size around 8 nm. The use of amines as the capping agent is important to obtain the monodisperse  $\text{Pt}_3\text{Co}$  nanocrystals and to stabilize the particles against aggregation.

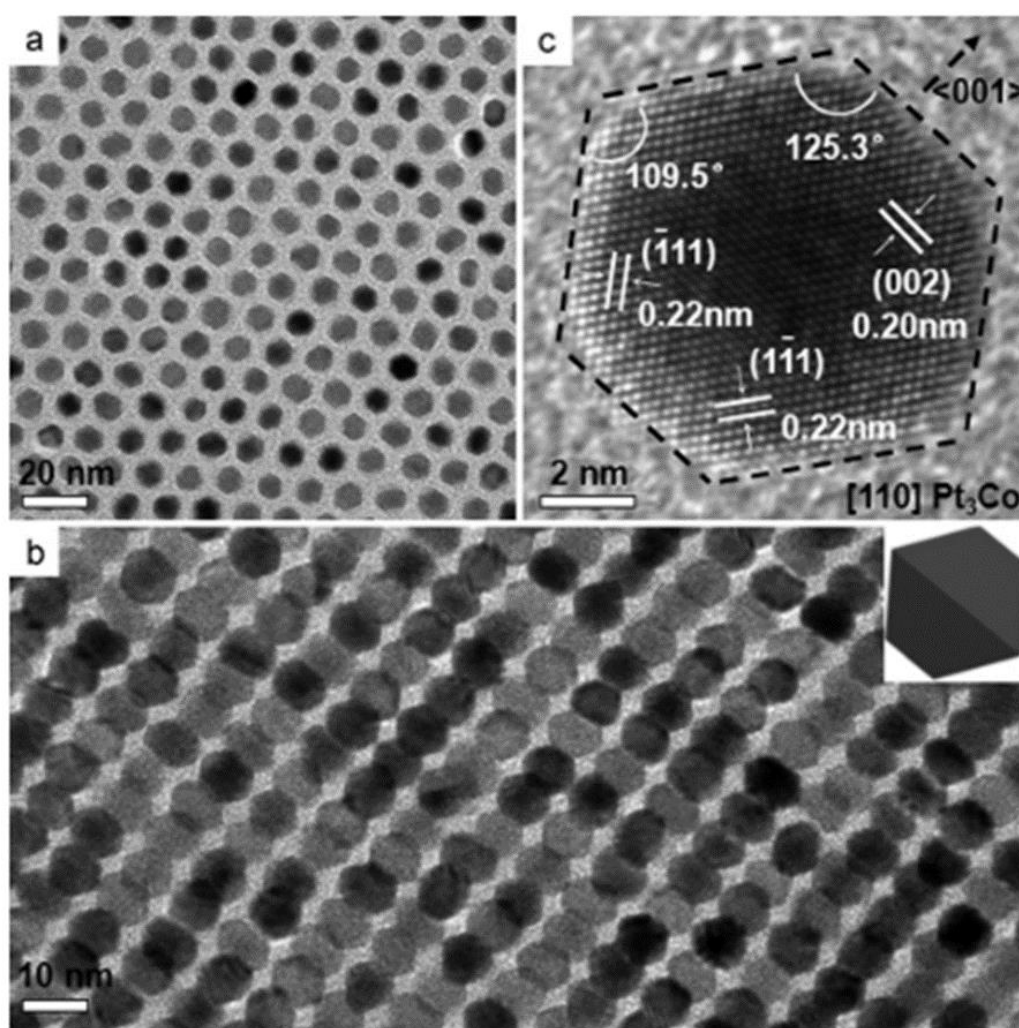


**Figure 1.3.** TEM of prepared  $\text{Pt}_3\text{Co}$  nanocrystals capped with amines <sup>[63]</sup>

Ethyl diamine (EDA) modified Pt nanowires have been prepared by using EDA as a capping agent <sup>[47]</sup>. Typically,  $\text{Pt}(\text{acac})_2$  and EDA were mixed in dimethylformamide (DMF) to get a homogeneous solution, and then the solution was heated up to 150°C

for 5 h with 0.2 MPa CO inside. The resulting colloidal products were collected by centrifugation and washed with ethanol several times. The diameter of ultrathin Pt NWs averaged to 1.1 nm; approximately 6 ~ 7 atoms thick. High-resolution STEM revealed that the as-prepared Pd NWs were highly crystalline, with two types of clearly observed lattice fringes having interplanar spacings of 0.227 and 0.196 nm, ascribed to the (111) and (200) planes of fcc Pt (*Figure 1.4*). PVP stabilized Au clusters have been obtained by mixing an aqueous solution of HAuCl<sub>4</sub>/PVP and a strong reducing agent NaBH<sub>4</sub> at 0 °C. By tuning the concentration of PVP and HAuCl<sub>4</sub>, the average size of the obtained Au cluster could be adjusted to 1.1 ~ 3.1 nm [41].

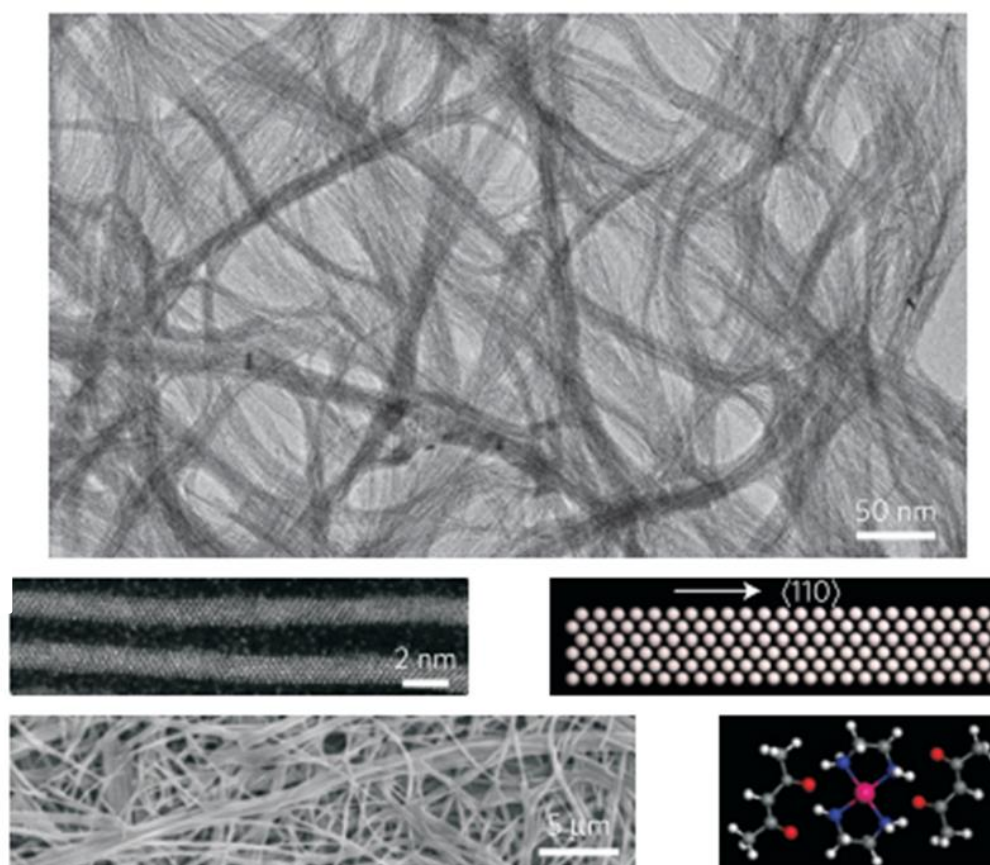
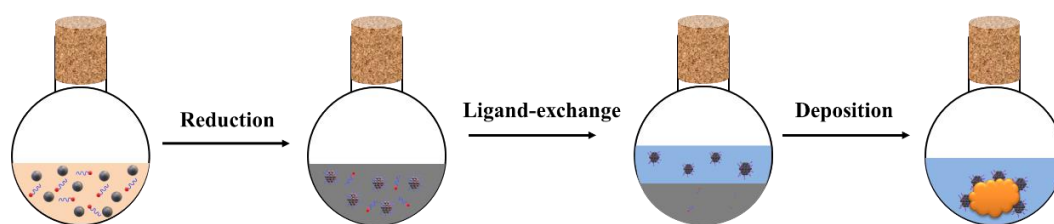


*Figure 1.4. Pt nanowires capped with ethyl diamine* [47]

To investigate the catalytic roles of capping agents around MNCs, different ligands-capping MNCs have to be prepared. One of the possible ways is to do the ligand-exchange process of as-synthesized MNCs to replace the ligands with others. For example, Ru nanoparticles were synthesized by thermal-reduction of  $\text{RuCl}_3$  in 1,2-propanediol [42]. At elevated temperatures, polyols are oxidized to various aldehyde and ketone species enabling the reduction of metal precursors. After the formation of Ru nanoparticles, 1-Ethynyl-4-hexylbenzene (EHB, a terminal alkyne) dissolved in toluene was added to extract the Ru nanoparticles from propanediol to the toluene phase, as a result of self-assembly of alkynes on the surface of metal nanoparticles. It is worth to note that the ligand-exchange process has been extensively extended for the different types of ligands. Another systematic study of chain-length of amines on the  $\text{Pt}_3\text{Co}$  surface has been conducted by Wu et al [63]. Amine-capped  $\text{Pt}_3\text{Co}$  NCs with different chain-length from  $\text{C}_4\text{NH}_2$  to  $\text{C}_{18}\text{NH}_2$  have been prepared by thermal-decomposition and ligand-exchange process. The influence of the chain-length on the catalytic performance was systematically studied.

The MNCs could be deposited on the supports after preparation, and this kind of supported MNCs catalysts could be easily separated from the reaction mixture after liquid-phase heterogeneous catalysis. This process is called the sol immobilization method. For example, 5 wt% PVA coated Pd NCs on  $\gamma\text{-Al}_2\text{O}_3$  have been prepared following this procedure [35]. Pd precursors ( $\text{Na}_2\text{PdCl}_4$ ) and PVA solutions were mixed to form an aqueous phase. Then, the  $\text{NaBH}_4$  solution was added to reduce the Pd salts

and a brown metallic Pd sol was immediately formed. Finally, the colloid has been immobilized by adding the Al<sub>2</sub>O<sub>3</sub> support under vigorous stirring



**Schema 1.2.** Illustration of general procedure for direct preparation of ligand-capped MNCs catalysts

To conclude, as shown in **Schema 1.2**, the direct catalyst preparation based on the solution approach is known to produce high-quality MNCs with tunable size and shape, narrow size dispersion, and high crystallinity. The preparation involves the mixing of metal precursor and protective ligands following by reduction to MNCs coated with ligands. This process is always accompanied by the darkening of the solution because of the formation of colloids. The ligands could be further exchange by the ligand-exchange process, which facilitates the studies of the catalytic role of ligands. The ligand-exchange process involves the MNCs transformation from one phase to another. Thus, a reverse immiscible solvent need to be added which contains the desired ligand molecules. With the replacement of the initial ligands with new ligands, the transfer of MNCs could be observed by the color change. Moreover, the prepared well-dispersed MNCs could be deposited on the supports to produce supported metal catalysts, which is called a sol immobilization approach. The supported ligand-capping metal catalysts prepared by this approach have narrow size distributions and easy for separation after liquid-phase reactions.

### 1.2.2. Post-modifications

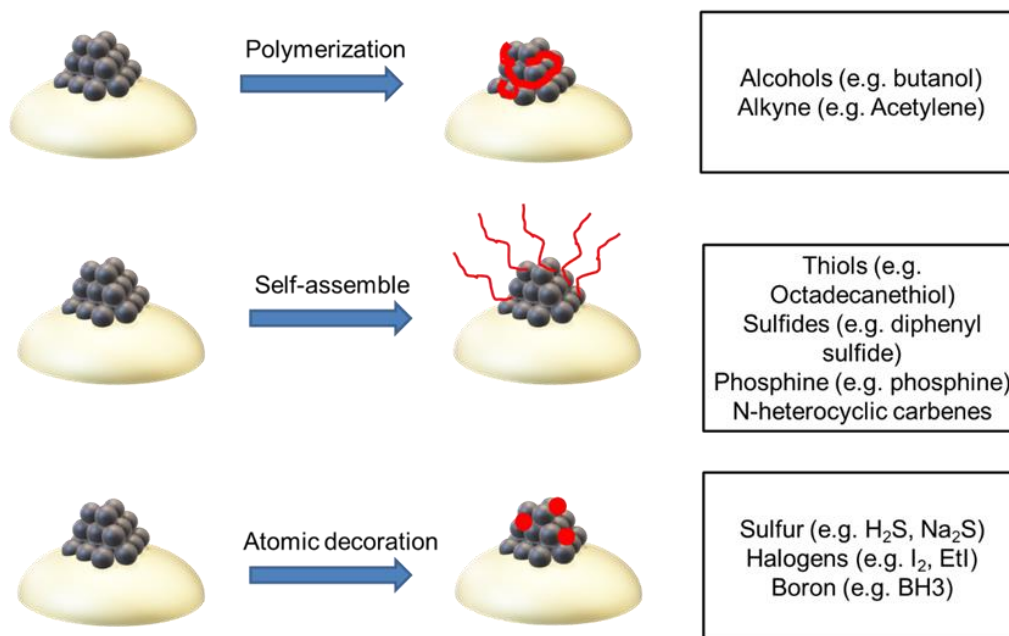
Due to the easy realization and close to industrial application, post-modification is attracting more and more attention. Post-modification was extensively used to modify supported metal catalysts, except several cases of colloidal metal NPs. According to the interaction between modifiers and metals, various preparation methods have been reported. Specifically, *Schema 1.3* summarizes the different approaches for the post-modification like (1) On-metal-surface polymerization [33, 40, 43]; (2) Self-assemble monolayers (SAM) [79, 86, 89, 102]; (3) Atomic element decoration [88, 60, 115].

The deposition of modifiers via the on-surface polymerization has been reported for metal single crystals like Cu (111) [112]. Concerning the on-surface polymerization for catalytic applications, the presence of polymeric species will block the metal sites and decrease the catalytic activity. However, few works have reported that controlled polymerization with the alcohols or alkynes could improve the catalytic performance of metal MNCs.

For example, Niu et al. have reported treatment of 15 wt% Co/Al<sub>2</sub>O<sub>3</sub> catalyst with butanol vapor at 250 °C using N<sub>2</sub> as carrier gas for selective amination of alcohols [43]. Butanol dehydrogenates to aldehyde and with subsequent aldol condensation produces polymeric species. STEM-EDS (*Figure 1.5*) analysis indicates the presence of carbonaceous species on the treated catalysts. It is worth to note that the treatment time is important for the catalytic activity. The long-time treatment caused severe



deactivations, while the optimization of the treatment time results in the promoting effects.



*Schema 1.3. Post-modification of metal nanoparticles with modifies*

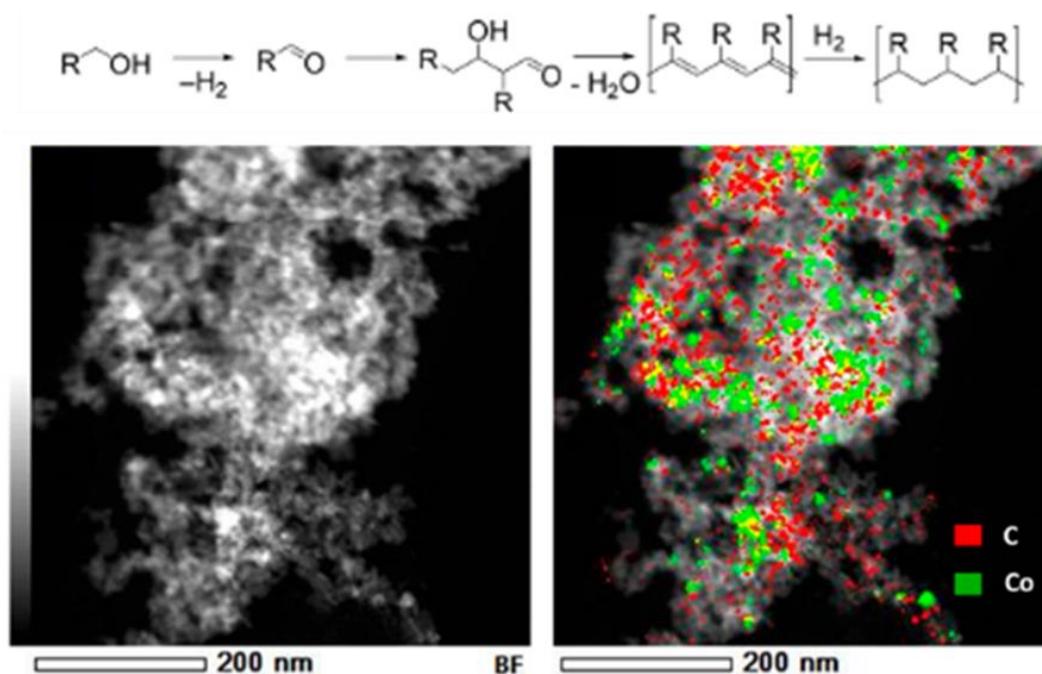


*Figure 1.5. Pre-treatment of Co/Al<sub>2</sub>O<sub>3</sub> with alcohols <sup>[43]</sup>*

The Pd catalysts have been treated by acetylene to produce a trans-polyacetylene layer on the Pd surface [33]. According to the preparation, the acetylene treatment was performed in a glass pressure vessel, with the Pd nanosheets dispersed in DMF. The vessel was charged with acetylene and heated at 30 °C for different time to control the polymerization degree. (*Figure 1.6*).

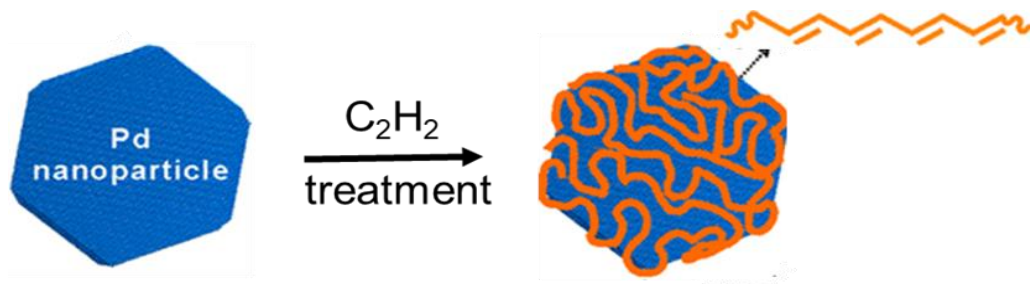


*Figure 1.6.* Pd NPs pre-treatment by  $C_2H_2$  [33]

Self-assembled monolayers (SAMs) have been widely used to endow steric and electronic properties of the metal surfaces. The usage of SAMs on metal nanoparticles for catalysis has been reviewed by J. Will Medlin et al [102]. SAMs are organic assemblies composed of molecules containing a headgroup that interacts strongly with a metal surface. The most used organic molecules for SAMs are thiols. When exposed to the metal surfaces, the thiols molecules covalently bond to the metal surface through a sulfur attachment group producing ordered and stable monolayer films.

The general procedure for the formation of thiols SAMs on metal catalysts includes the first cleaning of supported metal catalysts (Pd/Al<sub>2</sub>O<sub>3</sub> or Pt/Al<sub>2</sub>O<sub>3</sub>) by oxidation with oxygen and reduction with hydrogen at high temperature [86]. And then, thiols coating is deposited by immersing the catalyst at room temperature in an ethanolic solution of thiols (concentration: 1~10 mM) for 24 h. Finally, the catalysts were dried in an inert

gas flow before using. SAMs provide versatility as a modification platform due to the turnability of their tail-group. For example, 1-octadecanethiol, a straight-chain alkanethiol with nearest-neighbor spacing of  $\sim 0.5$  nm on palladium, was used to produce a densely packed monolayer on the Pd/Al<sub>2</sub>O<sub>3</sub> catalysts [81,99]. And another thiol, with a bulky “caged” tail moiety, 1-adamantanethiol, with an expected nearest-neighbor spacing of  $\sim 0.69$  nm on Pd, was used to create a sparser monolayer. The structures of both thiols are depicted in *Figure 1.7*.

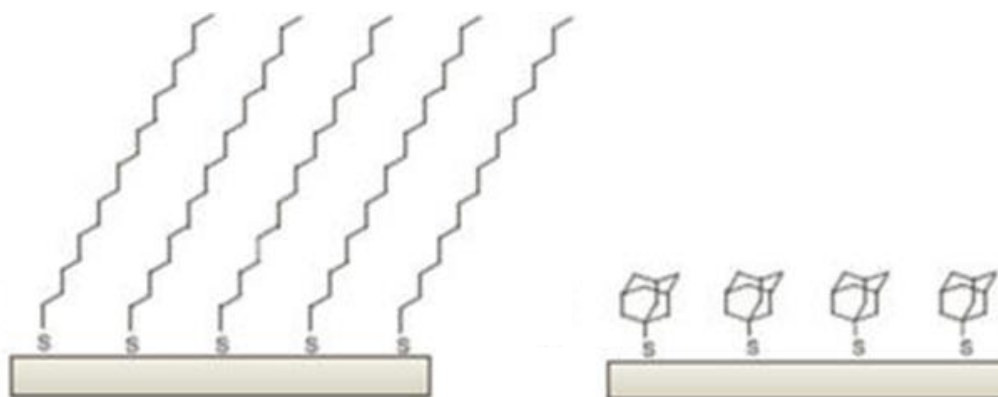


*Figure 1.7.* Pd/Al<sub>2</sub>O<sub>3</sub> modified with different thiols [102]

Thiols with multiple functional groups like phenyl rings, hydroxyl groups, and acid groups have been also reported to produce SAMs on the metal catalysts for selective reactions [97, 100, 101]. Besides thiols, organic sulfide like diphenyl sulfide (Ph<sub>2</sub>S) have been developed to modify the metal catalyst. For example, the Ph<sub>2</sub>S modified Pd/TiO<sub>2</sub> catalyst has been prepared by adding the reduced 1 wt % Pd/TiO<sub>2</sub> to a Ph<sub>2</sub>S in hexane solution at the appropriate concentration (0.2 mM) and stirred at 298 K for 30 min [93]. It is worth noting that organic sulfide on the metal surface is not stable, the C-S bond is easy to cleavage at an evaluated temperature in the presence of H<sub>2</sub>. For example, Ph<sub>2</sub>S

on the Pd surface easily decomposes by reduction at 120 °C with hydrogen, with sulfur atoms on the Pd surface [76, 91, 94, 96].

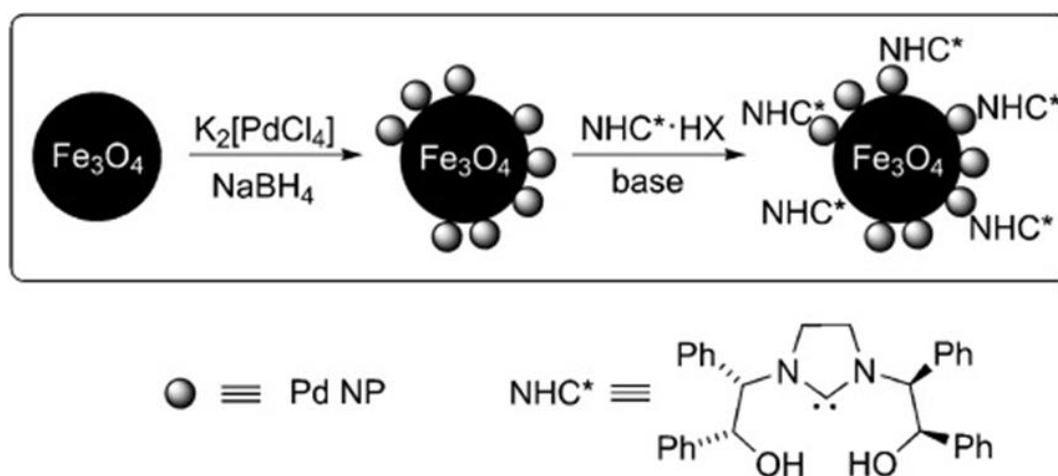


**Figure 1.8.** Pd/Fe<sub>3</sub>O<sub>4</sub> modified with NHCs [119]

Other modifiers such as phosphines and N-heterocyclic carbenes have also been reported to form monolayers on metal surface for selective reactions [69, 71, 73, 119, 53]. However, due to the relatively weak interaction between these modifiers and metal atoms, the catalysts are usually limited to gas-phase reaction or applied as an additive in the liquid-phase reaction. For example, triphenylphosphine (PPh<sub>3</sub>) has been used as a ligand for heterogeneous Pd/TiO<sub>2</sub> catalyst [71]. The reduced 1 wt% Pd/TiO<sub>2</sub> catalyst was added to a solution of PPh<sub>3</sub> dissolved in hexane. The resulting mixture was stirred in a rotary evaporator for 30 min before drying in a vacuum. The prepared catalyst was subjected to the gas-phase hydrogenation of acetylene. In another case, the PPh<sub>3</sub> modified Au/SiO<sub>2</sub> catalyst was applied for liquid-phase reaction, however, PPh<sub>3</sub> was added as a homogeneous capping ligand in the reaction mixture [69]. Due to relatively strong interaction between PPh<sub>3</sub> ligand and metal nanoparticles, the PPh<sub>3</sub> could chemically adsorb on the metal surface and form a monolayer. However, the P-Metal

bond is not strong enough with its leaching in liquid-phase reaction and suffers from poor ligand stability during heterogeneous catalysis.

N-heterocyclic carbenes (NHCs) have been emerged recently as modifiers to functionalize metal catalysts <sup>[64]</sup>. Since their first discovery in 1991, NHCs have been thoroughly studied for different applications. Due to their unique electronic and steric properties, they are widely used as ligands in metal-catalyzed reactions. In general, several advantages of NHC ligands have been revealed. Firstly, the easy introduction of sterically- and electronically-perturbing functional groups ensures high synthetic flexibility. Secondly, due to their particular geometry, the N-substituents of NHC ligands interact not only with the metallic surface but also with the adjacent ligands, while the high strength of the NHC-Metal bonds also enhanced the stabilization of MNPs. For example, Pd/Fe<sub>3</sub>O<sub>4</sub> has been modified with NHCs by using chiral, enantiomerically pure imidazolium salts under basic conditions to explore the possibility of achieving asymmetry reactions on active NPs (*Figure 1.8*) <sup>[119]</sup>. Typically, a calculated amount of Pd/Fe<sub>3</sub>O<sub>4</sub> was mixed with base (NaOtBu) and NHCs in toluene and heated to 50 °C for 6 h. After cooling to room temperature, the suspension was centrifuged and washed with toluene, ethanol, and acetone. The prepared NHCs-modified Pd/Fe<sub>3</sub>O<sub>4</sub> catalyst could be reused five times without any significant decrease in either activity or selectivity, confirming the high stability of NHCs ligands on the metal surface.

Atomic decoration was normally performed with H<sub>2</sub>S or inorganic sulfide to graft sulfur atoms on the metal surface, or graft atomic halogen and boron atoms on the metal

surface. However, due to the small atomic sizes, the S and B atoms migrate inside the metal lattice. As shown in *Figure 1.9*, Pd<sub>x</sub>S<sub>y</sub> was always produced when the Pd catalyst has been treated by Na<sub>2</sub>S at elevated temperatures <sup>[80]</sup>.

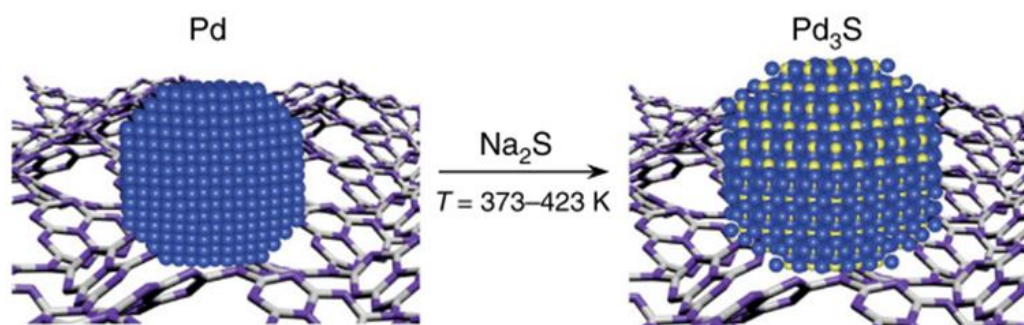


*Figure 1.9. Modification of Pd catalyst by Na<sub>2</sub>S*<sup>[80]</sup>

### 1.3. Identification of the role of promoters

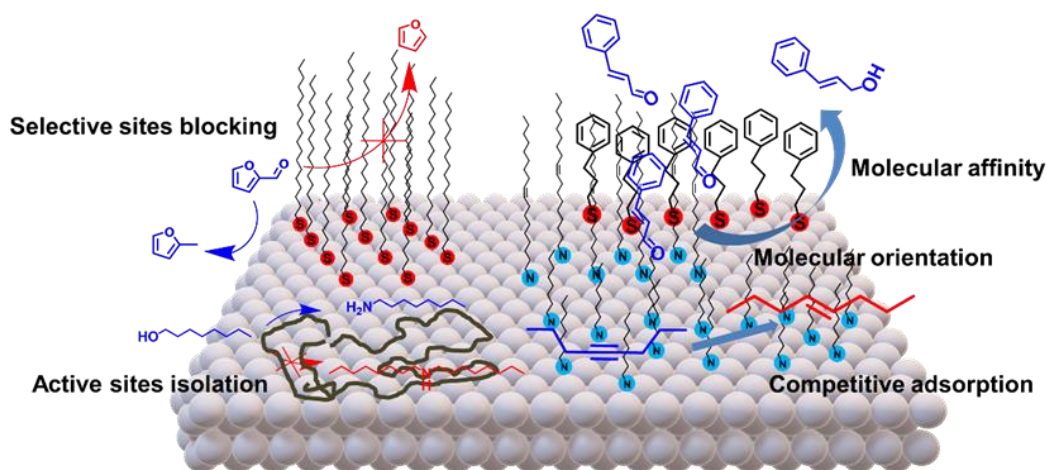
Coordination of non-metallic modifiers on the active metal surface results in several effects during the catalytic process. First of all, the presence of modifiers will change the structural geometry on-surface as well as the space arrangement outer-surface. The on-surface change involves blocking the active sites, which will prevent the adsorption of reactant molecules as well as limiting the diffusion of intermediates on the surface. The outer-surface changes derive from the modifiers, which have long and bulky “tail” such as the amphiphilic modules. These tails will interact with the reactant molecules via steric space hindrance and weak interaction (e.g. Van der Waals forces, hydrogen bonding, aromatic ring stacking) when the reactant molecules approaching the catalyst surface<sup>[22, 118]</sup>. All these on-surface or outer-surface structural changes could be ascribed to steric effects. Besides the steric effects, the coordination of modifiers will change the

electronic structure of the metal surface, e.g. the Fermi core level <sup>[120]</sup>. Understanding electronic effects could be more difficult compared to the steric effects. The electronic effect is relevant to changing the electronic structure of surface metal atoms <sup>[36, 38, 47]</sup>. Due to the demands to develop multiple-step reactions, bifunctional catalysts and sites derived from non-metallic modifiers attract a lot of attention <sup>[121]</sup>. The bifunctional effects introduced by modifiers can overcome the drawback coming from using two kinds of different catalysts in a single reaction system. Notably, bifunctional effects create a proximate metal-acid or metal-base site, which is important for efficient catalytic process.

### **1.3.1. Steric effects**

The steric effects strongly affect the accessibility of reactant molecules on the metal surface. The steric effects can be more significant when the reactant molecule has a large molecule size <sup>[43]</sup>. Since most of the fine chemical molecules have a relatively big molecular size, tuning of the steric effects is a popular way to control the selectivity during the catalytic process. Numerous papers have ascribed to steric effect the abnormal catalytic behavior after the modification, but only a few of them focus on the understanding of the interaction mechanism between the reactants and modifiers. The understanding of the way how the steric effects change the behavior of reactant molecules is important because it can guide the rational design of the smart catalytic surfaces.

It is easy to understand that when a surface of the metal was modified by a non-metallic modifier, not only the structural parameters will be changed but also the electronic state of metal atoms can be altered. During the real catalytic process, both the steric and electronic effects will impact the catalytic behavior, however, in some cases, either steric or electronic effect can be dominant or both of them are equally important. Identification of steric and electronic effects and their contributions to the catalytic behavior is therefore the primary task for the systematic and comprehensive understanding of heterogeneous catalysis.



**Schema 1.4.** Illustration of different kinds of steric effects on catalytic performance.

The steric effect can have different nature and can involve different modifiers. As shown in **Schema 1.4**, the non-metallic modifiers could be polymers, N-, S- based organic molecules. The presence of steric effects usually decreases the overall activity and changes the selectivity. Several mechanisms have been proposed to explain the abnormal catalytic performance by comparing it with the non-modified catalyst. These mechanisms involve on-surface effects of (1) selective sites blocking, (2) active sites



isolation, (3) competitive adsorption, and outer-surface effects of (4) molecular affinity, (5) molecular orientation [22, 25, 102].

### 1.3.1.1. Selective sites blocking

Polymers modifies are often used for selective blocking the active sites. Sebastiano et al, have reported the selectivity control in the palladium-catalyzed alcohol oxidation through selective blocking of specific active sites [35]. The authors modified Pd nanoparticles with PVA and found that PVA selectively blocked the Pd (111) facets. The supported Pd NPs protected by PVA showed a lower rate of benzaldehyde decarbonylation and suppressed further oxidation of benzaldehyde to benzoic acid compared with the unprotected Pd nanoparticles.

The alkyne modified ruthenium nanoparticles have been synthesized and compared with the non-modified counterparts for selective hydrogenation of styrene by Zhang et al [42]. As illustrated in *Figure 1.10*, two different kinds of alkynes have been used, terminal alkyne 4-ethynyltoluene and internal alkyne 1,2-di-p-tolyne. The alkyne showed different adsorption configurations on the surface of Ru (0001). The terminal alkyne adsorbs strongly in comparison with internal alkyne with the Ru=C-HCH- interfacial bonds. Internal alkyne adopted an  $\eta^2$  side-on configuration and formed a  $\delta$ - $\pi$  covalent bond. It means that the internal alkyne blocked the bridge sites and the terminal alkyne blocked the hole sites. The selective blocking of active sites leads to different catalytic results. Thus, Ru NPs capped with terminal alkynes exhibited catalytic activity towards hydrogenation of both the C=C and phenyl rings of styrene,

while Ru nanoparticle capped with internal alkynes exhibited activity towards the hydrogenation of the C=C bonds only. This discrepancy has been caused by the different sites needed for the hydrogenation of C=C bonds and phenyl rings.

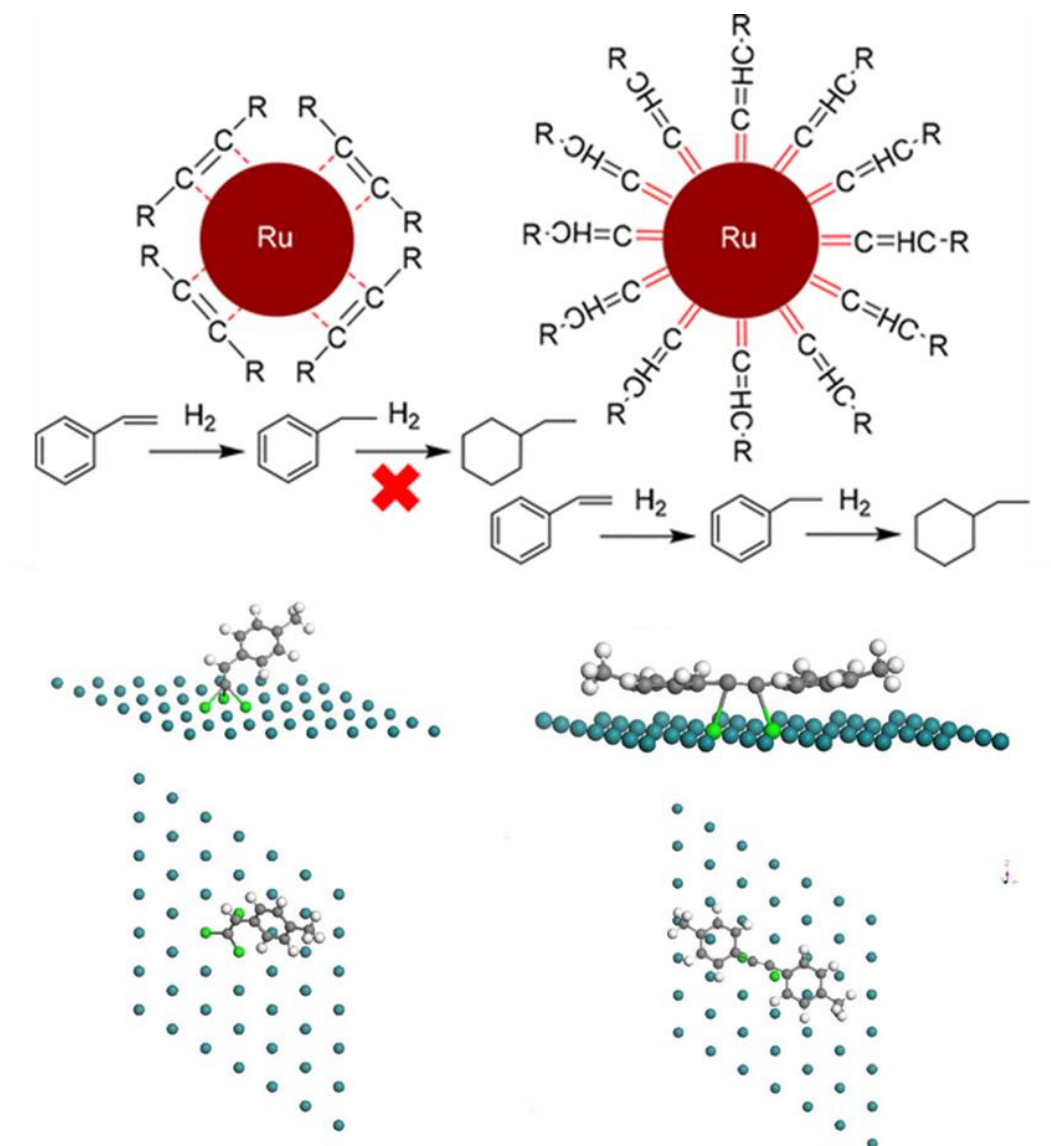


**Figure 1.10.** The adsorption configurations of terminal alkyne (4-ethynyltoluene) and internal alkyne (1,2-di-p-tolyethyne) on Ru (0001) <sup>[42]</sup>.

The sulfur-based modifiers like thiols have been extensively used as selective blocking agents for metal catalysts <sup>[102, 118]</sup>. For example, the reaction pathways for furfural hydrogenation have been well-controlled on supported Pd catalysts with self-assembled

thiols monolayers<sup>[81]</sup>. As shown in **Figure 1.11**, two different thiol molecules: linear 1-octadecanethiol (C18) and bulky 1-adamantanethiol (AT) were used to modify the Pd surface for catalytic hydrogenation of furfural. The C18 thiols selectively block the terrace sites, while AT thiols sparsely block the terraces, edges, and corners sites without discrimination. It means that the catalyst modified by the C18 thiol has the only accessible sites at particle edges and steps whereas AT modified catalyst provides access for the reacting molecules only to the sites on the particle terraces. The accessibility of different active sites results in different catalytic behaviors during the furfural hydrogenation. Pd modified by C18 thiol showed high activity in hydrogenation and deoxygenation of carbonyl group, while the AT modified Pd exhibited decarbonylation of aldehyde group and hydrogenation of furan rings.

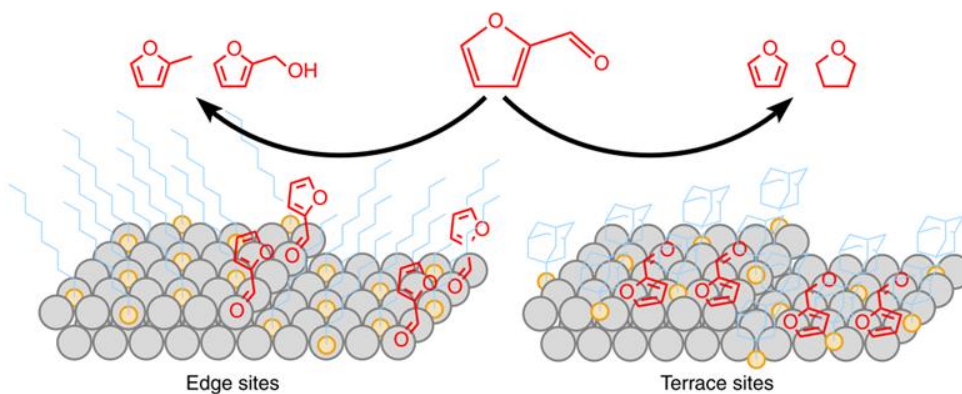


**Figure 1.11.** Proposed adsorption mechanism of furfural on C18 and AT modified catalysts<sup>[81]</sup>.

The hydrogenation of ethylene has been extensively studied in the literature. It has been suggested that the most reactive forms involve a  $\pi$ -bound state weakly adsorbed on the top sites<sup>[86]</sup>. With AT- and C18-modified Pd/Al<sub>2</sub>O<sub>3</sub> catalysts, ethylene hydrogenation

rates were measured to determine the effect of site availability on catalytic activity. The reactions were performed in a gas-phase plug flow reactor at 323 K using a 10:1 hydrogen to reactant feed ratio.

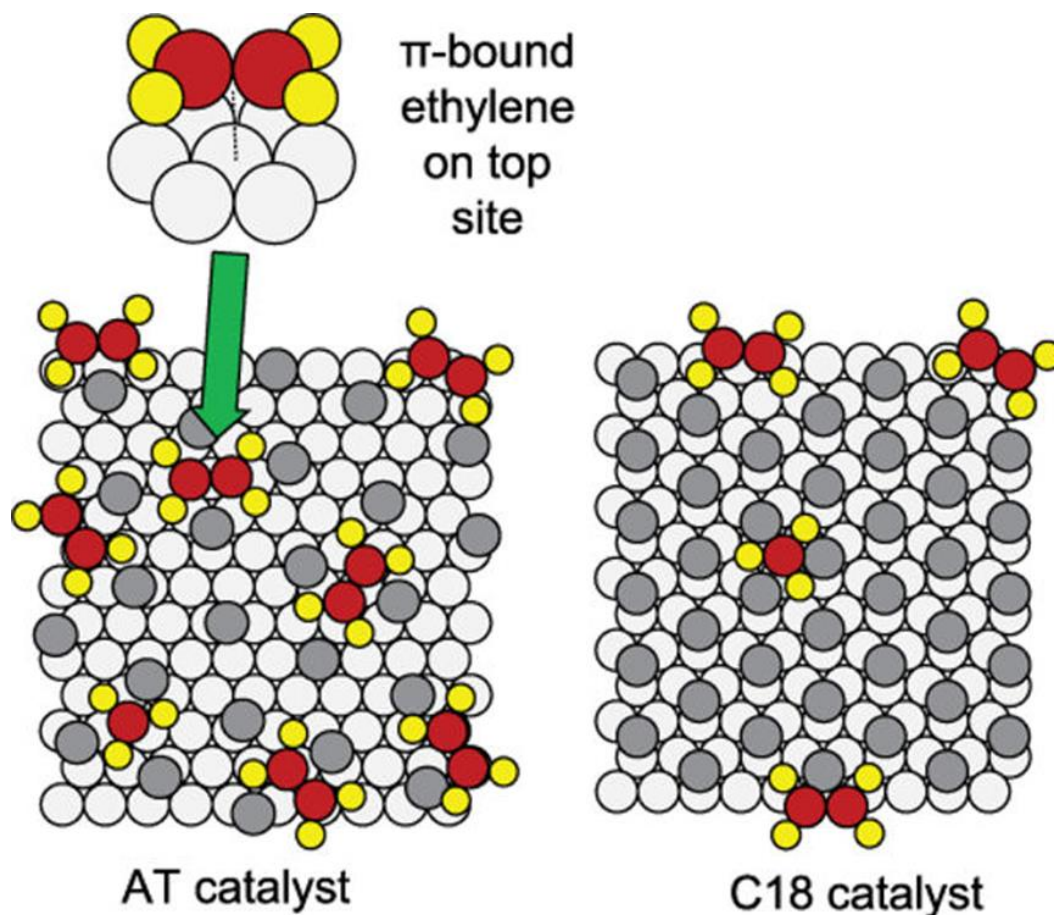


**Figure 1.12.** Proposed adsorption mechanism for ethylene on AT and C18 modified Pd/Al<sub>2</sub>O<sub>3</sub> catalysts<sup>[86]</sup>.

Results showed that the AT-modified catalysts converted ethylene into ethane with a factor of  $\sim 17\times$  faster than the C18-modified catalysts despite having twice lower thiolate surface coverage. The reaction rates were consistent with the availability of only top sites on the C18 catalysts at particle edges and corners, whereas AT catalysts allowed access to particle terraces. However, the adsorption isotherms suggested a difference in adsorption energy of only  $\sim 1$  kJ/mol between C18 and AT catalysts. The

proposed adsorption mechanism of ethylene on the SAM-modified catalysts is shown in *Figure 1.12*. This study demonstrated the successful use of SAMs for the control of the accessibility of specific active sites for a well-studied reaction.

### 1.3.1.2. Active sites isolation

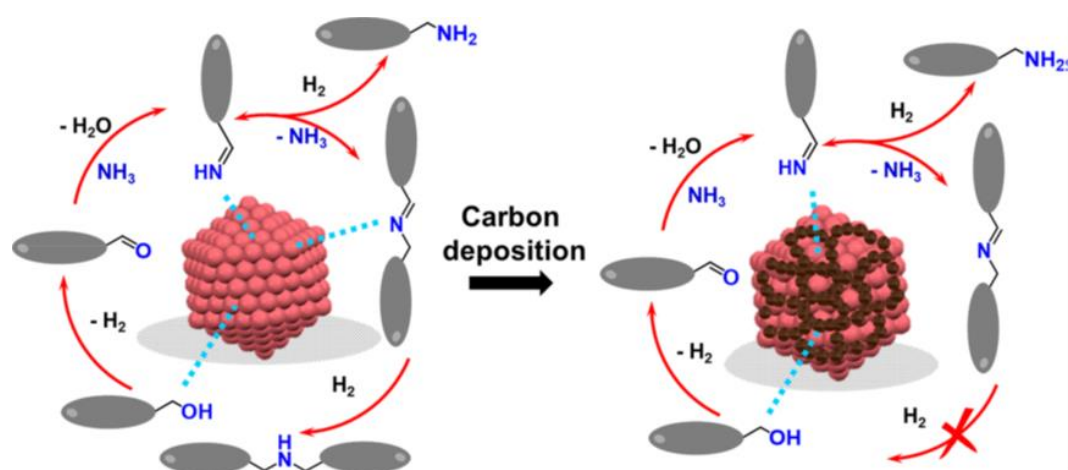


*Figure 1.13.* Prevent the reaction from the internal group by steric effect over alcohols treated Co catalysts <sup>[43]</sup>.

During heterogeneous catalysis, the reactant molecules need to be adsorbed and be activated on the metal surface. This process needs the participation of multiple metal atoms on the surface. The active site isolation is an effect that reduces the size of active assemblies and results in a change of the catalytic behavior for some specific reactions [87, 88, 92]. One of the important features in catalysis is selective activation of the terminal functional groups while preventing the reaction from internal groups. The terminal part of a molecule can much more easily access the active site than the internal part. For example, when the cobalt nanoparticles were treated by 1-butanol at high temperature, the polymeric carbon species were produced on the cobalt surface which has a strong steric effect during the amination of 1-butanol to 1-butyl amine <sup>[43]</sup>. The suppression of

hydrogenation of internal imine groups has been proposed as the key factor for the enhanced selectivity (As shown in [Figure 1.13](#)).

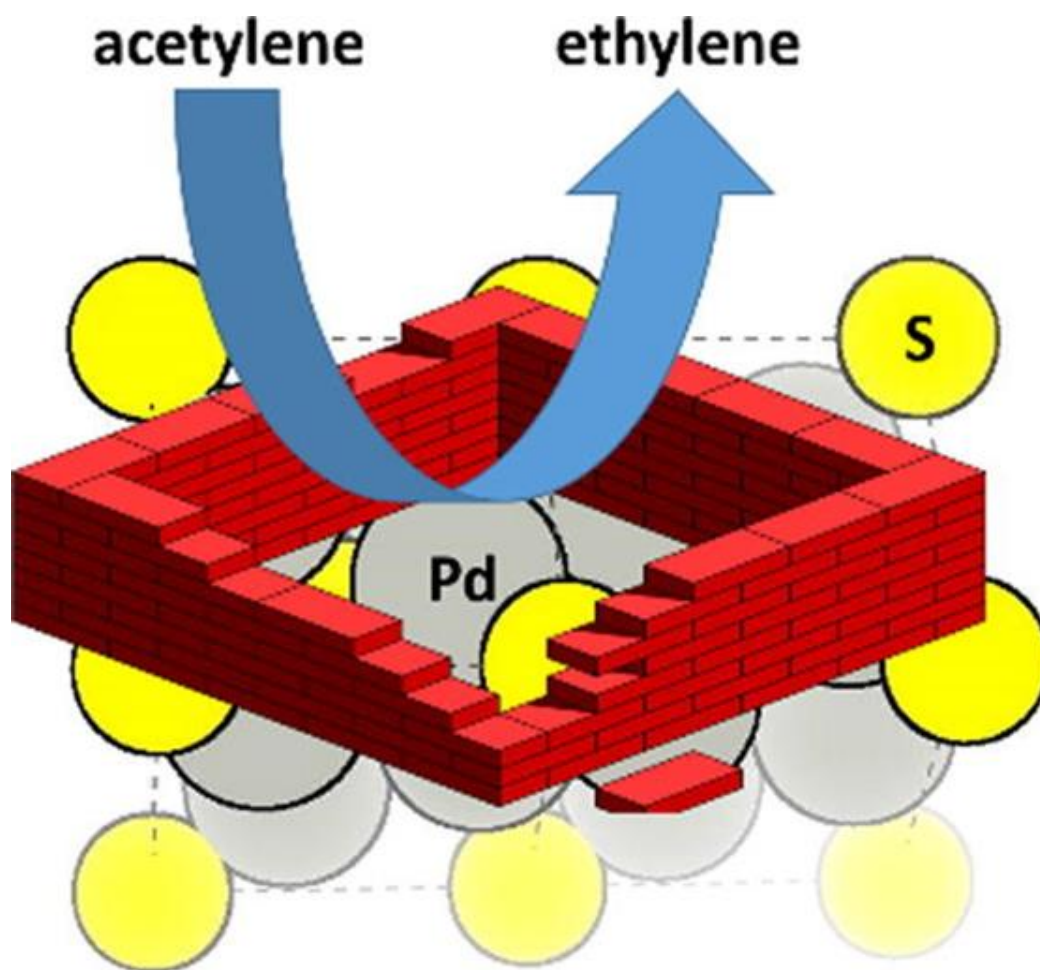


**Figure 1.14.** Modification with sulfur to create isolated Pd atoms <sup>[87]</sup>.

Another example is the selective hydrogenation of 4-nitrostyrene on the Pt/TiO<sub>2</sub> catalyst pretreated by organic thiol reported by Martin et al <sup>[101]</sup>. The authors found that after modification of Pt catalyst with organic thiols, a switch in selectivity from 4-ethylnitrobenzene and 4-ethylaniline toward 4-aminostyrene has been observed. This change was ascribed to the alteration of adsorption configuration of 4-nitrostyrene on the Pt surface due to active sites isolation by organic thiols. The adsorbed thiol modifiers prevent the flat adsorption of 4-nitrostyrene via benzene ring. Therefore, the

4-nitrostyrene can only be adsorbed via tilted-configuration. A preferential interaction of the nitro-group with the TiO<sub>2</sub> support leads to the observed switch in selectivity.

The changing of active ensembles on the Pd surface will significantly change the behavior during alkyne hydrogenation. It has been extensively reported that the Pd<sub>4</sub>S phase of palladium sulfide is known to provide highly selective assemblies for alkyne semi-hydrogenation to alkene (*Figure 1.14*)<sup>[87]</sup>.

### 1.3.1.3. Molecular affinity

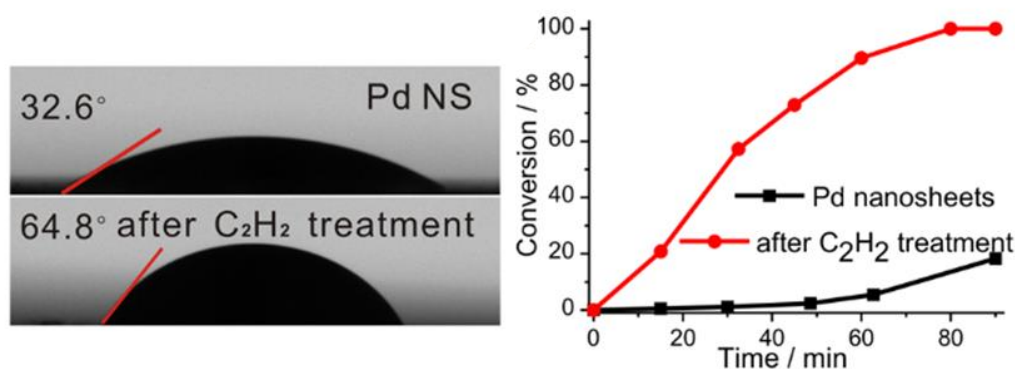


*Figure 1.15.* Static water contact angle and nitrobenzene hydrogenation catalytic activity over Pd nanosheet before and after C<sub>2</sub>H<sub>2</sub> treatment<sup>[33]</sup>.

Molecular affinity implies the strength and specificity of intermolecular interaction between the modifier and reactant molecules. It is an outer-surface effect and depends on the structure and tail of the modifier. The hydrophilic and hydrophobic properties of the modifiers are extremely important. The hydrophobic affinity is relevant to the presence of alkane chains and the hydrophilic affinity is associated with the polar groups which might be involved in H bonding on. Aromatic rings in modifiers also demonstrate an affinity to the aromatic reactants via  $\pi$ - $\pi$  stacking effect. The role of molecular affinity is: to attract the reactant molecules, to increase the concentration of

surface reactants, and to increase the rate of the reaction; to change the configuration of reactants and molecules.

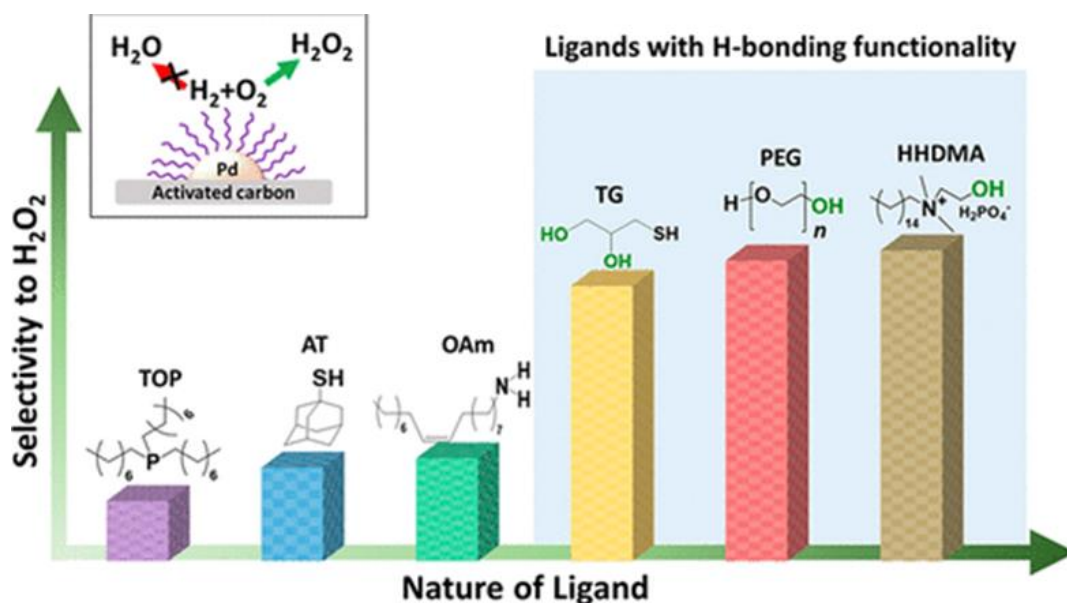


**Figure 1.16.** Effect of ligand on the selective to H<sub>2</sub>O<sub>2</sub> over Pd catalyst<sup>[98]</sup>.

For example, Dai et al. have reported C<sub>2</sub>H<sub>2</sub> treatment of Pd nanoparticle for enhancement of hydrogenation ability of hydrophobic substrates. The treatment with C<sub>2</sub>H<sub>2</sub> on Pd results in the polymerization of C<sub>2</sub>H<sub>2</sub> into trans-polyacetylene and makes the Pd surface hydrophobic<sup>[33]</sup>. Such a surface modification helps to accumulate more hydrophobic substrates during catalysis with the enhancement of catalytic activity. As shown in **Figure 1.15**, the contact angle of water droplets on the Pd surface increased from 32.6° to 64.8° after the C<sub>2</sub>H<sub>2</sub> polymerization, indicating the more hydrophobic properties of the Pd surface. Consequently, the modified catalysts exhibited high activity in the hydrogenation of hydrophobic nitrobenzene but poorer catalytic activity for hydrogenation of hydrophilic 4-nitrophenol.



Lucas et al. have reported modification of Pd surface by various modifiers such as phosphines and thiols. It was found that those H-bonding groups led to the highest H<sub>2</sub>O<sub>2</sub> production (*Figure 1.16*)<sup>[98]</sup>.

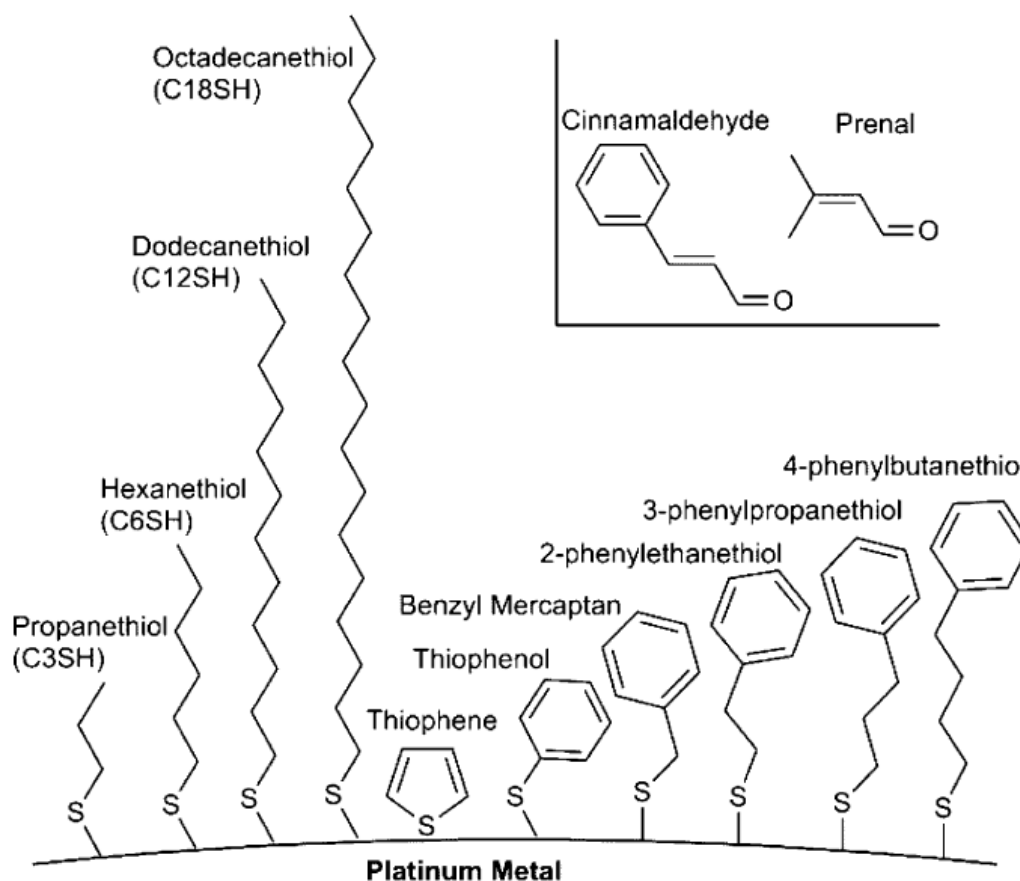


*Figure 1.17. Proposed adsorption mechanism depicting favorable orientation of cinnamaldehyde induced by 3-phenylpropanethiol SAM modifiers*<sup>[89]</sup>.

Molecule affinity has been demonstrated during the hydrogenation of cinnamaldehyde. Tuning the structure of the SAM tail facilitated appropriately positioned aromatic stacking interactions between the reactant and the modifier. Cinnamaldehyde is an  $\alpha$ ,  $\beta$ -unsaturated aldehyde of significant industrial importance<sup>[63]</sup>. Typically, on transition metal catalysts, the major product is formed via hydrogenation of the double bond to

produce hydrocinnamaldehyde. However, the more industrially valuable product is cinnamyl alcohol formed by hydrogenation of the aldehyde. Platinum is one of the most selective metals for producing cinnamyl alcohol. To demonstrate this concept, a variety of SAMs with organic tails were tested to determine their effect on the selectivity. The results demonstrate that the selectivity could be increased from ~25% on the uncoated Pt catalysts to over 95% using the catalyst modified with 3-phenylpropanethiol. This modifier provides aromatic stacking interactions between the modifier and reagent for selective conversion of the aldehyde moiety.

The proposed adsorption mechanism for this highly selective system is shown in *Figure 1.17*. Linear alkanes with no specific interaction with cinnamaldehyde provide modest improvement in selectivity over uncoated catalysts. This nonspecific effect was induced by the presence of sulfur independently of the alkanethiol tail length. Reducing the distance between the SAM phenyl moiety and the catalyst resulted in a low selectivity to the desired product. Earlier, it has been shown that binding in a horizontal configuration favors olefin hydrogenation while binding vertically favors hydrogenation of the aldehyde.

#### **1.3.1.4. Molecular orientation**

Molecular orientation is related to the changes of the reactant molecule configuration approaching the catalyst surface due to the presence of modifier tails. In comparison with molecular affinity, molecular orientation does not have any specific intermolecular interaction between modifiers and reactants but has spatial hindrance. The spatial

hindrance of modifiers allowed the penetration of the reactant molecules with a small functional group to the catalytic surface. Thus, molecular orientation favors the reaction happening on the small functional group of the molecules.

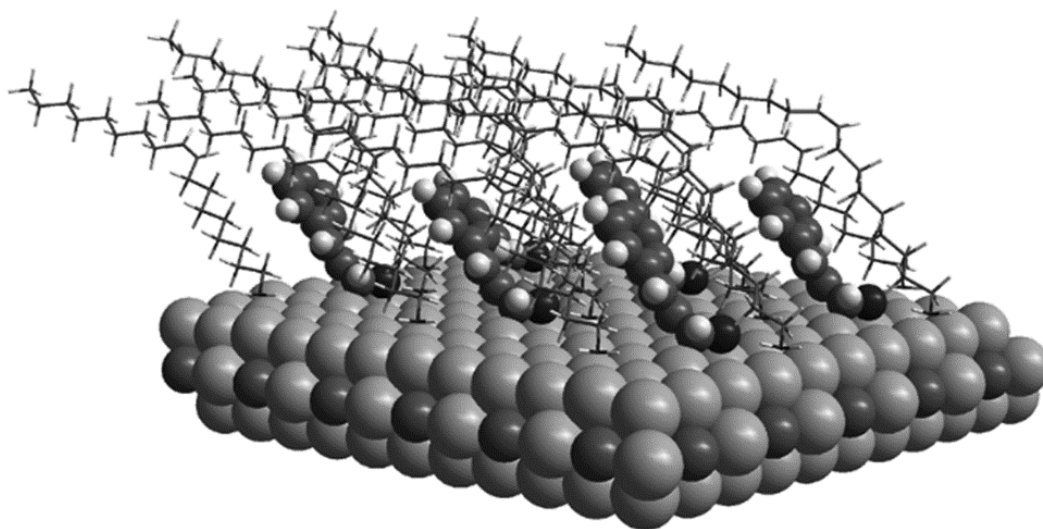


**Figure 1.18.** Optimized structure of CAS adsorption on the Pt<sub>3</sub>Co (100) surface capped by oAm <sup>[63]</sup>.

One example is the hydrogenation of cinnamaldehyde over amines-capped Pt<sub>3</sub>Co nanoparticles <sup>[63]</sup>. It is well known that hydrogenation of unsaturated aldehydes (CAL) over metal catalysts thermodynamically favors the formation of saturated aldehydes (hydrocinnamaldehyde, HCAL) rather than unsaturated alcohol (hydrocinnamyl alcohol, HCOL). oAm can form an ordered arrangement on the Pt surface and the long carbon chains impart steric hindrance so that the CAL molecules do not lie flatly on the nanoparticle surface. Computationally, the CAL molecules can only enter into the array of oAm molecules with their aldehyde groups interacting with the Pt<sub>3</sub>Co (100) surface. The C=C bonds are far away from the catalytically active surface (as shown in **Figure 1.18**)

### 1.3.1.5. Competitive adsorption

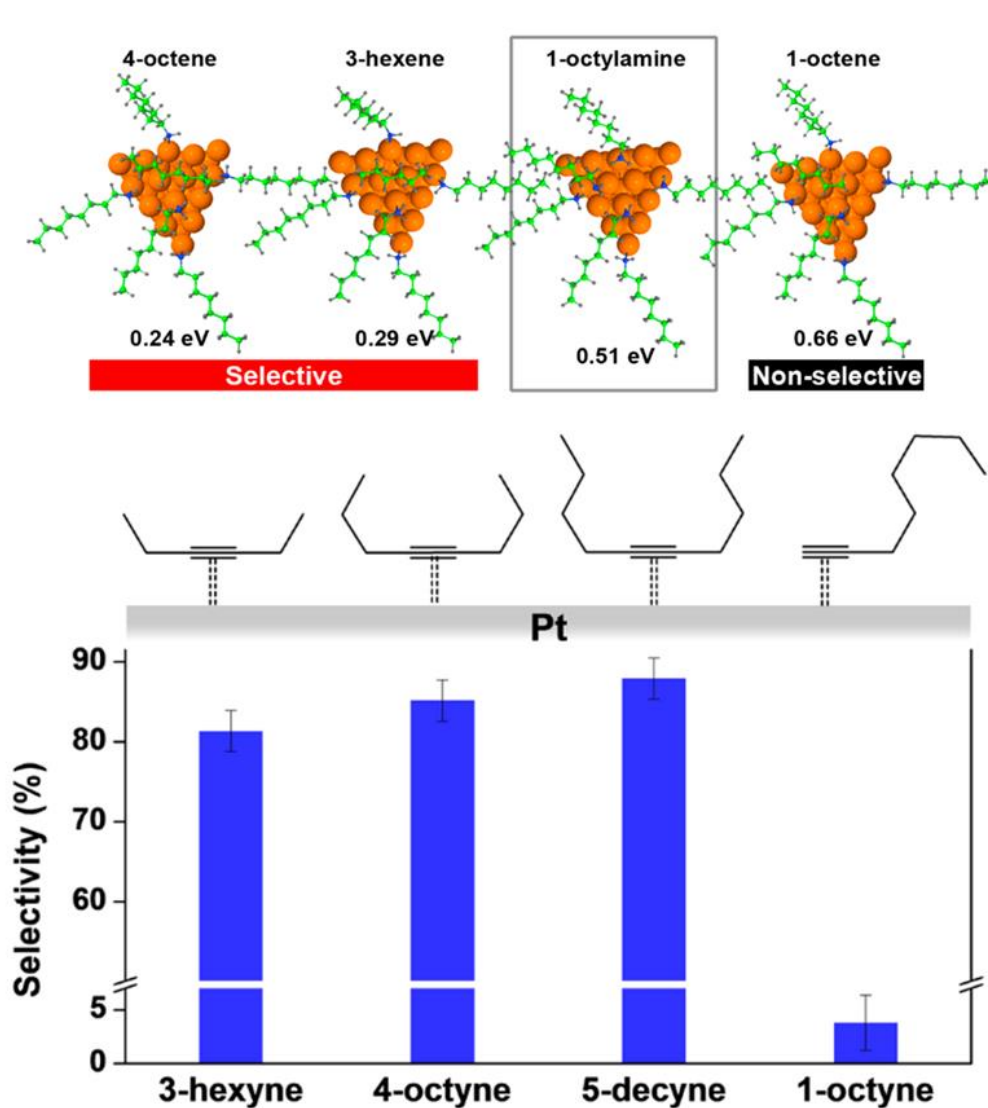


**Figure 1.19.** Calculated adsorption energy of different alkenes and 1-octylamine, and the selectivity to alkene during hydrogenation of corresponding alkynes <sup>[48]</sup>.

Weak adsorption of modifiers on the metal surface during catalysis could endow competitive adsorption with the reactant or intermediate molecules and thus affect the catalytic performance. The modifiers can be added directly to the reaction mixture.

For example, Kwon et al. have reported that the addition of primary alkylamines to Pt and CoPt<sub>3</sub> NPs can drastically increase the selectivity to alkene from 0 to > 90% without

affecting the catalytic activity <sup>[48]</sup>. The equilibrium between the adsorption of the reactant, intermediate molecules, and capping agents determines the selectivity and activity of the catalyst. The hydrogenation of alkyne results in semi-hydrogenation products such as alkene and full hydrogenated product such as alkane. The capping agent and reacting molecules should have comparable adsorption energy. Note that the use of a capping agent with too low adsorption energies in comparison with alkenes has little or no effect on selectivity. However, the capping agents with high adsorption energies significantly reduce the further conversion of alkene to alkane and increase the selectivity to intermediates alkene (*Figure 1.19*).

### **1.3.2. Electronic effects**

The electronic structure and density of active sites in metal catalysts is important for heterogeneous catalysis. The electronic effect is due to the surface metal atoms in the catalysts having different local electronic structures, which interact differently with molecules. Several theories have been developed to define the relationship between the electronic state of metal and its catalytic activity. For example, *d*-band center theory proposed and developed by Norskov et al. has described transition metal catalysis <sup>[24]</sup>. It has been reported that the modification of Pt (111) surface with subsurface 3*d* transition metals will change the *d*-band center of surface Pt. The dissociative adsorption energy of H<sub>2</sub> and O<sub>2</sub> on such Pt (111) surface exhibited a linear trend with the *d*-band center. The more positive is the *d*-band center, the lower is the dissociative adsorption energy of H<sub>2</sub> and O<sub>2</sub>. The description of the electronic effect of non-metallic

modifiers on the metal surface is still a challenge. Although the electronic effect of ligands has been widely applied to optimize homogeneous catalysis by metal complexes, it has been much less recognized in the field of heterogeneous catalysis. The interactions between non-metallic modifiers and metal atoms are more complex. The electronic effect of the modified metal catalysts is usually interpreted in terms of electron donation and electron withdrawal.

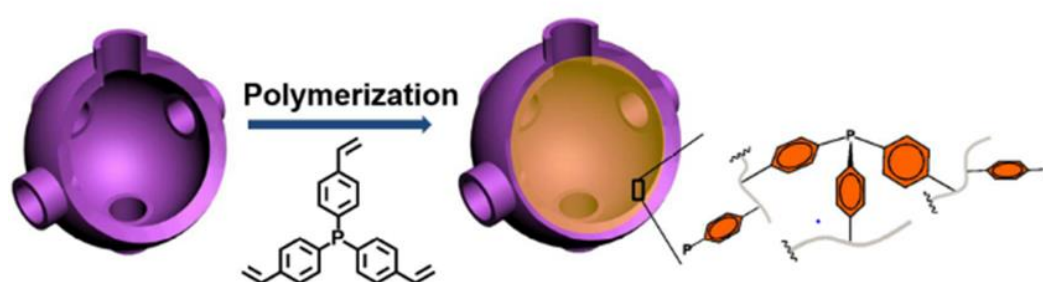


**Figure 1.20.** The preparation of Pd/PPh<sub>3</sub>@FOU-12 catalyst<sup>[75]</sup>.

The universal consequence of electron donation and electron withdrawal effect of modifiers is the modification of the electronic density of the surface metals. For example, the electron donation modifiers such as N- and P-based elements result in negatively charged active sites. Modification with electron withdrawal modifiers like S- and halogen-based species leads to the positively-charged metal surface. The changing of the electronic density of the metal surface will consequently alter the catalytic properties. For example, the negatively charged metal surface will enhance the adsorption of electron-deficient molecules but suppress the reaction with electron-rich counterparts. Guo et al. have investigated the effect of the electronic density of Pd nanoparticle on the hydrogenation reactions<sup>[75]</sup>. As shown in **Figure 1.20**, the authors deposited Pd nanoparticles on a PPh<sub>3</sub> cross-linked in the FDU-12 support. The electron

donating effect of  $\text{PPh}_3$  increased the surface electronic density of Pd NPs as well as the activity in the reactions involving electrophilic substrates.

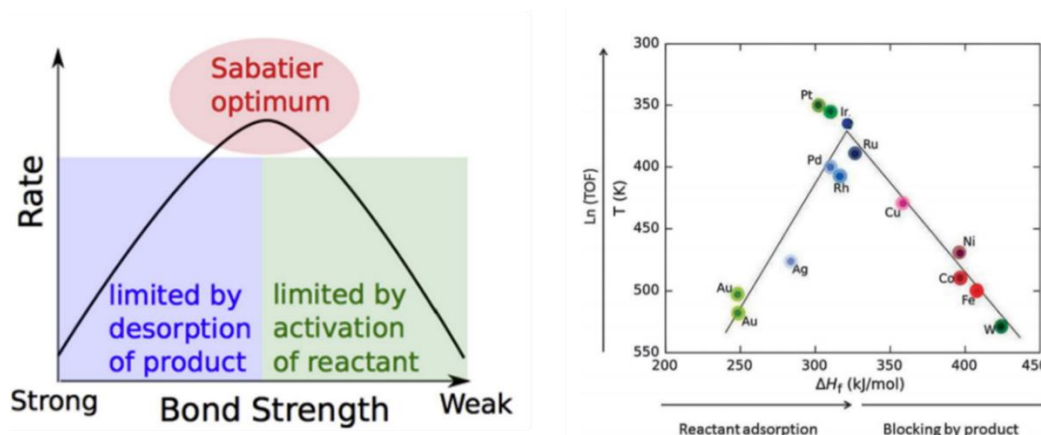


**Figure 1.21.** Volcano-type relationship between metals and its catalytic activity<sup>[24]</sup>.

The electronic structure of the metal surface strongly affects the catalytic properties.

**Figure 1.21** shows a volcano-type curve which relates the intrinsic activity and adsorption energy for different metals. This curve illustrates the Sabatier principle<sup>[24]</sup>.

It states that the interactions between the catalyst and the substrate should be "just right", neither too strong nor too weak. If the interaction is too weak, the substrate will fail to bind to the catalyst and no reaction will take place. On the other hand, if the interaction is too strong, the product fails to desorb. The observed abnormal catalytic results derived from electronic state changes could be often explained as the movement of the modified catalyst on the volcano-type curve.

### 1.3.2.1. Electronic donation

The electronic donation effect normally exists in the elements that have a lone pair of electrons. The usually used modifiers for electronic donation are N-based, P-based, and carbenes. Typical electron-donating modifiers are shown in **Figure 1.22**.

The polymers with good solubility are widely used as capping agents to control the growth of nanoparticles and protect them from aggregation. The polymers on the metal surface act as modifiers during heterogeneous catalysis. For example, PVP has been widely used as a capping agent for the transition metal nanoparticles synthesis. The electronic effects of Au nanoparticles modified by PVP have been studied by Hironori et al [41, 36]. The electronic density of PVP@Au nanoclusters was investigated by CO-FTIR. It is known that the CO molecules adsorb over clusters of Au atoms. Thus, the stretching frequency of adsorbed CO mainly reflects the electron density on the adsorption sites. The shifts of vibration frequency ( $\nu_{\text{CO}}$ ) towards higher and lower wavenumbers relative to that of free CO when CO is adsorbed over positively and negatively charged Au sites, respectively. Larger Au particles are less affected by PVP and the CO adsorption spectra is comparable to that for the bulk gold. However, the CO adsorption peaks over small Au nanoparticles are significantly shifted to lower frequency from those of large ones. The lower-frequency shift of  $\nu_{\text{CO}}$  on small Au nanoparticles have been assigned to CO adsorbed on negatively charged Au sites.

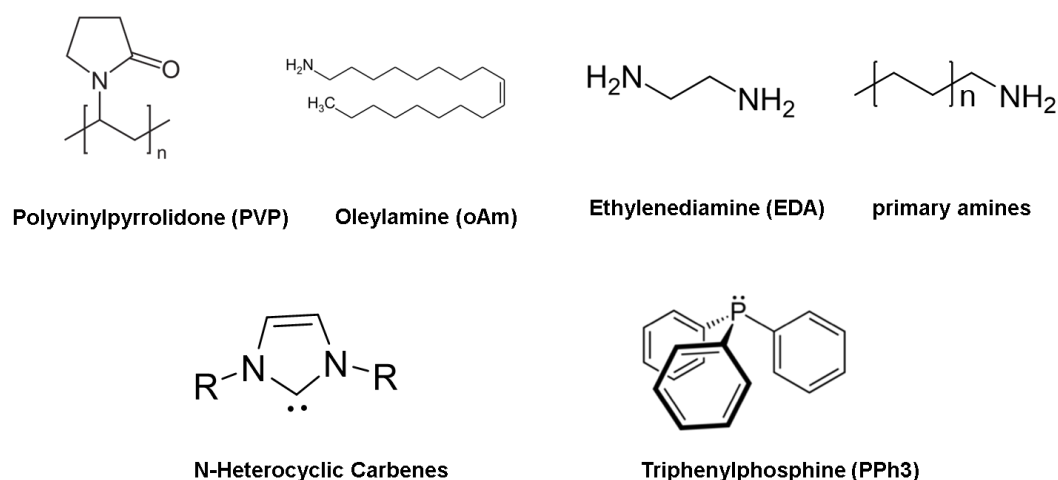


**Figure 1.22.** Represent modifiers with electron donation effects.



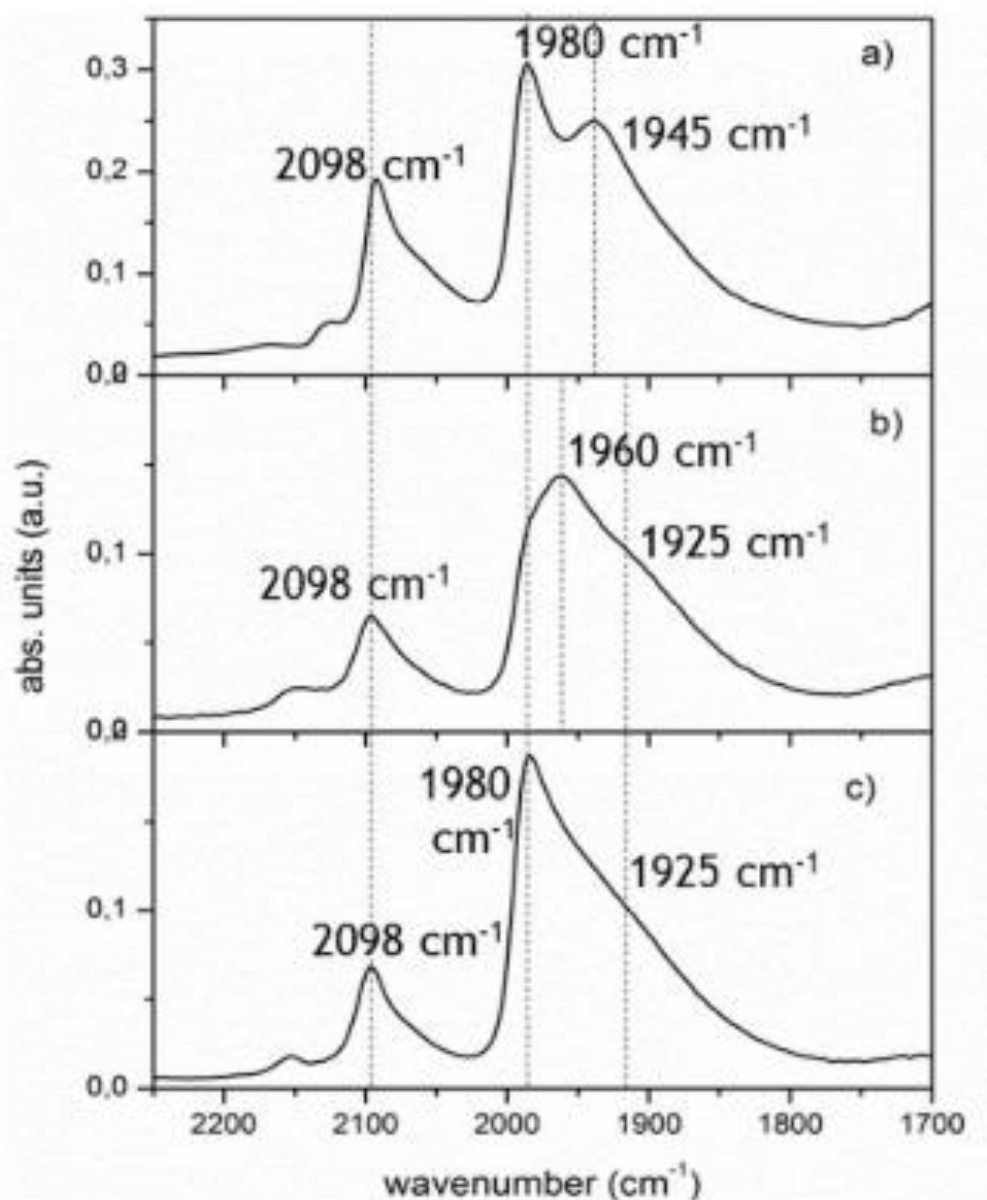


**Figure 1.23.** DRFTIR spectra of adsorbed CO on (a) 5 wt% Pd/Al<sub>2</sub>O<sub>3</sub>, (b) 5 wt% Pd@PVA/Al<sub>2</sub>O<sub>3</sub> and (c) calcined 5 wt% Pd@PVA/Al<sub>2</sub>O<sub>3</sub> [34].

Sebastiano et al. have reported using diffuse reflectance infrared spectroscopy (DRIFTS) the accessibility and electronic effect of metal sites by monitoring the adsorption of CO as a probe molecule. Pd NPs were synthesized with coating by PVA and deposited on Al<sub>2</sub>O<sub>3</sub> supports by sol immobilization [34, 35, 38]. As shown in **Figure 1.23**, adsorbed CO on Pd/Al<sub>2</sub>O<sub>3</sub> exhibits three main signals. The signal at 2098 cm<sup>-1</sup> is due to CO linearly

bound to the Pd particle corners. The signal at  $1980\text{ cm}^{-1}$  is related to  $\mu^2$  bridge-bonded CO on the Pd (100) facets, while that at  $1945\text{ cm}^{-1}$  is attributed to  $\mu^2$  bridge-bonded CO on the Pd (111) planes. After PVA coating, the new peak appears at  $1960\text{ cm}^{-1}$  and  $1925\text{ cm}^{-1}$ , which were ascribed to the perturbation of the  $\mu^2$  bridge-bonded CO on Pd (100) facets and  $\mu^2$  bridge-bonded CO on Pd (111) planes, respectively. This shift is due to the electron donation effect of PVA on the Pd surface. The back-donation from Pd to the  $\pi^*$  antibonding orbitals of CO lowers the vibrational frequency of adsorbed CO.

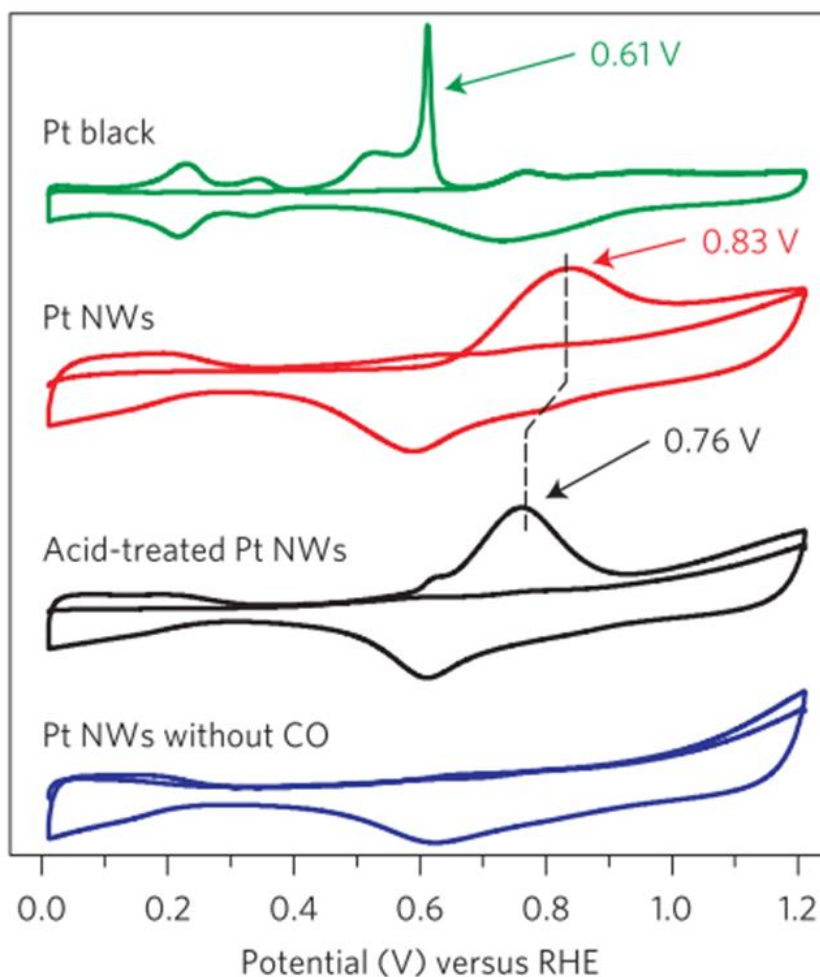


**Figure 1.24.** CO stripping voltammetry of Pt black, EDA-Pt NWs, sulphuric acid (1 M) treated EDA-Pt NWs and EDA-Pt NWs without CO<sup>[47]</sup>.

The electron-rich surface also enhanced CO binding by back-donating more electrons into CO. The CO stripping voltammetry is an effective technique to determine the surface electronic structure of noble metals. Chen et al. characterized the ethylenediamine (EDA) modified Pt nanowires (NWs) by CO stripping voltammetry (*Figure 1.24*). The CO tripping potential on EDA-Pt NWs was measured to be 0.83 V versus reversible hydrogen electrode (RHE), which is 0.22 V higher than that on Pd black (0.61 V versus RHE). EDA-coordinated Pt NWs displayed a higher oxidative stripping potential than that on Pt blacks. These results indicate that after the EDA adsorption, the surface of Pt NWs becomes electron-rich and donated more electrons to CO  $2\pi^*$  orbitals, thus strengthening CO adsorption and weakening C-O bonds.

Recently, N-heterocyclic carbenes (NHCs) have been proposed as a class of electronic donation modifiers for metal nanocatalysts. NHCs are a unique class of ligands, which is widely applied in the fields of coordination chemistry and homogeneous catalysis. Their electron-rich nature leads to strong bonding to metals. In general, they act as strong  $\sigma$ -donor and weak  $\pi$ -acceptor ligands and are capable to influence the reactivity and selectivity of homogeneous transition metal catalysts. For example, Johannes et al. have investigated the influence of the NHC ligands on the activity of the Pd/Al<sub>2</sub>O<sub>3</sub> catalyst <sup>[53]</sup>. They choose the hydrogenolysis of bromobenzene as the benchmark reaction to investigate the activating effect of NHCs. The activation of bromobenzene should be facilitated in the presence of electron-donating ligands similar to homogeneous catalysis. A significant accelerating effect of NHCs was observed with aromatic N-substituents being the most effective ligands (IPr, IMes). NHCs bearing

alkyl N-substituents (ICy, IMe) were less efficient in the promotion of hydrogenolysis but superior to unmodified Pd/Al<sub>2</sub>O<sub>3</sub>.

### 1.3.2.2. Electronic withdrawal

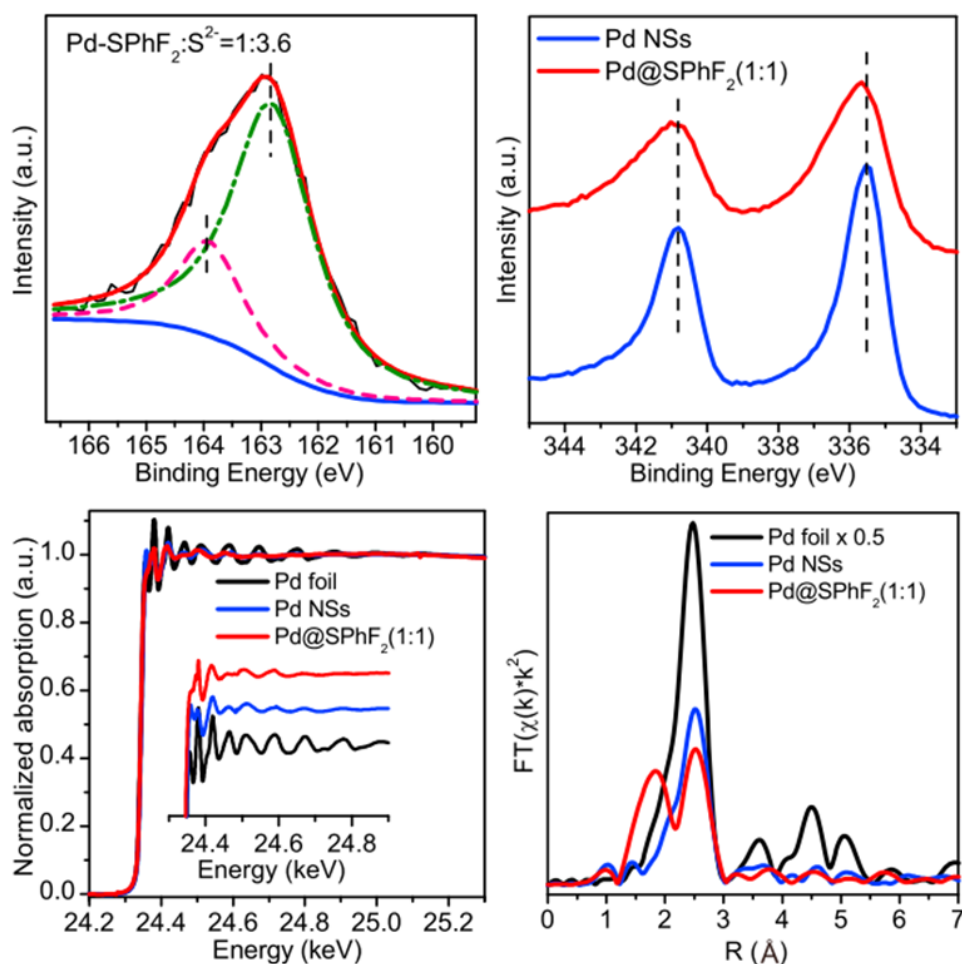


**Figure 1.25.** Structure analysis of the Pd@SPhF<sub>2</sub> (1:1) catalyst<sup>[92]</sup>.

The electronic withdrawal effect relevant to the use of non-metallic modifiers for metal catalysts is less reported. The most reported modifiers for electronic withdrawal are S-based species. For example, Zhao et al. have used the thiol-treated ultrathin Pd nanosheets as a model catalyst for semi hydrogenation of internal alkynes<sup>[92]</sup>. The ultrathin structure of Pd NSs makes it feasible to directly visualize the change in the

surface structure of Pd NSs upon their reaction with thiols via electron microscopy. They revealed that upon adsorption of 3,4-difluorothiols (HSPhF<sub>2</sub>), C-S bonds in thiols can be broken forming a Pd surface modified with both thiolates and sulfides.

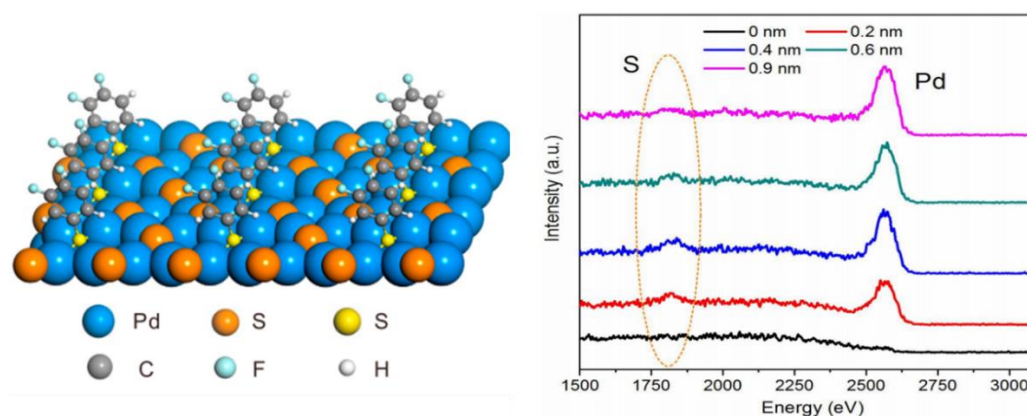


**Figure 1.25.** Illustration of structure and LEISS spectra for Pd@SPhF<sub>2</sub> (1:1) with different detected depths<sup>[92]</sup>.

As shown in **Figure 1.25**, the XPS data confirmed the co-presence of S<sup>2-</sup> and thiolate on the thiol-treated Pd NSs. Two main sulfur components at 162.9 and 163.8 eV were assigned to S<sup>2-</sup> and SR<sup>-</sup>, respectively. The presence of S<sup>2-</sup> proves the S-C bond cleavage in the thiol modification process. Moreover, the binding energy of Pd 3d in distorted Pd NSs displayed a slight shift toward higher binding energy than that of unmodified NSs, indicating that Pd had been partially oxidized. To better understand the local environment of Pd, the Pd@SPhF<sub>2</sub>(1:1) catalyst was further characterized by EXAFS. EXAFS demonstrated that the coordination environment of Pd experienced a dramatic change in thiol treatment. Although the Pd-Pd coordination number was decreased from 9.7 to 4.7, a Pd-S scattering path appeared with the coordination number of 1.7. These results demonstrate the interaction of Pd with S, which yields the Pd<sub>x</sub>S species and withdrawal of electrons from Pd.

It is worth noting that modification with sulfur will lead to the sulfur atoms entering the first coordination shell around the Pd atoms. The 3D distributions of Pd and S elements were characterized by high-sensitivity low-energy ion scattering spectroscopy (*Figure 1.25*). Even with the increased depth of analysis enabled by Ar ion sputtering, the presence of sulfur species was still revealed, indicating the incorporation of  $S^{2-}$  into the inner lattice of Pd.

### 1.3.3. Bifunctionality

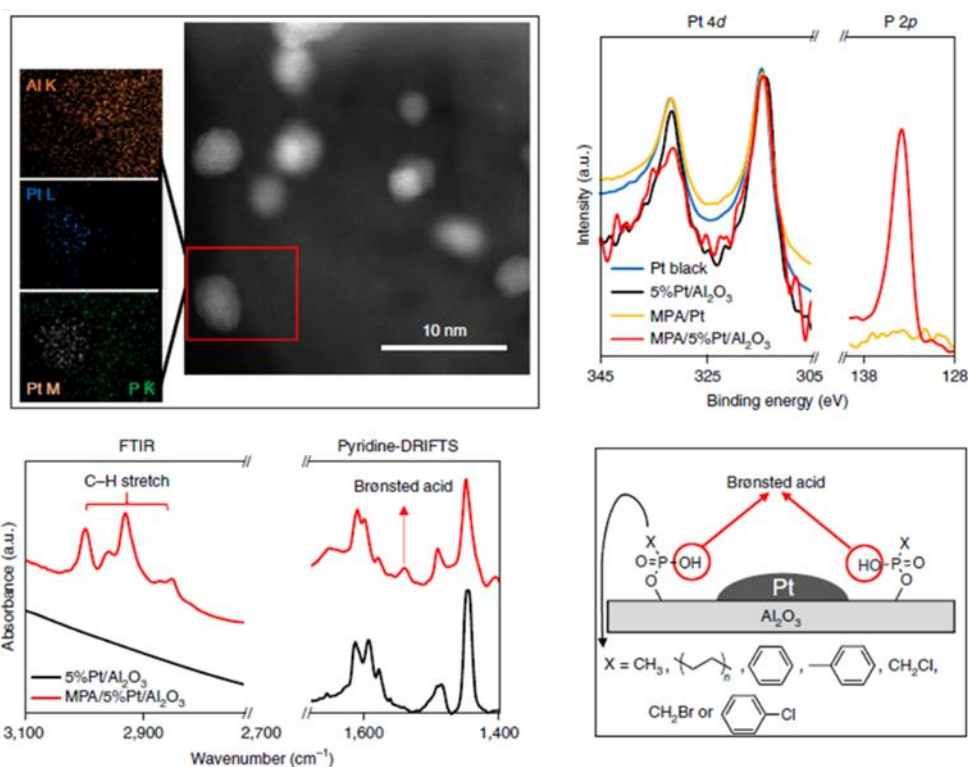


*Figure 1.26. Phosphoric acid modified Pt/Al<sub>2</sub>O<sub>3</sub> catalysts* <sup>[9]</sup>.

Besides modulation of the activity of metal sites, the presence of the non-metallic modifier can also create bifunctional active sites like metal-acid or metal-basic sites. The introduction of bifunctionality on metal catalysts by surface modification is an

alternative way for the design of a single heterogeneous catalyst for multiple step or cascade reactions (e.g. hydrogenation and deoxygenation, acetalization and hydrogenolysis). In comparison with the conventional strategies for cascade reactions (e.g. introducing homogeneous acid, deposition of metal nanoparticle on acidic or basic supports), the modification by non-metallic species provide tunable metal-acid or metal-basic sites. Several papers have reported the construction of a bifunctional interface between metal nanoparticle and supports by surface modifications. For example, Zhang et al. have reported to modify the Pt/Al<sub>2</sub>O<sub>3</sub> catalysts with organic phosphonic acids by grafting phosphonate ligands on the Al<sub>2</sub>O<sub>3</sub> support<sup>[9]</sup>. As shown in **Figure 1.26**, 5 wt% Pt/Al<sub>2</sub>O<sub>3</sub> catalyst modified by methyl phosphonic acid (MPA) was characterized by STEM-EDS, XPS, and FTIR. The deposition of MPA on Al<sub>2</sub>O<sub>3</sub> was demonstrated by STEM-EDS. The EDS peak deconvolution collected from platinum nanoparticles demonstrated that negligible phosphorus was present on the platinum nanoparticles. Deposition of MPA on platinum black showed minimal phosphorus signal (phosphorus 2p) according to XPS analysis, whereas MPA/5%Pt/Al<sub>2</sub>O<sub>3</sub> showed significant phosphorus coverage. Also, the MPA deposition on 5%Pt/Al<sub>2</sub>O<sub>3</sub> does not alter the platinum 4d binding energy, further confirming the absence of MPA on platinum. The FTIR spectra showed the appearance of C-H stretching vibration peaks after the MPA deposition on 5%Pt/Al<sub>2</sub>O<sub>3</sub>. Moreover, phosphonic acid deposition was found to introduce Brønsted acid sites to the catalyst. A characteristic pyridinium ion peak around 1540 cm<sup>-1</sup> was observed in the diffuse reflectance infrared Fourier transform spectra (DRIFTS) after pyridine adsorption. The introduced Brønsted acidity

suggests retention of P-OH groups when phosphonic acids were bound on the Al<sub>2</sub>O<sub>3</sub> support. Overall, the characterization results showed that: (1) phosphonic acid was bounded selectively to Al<sub>2</sub>O<sub>3</sub> rather than platinum, (2) modification with phosphonic acid introduced Brønsted acid sites and (3) phosphonic acid retained their organic functionality and did not restructure Al<sub>2</sub>O<sub>3</sub>.

Construction of basic sites on the surface of metal catalyst was achieved by Liu et al [122, 123]. They reported a Schiff base modified Au catalyst for catalytic decomposition of formic acid to hydrogen. The Au@Schiff-SiO<sub>2</sub> catalyst was prepared by one-pot aldimine condensation (formaldehyde and 3-aminopropyl-triethoxysilane) and in situ reduction of gold precursor. The illustration of the preparation and structure of the Au@Schiff-SiO<sub>2</sub> catalyst is shown in [Figure 1.27](#).

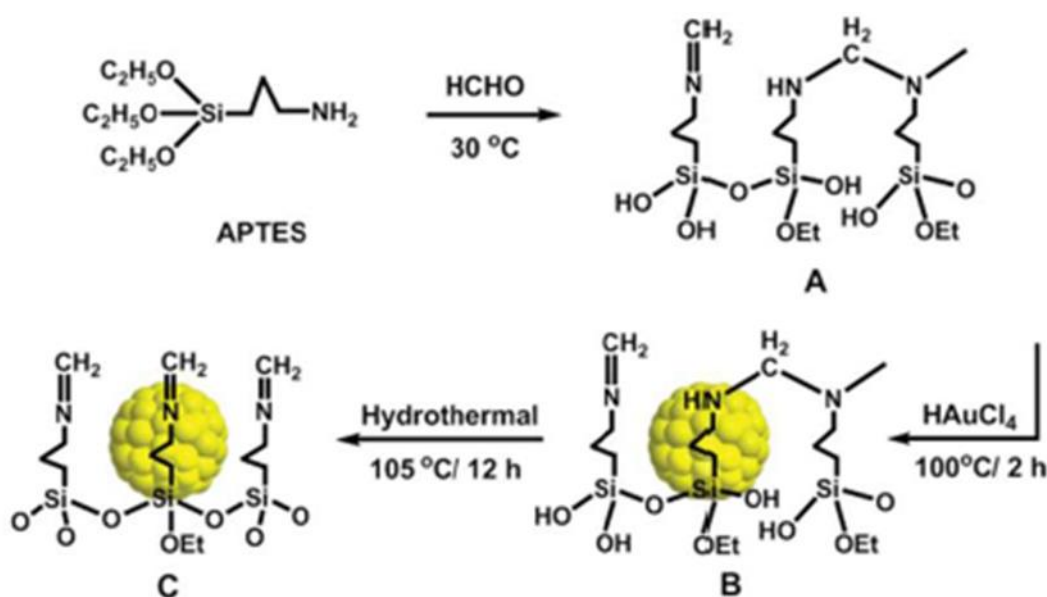


[Figure 1.27](#). Schiff base modified Au catalysts [122].

#### 1.4. Catalytic hydrogenation over modified metal catalysts



Hydrogenation is the most studied model reaction over the modified metal catalysts. The presence of non-metallic modifiers could significantly change the catalytic behaviors of substrates on the metal surface. The non-metallic modifiers may have two effects on the catalytic reactions, the first one is relevant to the activity and the second one to the selectivity. While in most cases, the presence of non-metallic modifiers will decrease the activity due to active site blocking, some studies revealed that the presence of modifiers could increase the TOF numbers for conversion of some specific substrates. Most studies have reported the change of the selectivity after modification. In this part, the most studied and industrially potential hydrogenation reactions that have been performed with non-metallic modifiers are summarized and discussed. We will discuss how the steric and electronic effects influence the catalytic performance of specific reactions and introduce the molecular-level interaction between substrates and catalysts. Our target is to propose a general concept about enhancing and tuning the reaction behaviors by surface modification.

The evaluation of a modified catalyst in several reactions is necessary to understand the changes of steric, electronic, and functionalities. For example, hydrogenation of cinnamaldehyde is usually used as a model reaction for checking the steric orientation of modifiers on the metal surface. The partial hydrogenation of alkyne to an alkene is well studied over modified metal catalysts. Other reactions such as hydrogenation of nitrobenzene to aniline or N-benzylhydroxylamine, hydrogenolysis of halogen substituted arenes, and hydrogen peroxide production will be discussed in the following sections.

### 1.4.1. Partial hydrogenation of alkynes to alkenes

Partial hydrogenation of alkynes to alkenes is the most widely studied model reaction over modified metal catalysts <sup>[124]</sup>. Hydrogenation of alkynes over metals suffers from over-hydrogenation to alkanes <sup>[46, 80, 125, 126]</sup>. Numerous works indicate that this process requires a major modification of the metal surface, which makes this reaction suitable for studies of the modifier effects. Another reason is the industrial significance of this reaction towards the manufacturing of polymers, pharmaceuticals, vitamins, and fragrances. The modification by non-metallic species aims to endow high activity for alkynes hydrogenation to alkenes but prevents further hydrogenation of alkenes to alkanes. To realize this purpose, various modifiers including N-, P-, and S-based have been developed. It is worth noting that N- and P-modifiers are normally electronic donors, whereas S-based compounds are electronic withdrawal modifiers.

In the partial hydrogenation of alkynes, the selectivity can be controlled by thermodynamics or kinetics (reaction mechanism) (*Figure 1.28*) <sup>[127]</sup>. The kinetic control takes place when the hydrogenation of the adsorbed alkyne is favored in comparison with the adsorbed alkene ( $k_2 \gg k_4$ ). In contrast, thermodynamic selectivity implies the ability of a metal to preferentially adsorb the alkyne in the presence of the alkene ( $k_1/k_{-1} \gg k_3/k_{-3}$ ), thus suppressing the consecutive hydrogen addition which results in the production of alkane. For most of the metals studied in the literature, however, the alkene hydrogenation rate is faster than that of alkyne hydrogenation and

consequently, the selectivity pattern is usually attributed to the stronger adsorption of the alkyne compared with that of the alkene (thermodynamic selectivity).

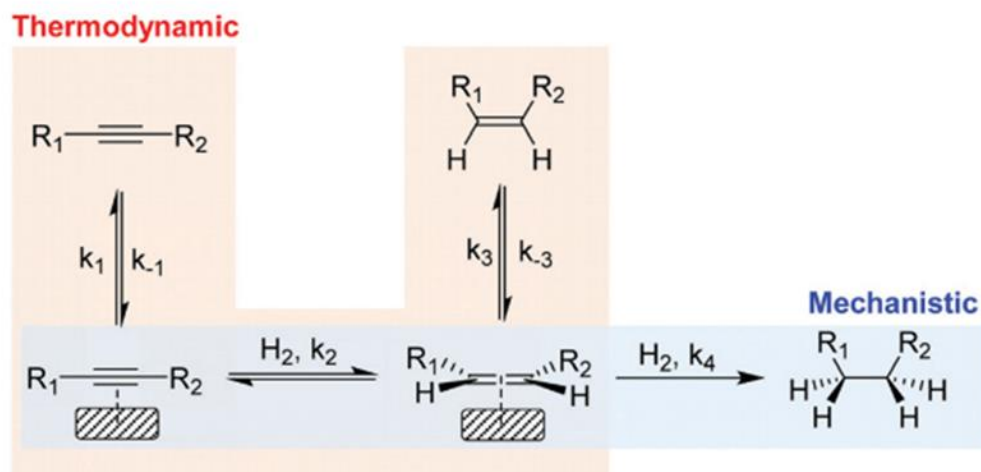


**Figure 1.28.** Illustration of the mechanistic and thermodynamic selectivity of alkynes partial hydrogenation <sup>[127]</sup>.

It is generally accepted that the presence of hydrides, either on or below the metal surface, favors the over-hydrogenation and thus the formation of alkanes. For example, as shown in **Figure 1.29**, the Pd NanoSelect catalyst developed by BASF is prepared by a chemical reduction method employing HHDMA as a reducing agent, stabilizer, and modifier consequently <sup>[46]</sup>. This catalyst consists of palladium nanoparticles of 5 ~ 8 nm supported on carbon or titanium silicate that exhibit alkene selectivity comparable to those provided by the Lindlar's catalyst in the semi-hydrogenation of alkynes. Pérez-Ramírez et al. have studied the promotion effect of HHDMA on the NanoSelect Pd catalyst by experimental and theoretical methods <sup>[26]</sup>. According to DFT calculations, HHDMA is adsorbed rigidly over the Pd surface and restricts the accessibility of the substrate to the active sites of the catalyst (forming cavities with elliptical shape), providing exceptional performance for the hydrogenation of terminal alkynes but low

activity for disubstituted and bulky alkynes (*Figure 1.29*). Meanwhile, the presence of rigidly adsorbed HDDMA reduced the hydride coverage at the Pd surface via electronic effects.

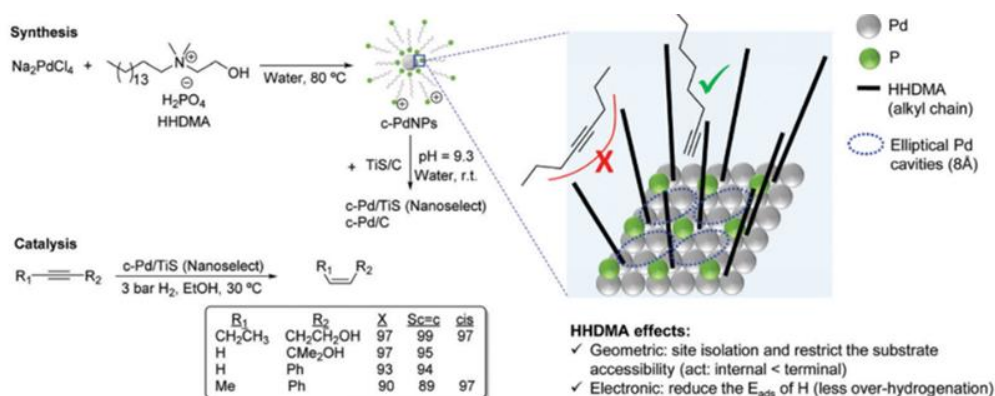


*Figure 1.29. Illustration of the preparation of Pd catalyst capped with HDDMA [26].*

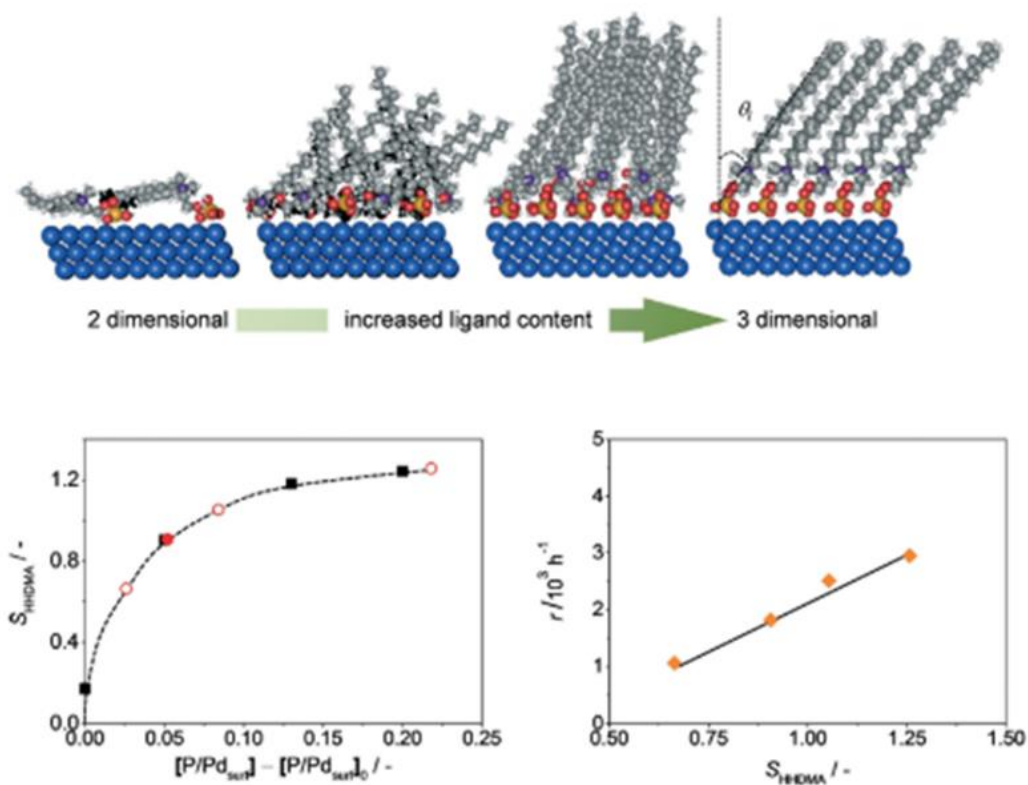


*Figure 1.30. Schematic representation of the catalyst's structures with variable ligand concentration [26].*

DFT calculations indicated that the ligand changes the adsorption configuration. At low coverage, the organic layer lies almost flatly on the surface of the PdNPs blocking a

large number of metal sites. A high HHDMA coverage favors an extended three-dimensional configuration of the alkyl chains and exposes more available Pd sites (As indicated in *Figure 1.30*).

#### 1.4.2. Selective hydrogenation of unsaturated aldehydes to unsaturated alcohols

The selective hydrogenation of unsaturated aldehydes (UAL) to saturated aldehydes (SAL) and unsaturated alcohols (UOL) is an important industrial process for producing fine chemicals (*Figure 1.31*). A lot of efforts have been made on the selective hydrogenation of C=O to UOL, because the C=C hydrogenation is thermodynamically favored over the C=O hydrogenation <sup>[128]</sup>. A crucial step toward high selectivity is the rational design of heterogeneous catalysts. Therefore, this reaction is a good model reaction for the fundamental study of the steric and electronic effects.

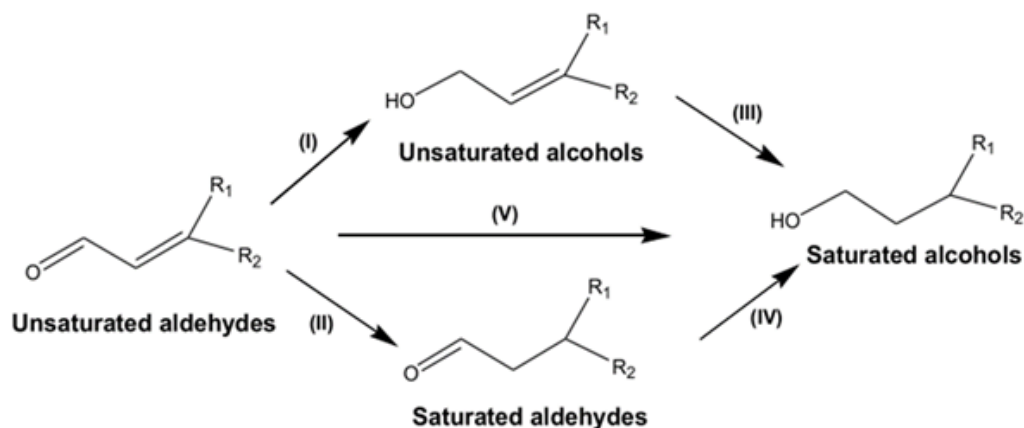


*Figure 1.31.* Reaction pathway for hydrogenation of UAL <sup>[128]</sup>.

Zhong et al. have prepared the polyvinylpyrrolidone (PVP)-stabilized Au nanoparticles immobilized on the SiO<sub>2</sub> support <sup>[41]</sup>. Prepared Au-PVP/SiO<sub>2</sub> was subjected to ultraviolet-ozone (UVO) treatment to remove the residues PVP. The hydrogenation of

CAL could occur at either C=C or C=O bond to hydrocinnamaldehyde (HCAL) or cinnamyl alcohol (COL), respectively. Hydrogenation of both C=C and C=O bonds leads to hydrocinnamyl alcohol (HCOL). Residual PVP significantly decreased the activity for CAL hydrogenation. The selectivity changes to the hydrogenation of C=C bond were observed after the removal of the residues (*Figure 1.32*).

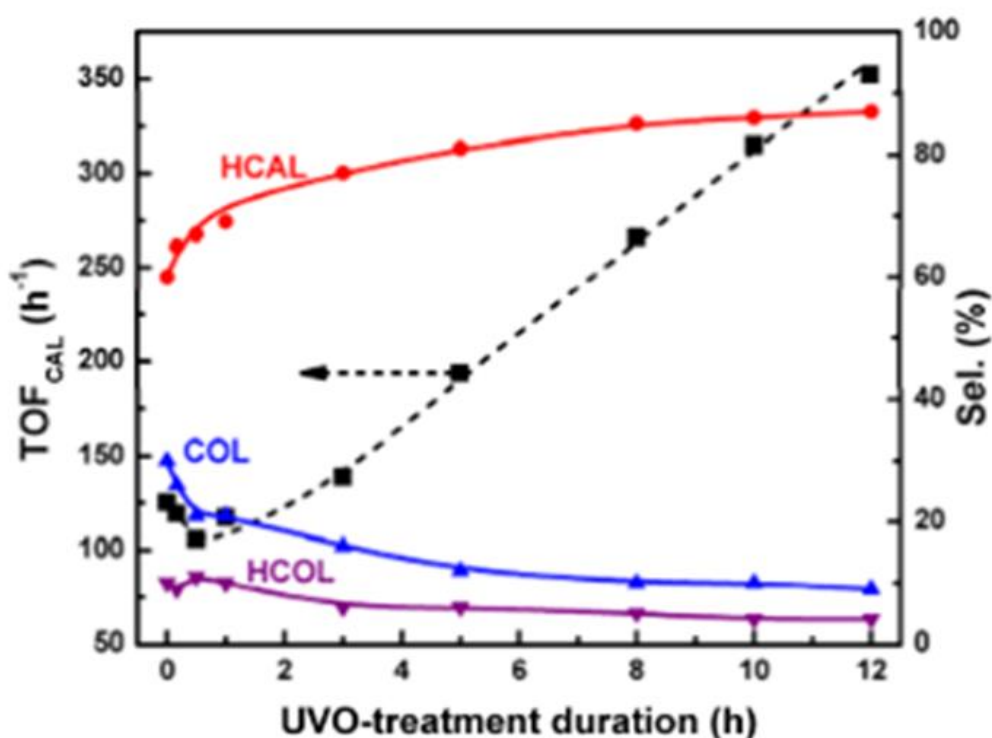


*Figure 1.32.* Effects of UVO-treatment duration on the Au-PVP/SiO<sub>2</sub> catalytic performance for CAL hydrogenation<sup>[41]</sup>.

In another case, air-stable AuNPs modified by strong donor ligands such as secondary phosphine oxides (SPO) have been prepared by Israel et al<sup>[69]</sup>. As shown in *Figure 1.33*, high conversion and selectivity to  $\alpha$ ,  $\beta$ -unsaturated alcohols were obtained. The ligand-metal cooperative effect between Au and SPO plays a crucial role in this reaction. An H/D exchange experiment was performed over the catalyst by exposure of a benzene solution to an equimolar mixture of H<sub>2</sub> and D<sub>2</sub> (ca. 1 bar) with the generation of HD.

Considering that Au has a very limited capacity for hydrogen dissociation, the surprising preference for hydrogen activation could be ascribed to the cooperative effect between Au and SPO ligands. Therefore, the mechanism which suggests that the ligand promotes a heterolytic hydrogenation was proposed to explain the abnormal catalytic behavior.

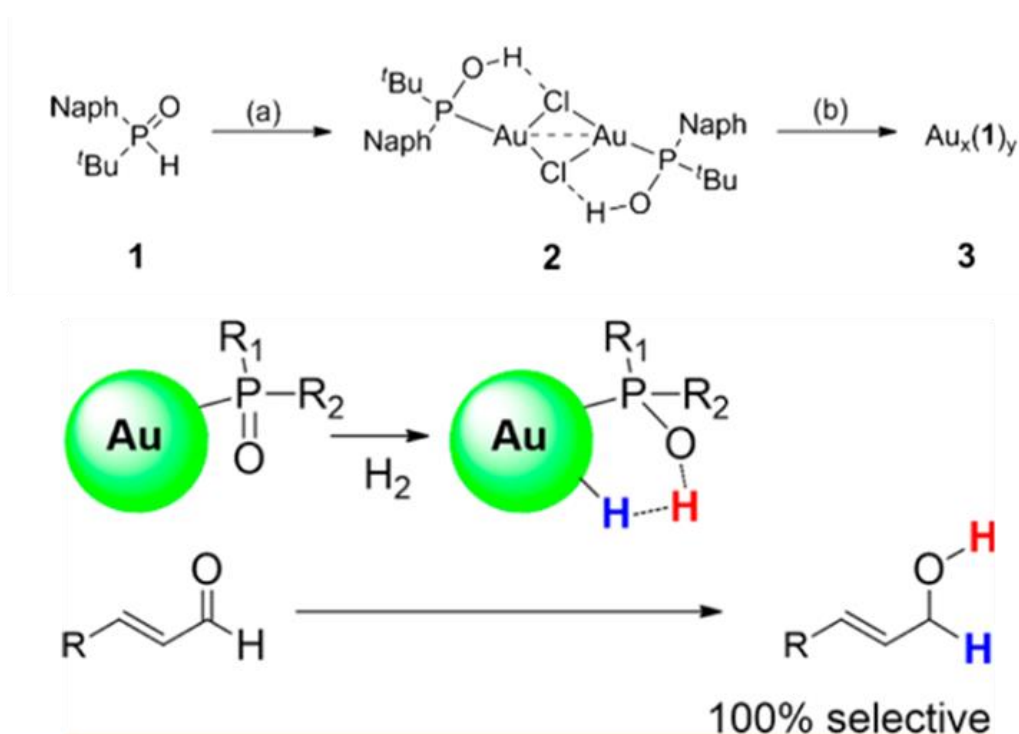


**Figure 1.33.** Mechanism of SPO modified Au nanoparticle for hydrogenation of UAL [69].

### 1.4.3. Hydrogenation of nitroarenes to N-hydroxylanilines

Hydrogenation of nitroaromatics to N-hydroxylanilines is an industrially important reaction. Chen et al. have reported the preparation of uniform ultrathin (~1.1 nm in diameter) Pt nanowires with ethylenediamine (EDA) chelated on their surfaces (denoted as EDA-Pt NWs). The promoted Pt nanowires were used as model catalysts for the hydrogenation of nitroaromatics [47]. Due to the electron donation from EDA to

Pt NWs, the surface of Pt NWs become electron-rich. This interfacial electronic effect makes the Pt NWs favorable for the adsorption of electron-deficient reactants but disfavors the adsorption of electron-rich substances (N-hydroxylanilines). The reaction mechanism has been supported by DFT calculation. The adsorption free energies ( $\Delta G_{\text{ads}}$ ) of nitrobenzene, nitrosobenzene, and N-hydroxylaniline on bare Pt NWs are  $-1.27$ ,  $-1.48$  and  $-0.89$  eV, respectively. It indicates that all of these N-containing aromatics are readily adsorbed on the pristine Pt catalysts and undergo hydrogenation. This explains the poor selectivity for N-hydroxylaniline over Pt black.

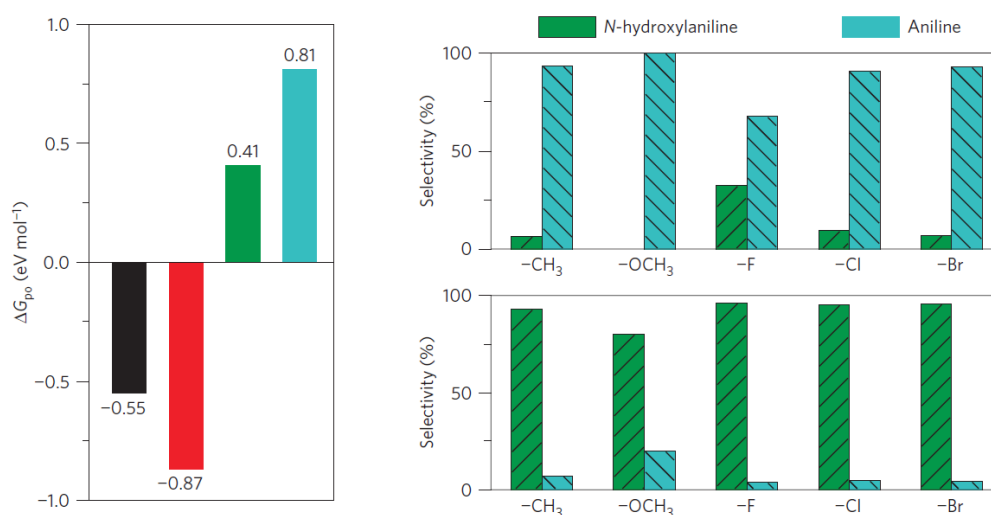


**Figure 1.34.** Mechanism of catalytic selectivity of EDA-Pt NWs<sup>[47]</sup>.

As shown in **Figure 1.34**,  $\Delta G_{\text{p0}}$  for nitrobenzene and nitrosobenzene were calculated to be  $-0.55$  and  $-0.87$  eV, respectively, whereas  $\Delta G_{\text{p0}}$  for N-hydroxylaniline was  $0.41$  eV. These changes in free energy can be explained in terms of the change in the spatial distribution of the electronic density. In the presence of EDA,  $d$  orbitals of Pt are nearly fully occupied. This favors the adsorption of electron-deficient substrates through  $d-\pi^*$  donation but disfavors electron-rich substrates because of the negatively charged Pt



surface. Moreover, Pt black was treated with  $[\text{Pt}(\text{EDA})_2](\text{acac})_2$  to allow the deposition of Pt-EDA chelating units on its surface. A series of nitroaromatics with various substitutions (1-fluoro-4-nitrobenzene, 1-chloro-4-nitrobenzene, 1-bromo-4-nitrobenzene, 1-methyl-4-nitrobenzene and 1-methoxy-4-nitrobenzene) have been examined for hydrogenation over the modified Pt black. A significant enhancement of the selectivity towards the N-hydroxylaniline derivatives was observed.

#### 1.4.4. Hydrogen peroxide production

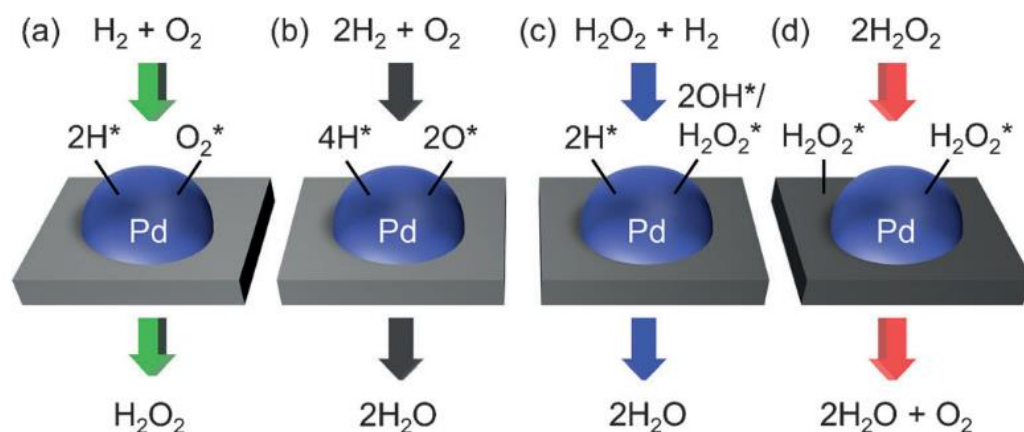


**Figure 1.35.** Reactants, products, and relevant adsorbed intermediates in the  $\text{H}_2\text{O}_2$  production on Pd catalysts <sup>[129]</sup>.

Hydrogen peroxide ( $\text{H}_2\text{O}_2$ ) attracts growing attention as a green stoichiometric oxidant in a wide range of applications.  $\text{H}_2\text{O}_2$  is commercially synthesized by the sequential hydrogenation and oxidation of anthraquinones in a mixture of organic solvents. This process suffers from high energy input, a significant generation of waste, and complex liquid-liquid separations. The direct synthesis of  $\text{H}_2\text{O}_2$  from molecular hydrogen ( $\text{H}_2$ ) and oxygen ( $\text{O}_2$ ) at (sub)ambient temperatures is an attractive approach due to the (1)

absence of organic substrates; (2) use of green solvents such as water or methanol; and (3) simplified purification. Pd is widely used to catalyze this process. Achieving selectivity >50% is a challenge using unmodified Pd-based catalysts, because of the promotion of the O-O bond activation that leads to undesired H<sub>2</sub>O production (*Figure 1.35*)<sup>[129]</sup>.

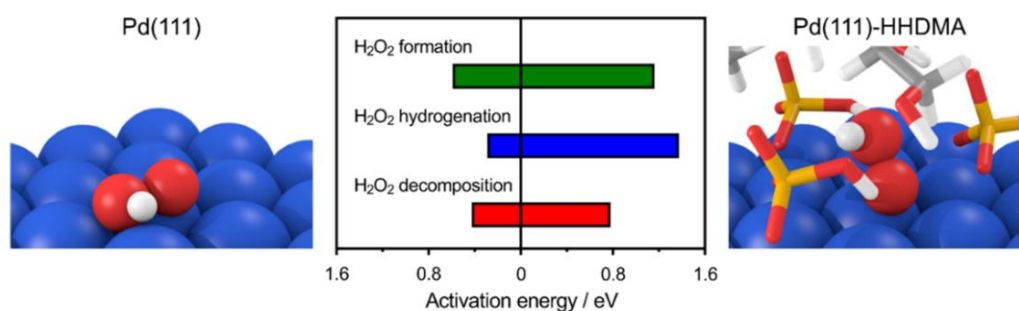


*Figure 1.36.* Activation energies for the direct synthesis of H<sub>2</sub>O<sub>2</sub> and the side reactions leading to water formation by H<sub>2</sub>O<sub>2</sub> hydrogenation and decomposition<sup>[129]</sup>.

Lari et al. have disclosed that the ligand-modified palladium nanoparticles deposited on a carbon carrier efficiently catalyze the direct synthesis of H<sub>2</sub>O<sub>2</sub><sup>[129]</sup>. Catalytic testing demonstrated that the selectivity increases with the HHDMA ligand content from 10% for naked nanoparticles up to 80%. As rationalized by DFT calculations, this behavior arises from the adsorption of O<sub>2</sub> and hydroperoxyl radicals. These intermediates are flattened on the Pd (111) surface (*Figures 1.36*), thus favoring the cleavage of the O-O bond. In contrast, on Pd (111)-HHDMA, the electrostatic interaction of the adsorbed intermediates with the H<sub>2</sub>PO<sub>4</sub><sup>-</sup> group and quaternary ammonium headgroups of the HHDMA molecule enables the peculiar vertical configuration of the intermediate, impeding the cleavage of the O-O bond and its over-hydrogenation. Such a ligand-imposed geometry resembles the active site of metalloenzymes.

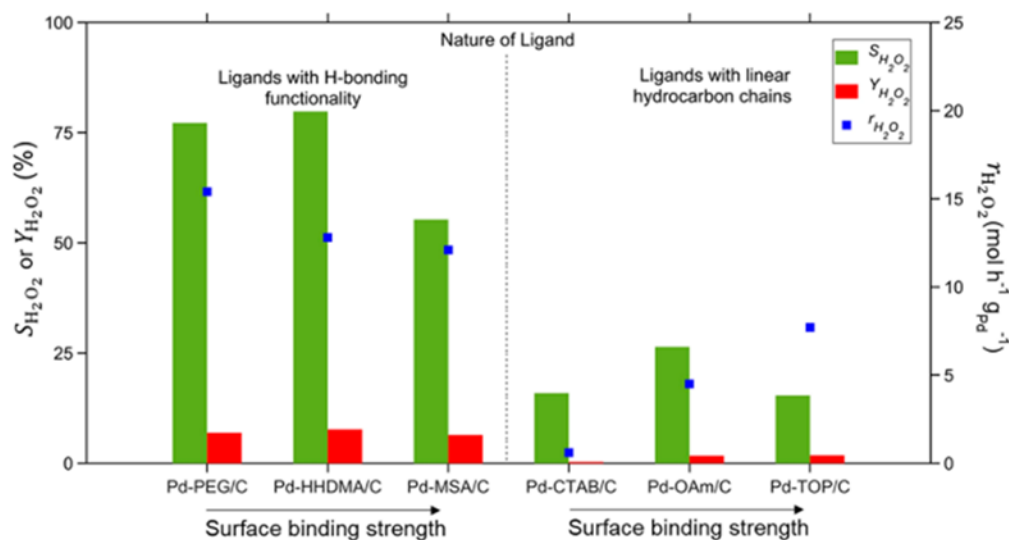


**Figure 1.37.** Catalytic performance of  $H_2O_2$  production of Pd NPs with various ligands supported on activated carbon<sup>[98]</sup>.

While the steric effect derived from the surface modifiers plays an important role in the  $H_2O_2$  selectivity, Lucas et al. have confirmed that ligands with H-bonding groups result in significant enhancement of the selectivity to  $H_2O_2$ <sup>[98]</sup>. They screened a wide range of surface-bound ligands with varying functionalities such as polyethylene glycol (PEG), hexadecyltrimethylammonium bromide (CTAB), mercaptosuccinic acid (MSA), oleylamine (OAm), trioctylphosphine (TOP). The highest selectivity had been related to the ligands with the OH functionality in their structure (**Figure 1.37**), which promotes hydrogenation of the OOH intermediate to  $H_2O_2$ . In the case of the ligands without OH functionality, the authors observed an increase in the rate of the  $H_2O_2$  production that scaled with the bulkiness of the ligands (TOP > OAm > CTAB). This suggests a possible effect induced by steric hindrance arising from the ligands. Deep characterization suggested a positive relationship between the rate of  $PdH_x$  formation and  $H_2O_2$  selectivity.

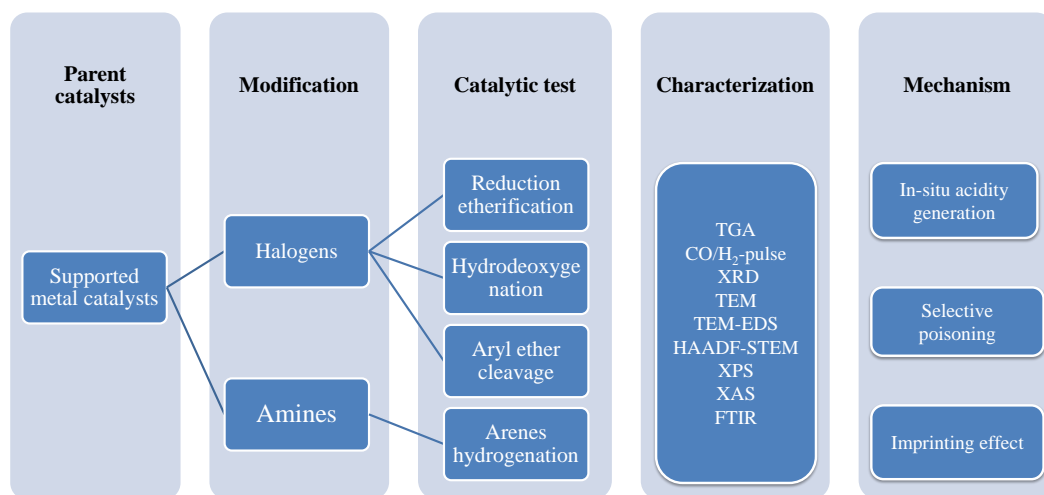
## 1.5. Goals and strategies of the thesis

The post-modification of the metal catalysts with suitable modifiers could significantly change the catalytic performance of the metal catalysts. The post-modification strategy does not require often sophisticated synthesis of new catalysts and can be easily adapted for the available commercial catalysts. The goal of this thesis is to develop and understand highly selective metal catalyst prepared by post-modification with non-metallic modifiers.

Based on the analysis of the literature, we realized that strong coordination between metal nanoparticles and modifiers could be formed by using heteroatoms such as S, N, P, and halogens. Polymers usually induce strong steric hindrances during catalysis, causing low activity of the catalysts. Modification of the metal catalyst by small molecules containing heteroatoms could be interesting for the tunable selectivity and high activity. Considering that S has already been studied extensively and the indiscriminate poisoning of S atoms leads to a decrease in the activity of metal nanoparticles, the role of halogens and amines on the modification of metal catalysts is still not clear.

Our strategy is illustrated in *Schema 1.6*. First of all, industrial and commercialized supported metal catalysts were selected as parent catalysts. Several methods have been used for the modification with promoters (such as halogens and amines). The catalytic performance has been tested using biomass-derived molecules and compared with the parent catalysts. Consequently, the modified catalyst was subjected to various

characterization methods to identify the steric, electronic and bifunctional effect introduced by modifiers. Finally, a reaction mechanism has been proposed to explain the structure-performance relationships.



**Schema 1.6.** Experiment route for the thesis.

## 1.6. Thesis structure

First of all (Chapter 3), the modification of supported Pd catalyst by iodine has been studied in hydrogenation reactions for fine chemical synthesis. We found that the modification of Pd catalysts by iodine atoms leads to the formation of Pd-I bifunctional sites on the Pd surface. The Pd-I sites could promote the reductive etherification of carbonyl compounds with alcohols. Characterizations disclose the electronic interaction and bifunctionality of the Pd-I catalyst. The developed Pd-I catalyst exhibited promising applications in the production of bio-solvent from biomass-derived carbonyl compounds.

In Chapter 4, the halogen modification of Pd catalysts has been extended to Pd-Br systems. Due to the higher electronegativity of Br, the Pd-Br catalyst demonstrated strong Brønsted acidity during hydrogenation reactions with the deoxygenation of

active hydroxyl groups. The prepared Pd-Br catalyst was tested for hydrodeoxygenation reactions of biomass-derived HMF to dimethylfuran, which shows high selectivity and activity at ambient temperature. The direct generation of bifunctionality on the metal surface leads to maximum catalytic efficiency.

In Chapter 5, the modification of metal catalysts by halogens was further investigated over Ru-Br system. The introduction of Br on the Ru nanoparticle surface can selectively deactivate the terrace sites, which is responsible for aromatic rings hydrogenation, while the defect sites (edges and corners) are not affected. The Ru-Br catalyst was found to be efficient for the production of single-ring aromatic molecules (benzene and phenol) from diphenyl ether, which is a lignin-derived model compound.

In Chapter 6, we proposed a molecular imprinting strategy for selective poisoning of Pd surface by the preparation of active islands. The imprinted Pd catalyst was prepared by adsorption of aromatic template molecules with subsequent selectively poisoning using amines. The pre-adsorption of templates protects the active sites with pre-determined size and shape during the poisoning process. Catalytic tests showed that after imprinting, the Pd catalysts exhibited reactivity for the molecules displaying similar size and shape to template molecules. The imprinted Pd catalyst was further applied for the selective removal of carcinogenic benzene from mixed aromatics.

The last chapter gives a general conclusion of the thesis. We emphasize the new knowledge which has been generated for the last 3 years in the field of surface chemistry and mechanism of catalytic reactions. Finally, we provide perspectives and future research which could be conducted in this field.

## Reference

1. Yang, F.; Deng, D.; Pan, X.; Fu, Q.; Bao, X., Understanding nano effects in catalysis. *Natl. Sci. Rev.* **2015**, *2* (2), 183-201.
2. Coperet, C.; Comas-Vives, A.; Conley, M. P.; Estes, D. P.; Fedorov, A.; Mougel, V.; Nage, H.; Nunez-Zarur, F.; Zhizhko, P. A., Surface Organometallic and Coordination Chemistry toward Single-Site Heterogeneous Catalysts: Strategies, Methods, Structures, and Activities. *Chem. Rev.* **2016**, *116* (2), 323-421.
3. Astruc, D.; Lu, F.; Aranzaes, J. R., Nanoparticles as recyclable catalysts: the frontier between homogeneous and heterogeneous catalysis. *Angew. Chem. Int. Ed.* **2005**, *44* (48), 7852-7872.
4. Samantaray, M. K.; D'Elia, V.; Pump, E.; Falivene, L.; Harb, M.; Ould Chikh, S.; Cavallo, L.; Basset, J. M., The Comparison between Single Atom Catalysis and Surface Organometallic Catalysis. *Chem. Rev.* **2020**, *120* (2), 734-813.
5. Gilroy, K. D.; Ruditskiy, A.; Peng, H. C.; Qin, D.; Xia, Y., Bimetallic Nanocrystals: Syntheses, Properties, and Applications. *Chem. Rev.* **2016**, *116* (18), 10414-10472.
6. Xu, C.; Paone, E.; Rodriguez-Padron, D.; Luque, R.; Mauriello, F., Recent catalytic routes for the preparation and the upgrading of biomass derived furfural and 5-hydroxymethylfurfural. *Chem. Soc. Rev.* **2020**, *49* (13), 4273-4306.
7. Chen, S.; Wojcieszak, R.; Dumeignil, F.; Marceau, E.; Royer, S., How Catalysts and Experimental Conditions Determine the Selective Hydroconversion of Furfural and 5-Hydroxymethylfurfural. *Chem. Rev.* **2018**, *118* (22), 11023-11117.
8. Liu, Y.; Zhao, G.; Wang, D.; Li, Y., Heterogeneous catalysis for green chemistry based on nanocrystals. *Natl. Sci. Rev.* **2015**, *2* (2), 150-166.
9. Zhang, J.; Ellis, L. D.; Wang, B.; Dzara, M. J.; Sievers, C.; Pylypenko, S.; Nikolla, E.; Medlin, J. W., Control of interfacial acid-metal catalysis with organic monolayers. *Nat. Catal.* **2018**, *1* (2), 148-155.
10. Guo, M.; Peng, J.; Yang, Q.; Li, C., Highly Active and Selective RuPd Bimetallic NPs for the Cleavage of the Diphenyl Ether C–O Bond. *ACS Catal.* **2018**, *8* (12), 11174-11183.
11. Sergeev, A. G.; Hartwig, J. F., Selective, nickel-catalyzed hydrogenolysis of aryl ethers. *Science* **2011**, *332* (6028), 439-443.
12. Sergeev, A. G.; Webb, J. D.; Hartwig, J. F., A heterogeneous nickel catalyst for the hydrogenolysis of aryl ethers without arene hydrogenation. *J. Am. Chem. Soc.* **2012**, *134* (50), 20226-20229.

13. Luo, Z.; Zheng, Z.; Wang, Y.; Sun, G.; Jiang, H.; Zhao, C., Hydrothermally stable Ru/HZSM-5-catalyzed selective hydrogenolysis of lignin-derived substituted phenols to bio-arenes in water. *Green Chem.* **2016**, *18* (21), 5845-5858.
14. Xu, G.-Y.; Guo, J.-H.; Qu, Y.-C.; Zhang, Y.; Fu, Y.; Guo, Q.-X., Selective hydrodeoxygenation of lignin-derived phenols to alkyl cyclohexanols over a Ru-solid base bifunctional catalyst. *Green Chem.* **2016**, *18* (20), 5510-5517.
15. Wu, H.; Song, J.; Xie, C.; Wu, C.; Chen, C.; Han, B., Efficient and Mild Transfer Hydrogenolytic Cleavage of Aromatic Ether Bonds in Lignin-Derived Compounds over Ru/C. *ACS Sustain. Chem. Eng.* **2018**, *6* (3), 2872-2877.
16. Li, H.; Song, G., Ru-Catalyzed Hydrogenolysis of Lignin: Base-Dependent Tunability of Monomeric Phenols and Mechanistic Study. *ACS Catal.* **2019**, *9* (5), 4054-4064.
17. Zhou, Y. N.; Li, J. J.; Wu, Y. Y.; Luo, Z. H., Role of External Field in Polymerization: Mechanism and Kinetics. *Chem. Rev.* **2020**, *120* (5), 2950-3048.
18. Thomas, B.; Raj, M. C.; B, A. K.; H, R. M.; Joy, J.; Moores, A.; Drisko, G. L.; Sanchez, C., Nanocellulose, a Versatile Green Platform: From Biosources to Materials and Their Applications. *Chem. Rev.* **2018**, *118* (24), 11575-11625.
19. Gerardy, R.; Debecker, D. P.; Estager, J.; Luis, P.; Monbaliu, J. M., Continuous Flow Upgrading of Selected C<sub>2</sub>-C<sub>6</sub> Platform Chemicals Derived from Biomass. *Chem. Rev.* **2020**, *120* (15), 7219-7347.
20. Zaera, F., Regio-, stereo-, and enantioselectivity in hydrocarbon conversion on metal surfaces. *Acc. Chem. Res.* **2009**, *42* (8), 1152-1160.
21. Wu, B.; Zheng, N., Surface and interface control of noble metal nanocrystals for catalytic and electrocatalytic applications. *Nano Today* **2013**, *8* (2), 168-197.
22. Liu, P.; Qin, R.; Fu, G.; Zheng, N., Surface Coordination Chemistry of Metal Nanomaterials. *J. Am. Chem. Soc.* **2017**, *139* (6), 2122-2131.
23. Kano, S.; Tada, T.; Majima, Y., Nanoparticle characterization based on STM and STS. *Chem. Soc. Rev.* **2015**, *44* (4), 970-987.
24. Norskov, J. K.; Bligaard, T.; Hvolbaek, B.; Abild-Pedersen, F.; Chorkendorff, I.; Christensen, C. H., The nature of the active site in heterogeneous metal catalysis. *Chem. Soc. Rev.* **2008**, *37* (10), 2163-2171.
25. Wu, W.; Shevchenko, E. V., The surface science of nanoparticles for catalysis: electronic and steric effects of organic ligands. *J. Nanopart. Res.* **2018**, *20* (9), 225.
26. Rossi, L. M.; Fiorio, J. L.; Garcia, M. A. S.; Ferraz, C. P., The role and fate of capping ligands in colloiddally prepared metal nanoparticle catalysts. *Dalton Trans.* **2018**, *47* (17), 5889-5915.



27. Niu, Z.; Li, Y., Removal and Utilization of Capping Agents in Nanocatalysis. *Chem. Mater.* **2013**, *26* (1), 72-83.
28. Shifrina, Z. B.; Matveeva, V. G.; Bronstein, L. M., Role of Polymer Structures in Catalysis by Transition Metal and Metal Oxide Nanoparticle Composites. *Chem. Rev.* **2020**, *120* (2), 1350-1396.
29. Nguyen, L.; Tao, F. F.; Tang, Y.; Dou, J.; Bao, X. J., Understanding Catalyst Surfaces during Catalysis through Near Ambient Pressure X-ray Photoelectron Spectroscopy. *Chem. Rev.* **2019**, *119* (12), 6822-6905.
30. Gavia, D. J.; Shon, Y. S., Catalytic Properties of Unsupported Palladium Nanoparticle Surfaces Capped with Small Organic Ligands. *ChemCatChem* **2015**, *7* (6), 892-900.
31. Jin, L.; Liu, B.; Duay, S.; He, J., Engineering Surface Ligands of Noble Metal Nanocatalysts in Tuning the Product Selectivity. *Catalysts* **2017**, *7* (12), 44.
32. Campisi, S.; Schiavoni, M.; Chan-Thaw, C.; Villa, A., Untangling the Role of the Capping Agent in Nanocatalysis: Recent Advances and Perspectives. *Catalysts* **2016**, *6* (12), 185.
33. Dai, Y.; Liu, S.; Zheng, N., C<sub>2</sub>H<sub>2</sub> treatment as a facile method to boost the catalysis of Pd nanoparticulate catalysts. *J. Am. Chem. Soc.* **2014**, *136* (15), 5583-5586.
34. Chen, K.; Wu, H.; Hua, Q.; Chang, S.; Huang, W., Enhancing catalytic selectivity of supported metal nanoparticles with capping ligands. *Phys. Chem. Chem. Phys.* **2013**, *15* (7), 2273-2277.
35. Campisi, S.; Ferri, D.; Villa, A.; Wang, W.; Wang, D.; Kröcher, O.; Prati, L., Selectivity Control in Palladium-Catalyzed Alcohol Oxidation through Selective Blocking of Active Sites. *J. Phys. Chem. C* **2016**, *120* (26), 14027-14033.
36. Tsunoyama, H.; Ichikuni, N.; Sakurai, H.; Tsukuda, T., Effect of electronic structures of Au clusters stabilized by poly(N-vinyl-2-pyrrolidone) on aerobic oxidation catalysis. *J. Am. Chem. Soc.* **2009**, *131* (20), 7086-7093.
37. Villa, A.; Wang, D.; Veith, G. M.; Vindigni, F.; Prati, L., Sol immobilization technique: a delicate balance between activity, selectivity and stability of gold catalysts. *Catal. Sci. Technol.* **2013**, *3* (11), 3036-3041.
38. Jones, S.; Qu, J.; Tedsree, K.; Gong, X. Q.; Tsang, S. C., Prominent electronic and geometric modifications of palladium nanoparticles by polymer stabilizers for hydrogen production under ambient conditions. *Angew. Chem. Int. Ed.* **2012**, *51* (45), 11275-11278.
39. Yang, Y.; Liu, H.; Li, S.; Chen, C.; Wu, T.; Mei, Q.; Wang, Y.; Chen, B.; Liu, H.; Han, B., Hydrogenolysis of 5-Hydroxymethylfurfural to 2,5-Dimethylfuran under Mild Conditions without Any Additive. *ACS Sustain. Chem. Eng.* **2019**, *7* (6), 5711-5716.

40. Koch, M.; Hecht, S.; Grill, L., On-Surface Polymerization: From Polyarylenes to Graphene Nanoribbons and Two-Dimensional Networks. In *From Polyphenylenes to Nanographenes and Graphene Nanoribbons*, **2017**; pp 99-125.
41. Zhong, R.-Y.; Sun, K.-Q.; Hong, Y.-C.; Xu, B.-Q., Impacts of Organic Stabilizers on Catalysis of Au Nanoparticles from Colloidal Preparation. *ACS Catal.* **2014**, *4* (11), 3982-3993.
42. Zhang, F.; Fang, J.; Huang, L.; Sun, W.; Lin, Z.; Shi, Z.; Kang, X.; Chen, S., Alkyne-Functionalized Ruthenium Nanoparticles: Impact of Metal–Ligand Interfacial Bonding Interactions on the Selective Hydrogenation of Styrene. *ACS Catal.* **2018**, *9* (1), 98-104.
43. Niu, F.; Xie, S.; Bahri, M.; Ersen, O.; Yan, Z.; Kusema, B. T.; Pera-Titus, M.; Khodakov, A. Y.; Ordonsky, V. V., Catalyst Deactivation for Enhancement of Selectivity in Alcohols Amination to Primary Amines. *ACS Catal.* **2019**, *9* (7), 5986-5997.
44. Schrader, I.; Neumann, S.; Šulce, A.; Schmidt, F.; Azov, V.; Kunz, S., Asymmetric Heterogeneous Catalysis: Transfer of Molecular Principles to Nanoparticles by Ligand Functionalization. *ACS Catal.* **2017**, *7* (6), 3979-3987.
45. Stolaś, A.; Darmadi, I.; Nugroho, F. A. A.; Moth-Poulsen, K.; Langhammer, C., Impact of Surfactants and Stabilizers on Palladium Nanoparticle–Hydrogen Interaction Kinetics: Implications for Hydrogen Sensors. *ACS Appl. Nano Mater.* **2020**, *3* (3), 2647-2653.
46. Witte, P. T.; Berben, P. H.; Boland, S.; Boymans, E. H.; Vogt, D.; Geus, J. W.; Donkervoort, J. G., BASF NanoSelect™ Technology: Innovative Supported Pd- and Pt-based Catalysts for Selective Hydrogenation Reactions. *Top. Catal.* **2012**, *55* (7-10), 505-511.
47. Chen, G.; Xu, C.; Huang, X.; Ye, J.; Gu, L.; Li, G.; Tang, Z.; Wu, B.; Yang, H.; Zhao, Z.; Zhou, Z.; Fu, G.; Zheng, N., Interfacial electronic effects control the reaction selectivity of platinum catalysts. *Nat. Mater.* **2016**, *15* (5), 564-569.
48. Kwon, S. G.; Krylova, G.; Sumer, A.; Schwartz, M. M.; Bunel, E. E.; Marshall, C. L.; Chattopadhyay, S.; Lee, B.; Jellinek, J.; Shevchenko, E. V., Capping ligands as selectivity switchers in hydrogenation reactions. *Nano. Lett.* **2012**, *12* (10), 5382-5388.
49. Duran Pachon, L.; Yosef, I.; Markus, T. Z.; Naaman, R.; Avnir, D.; Rothenberg, G., Chiral imprinting of palladium with cinchona alkaloids. *Nat. Chem.* **2009**, *1* (2), 160-164.
50. Nohair, B.; Especel, C.; Lafaye, G.; Marécot, P.; Hoang, L. C.; Barbier, J., Palladium supported catalysts for the selective hydrogenation of sunflower oil. *J. Mol. Catal. A Chem.* **2005**, *229* (1-2), 117-126.

51. Cure, J.; Coppel, Y.; Dammak, T.; Fazzini, P. F.; Mlayah, A.; Chaudret, B.; Fau, P., Monitoring the coordination of amine ligands on silver nanoparticles using NMR and SERS. *Langmuir* **2015**, *31* (4), 1362-1367.
52. Šulce, A.; Flaherty, D. W.; Kunz, S., Kinetic analysis of the asymmetric hydrogenation of  $\beta$ -keto esters over  $\alpha$ -amino acid-functionalized Pt nanoparticles. *J. Catal.* **2019**, *374*, 82-92.
53. Ernst, J. B.; Schwermann, C.; Yokota, G. I.; Tada, M.; Muratsugu, S.; Doltsinis, N. L.; Glorius, F., Molecular Adsorbates Switch on Heterogeneous Catalysis: Induction of Reactivity by N-Heterocyclic Carbenes. *J. Am. Chem. Soc.* **2017**, *139* (27), 9144-9147.
54. Fiorio, J. L.; Barbosa, E. C. M.; Kikuchi, D. K.; Camargo, P. H. C.; Rudolph, M.; Hashmi, A. S. K.; Rossi, L. M., Piperazine-promoted gold-catalyzed hydrogenation: the influence of capping ligands. *Catal. Sci. Technol.* **2020**, *10* (7), 1996-2003.
55. Albani, D.; Vilé, G.; Mitchell, S.; Witte, P. T.; Almora-Barrios, N.; Verel, R.; López, N.; Pérez-Ramírez, J., Ligand ordering determines the catalytic response of hybrid palladium nanoparticles in hydrogenation. *Catal. Sci. Technol.* **2016**, *6* (6), 1621-1631.
56. Šulce, A.; Backenköhler, J.; Schrader, I.; Piane, M. D.; Müller, C.; Wark, A.; Ciacchi, L. C.; Azov, V.; Kunz, S., Ligand-functionalized Pt nanoparticles as asymmetric heterogeneous catalysts: molecular reaction control by ligand–reactant interactions. *Catal. Sci. Technol.* **2018**, *8* (23), 6062-6075.
57. Witte, P. T.; Boland, S.; Kirby, F.; van Maanen, R.; Bleeker, B. F.; de Winter, D. A. M.; Post, J. A.; Geus, J. W.; Berben, P. H., NanoSelect Pd Catalysts: What Causes the High Selectivity of These Supported Colloidal Catalysts in Alkyne Semi-Hydrogenation? *ChemCatChem* **2013**, *5* (2), 582-587.
58. Abate, S.; Freni, M.; Arrigo, R.; Schuster, M. E.; Perathoner, S.; Centi, G., On the Nature of Selective Palladium-Based Nanoparticles on Nitrogen-Doped Carbon Nanotubes for the Direct Synthesis of  $H_2O_2$ . *ChemCatChem* **2013**, *5* (7), 1899-1905.
59. Šulce, A.; Mitschke, N.; Azov, V.; Kunz, S., Molecular Insights into the Ligand–Reactant Interactions of Pt Nanoparticles Functionalized with  $\alpha$ -Amino Acids as Asymmetric Catalysts for  $\beta$ -Keto Esters. *ChemCatChem* **2019**, *11* (11), 2732-2742.
60. Wu, D.; Hernández, W. Y.; Zhang, S.; Vovk, E. I.; Zhou, X.; Yang, Y.; Khodakov, A. Y.; Ordonsky, V. V., In Situ Generation of Brønsted Acidity in the Pd-I Bifunctional Catalysts for Selective Reductive Etherification of Carbonyl Compounds under Mild Conditions. *ACS Catal.* **2019**, *9* (4), 2940-2948.
61. Vile, G.; Almora-Barrios, N.; Mitchell, S.; Lopez, N.; Perez-Ramirez, J., From the Lindlar catalyst to supported ligand-modified palladium nanoparticles: selectivity patterns and accessibility constraints in the continuous-flow three-phase hydrogenation of acetylenic compounds. *Chemistry* **2014**, *20* (20), 5926-5937.

62. Abate, S.; Arrigo, R.; Schuster, M. E.; Perathoner, S.; Centi, G.; Villa, A.; Su, D.; Schlögl, R., Pd nanoparticles supported on N-doped nanocarbon for the direct synthesis of H<sub>2</sub>O<sub>2</sub> from H<sub>2</sub> and O<sub>2</sub>. *Catal. Today* **2010**, *157* (1-4), 280-285.
63. Wu, B.; Huang, H.; Yang, J.; Zheng, N.; Fu, G., Selective hydrogenation of alpha,beta-unsaturated aldehydes catalyzed by amine-capped platinum-cobalt nanocrystals. *Angew. Chem. Int. Ed.* **2012**, *51* (14), 3440-3443.
64. Shen, H.; Deng, G.; Kaappa, S.; Tan, T.; Han, Y. Z.; Malola, S.; Lin, S. C.; Teo, B. K.; Hakkinen, H.; Zheng, N., Highly Robust but Surface-Active: An N-Heterocyclic Carbene-Stabilized Au<sub>25</sub> Nanocluster. *Angew. Chem. Int. Ed.* **2019**, *58* (49), 17731-17735.
65. da Silva, F. P.; Fiorio, J. L.; Rossi, L. M., Tuning the Catalytic Activity and Selectivity of Pd Nanoparticles Using Ligand-Modified Supports and Surfaces. *ACS Omega* **2017**, *2* (9), 6014-6022.
66. Chu, C.; Huang, D.; Zhu, Q.; Stavitski, E.; Spies, J. A.; Pan, Z.; Mao, J.; Xin, H. L.; Schmuttenmaer, C. A.; Hu, S.; Kim, J.-H., Electronic Tuning of Metal Nanoparticles for Highly Efficient Photocatalytic Hydrogen Peroxide Production. *ACS Catal.* **2018**, *9* (1), 626-631.
67. Liu, Y.; McCue, A. J.; Miao, C.; Feng, J.; Li, D.; Anderson, J. A., Palladium phosphide nanoparticles as highly selective catalysts for the selective hydrogenation of acetylene. *J. Catal.* **2018**, *364*, 406-414.
68. Fedorov, A.; Liu, H. J.; Lo, H. K.; Coperet, C., Silica-Supported Cu Nanoparticle Catalysts for Alkyne Semihydrogenation: Effect of Ligands on Rates and Selectivity. *J. Am. Chem. Soc.* **2016**, *138* (50), 16502-16507.
69. Cano, I.; Chapman, A. M.; Urakawa, A.; van Leeuwen, P. W., Air-stable gold nanoparticles ligated by secondary phosphine oxides for the chemoselective hydrogenation of aldehydes: crucial role of the ligand. *J. Am. Chem. Soc.* **2014**, *136* (6), 2520-2528.
70. Rafter, E.; Gutmann, T.; Löw, F.; Buntkowsky, G.; Philippot, K.; Chaudret, B.; van Leeuwen, P. W. N. M., Secondary phosphineoxides as pre-ligands for nanoparticle stabilization. *Catal. Sci. Technol.* **2013**, *3* (3), 595-599.
71. McCue, A. J.; McKenna, F.-M.; Anderson, J. A., Triphenylphosphine: a ligand for heterogeneous catalysis too? Selectivity enhancement in acetylene hydrogenation over modified Pd/TiO<sub>2</sub> catalyst. *Catal. Sci. Technol.* **2015**, *5* (4), 2449-2459.
72. Snelders, D. J. M.; Yan, N.; Gan, W.; Laurency, G.; Dyson, P. J., Tuning the Chemoselectivity of Rh Nanoparticle Catalysts by Site-Selective Poisoning with Phosphine Ligands: The Hydrogenation of Functionalized Aromatic Compounds. *ACS Catal.* **2012**, *2* (2), 201-207.

73. Ortuño, M. A.; López, N., Creating Cavities at Palladium–Phosphine Interfaces for Enhanced Selectivity in Heterogeneous Biomass Conversion. *ACS Catal.* **2018**, *8* (7), 6138-6145.
74. Chatterjee, A.; Jensen, V. R., A Heterogeneous Catalyst for the Transformation of Fatty Acids to  $\alpha$ -Olefins. *ACS Catal.* **2017**, *7* (4), 2543-2547.
75. Guo, M.; Li, H.; Ren, Y.; Ren, X.; Yang, Q.; Li, C., Improving Catalytic Hydrogenation Performance of Pd Nanoparticles by Electronic Modulation Using Phosphine Ligands. *ACS Catal.* **2018**, *8* (7), 6476-6485.
76. Love, J. C.; Wolfe, D. B.; Haasch, R.; Chabynyc, M. L.; Paul, K. E.; Whitesides, G. M.; Nuzzo, R. G., Formation and structure of self-assembled monolayers of alkanethiolates on palladium. *J. Am. Chem. Soc.* **2003**, *125* (9), 2597-2609.
77. Centrone, A.; Penzo, E.; Sharma, M.; Myerson, J. W.; Jackson, A. M.; Marzari, N.; Stellacci, F., The role of nanostructure in the wetting behavior of mixed-monolayer-protected metal nanoparticles. *Proc. Natl. Acad. Sci. USA* **2008**, *105* (29), 9886-9891.
78. Rogers, S. M.; Dimitratos, N.; Jones, W.; Bowker, M.; Kanaras, A. G.; Wells, P. P.; Catlow, C. R.; Parker, S. F., The adsorbed state of a thiol on palladium nanoparticles. *Phys. Chem. Chem. Phys.* **2016**, *18* (26), 17265-17271.
79. Marshall, S. T.; O'Brien, M.; Oetter, B.; Corpuz, A.; Richards, R. M.; Schwartz, D. K.; Medlin, J. W., Controlled selectivity for palladium catalysts using self-assembled monolayers. *Nat. Mater.* **2010**, *9* (10), 853-858.
80. Albani, D.; Shahrokhi, M.; Chen, Z.; Mitchell, S.; Hauert, R.; Lopez, N.; Perez-Ramirez, J., Selective ensembles in supported palladium sulfide nanoparticles for alkyne semi-hydrogenation. *Nat. Commun.* **2018**, *9* (1), 2634.
81. Pang, S. H.; Schoenbaum, C. A.; Schwartz, D. K.; Medlin, J. W., Directing reaction pathways by catalyst active-site selection using self-assembled monolayers. *Nat. Commun.* **2013**, *4*, 2448.
82. Huang, L.; Subramanian, R.; Wang, J.; Kwon Oh, J.; Ye, Z., Ligand screening for palladium nanocatalysts towards selective hydrogenation of alkynes. *Mol. Catal.* **2020**, *488*, 110923
83. Weng, Z.; Zaera, F., Increase in Activity and Selectivity in Catalysis via Surface Modification with Self-Assembled Monolayers. *J. Phys. Chem. C* **2014**, *118* (7), 3672-3679.
84. Altmann, L.; Kunz, S.; Bäumer, M., Influence of Organic Amino and Thiol Ligands on the Geometric and Electronic Surface Properties of Colloidally Prepared Platinum Nanoparticles. *J. Phys. Chem. C* **2014**, *118* (17), 8925-8932.
85. Haider, P.; Urakawa, A.; Schmidt, E.; Baiker, A., Selective blocking of active sites on supported gold catalysts by adsorbed thiols and its effect on the catalytic behavior:

- A combined experimental and theoretical study. *J. Mol. Catal. A Chem.* **2009**, *305* (1-2), 161-169.
86. Schoenbaum, C. A.; Schwartz, D. K.; Medlin, J. W., Controlling surface crowding on a Pd catalyst with thiolate self-assembled monolayers. *J. Catal.* **2013**, *303*, 92-99.
87. McKenna, F.-M.; Anderson, J. A., Selectivity enhancement in acetylene hydrogenation over diphenyl sulphide-modified Pd/TiO<sub>2</sub> catalysts. *J. Catal.* **2011**, *281* (2), 231-240.
88. McCue, A. J.; Guerrero-Ruiz, A.; Ramirez-Barria, C.; Rodríguez-Ramos, I.; Anderson, J. A., Selective hydrogenation of mixed alkyne/alkene streams at elevated pressure over a palladium sulfide catalyst. *J. Catal.* **2017**, *355*, 40-52.
89. Kahsar, K. R.; Schwartz, D. K.; Medlin, J. W., Control of metal catalyst selectivity through specific noncovalent molecular interactions. *J. Am. Chem. Soc.* **2014**, *136* (1), 520-526.
90. McKenna, F. M.; Mantarosie, L.; Wells, R. P. K.; Hardacre, C.; Anderson, J. A., Selective hydrogenation of acetylene in ethylene rich feed streams at high pressure over ligand modified Pd/TiO<sub>2</sub>. *Catal. Sci. Technol.* **2012**, *2* (3), 632-638.
91. Zhang, Q.; Su, C.; Cen, J.; Feng, F.; Ma, L.; Lu, C.; Li, X., The Modification of Diphenyl Sulfide to Pd/C Catalyst and Its Application in Selective Hydrogenation of p-Chloronitrobenzene. *Chin. J. Chem. Eng.* **2014**, *22* (10), 1111-1116.
92. Zhao, X.; Zhou, L.; Zhang, W.; Hu, C.; Dai, L.; Ren, L.; Wu, B.; Fu, G.; Zheng, N., Thiol Treatment Creates Selective Palladium Catalysts for Semihydrogenation of Internal Alkynes. *Chem* **2018**, *4* (5), 1080-1091.
93. McKenna, F. M.; Wells, R. P.; Anderson, J. A., Enhanced selectivity in acetylene hydrogenation by ligand modified Pd/TiO<sub>2</sub> catalysts. *Chem. Commun.* **2011**, *47* (8), 2351-2353.
94. Kahsar, K. R.; Schwartz, D. K.; Medlin, J. W., Liquid- and vapor-phase hydrogenation of 1-epoxy-3-butene using self-assembled monolayer coated palladium and platinum catalysts. *Appl. Catal. A* **2012**, *445-446*, 102-106.
95. Taguchi, T.; Isozaki, K.; Miki, K., Enhanced catalytic activity of self-assembled-monolayer-capped gold nanoparticles. *Adv. Mater.* **2012**, *24* (48), 6462-6467.
96. Mori, A.; Mizusaki, T.; Kawase, M.; Maegawa, T.; Monguchi, Y.; Takao, S.; Takagi, Y.; Sajiki, H., Novel Palladium-on-Carbon/Diphenyl Sulfide Complex for Chemoselective Hydrogenation: Preparation, Characterization, and Application. *Adv. Synth. Catal.* **2008**, *350* (3), 406-410.
97. Sadeghmoghaddam, E.; Gu, H.; Shon, Y. S., Pd Nanoparticle-Catalyzed Isomerization vs Hydrogenation of Allyl Alcohol: Solvent-Dependent Regioselectivity. *ACS Catal.* **2012**, *2* (9), 1838-1845.

98. F. de L. e Freitas, L.; Puértolas, B.; Zhang, J.; Wang, B.; Hoffman, A. S.; Bare, S. R.; Pérez-Ramírez, J.; Medlin, J. W.; Nikolla, E., Tunable Catalytic Performance of Palladium Nanoparticles for H<sub>2</sub>O<sub>2</sub> Direct Synthesis via Surface-Bound Ligands. *ACS Catal.* **2020**, *10* (9), 5202-5207.
99. Pang, S. H.; Schoenbaum, C. A.; Schwartz, D. K.; Medlin, J. W., Effects of Thiol Modifiers on the Kinetics of Furfural Hydrogenation over Pd Catalysts. *ACS Catal.* **2014**, *4* (9), 3123-3131.
100. Kahsar, K. R.; Schwartz, D. K.; Medlin, J. W., Selective Hydrogenation of Polyunsaturated Fatty Acids Using Alkanethiol Self-Assembled Monolayer-Coated Pd/Al<sub>2</sub>O<sub>3</sub> Catalysts. *ACS Catal.* **2013**, *3* (9), 2041-2044.
101. Makosch, M.; Lin, W.-I.; Bumbálek, V.; Sá, J.; Medlin, J. W.; Hungerbühler, K.; van Bokhoven, J. A., Organic Thiol Modified Pt/TiO<sub>2</sub> Catalysts to Control Chemoselective Hydrogenation of Substituted Nitroarenes. *ACS Catal.* **2012**, *2* (10), 2079-2081.
102. Schoenbaum, C. A.; Schwartz, D. K.; Medlin, J. W., Controlling the surface environment of heterogeneous catalysts using self-assembled monolayers. *Acc. Chem. Res.* **2014**, *47* (4), 1438-1445.
103. Andryushechkin, B. V.; Pavlova, T. V.; Eltsov, K. N., Adsorption of halogens on metal surfaces. *Surf. Sci. Rep.* **2018**, *73* (3), 83-115.
104. Ma, X.; Liu, S.; Liu, Y.; Gu, G.; Xia, C., Comparative study on catalytic hydrodehalogenation of halogenated aromatic compounds over Pd/C and Raney Ni catalysts. *Sci. Rep.* **2016**, *6*, 25068.
105. Roman, T.; Gossenberger, F.; Forster-Tonigold, K.; Gross, A., Halide adsorption on close-packed metal electrodes. *Phys. Chem. Chem. Phys.* **2014**, *16* (27), 13630-13634.
106. Meng, Q.; Hou, M.; Liu, H.; Song, J.; Han, B., Synthesis of ketones from biomass-derived feedstock. *Nat. Commun.* **2017**, *8*, 14190.
107. Zhu, Q.; Wang, S.-q., Trends and Regularities for Halogen Adsorption on Various Metal Surfaces. *J. Electrochem. Soc.* **2016**, *163* (9), H796-H808.
108. Tundo, P., Modifier effects on Pt/C, Pd/C, and Raney-Ni catalysts in multiphase catalytic hydrogenation systems. *J. Mol. Catal. A Chem.* **2003**, *204-205*, 747-754.
109. Rocha, T. C. R.; Hävecker, M.; Knop-Gericke, A.; Schlögl, R., Promoters in heterogeneous catalysis: The role of Cl on ethylene epoxidation over Ag. *J. Catal.* **2014**, *312*, 12-16.

110. Harris, J. W.; Herron, J. A.; DeWilde, J. F.; Bhan, A., Molecular characteristics governing chlorine deposition and removal on promoted Ag catalysts during ethylene epoxidation. *J. Catal.* **2019**, *377*, 378-388.
111. Choudhary, V.; Samanta, C., Role of chloride or bromide anions and protons for promoting the selective oxidation of H<sub>2</sub> by O<sub>2</sub> to H<sub>2</sub>O<sub>2</sub> over supported Pd catalysts in an aqueous medium. *J. Catal.* **2006**, *238* (1), 28-38.
112. Bjork, J.; Hanke, F.; Stafstrom, S., Mechanisms of halogen-based covalent self-assembly on metal surfaces. *J. Am. Chem. Soc.* **2013**, *135* (15), 5768-5775.
113. Oliveira, V.; Cremer, D., Transition from metal-ligand bonding to halogen bonding involving a metal as halogen acceptor a study of Cu, Ag, Au, Pt, and Hg complexes. *Chem. Phys. Lett.* **2017**, *681*, 56-63.
114. Ramirez, A.; Hueso, J. L.; Suarez, H.; Mallada, R.; Ibarra, A.; Irusta, S.; Santamaria, J., A Nanoarchitecture Based on Silver and Copper Oxide with an Exceptional Response in the Chlorine-Promoted Epoxidation of Ethylene. *Angew. Chem. Int. Ed.* **2016**, *55* (37), 11158-11161.
115. Zhao, Y.; Ling, T.; Chen, S.; Jin, B.; Vasileff, A.; Jiao, Y.; Song, L.; Luo, J.; Qiao, S. Z., Non-metal Single-Iodine-Atom Electrocatalysts for the Hydrogen Evolution Reaction. *Angew. Chem. Int. Ed.* **2019**, *58* (35), 12252-12257.
116. Seshu Babu, N.; Lingaiah, N.; Sai Prasad, P. S., Characterization and reactivity of Al<sub>2</sub>O<sub>3</sub> supported Pd-Ni bimetallic catalysts for hydrodechlorination of chlorobenzene. *Appl. Catal. B* **2012**, *111-112*, 309-316.
117. Favier, I.; Pla, D.; Gomez, M., Palladium Nanoparticles in Polyols: Synthesis, Catalytic Couplings, and Hydrogenations. *Chem. Rev.* **2020**, *120* (2), 1146-1183.
118. Sá, J.; Medlin, J. W., On-the-fly Catalyst Modification: Strategy to Improve Catalytic Processes Selectivity and Understanding. *ChemCatChem* **2019**, *11* (15), 3355-3365.
119. Ranganath, K. V.; Kloesges, J.; Schafer, A. H.; Glorius, F., Asymmetric nanocatalysis: N-heterocyclic carbenes as chiral modifiers of Fe<sub>3</sub>O<sub>4</sub>/Pd nanoparticles. *Angew. Chem. Int. Ed.* **2010**, *49* (42), 7786-7789.
120. Scanlon, M. D.; Peljo, P.; Mendez, M. A.; Smirnov, E.; Girault, H. H., Charging and discharging at the nanoscale: Fermi level equilibration of metallic nanoparticles. *Chem. Sci.* **2015**, *6* (5), 2705-2720.
121. Fogg, D. E.; dos Santos, E. N., Tandem catalysis: a taxonomy and illustrative review. *Coord. Chem. Rev.* **2004**, *248* (21-24), 2365-2379.
122. Liu, Q.; Yang, X.; Huang, Y.; Xu, S.; Su, X.; Pan, X.; Xu, J.; Wang, A.; Liang, C.; Wang, X.; Zhang, T., A Schiff base modified gold catalyst for green and efficient H<sub>2</sub> production from formic acid. *Energy Environ. Sci.* **2015**, *8* (11), 3204-3207.



123. Liu, Q.; Yang, X.; Li, L.; Miao, S.; Li, Y.; Li, Y.; Wang, X.; Huang, Y.; Zhang, T., Direct catalytic hydrogenation of CO<sub>2</sub> to formate over a Schiff-base-mediated gold nanocatalyst. *Nat. Commun.* **2017**, *8* (1), 1407.
124. Teschner, D.; Borsodi, J.; Wootsch, A.; Revay, Z.; Havecker, M.; Knop-Gericke, A.; Jackson, S. D.; Schlogl, R., The roles of subsurface carbon and hydrogen in palladium-catalyzed alkyne hydrogenation. *Science* **2008**, *320* (5872), 86-89.
125. Wei, Z.; Yao, Z.; Zhou, Q.; Zhuang, G.; Zhong, X.; Deng, S.; Li, X.; Wang, J., Optimizing Alkyne Hydrogenation Performance of Pd on Carbon in Situ Decorated with Oxygen-Deficient TiO<sub>2</sub> by Integrating the Reaction and Diffusion. *ACS Catal.* **2019**, *9* (12), 10656-10667.
126. Chan, C. W.; Mahadi, A. H.; Li, M. M.; Corbos, E. C.; Tang, C.; Jones, G.; Kuo, W. C.; Cookson, J.; Brown, C. M.; Bishop, P. T.; Tsang, S. C., Interstitial modification of palladium nanoparticles with boron atoms as a green catalyst for selective hydrogenation. *Nat. Commun.* **2014**, *5*, 5787.
127. Delgado, J. A.; Benkirane, O.; Claver, C.; Curulla-Ferre, D.; Godard, C., Advances in the preparation of highly selective nanocatalysts for the semi-hydrogenation of alkynes using colloidal approaches. *Dalton Trans.* **2017**, *46* (37), 12381-12403.
128. Lan, X.; Wang, T., Highly Selective Catalysts for the Hydrogenation of Unsaturated Aldehydes: A Review. *ACS Catal.* **2020**, *10* (4), 2764-2790.
129. Lari, G. M.; Puertolas, B.; Shahrokhi, M.; Lopez, N.; Perez-Ramirez, J., Hybrid Palladium Nanoparticles for Direct Hydrogen Peroxide Synthesis: The Key Role of the Ligand. *Angew. Chem. Int. Ed.* **2017**, *56* (7), 1775-1779.
130. Wu, J.; Wang, X.; Wang, Q.; Lou, Z.; Li, S.; Zhu, Y.; Qin, L.; Wei, H., Nanomaterials with enzyme-like characteristics (nanozymes): next-generation artificial enzymes (II). *Chem. Soc. Rev.* **2019**, *48* (4), 1004-1076.
131. Wu, W.; Huang, L.; Wang, E.; Dong, S., Atomic engineering of single-atom nanozymes for enzyme-like catalysis. *Chem. Sci.* **2020**, *11*, 9741-9756



## 2. Experiment Section

### 2.1. Catalyst preparation

#### 2.1.1. Chemicals

Commercial supported metal catalyst (5 wt. % Pd/Al<sub>2</sub>O<sub>3</sub>, 5 wt. % Pd/C, 5 wt. % Pt/C, 5 wt. % Ru/C and 5 wt. % Ru/Al<sub>2</sub>O<sub>3</sub>) were purchased from Johnson Matthey Chemicals Company. Palladium chloride, ethyl iodide, isobutyl iodide, iodobenzene, bromobenzene, chlorobenzene, chlorobutane, bromobutane, molecule I<sub>2</sub>, sodium iodide, ammonium bromide, 1-bromohexadecane, toluene anhydrous, mesitylene, 1,3,5-triisopropylbenzene, *p*-xylene, dimethylaminopropylamine, biphenyl, *n*-decane, isopropanol, methanol, tetrahydrofuran, furfural, hydroxymethylfurfural, octanal, benzyl aldehyde, benzyl alcohol, octanol, acetophenone, and pyridine were supplied by Sigma-Aldrich company. Silicon dioxide and alumina were purchased from Sasol company. Air, nitrogen, and hydrogen were supplied by Air Liquide company. Deionized water was obtained from a Millipore system. All chemicals were analytical grade and used as received without further purification.

#### 2.1.2. Preparation of I modified Pd catalyst

*I-Pd/Al<sub>2</sub>O<sub>3</sub> and I-Pd/C*: 5 wt. % of Pd on alumina or carbon supports (Pd/Al<sub>2</sub>O<sub>3</sub> or Pd/C) has been used as parent catalysts. Deposition of iodine has been performed by addition of 0.2 g of Pd/Al<sub>2</sub>O<sub>3</sub> or Pd/C together with 50 mg of ethyl iodide (EtI) in 6 g of isopropanol into 40 ml stainless-steel reactor. The reactor was pressurized with 10 bar

of H<sub>2</sub> and stirred at 60 °C for 1 h. Afterwards, the catalyst has been separated, thoroughly washed with isopropanol and dried in the vacuum oven at 80 °C overnight. The synthesized samples were denoted as I-Pd/C and I-Pd/Al<sub>2</sub>O<sub>3</sub>.

*I-Pd/Al<sub>2</sub>O<sub>3</sub> (N<sub>2</sub>)*: 200 mg of initial 5 wt.% Pd/Al<sub>2</sub>O<sub>3</sub>, 50 mg ethyl iodide, and 6 g isopropanol were added in a 40 ml autoclave, flushed with N<sub>2</sub> for 5 times and stirring at 60°C for 1 h. Finally, the catalyst was washed with isopropanol thoroughly and dried in the vacuum oven at 80°C overnight. The resultant catalyst was named as I-Pd/Al<sub>2</sub>O<sub>3</sub>(N<sub>2</sub>).

*NaI-Pd/Al<sub>2</sub>O<sub>3</sub>*: 200 mg of initial 5 wt.% Pd/Al<sub>2</sub>O<sub>3</sub>, 50 mg NaI, and 6 g H<sub>2</sub>O were added in a 40 ml autoclave, then flushed with H<sub>2</sub> for 5 times and pressurized at 10 bar of H<sub>2</sub> and stirring at 60°C for 1 h. Finally, the catalyst was washed with water thoroughly and dried in the vacuum oven at 80°C overnight. The resultant catalyst was named as NaI-Pd/Al<sub>2</sub>O<sub>3</sub>.

*I<sub>2</sub>-Pd/Al<sub>2</sub>O<sub>3</sub>*: 200 mg of initial 5 wt% Pd/Al<sub>2</sub>O<sub>3</sub>, 40 mg I<sub>2</sub>, and 6 g isopropanol were added in a 40 ml autoclave, then flushed with N<sub>2</sub> for 5 times and stirring at 60°C for 1 h. Finally, the catalyst was washed with isopropanol thoroughly and dried in the vacuum oven at 80°C overnight. The resultant catalyst was named as I<sub>2</sub>-Pd/Al<sub>2</sub>O<sub>3</sub>.

*I<sub>2</sub>/Al<sub>2</sub>O<sub>3</sub>*: The catalyst was prepared by mixing 200 mg of alumina with a solution of 10 mg of iodine in 2 mL of dichloromethane. The slurry was stirred magnetically at room temperature for 30 minutes. Then the solvent was removed by evaporation under reduced pressure at 50°C. The catalyst was collected and named as I<sub>2</sub>/Al<sub>2</sub>O<sub>3</sub> after drying.

### **2.1.3. Preparation of Br modified Pd catalyst**

*Br-Pd/Al<sub>2</sub>O<sub>3</sub>, Br-Pd/C, Br-Pd/SiO<sub>2</sub>*: To prepare the Br pre-treated catalysts, typically, 200 mg of Pd/Al<sub>2</sub>O<sub>3</sub>, Pd/C, Pd/SiO<sub>2</sub>, or Pd black catalyst, together with 50 µl BrBen and 5 g THF were added in the autoclave reactor. Afterwards, the reactor was sealed and pressurized by 20 bar of hydrogen, followed by heating up to 60°C with continuous magnetic stirring for 1 h. Finally, the catalyst and liquid phase were separated by centrifugation and washed with THF for 3 times and dried at 60°C overnight.

### **2.1.4. Preparation of Br modified Ru catalyst**

*Br-Ru/C, Br-Ru/SiO<sub>2</sub>*: To prepare the Br pre-treated catalysts, typically, 200 mg of Ru/C, or Ru/SiO<sub>2</sub>, together with 50 µl BrBen and 5 g THF were added in the autoclave reactor. Afterwards, the reactor was sealed and pressurized by 20 bar of hydrogen, followed by heating up to 60°C with continuous magnetic stirring for 1 h. Finally, the catalyst and liquid phase were separated by centrifugation and washed with THF for 3 times and dried at 60°C overnight.

### **2.1.5. Preparation of Pd/SiO<sub>2</sub> catalyst**

*10 w.t.% Pd/SiO<sub>2</sub> catalyst*: Pd on SiO<sub>2</sub> catalyst was prepared by incipient wetness impregnation. Typically, 2 g of SiO<sub>2</sub> was impregnated with 0.34 g PdCl<sub>2</sub> in H<sub>2</sub>O solutions. The prepared sample aged at room temperature overnight and then dried in the oven at 80°C for 12 h. Finally, the catalyst was calcined at 550°C for 6 h.

### **2.1.6. Preparation of imprinted Pd/SiO<sub>2</sub> catalyst**

*Print-Pd/SiO<sub>2</sub>*: 200 mg Pd/SiO<sub>2</sub> catalyst was firstly subjected to reduction with H<sub>2</sub> [5 mL (STP) / min] at 200°C for 3 h in a home-made fix-bed reactor, and then cooled down to 80°C for template adsorption and DMAPA poisoning. Template (toluene, mesitylene, TPB) was injected by a syringe pump with 10 ml (STP)/min N<sub>2</sub> flow as carrier gas under atmospheric pressure. Next, the template adsorbed Pd catalyst was poisoned by bubbling DMAPA liquid under 60°C and atmospheric pressure with 1 ml (STP) / min N<sub>2</sub> flow. Finally, the resultant catalyst was heated up to 150°C in the H<sub>2</sub> flow [10 ml (STP) / min] for 1 h to remove the template from the catalyst. The imprinted Pd catalyst was named as TL-Print-Pd/SiO<sub>2</sub>, ML-Print-Pd/SiO<sub>2</sub> and TPB-Print-Pd/SiO<sub>2</sub>, representing toluene, mesitylene and TPB imprinted Pd/SiO<sub>2</sub>, respectively. To study the poisoning behavior, D-Pd/SiO<sub>2</sub> catalyst was prepared by poisoning with DMAPA in the same manner without adsorption of template.

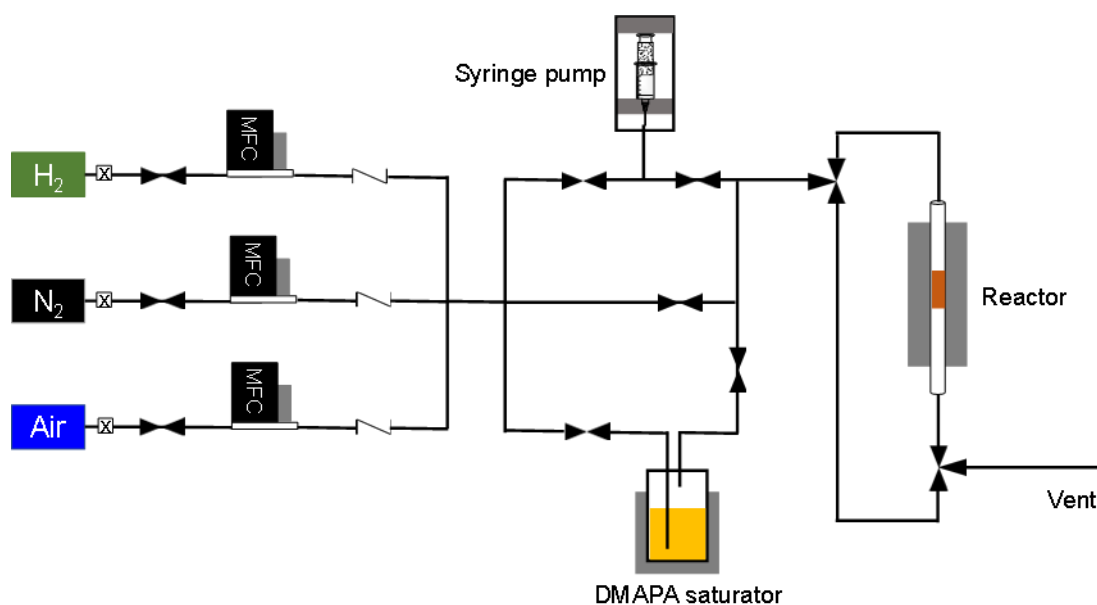


**Figure 2.1.** Schematic diagram of the home-made fixed-bed system for imprinting studies.

## 2.2. Catalyst Characterization

### **2.2.1. X-ray diffraction (XRD)**

The X-ray diffraction (XRD) were recorded on a PANalytical Empyrean X-ray diffractometer in Bragg-Brentano configuration with the  $0.02^\circ$  step size and 1 s step time. The Cu K $\alpha$  radiation (40 kV and 30 mA) was used as the X-ray source. The crystalline phases were identified by comparing the diffraction patterns with those of the standard powder XRD files (JCPDS). Crystal average size was calculated using the Scherrer equation.

### **2.2.2. Transmission electron microscopy (TEM)**

For transmission electron microscopy (TEM) analysis, the scanning mode was carried out on a JEOL 2100 FEG S/TEM microscope operated at 200 kV and equipped with a spherical aberration probe corrector. Before the analysis, the samples were dispersed in ethanol and deposited on a holey carbon-coated TEM grid. In STEM, the images were recorded using a high-angular annular dark field (HAADF) detector with inner and outer diameters of about 73 and 194 mrad. Energy Dispersive X-ray Spectroscopy (EDS) analyses allowing for the elemental mapping of Pd and Br, were performed in STEM using a JEOL Silicon Drift Detector (DrySD60GV, sensor size 60 mm<sup>2</sup>) with a solid angle of approximately 0.6 srad.

### **2.2.3. Chemisorption**

*CO-pulse:* The CO pulse adsorption was performed using AutoChem II 2920 apparatus from Micromeritics. 50 mg of sample was put in a quartz reactor, and then the samples

were reduced in a flow of 5% H<sub>2</sub>/Ar flow (60 ml/min) with a heating rate 10 °C/min at 60 °C for 0.5 h. After cooling down to 45 °C the catalyst has been treated by CO pulses in He flow till full saturation. H<sub>2</sub>-TPR has been performed in the same unit using CryoCooler for sub-ambient (-70°C) measurements with heating rate 10 °C/min in 5% H<sub>2</sub>/Ar flow.

*H<sub>2</sub>-pulse:* The H<sub>2</sub> pulse chemisorption was carried out on the same instrument. 50 mg of sample was put in a quartz reactor, and then the samples were reduced in a flow of 5% H<sub>2</sub>/Ar flow (60 ml/min) with heating rate 10°C/min at 200°C for 0.5 h, then flushed under Ar flow (60 ml/min) at 250°C for 0.5 h. The catalyst after reduction has been cooled down to 45°C followed by pulses of 5% H<sub>2</sub>/Ar till saturation of H<sub>2</sub> signal.

*H<sub>2</sub>-TPR:* The H<sub>2</sub> temperature programmed reduction (H<sub>2</sub> TPR) experiments were carried out on the same instrument using 50 mg of the sample in a flow of 5% H<sub>2</sub>/Ar. The temperature was increased from room temperature to 600°C at a rate of 10°C/min.

#### **2.2.4. Thermogravimetric analysis (TGA)**

Thermogravimetric analysis (TGA) was carried out under air flow [10 mL(STP)/min] in the temperature range of 20 ~ 800°C using a heating rate of 5°C/min on a Mettler Toledo SMP/PF7458/MET/600W instrument.

#### **2.2.5. X-ray photoelectron spectrometry (XPS)**

X-ray photoelectron spectroscopy (XPS) analysis has been performed in a ThermoFischer ESCALAB 250Xi photoelectron spectrometer using monochromatic X-ray radiation Al K $\alpha$  (1486.7 eV) and 180° double-focusing hemispherical analyzer



with a six-channel detector. The binding energy (BE) of the photoemission spectra was calibrated to Al 2p peak with BE 74.5 eV for Al-containing samples and to adventitious carbon C 1s peak with BE 284.8 eV for others.

### **2.2.6. Fourier transform Infrared spectroscopy (IR)**

Fourier transform infrared (FTIR) spectra were recorded using a Thermo Fisher Scientific Nicolet 6700 FTIR (32 scans at a resolution of  $4\text{ cm}^{-1}$ ) equipped with a mercury cadmium telluride (MCT) detector. Pyridine and CO-FTIR experiments were performed in a vacuum cell (less than  $10^{-5}$  torr). The catalyst samples for analysis were pressed in a  $40 \sim 50\text{ mg/cm}^2$  ( $D=13\text{ mm}$ ) self-supporting discs. Before the analysis, all the samples were reduced at  $60^\circ\text{C}$  for 1 h with subsequent vacuum treatment for 3 h. CO adsorption has been performed by the addition of CO doses in the cell at room temperature till full saturation. Pyridine (Py) adsorption has been performed in the same way by the addition of Py doses. For some experiments, 500 torr of hydrogen have been introduced in the cell after Py adsorption.

### **2.2.7. X-ray fluorescence analysis (XRF)**

X-ray fluorescence (XRF) analysis was performed with the use of an energy dispersive micro-X Ray Fluorescence spectrometer M4 TORNADO (Bruker). This instrument is equipped with 2 anodes a Rhodium X-ray tube 50 kV/600 mA (30 W) and a Tungsten X-Ray tube 50 kV/700 mA (35 W). For sample characterization, the X-rays Rhodium with a polycapillary lens enabling excitation of an area of  $200\text{ }\mu\text{m}$  was used. The detector used was a Silicon-Drift-Detector Si (Li) with  $<145\text{ eV}$  resolution at 100000

cps (Mn K $\alpha$ ) and cooled with a Peltier cooling (253°K). The measurement was done under vacuum (20 mbar). The elements, that can be measured by this instrument unit range from sodium (Na) to uranium (U). Quantitative analysis was done using a fundamental parameter (FP) (standardless). As elements are present in stoichiometric compounds, its formula was used for quantification of the weight percent of each element.

## **2.3. Evaluation of catalytic reactions**

### **2.3.1. Reductive etherification**

The etherification reaction has been conducted in a 40 ml stainless-steel autoclave equipped with a magnetic stirrer, pressure gauge and an automatic temperature controller. In a typical experiment, 2 g of isopropanol, 0.1 g of furfural and 50 mg of catalyst with or without 15 mg of organic iodide were loaded into the reactor. Afterwards, the reactor was sealed and pressurized by 20 bar of H<sub>2</sub>, followed by heating up to the target temperature with continuous magnetic stirring. After reaction, the autoclave was cooled down, the pressure was released and the solution was separated by filtration and analyzed by gas chromatography (GC) with biphenyl as the internal standard. In some experiments, other alcohols and carbonyl compounds have been used instead of furfural and isopropanol.

The products of the reaction have been analyzed by GC (Agilent Technologies 7820A) equipped with a polar column of HP-5 and flame ionization detector (FID), with an inlet temperature of 250°C. The products have been separated using the temperature

program. The initial temperature was 75°C and hold for 5 min with subsequent heating to 260°C with the ramping rate 10°C/min. GC-MS analysis (Agilent Technologies 5977A MSD with Agilent Technologies 7890B GC system equipped with HP-5 capillary column) was used to identify the organic compounds.

The conversion of carbonyl compound, selectivity and yield to corresponding products were defined as follows:

$$\text{Conversion (\%)} = 1 - \frac{n_A}{n_A^o}$$

$$\text{Selectivity to the product p (\%)} = \frac{n_p}{n_A^o - n_A}$$

$$\text{Yield (\%)} = \text{Conversion} \times \text{Selectivity}$$

$n_A$ ,  $n_A^o$  and  $n_p$  refers to the final, initial moles of carbonyl compound and final moles of product, respectively. Biphenyl was used as internal standard for the GC analysis.

### 2.3.2. Hydrodeoxygenation

The hydrodeoxygenation reaction has been performed in a 25 ml stainless-steel autoclave equipped with a magnetic stirrer, pressure gauge and an automatic temperature controller. Typically, for the hydrodeoxygenation of HMF, 5 g of THF, 0.1 g of HMF and 50 mg of catalyst with or without 10 µl of bromobenzene were added into the reactor. Afterward, the reactor was sealed and pressurized by 5 or 20 bar of hydrogen, followed by heating up to the target temperature with continuous magnetic stirring. After the reaction, the reactor was cooled down, the solution was separated by filtration and the products were identified by GC-MS (Agilent Technologies 5977A

MSD with Agilent Technologies 7890B GC system equipped with HP-5 capillary column) and quantified by GC (Agilent Technologies 7820A, equipped with HP-5 capillary column and flame ionization detector) with biphenyl as the internal standard. The conversion of HMF, selectivity and yield to corresponding products were defined as follows:

$$\text{Conversion (\%)} = 1 - \frac{n_A}{n_A^o}$$

$$\text{Selectivity to the product p (\%)} = \frac{n_p}{n_A^o - n_A}$$

$$\text{Yield (\%)} = \text{Conversion} \times \text{Selectivity}$$

$n_A$  and  $n_A^o$  refers to the final, initial number of the moles of HMF, respectively.  $n_p$  is number of the moles of converted HMF to product p. Biphenyl was used as an internal standard for quantification.

### 2.3.3. Hydrogenolysis of diphenyl ether

50 ~ 100 mg catalyst (e.g. Br-Ru/C), 100 mg diphenyl ether, and 5 g methanol were put together in a 50 ml batch reactor. Then, the reactor was pressurized by 5 ~ 20 bar of H<sub>2</sub> and heated at 100 ~ 200 °C for 0.5 ~ 12 h. The products were analyzed by GC and GC-MS, with biphenyl as the internal standard. The conversion and selectivity were calculated based on the numbers of phenyl rings.

$$\text{Conversion (\%)} = 1 - \frac{n_A}{n_A^o}$$

$$\text{Selectivity to the product p (\%)} = \frac{n_p}{n_A^o - n_A}$$

$$\text{Yield (\%)} = \text{Conversion} \times \text{Selectivity}$$

$n_A$  and  $n_A^o$  refers to the final, initial number of the moles of phenyl rings in biphenyl ether, respectively.  $n_p$  is the number of the moles of phenyl rings in converted biphenyl ether to product p. Biphenyl has been used as an internal standard for quantification.

### 2.3.4. Aromatics hydrogenation

50 ~ 100 mg Pd/SiO<sub>2</sub> or imprinted Pd/SiO<sub>2</sub> catalyst, 5 g n-decane, 100 mg reactant (toluene, mesitylene and TPB), were put in a 25 ml batch-reactor. Then, the reactor was flushed with H<sub>2</sub> 3 times and pressurized 20 bar H<sub>2</sub>. After heated up at 120°C for 1 ~ 6 h, the catalyst was separated and the liquid phase was analyzed by GC with biphenyl as the internal standard.

The TOF number was defined as:

$$\text{TOF} = \frac{N_p}{t \times N_{\text{active sites}}}$$

Where  $N_p$  represents the converted mole number of aromatics, and  $N_{\text{active sites}}$  represents the mole number of active sites measured by H<sub>2</sub> pulse chemistry, and  $t$  represents the reaction time (h).

### 2.3.5. Selective benzene removal

100 mg Pd/SiO<sub>2</sub> or imprinted Pd/SiO<sub>2</sub> catalyst, 5 g n-decane, 100 mg benzene and 100 mg other aromatics (toluene, mesitylene or TPB), were put in a 25 ml batch-reactor. Then, the reactor was flushed with H<sub>2</sub> for 3 times and pressurized at 20 bar H<sub>2</sub>. After heating up at 120 °C for 1 ~ 24 h, the catalyst was separated and the liquid phase was analyzed by GC with biphenyl as the internal standard.

The selective to benzene was defined as:

$$\text{Selectivity to benzene} = \frac{N_{benzene}}{N_{aromatics}}$$

Where  $N_{benzene}$  represents the converted mole number of benzene in the mixed-aromatics,  $N_{aromatics}$  represents the converted mole number of all aromatic molecules.

### **3. Modification of Pd Catalyst with Iodide: In-situ Generation of Brønsted Acidity for Selective Reductive Etherification**

#### **ABSTRACT.**

Selective synthesis of ethers from biomass-derived carbonyl compounds is an important academic and industrial challenge. The existing processes based on strong acid or metallic catalysts cannot provide high selectivity to ethers due to the occurrence of side reactions. In this chapter, we propose a Pd-I bifunctional heterogeneous catalyst for selective reductive etherification of aldehydes with alcohols. The catalyst was prepared by simply post-modification of supported or non-supported Pd catalyst by organic iodide under reductive conditions. Extensive catalyst characterizations uncovered the presence of iodine species on the surface of Pd nanoparticles. Heterolytic dissociation of hydrogen on the Pd-I surface sites leads to the “in-situ” generation of Brønsted acidity, which promotes reaction toward corresponding ethers with extremely high selectivity at very mild reaction conditions.

**KEYWORDS.** Acidity generation, Surface modification, Palladium and iodine, Reductive etherification, Biomass upgrading.

Some content in chapter have been published in the following publications:

Dan Wu, Willinton Y. Hernández, Songwei Zhang, Evgeny I. Vovk, Xiaohong Zhou, Yong Yang, Andrei Y. Khodakov\*, and Vitaly V. Ordomsky\*. *ACS Catalysis*, **2019**, *9*, 2940-2948.



### 3.1. Introduction

Ethers and its derivatives are widely used as solvent, surfactants, pharmaceuticals, polymers and liquid fuels <sup>[1-3]</sup>. Traditional routes for the synthesis of ethers normally involve dehydration of alcohols over mineral acids or heterogeneous polymer Nafion-H at elevated temperatures (>150 °C) <sup>[4-6]</sup>. The Williamson ether synthesis by reaction of alcohol with an alkyl halide is another possible approach for the ether production <sup>[7-8]</sup>. However, this reaction requires synthesis of environmentally harmful halides as intermediates.

The selectivity is the most important challenge in the synthesis of ethers from biomass-derived feedstocks. The reaction selectivity is usually insufficient in the traditional synthesis routes, because of complex structure of the biomass-derived substrates, which simultaneously contain several functional groups like carbonyls and hydroxyls. The reductive condensation of alcohols with aldehydes and ketones yielding ethers has been recently proposed as an innovative route to valorize bio-sourced platform molecules <sup>[9-11]</sup>. The reaction mechanism involves intermediate acetalization of carbonyl group over an acid catalyst with subsequent hydrogenolysis of the reaction intermediates to ethers over metal sites. For example, combination of Pt and Amberlyst-15 has been used for transformation of 5-(hydroxymethyl)furfural (HMF) to 2,5-bis(alkoxymethyl)furan with an yield close to 60 % <sup>[9]</sup>. The proximity of acid and metal sites in the bifunctional metal-acid catalysts is commonly enhanced by using liquid acids or their solutions (H<sub>2</sub>SO<sub>4</sub>, HCl etc) <sup>[12]</sup>. Recently metal chlorides have been proposed for this reaction as

catalysts combining both hydrogenation and acidic properties<sup>[13]</sup>. Beside acetalization and hydrogenolysis reaction pathway, another option was using Lewis acid zeolite such as Sn-Beta or Zr-Beta, where reaction involves transfer hydrogenation of HMF to 2,5-bis(hydroxymethyl)furan (BHMF) followed by etherification<sup>[14-15]</sup>. However, poor selectivity, high temperature, low catalytic activity and difficult catalyst separation from the reaction products have been so far serious drawbacks for the implementation of reductive etherification in an industrial scale. In another report, with generation of PdH species as acid sites during hydrogenation reaction, Pd on carbon with 0.7% loading is able to catalyze furfural reductive etherification to furfuryl ethyl ether in ethanol with 81% yield<sup>[16]</sup>. However, this process suffers from narrow reaction temperature windows, limitation of substrates and catalyst degradation.

Molecular iodine has been reported as an effective catalyst for the acetalization reactions, which has been widely used as a protection method for the carbonyl groups in organic synthesis<sup>[17-18]</sup>. One of possible catalytic effects of iodine is related to the generation of hydrogen iodide, which acts in liquid solutions as a Brønsted acid and activates the carbonyl groups by hydrogen bonding effects<sup>[19-20]</sup>. Recently, surface modification of heterogeneous catalysts, which often results in major enhancement in chemoselectivities in numerous reactions, has gained significant interests<sup>[21-23]</sup>. Modification of metal-supported catalysts with iodine could be therefore, favorable for the selective synthesis of ethers from aldehydes and alcohols, since both acetalization and hydrogenolysis functions will be combined in proximity over a single catalyst.

However, this strategy of catalyst design has not yet been explored given the well-known strong poisoning effect of iodine on metal catalysts such as Pt, Au and Pd<sup>[24-25]</sup>. Herein, we developed an extremely efficient Pd-I catalyst (**Figure 3.1**) for reductive condensation of aldehydes and ketones with alcohols with high ether productivity and operating at very mild reaction conditions. The catalyst described in this work can be prepared by “in situ” modification of a commercially available Pd-supported catalyst with organic iodide. This substantially simplifies its preparation process.

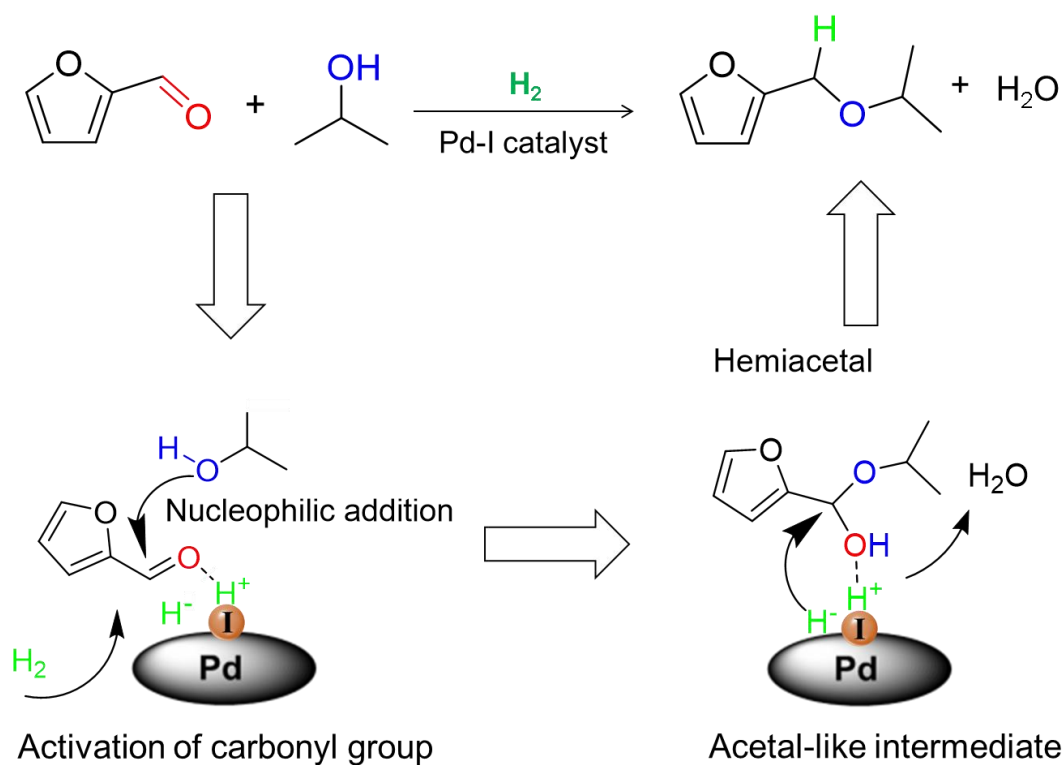


**Figure 3.1.** Scheme of the synthesis of ether from aldehyde and alcohol involving in-situ Brønsted acidity generation in the presence of hydrogen over heterogeneous Pd-I catalyst.

## 3.2. Results and discussion

### 3.2.1. Etherification over the Pd-I catalysts

**Table 3.1.** Etherification reaction of furfural over Pd catalysts treated and non-treated by iodine compounds ( $T=60\text{ }^{\circ}\text{C}$ , 20 bar  $\text{H}_2$ , 0.1 g furfural, 2 g isopropanol, 50 mg catalyst, 1h)

Furfural +  $\text{H}_2$  → FA + THFA + Ether + Acetal + Hemiacetal

Entry	Catalytic system	Furfural Conv., %	Selectivity, %					
			FA	THFA	Ether	Acetal	Hemiacetal	Others <sup>f</sup>
1	Pd/Al <sub>2</sub> O <sub>3</sub>	87.8	0	99.1	0	0	0	0.9
2	Pd/Al <sub>2</sub> O <sub>3</sub> + EtI <sup>a</sup>	72.1	3.9	0.2	91.8	1.3	1.7	1.1
3	I-Pd/Al <sub>2</sub> O <sub>3</sub>	35.8	0	0	83	12	1.4	3.6
4	I-Pd/Al <sub>2</sub> O <sub>3</sub> (N <sub>2</sub> ) <sup>b</sup>	59.7	0	92.6	0	0	0	7.3
5	NaI-Pd/Al <sub>2</sub> O <sub>3</sub> <sup>c</sup>	34.5	2	83.4	0	0	0	14.6
6	Pd/Al <sub>2</sub> O <sub>3</sub> + iBuI <sup>a</sup>	92.5	7.8	0	86.2	1.3	0	4.7
7	Pd/Al <sub>2</sub> O <sub>3</sub> + IBn <sup>a</sup>	55.4	3.4	0	84.6	1.4	2.8	7.8
8	Pd/Al <sub>2</sub> O <sub>3</sub> + I <sub>2</sub> <sup>a</sup>	38.2	0	0	65.6	32.7	0.5	1.2
9	I <sub>2</sub> -Pd/Al <sub>2</sub> O <sub>3</sub>	68.7	3.8	0	90	2.1	1.7	2.3
10	Pd/C	99.9	0	43.3	0	0	0	56.7
11	Pd/C + EtI <sup>a</sup>	88.1	19.7	1.5	69.4	0.3	2.8	6.3
12	I-Pd/C	16.8	0	0	39.7	54.5	0	5.8
13	Pd powder	52.4	8.9	90.6	0	0	0	0.5
14	Pd powder + EtI <sup>a</sup>	24.3	0.3	0	33.3	64.3	0	2.1
15	PdI <sub>2</sub>	54.8	0	0	0	99.3	0	0.7
16	I <sub>2</sub> /Al <sub>2</sub> O <sub>3</sub> <sup>d</sup>	36.6	0	0	0	99.9	0	0.1
17	Pd/Al <sub>2</sub> O <sub>3</sub> + BuCl <sup>a</sup>	53.5	0	72.3	0	0	0	27.7
18	Pd/Al <sub>2</sub> O <sub>3</sub> + BuBr <sup>a</sup>	46	0	41.1	0	0	0	58.9
19	Pd/Al <sub>2</sub> O <sub>3</sub> + EtI <sup>e</sup>	99.6	7	0	82.5	0.8	6.9	2.7

<sup>a</sup> 15 mg of EtI, iBuI, IBn, I<sub>2</sub>, BuCl or BuBr have been added in the reaction mixture before reaction

<sup>b</sup> Pd/Al<sub>2</sub>O<sub>3</sub> was pre-treated with EtI in isopropanol under N<sub>2</sub> atmosphere

<sup>c</sup> Pd/Al<sub>2</sub>O<sub>3</sub> was pre-treated with NaI in water in H<sub>2</sub> atmosphere

<sup>d</sup> The I<sub>2</sub>/Al<sub>2</sub>O<sub>3</sub> was prepared by impregnation method according to ref [32]

<sup>e</sup> This experiment was performed at 35°C for 6 h

<sup>f</sup> The main other products are methylfuran and methyltetrahydrofuran.

The commercial catalyst Pd/Al<sub>2</sub>O<sub>3</sub> (5 wt. %) has been used for hydrogenation of furfural in isopropanol solution. The catalyst demonstrated high activity with formation of tetrahydrofurfuryl alcohol (THFA) as the main product (**Table 3.1, Entry 1**). Addition

of traces of ethyl iodine (EtI) in the reactor leads to a total change of the reaction route (*Table 3.1, Entry 2*), causing a favored formation of ether (2-(isopropoxymethyl)furan) as the main product (91.8 % selectivity) and traces of acetal (2-(diisopropoxymethyl)furan). Note that this dramatic change in the selectivity could be explained either by the presence of EtI as co-catalyst during the reaction, for example, by generation of HI or as modifier of the Pd-supported catalyst.

In order to identify the role of EtI, we did the treatment of Pd/Al<sub>2</sub>O<sub>3</sub> with EtI in isopropanol solution, at the reaction conditions, but without furfural. Afterwards, the solid catalyst was washed thoroughly with isopropanol and dried in vacuum oven overnight to remove the physically adsorbed iodine species. The modified I-Pd/Al<sub>2</sub>O<sub>3</sub> catalyst demonstrated lower catalytic activity compared with the mixed system Pd/Al<sub>2</sub>O<sub>3</sub> and EtI but showed very similar selectivity towards formation of the ether (*Table 3.1, Entry 3*).

Another indication on modification of the catalyst by iodine species is in its stable catalytic performance after 5 cycles with intermediate separation by centrifugation and addition of fresh substrate without EtI (*Figure 3.2*). Comparable reaction rates were observed in several consecutive reaction cycles (*Figure 3.3*). The decline of selectivity after 15 min of test for 2 and 3 cycles could be explained by accumulation of water in the catalyst leading to higher formation of hemiacetal at the initial stage of the reaction. In order to check the role of hydrogen in the genesis of active sites, we have performed the treatment of Pd/Al<sub>2</sub>O<sub>3</sub> by EtI in inert atmosphere of nitrogen. The catalyst demonstrates the catalytic performance similar to initial Pd/Al<sub>2</sub>O<sub>3</sub> catalyst with THFA

as the main product of the reaction (92.6 %, *Table 3.1, Entry 4*). Thus, hydrogen atmosphere is necessary for the effective modification of the palladium catalyst.

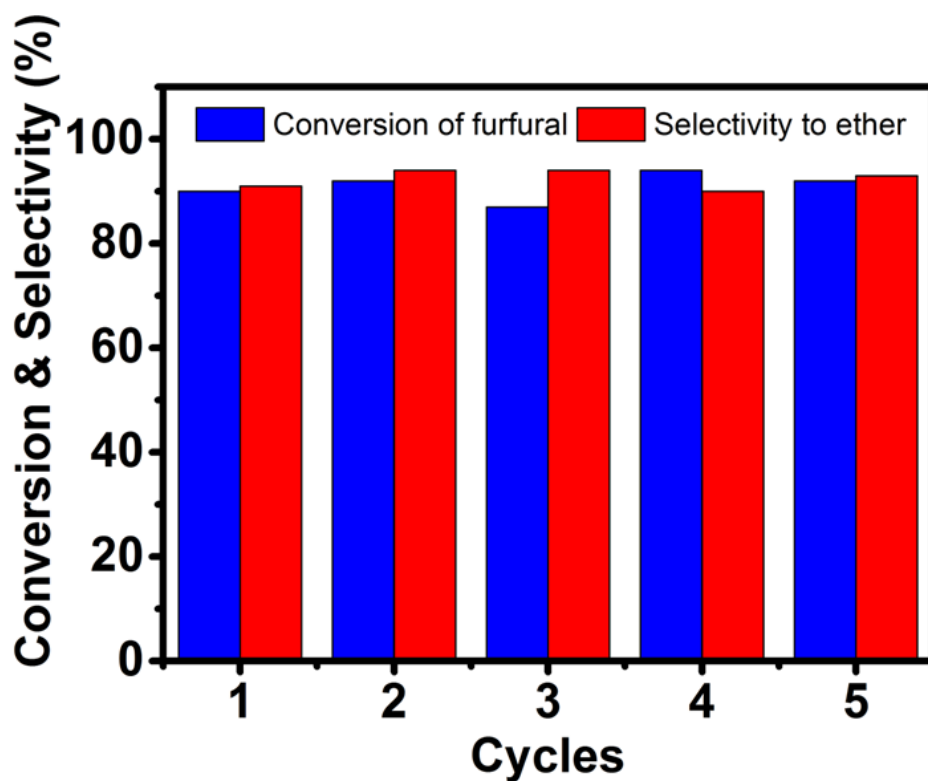


**Figure 3.2.** Catalytic performance of Pd/Al<sub>2</sub>O<sub>3</sub>+EtI catalyst with addition of EtI only for the first cycle.

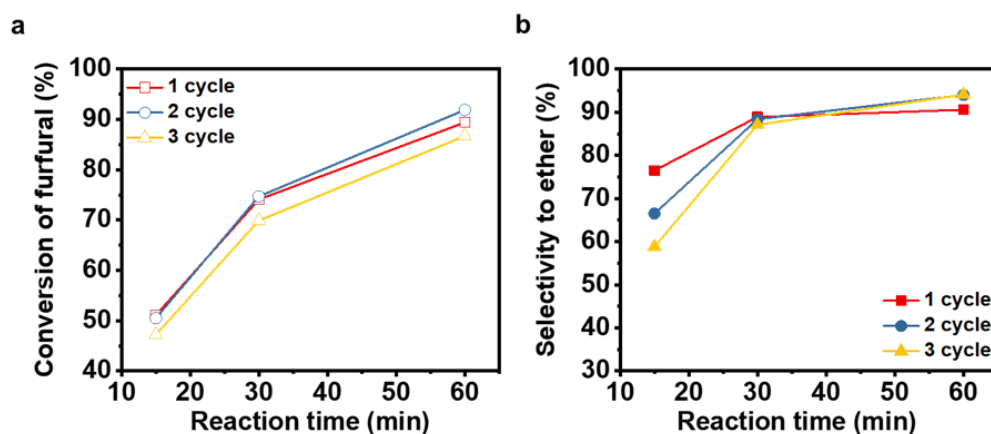


**Figure 3.3.** Evolution of conversion (a) and selectivity (b) for the first 3 cycles with reaction time. Reaction conditions: 50 mg I-Pd/Al<sub>2</sub>O<sub>3</sub>, 100 mg furfural, 2 g isopropanol, 60°C, 20 bar H<sub>2</sub>.

In order to verify the role of iodine species on the catalytic performance we have performed modification of the catalyst by the NaI salt which resulted only in partial catalyst deactivation without affecting the selectivity observed for non-promoted Pd/Al<sub>2</sub>O<sub>3</sub> catalyst (*Table 3.1, Entry 5*). Thus, the modification of the catalyst might be explained by reaction of Pd with organic iodide in the presence of hydrogen with formation of atomic iodine on the surface. Numerous previous studies demonstrated that alkyl iodides could dissociate on metal surface with generation of iodine atoms and alkanes species in the presence of H<sub>2</sub> [26]. To confirm the dissociation of alkyl iodides, isobutyl iodide (iBuI) and iodobenzene (IBn) were also used as iodine source in the reaction mixture. Notably, high yield of ether (*Table 3.1, Entry 6 & 7*) was observed in both experiments. Moreover, the analysis of the products from Pd/Al<sub>2</sub>O<sub>3</sub> promoted with IBn had shown the presence of benzene in the products (*Figure 3.4*). This indicates on the dissociation of IBn with formation of iodine species, which might modify the Pd catalyst. Moreover, the iodine molecule has been also used as an additive (*Table 3.1, Entry 8*). Although the formation of ether was observed in the products, conversion of furfural was quite low. The main side product was acetal due to the presence of I<sub>2</sub> in the reaction mixture, which is well known as a catalyst for acetalization reaction. However, the catalyst pretreated by molecular I<sub>2</sub> in isopropanol solution has demonstrated relatively high activity and selectivity to ether (*Table 3.1, Entry 9*). It has been reported that I<sub>2</sub> can dissociate on the metal surface with formation of adsorbed iodine atoms [27]. Thus, organic iodides as well as molecular iodine can be used for modification of the surface of Pd.

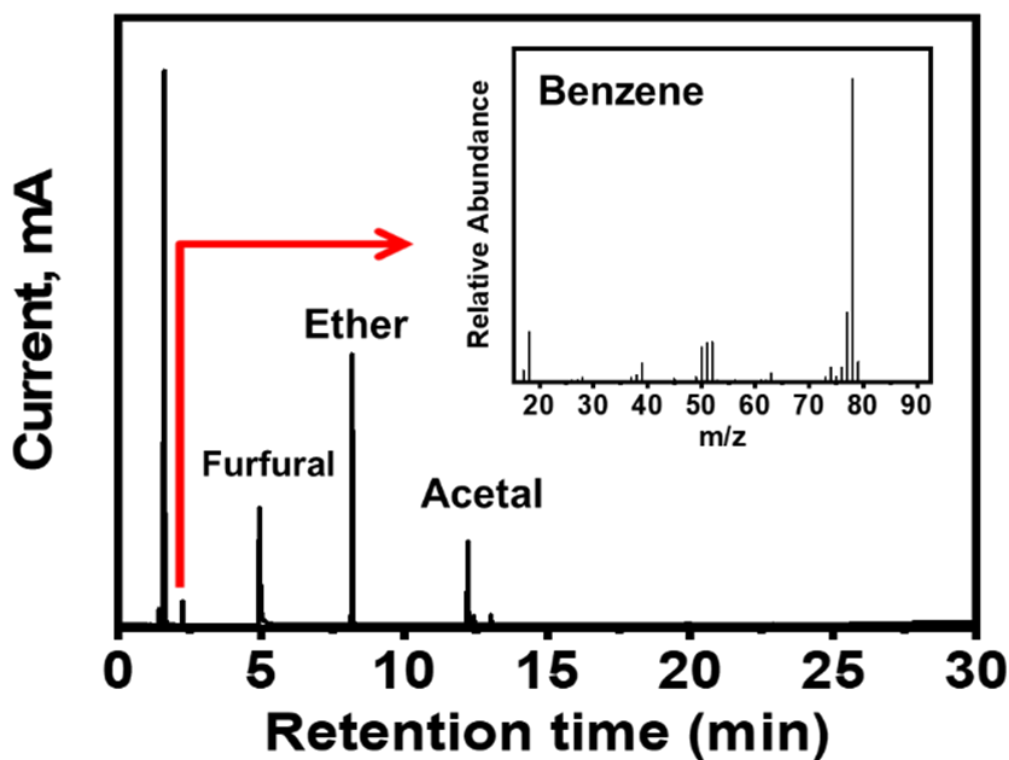


**Figure 3.4.** GC-MS analysis of products from Pd/Al<sub>2</sub>O<sub>3</sub> with IBn.

Note that iodine could modify both the alumina support and Pd. In order to verify the role of support in this reaction we have tested Pd/C (5 wt. % Pd) in hydrogenation of furfural in the presence of EtI ([Table 3.1, Entry 10-11](#)). The non-promoted Pd/C catalyst demonstrated high selectivity to THFA similar to Pd/Al<sub>2</sub>O<sub>3</sub>. However, additionally the catalyst yields 2-methyltetrahydrofuran as the product of deeper hydrogenation and tetrahydropyran derivatives as the products of ring opening and re-cyclization. High activity of Pd/C catalyst in deep hydrogenation reactions has been explained earlier by inert support and presence of unsaturated sites over Pd nanoparticles <sup>[28-29]</sup>. Similar to the alumina supported catalyst, promotion of Pd/C with EtI also shifts the selectivity of the reaction towards the ether. The same effect is also observed after pre-treatment of the Pd/C catalyst by EtI ([Table 3.1, Entry 12](#)). It means that the pre-treatment of



alumina with iodide does not play a key role in the modification of the selectivity of the reaction.

**Table 3.2.** CO-adsorption analysis of different samples.

Samples	CO adsorption (mmol/g)	Surface metal (%)	Particle size (nm)
Pd/Al <sub>2</sub> O <sub>3</sub>	0.14	29	3.8
I-Pd/Al <sub>2</sub> O <sub>3</sub>	0.0063	1.3	-
I-Pd/Al <sub>2</sub> O <sub>3</sub> (N <sub>2</sub> )	0.11	24	-
NaI-Pd/Al <sub>2</sub> O <sub>3</sub>	0.061	13	-
Pd/C	0.19	40	2.8
I-Pd/C	0.041	8.7	-
Pd powder	0.054	0.58	194
I-Pd powder	0.017	0.18	-
Pd/Al <sub>2</sub> O <sub>3</sub> + BuCl	0.11	23	
Pd/Al <sub>2</sub> O <sub>3</sub> + BuBr	0.092	19	

Non-supported Pd powder was tested in this reaction as well (*Table 3.1, Entry 13 & 14*). In the presence of traces of EtI, the selectivity to ether increased from 0 to 33.3 %. The low conversion of furfural on non-supported Pd resulted from the low metal surface area (*Table 3.2*). These results indicate that iodine most probably modifies Pd, leading to the new active species for selective synthesis of ether. In this case, the formation of PdI<sub>2</sub> could be responsible for change of the reaction route. Test of PdI<sub>2</sub> salt in the reaction has shown formation of acetal as the main product of the reaction without ether in the products (*Table 3.1, Entry 15*). The absence of ether could be explained by absence of metallic sites for acetal hydrogenolysis.

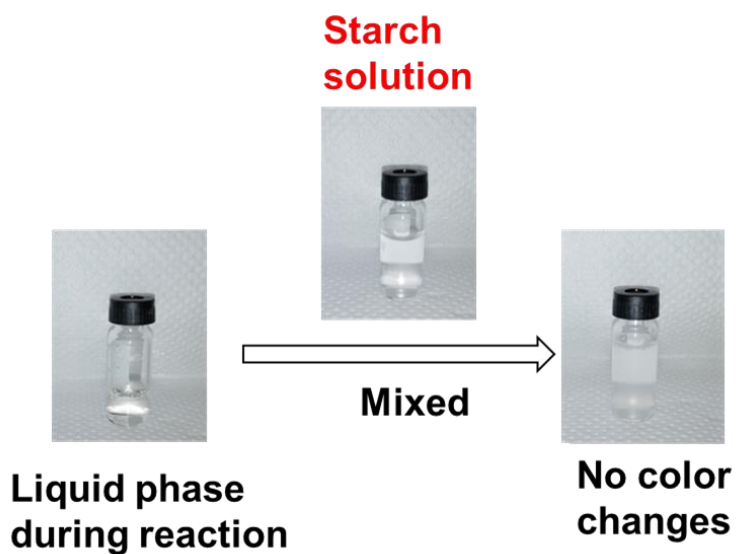


**Figure 3.5.** Analysis of  $I_2$  produced during reaction condition.

Iodine molecule itself has been shown earlier as an active catalyst in transformation of aldehydes<sup>[17]</sup>. We have checked the presence of  $I_2$  in the solution after reaction over  $I$ - $Pd/Al_2O_3$  by a test with addition of starch. The solution was clear and colorless which means absence of  $I_2$  formation (**Figure 3.5**). Additionally,  $I_2$  on  $Al_2O_3$  catalyst has been prepared by impregnation of  $I_2$  over alumina which has been used for several reactions<sup>[30-33]</sup>. However, only acetal was observed as the product of the reaction without ether formation (**Table 3.1, Entry 16**). The potential application of other halogens for pretreatment of Pd has been investigated by using chlorobutane (BuCl) and bromobutane (BuBr) as additives. However, the presence of BuCl and BuBr only decreased the hydrogenation ability of  $Pd/Al_2O_3$ . Notably, no ether was produced over these catalysts (**Table 3.1, Entry 17 & 18**). CO adsorption over the catalysts after pretreatment shows similar adsorption capacity in comparison with the parent catalyst, which indicates low adsorption of Cl and Br over Pd metal surface (**Table 3.2**).

Thus, I-Pd/Al<sub>2</sub>O<sub>3</sub> is an efficient and stable catalyst for reductive etherification of furfural. Moreover, we have performed the etherification reaction at even lower temperature (35 °C) for 6 h (*Table 3.1, Entry 19*) with similar activity and selectivity. Consistently, an approximate 80 % selectivity to ether product was identified by NMR analysis after the removal of non-reacted isopropanol by rotary evaporation and filtration of catalyst. <sup>1</sup>H and <sup>13</sup>C NMR spectra of the ether are displayed in *Figure 3.6 and Figure 3.7*. The further purification of the product by extraction of furfural and furfuryl alcohol by water shows high purity of formed ether according to NMR analysis (*Figure 3.8 and Figure 3.9*) with isolated yield of 76 %. This demonstrates the practicality of this route.

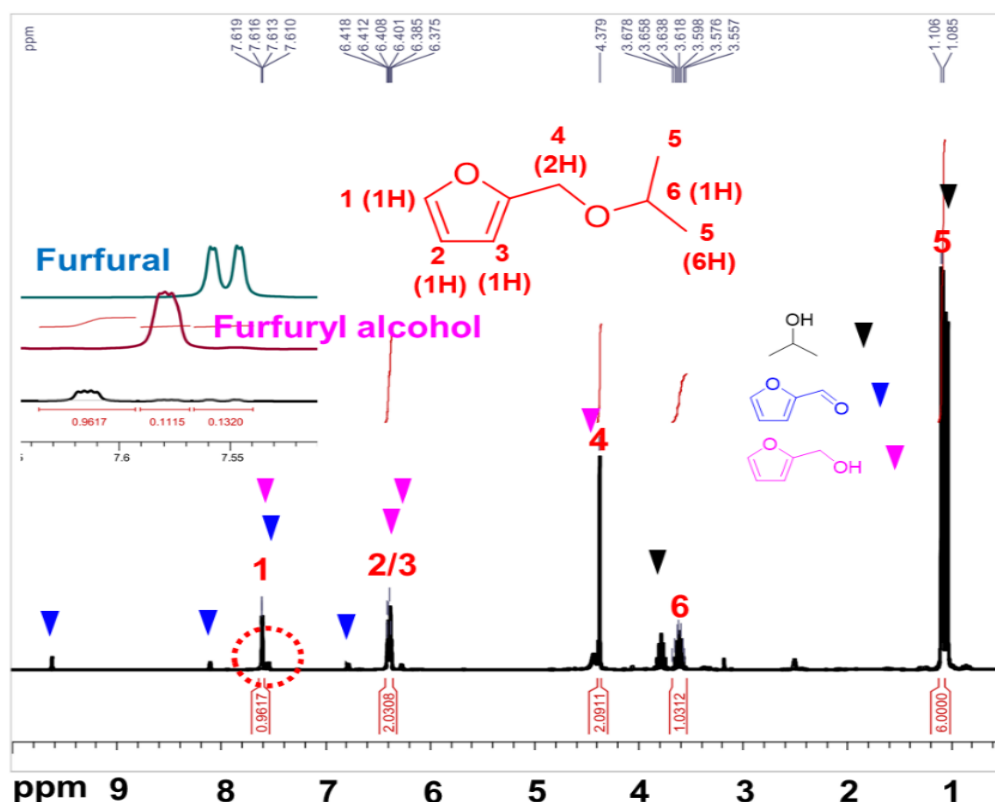


*Figure 3.6.* <sup>1</sup>H NMR spectrum of crude product of 2-(isopropoxymethyl)furan. The main impurities are residual furfural, furfuryl alcohol and isopropanol.

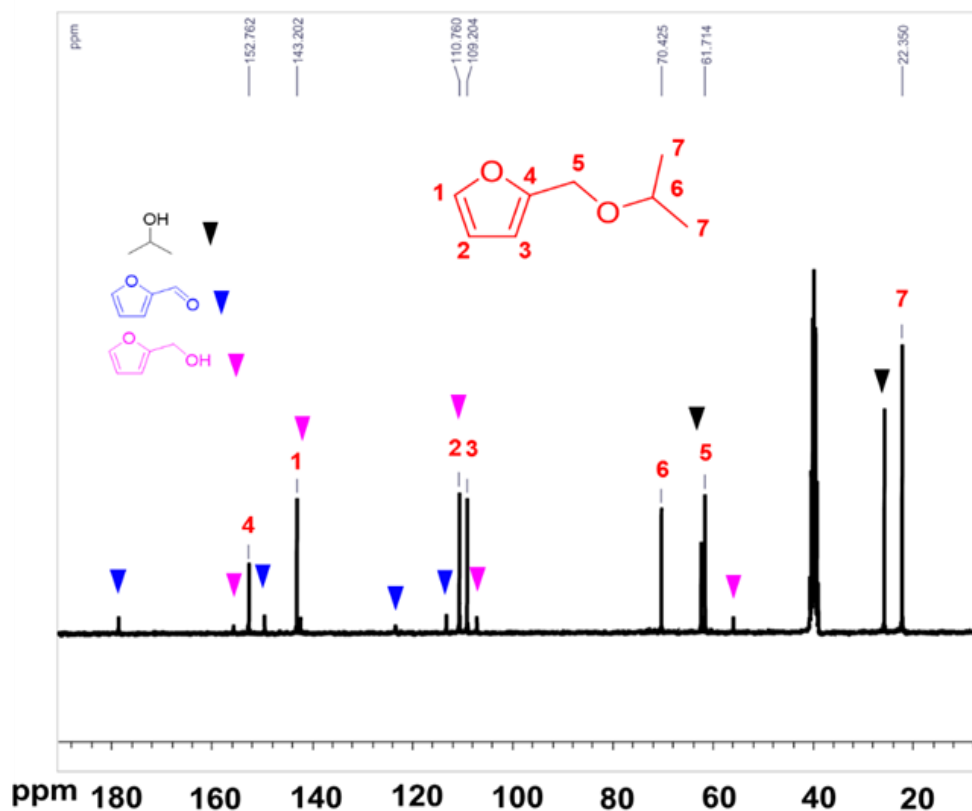


**Figure 3.7.**  $^{13}\text{C}$  NMR spectrum of crude product of 2-(isopropoxymethyl)furan. The main impurities are residual furfural, furfuryl alcohol and isopropanol.

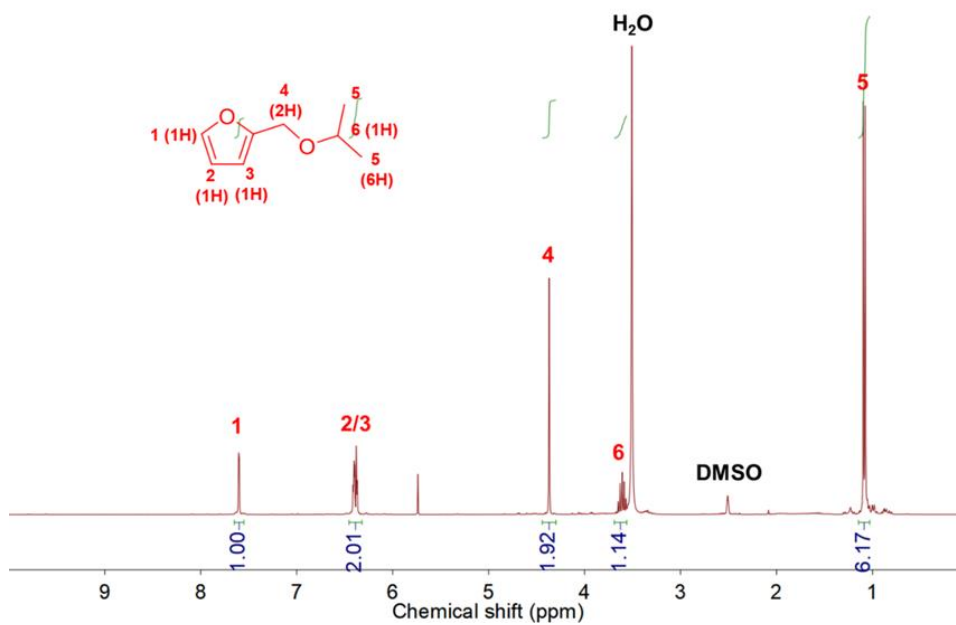


**Figure 3.8.**  $^1\text{H}$  NMR spectrum of purified product of 2-(isopropoxymethyl)furan after washing with  $\text{H}_2\text{O}$ .

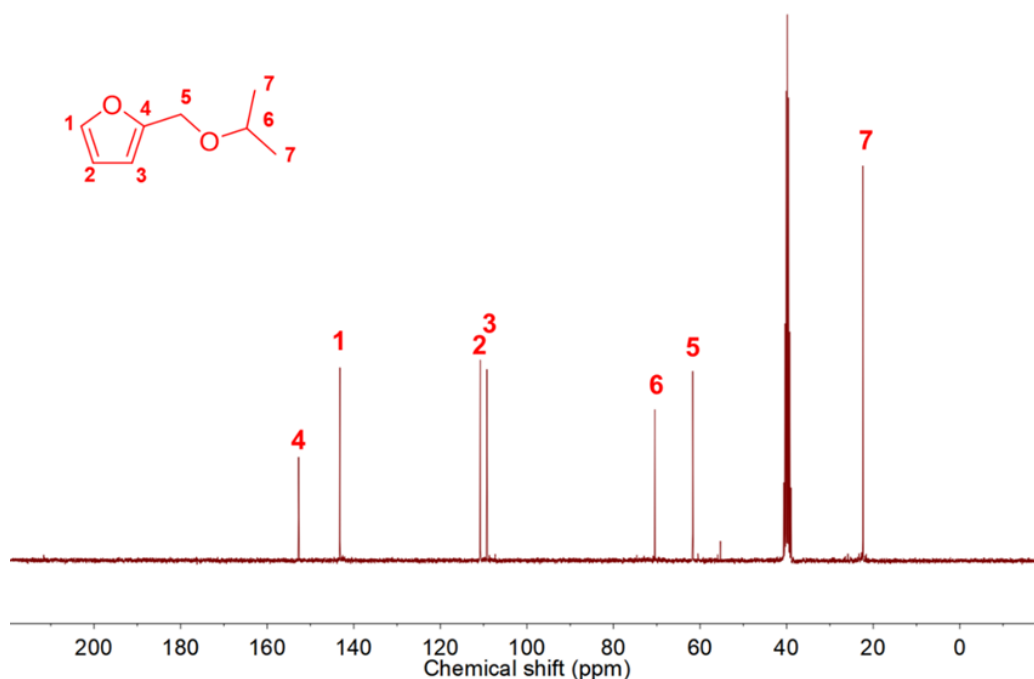


**Figure 3.9.**  $^{13}\text{C}$  NMR spectrum of purified product of 2-(isopropoxymethyl)furan after washing with  $\text{H}_2\text{O}$ .

### 3.2.2. Characterization of the catalyst

Deep characterization of the catalysts was performed in order to gain insights on the structure-activity relationships. HRTEM and EDS mapping analysis were carried out to identify the changes after modification of EtI and preferred location of the iodine species on the I-Pd/ $\text{Al}_2\text{O}_3$  catalyst (**Figure 3.10**). The particle size distribution of Pd in I-Pd/ $\text{Al}_2\text{O}_3$  catalyst was in the range of 3 ~ 5 nm, which is similar to the parent catalyst. According to HRTEM images, the distance between crystallographic planes was 0.225 nm, in a good agreement with the (111) lattice spacing (0.226 nm) of the face-centered cubic (fcc) Pd, which is in consistent with parent Pd/ $\text{Al}_2\text{O}_3$  [34]. In addition, according to **Figure 3.10d**, most intense iodine EDS signals come from the same locations as Pd and only negligible iodine is detected on the  $\text{Al}_2\text{O}_3$  support. This observation suggests

that most of iodine is adsorbed on the Pd surface and not on the support. Moreover, from EDS elemental analysis ([Table 3.3](#)), the loading of iodine on the I-Pd/Al<sub>2</sub>O<sub>3</sub> catalyst is estimated to be 0.39 wt. %, which corresponds to 0.03 mmol of iodine per 1 g of catalyst.

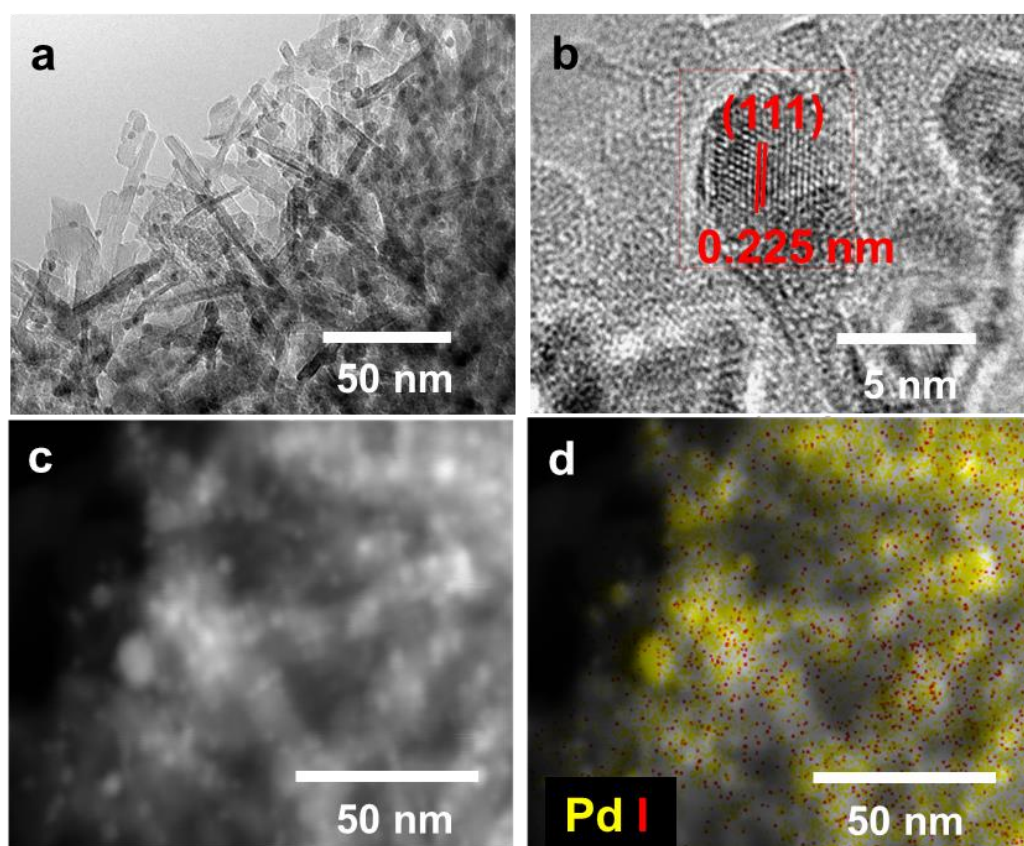


**Figure 3.10.** Characterization of I-Pd/Al<sub>2</sub>O<sub>3</sub> catalyst by TEM analysis (a) TEM image; (b) HRTEM image; (c) STEM image and (d) corresponding EDS mapping image.

**Table 3.3.** Characterizations of Pd/Al<sub>2</sub>O<sub>3</sub> and I-Pd/Al<sub>2</sub>O<sub>3</sub>.

Catalyst	Elemental analysis, wt%		Pd <sup>2+</sup> /P d, %	CO adsorption, mmol/g	H <sub>2</sub> consumption, mmol/g	Pd <sub>CO</sub> /Pd, %
	Pd	I				
	Pd/Al <sub>2</sub> O <sub>3</sub>	5				
I-Pd/Al <sub>2</sub> O <sub>3</sub>	5.7	0.39	16	0.0063	0.07	1.3

CO chemisorption analysis of I-Pd/Al<sub>2</sub>O<sub>3</sub> catalyst also suggests interaction of I species with the Pd surface atoms ([Table 3.3](#)). The CO uptake decreases from 0.14 mmol/g for

initial Pd/Al<sub>2</sub>O<sub>3</sub> to 0.0063 mmol/g for I-Pd/Al<sub>2</sub>O<sub>3</sub>. The dramatic decrease in the CO uptake indicates on deactivation of several Pd atoms by adsorbed I atoms. Interestingly, for the I-Pd/Al<sub>2</sub>O<sub>3</sub> (N<sub>2</sub>) and NaI-Pd/Al<sub>2</sub>O<sub>3</sub> samples, the CO-adsorption uptakes did not change a lot after treatment with the iodine compounds indicating that the iodine is not effectively bonded to the Pd surface (*Table 3.2*).

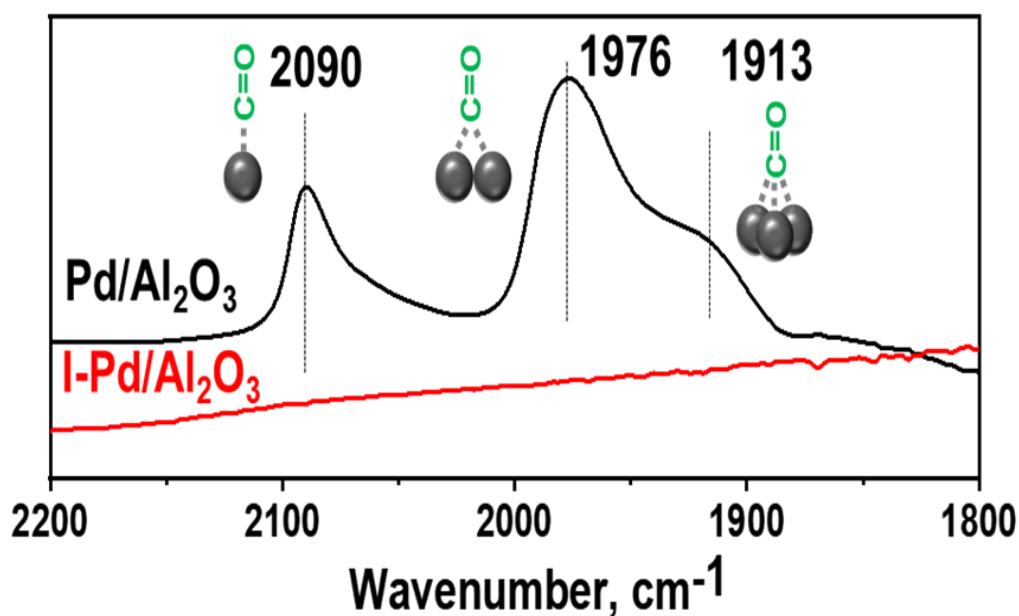


**Figure 3.11.** FTIR for CO adsorption over Pd/Al<sub>2</sub>O<sub>3</sub> and I-Pd/Al<sub>2</sub>O<sub>3</sub> under vacuum conditions.

CO-FTIR analysis was performed to confirm the interaction of CO and Pd. *Figure 3.11* shows a set of CO absorption band on initial Pd/Al<sub>2</sub>O<sub>3</sub> with linear at 2090 cm<sup>-1</sup> and bridged and multiple species at 1976 cm<sup>-1</sup> and 1913 cm<sup>-1</sup>, respectively [35]. However, there are no peaks of CO over I-Pd/Al<sub>2</sub>O<sub>3</sub>, which indicates electron withdrawing and hindrance effect of I species over Pd surface.

The electronic state of palladium and iodine in the I-Pd/Al<sub>2</sub>O<sub>3</sub> catalyst was characterized by XPS. *Figure 3.12* demonstrates Pd 3d and I 3d core level spectra of I-Pd/Al<sub>2</sub>O<sub>3</sub> before and after reaction compared with spectra of Pd/Al<sub>2</sub>O<sub>3</sub> and PdI<sub>2</sub>.

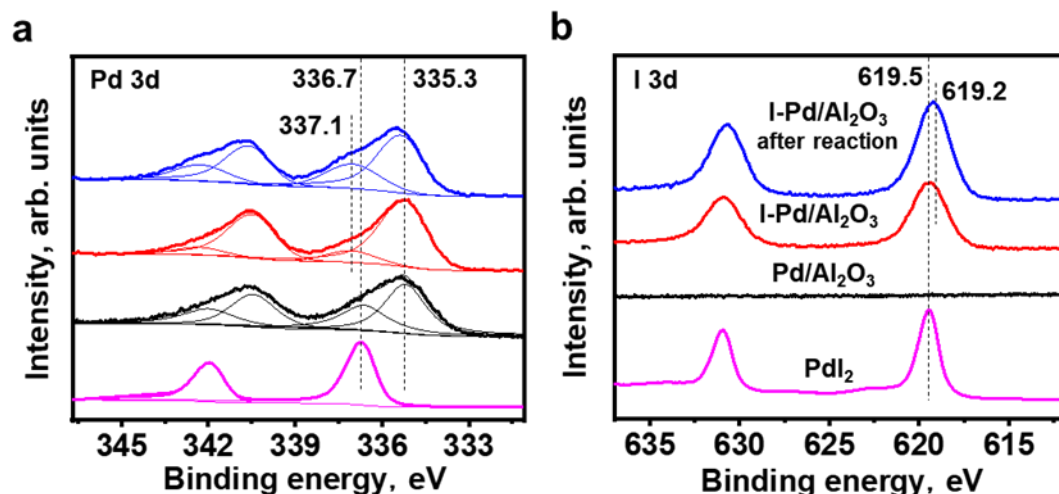


**Figure 3.12.** XPS Pd 3d (a) and I 3d (b) core level spectra of PdI<sub>2</sub>, Pd/Al<sub>2</sub>O<sub>3</sub>, I-Pd/Al<sub>2</sub>O<sub>3</sub>, and I-Pd/Al<sub>2</sub>O<sub>3</sub> after reaction.

A Pd 3d spectrum of one chemical state has 3d<sub>5/2</sub> and 3d<sub>3/2</sub> components with 5.26 eV spin-orbit splitting. Pd 3d spectrum of Pd/Al<sub>2</sub>O<sub>3</sub> catalyst, as shown in [Figure 3.12a](#), has two doublets with BE (Pd 3d<sub>5/2</sub>) 335.3 eV and 336.7 eV attributed to metallic Pd<sup>0</sup> and Pd<sup>2+</sup> (PdO) respectively [36-37]. Both of these states coexist on the surface with domination of the metallic state. A minor shift of Pd 3d peaks to higher BE for I-Pd/Al<sub>2</sub>O<sub>3</sub> catalysts (both before and after reaction) can be attributed to interaction of Pd with iodine. This interaction leads to the electron withdrawal from Pd to I. In I-Pd/Al<sub>2</sub>O<sub>3</sub> catalyst, Iodine has access to electrons from Pd nanoparticles resulting in lower electron density and partial positive charge of the Pd nanoparticles [38-39]. It is interesting that Pd<sup>2+</sup>/Pd<sup>0</sup> ratio is lower for I-Pd/Al<sub>2</sub>O<sub>3</sub> sample (before reaction) comparing to that of Pd/Al<sub>2</sub>O<sub>3</sub> (16% vs. 32%, [Table 3.3](#)). Additional information about Pd oxidation state has been obtained from H<sub>2</sub>-TPR analysis ([Figure 3.13](#)). Broad peak of hydrogen consumption over Pd/Al<sub>2</sub>O<sub>3</sub> is observed at 15 °C. For the I-Pd/Al<sub>2</sub>O<sub>3</sub> catalyst, a very weak reduction peak is observed at approximately 50 °C. The consumption of H<sub>2</sub> for



Pd/Al<sub>2</sub>O<sub>3</sub> and I-Pd/Al<sub>2</sub>O<sub>3</sub> is 0.41 and 0.07 mmol/g, respectively ([Table 3.3](#)). It also points on a lower fraction of PdO phase in I-Pd/Al<sub>2</sub>O<sub>3</sub> catalyst. This might suggest that I atoms coordinate over Pd surface and protect them from oxidation, preventing formation of PdO in I-Pd/Al<sub>2</sub>O<sub>3</sub> catalyst.

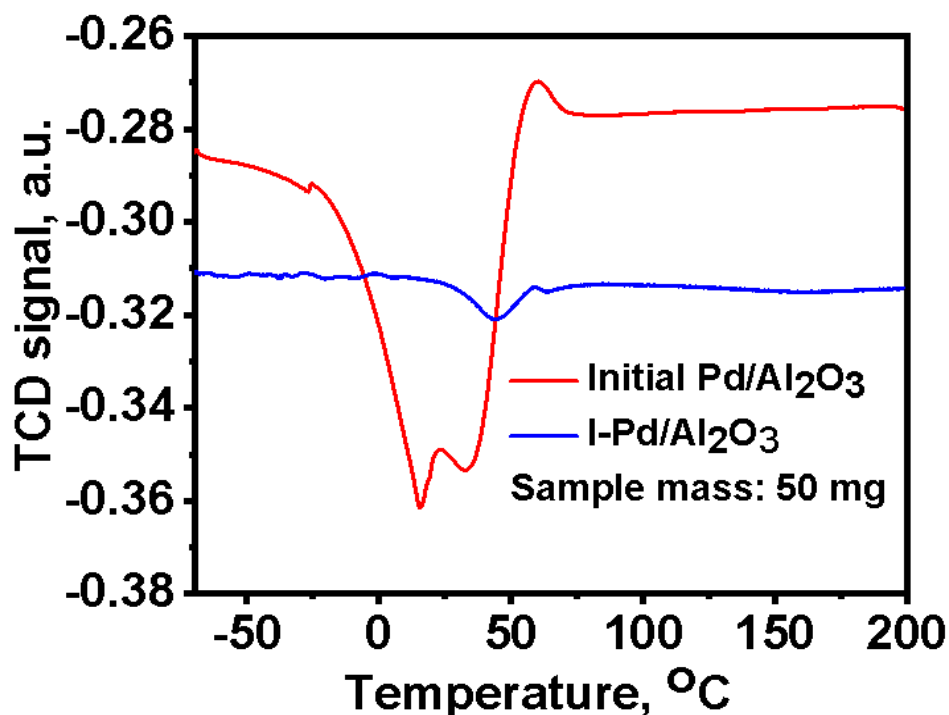


**Figure 3.13.** *H<sub>2</sub>-TPR analysis for Pd/Al<sub>2</sub>O<sub>3</sub> and I-Pd/Al<sub>2</sub>O<sub>3</sub>.*

I 3d spectra of the considered samples are shown in [Figure 3.12b](#), demonstrating 3d<sub>5/2</sub> and 3d<sub>3/2</sub> spin-orbit doublets with 11.5 eV splitting. For I-Pd/Al<sub>2</sub>O<sub>3</sub> catalyst the I 3d<sub>5/2</sub> peak BE is 619.5 eV. The I 3d<sub>5/2</sub> peak of PdI<sub>2</sub> demonstrates the same BE of 619.5 eV. The I 3d<sub>5/2</sub> BE for I atomically located on metal surfaces is expected between 618.5 and 619.7 eV <sup>[40]</sup>. An observed value within this region suggests dissociation of EtI over palladium. The relative broadening of I 3d peaks of I-Pd/Al<sub>2</sub>O<sub>3</sub> catalyst is probably a result of irregular localization of I on the planes, edges and corners of Pd nanoparticles.

I-Pd/Al<sub>2</sub>O<sub>3</sub> after reaction shows similar Pd 3d and I 3d spectra suggesting high stability of the catalyst.

### 3.2.3. Mechanism of the reaction

Acetalization of carbonyl groups is usually considered as an acid catalyzed reaction and takes place in the presence of Brønsted acid sites<sup>[19-20]</sup>. Therefore, we deduce that the generation of Brønsted acid sites in the Pd-I catalysts maybe a key step for the carbonyl group activation.

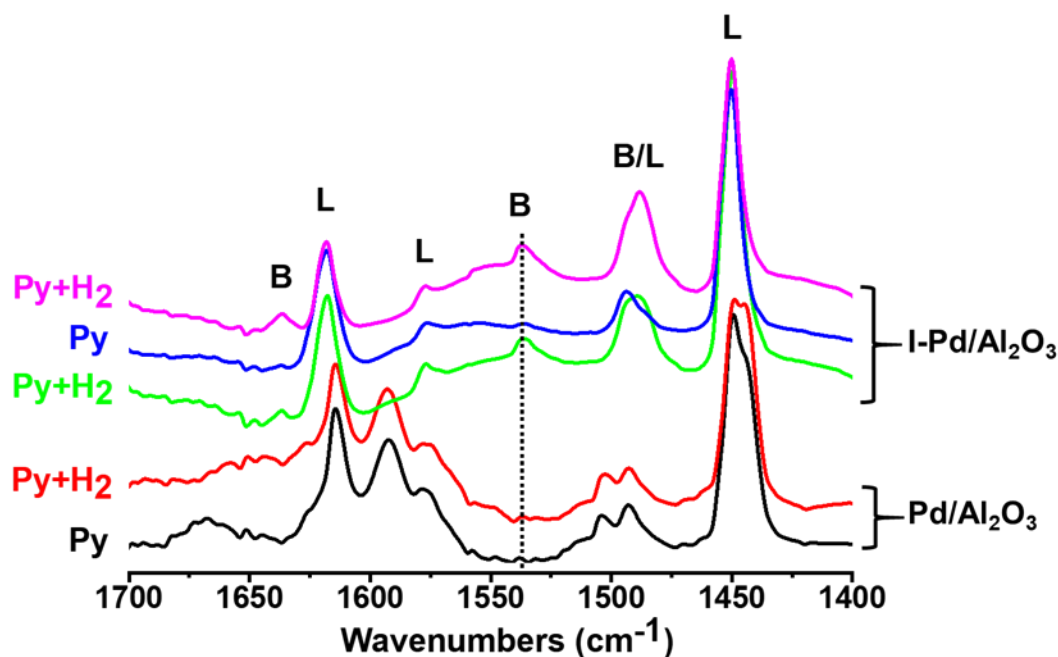


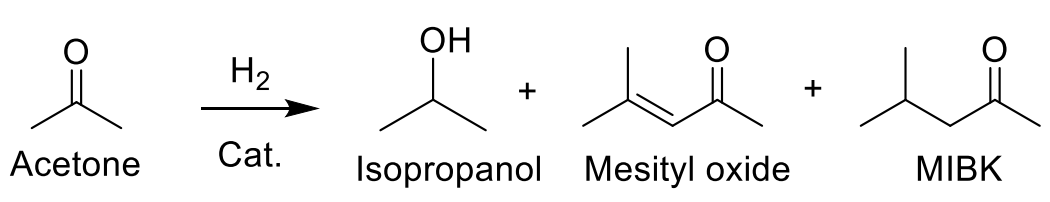
**Figure 3.14.** FTIR spectra of Py adsorption over Pd/Al<sub>2</sub>O<sub>3</sub> and I-Pd/Al<sub>2</sub>O<sub>3</sub> with and without hydrogen.

To confirm the presence of Brønsted acid sites, an in-situ pyridine-FTIR analysis was carried out on Pd/Al<sub>2</sub>O<sub>3</sub> and I-Pd/Al<sub>2</sub>O<sub>3</sub>. As shown in **Figure 3.14**, after adsorption of pyridine, both initial Pd/Al<sub>2</sub>O<sub>3</sub> and the I-Pd/Al<sub>2</sub>O<sub>3</sub> show a peak at 1450 cm<sup>-1</sup> assigned to the Lewis acid sites probably present on the Al<sub>2</sub>O<sub>3</sub> support. No peak related to the

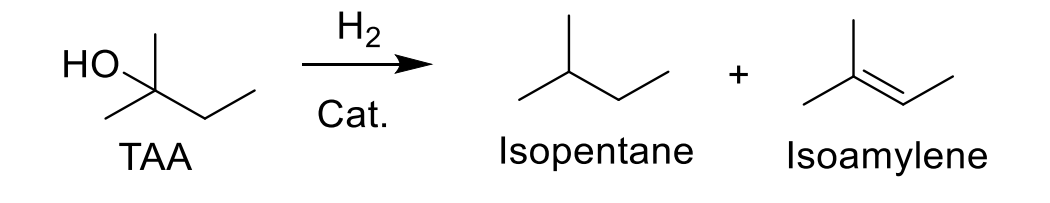
adsorption of Py over Brønsted acid sites ( $1540\text{ cm}^{-1}$ ) was detected for both catalysts [41]. Then, we added hydrogen at  $60^\circ\text{C}$  to check the acidity of I-Pd/ $\text{Al}_2\text{O}_3$  close to the reaction conditions. Surprisingly, we observed appearance of a Py-IR peak at  $1540\text{ cm}^{-1}$ . This might indicate generation of Brønsted acidity on the catalyst under hydrogen atmosphere. Removal of hydrogen from the cell led to disappearance of this peak. However, it could be recovered by dosing again hydrogen. This result indicates that the acidity generation on the Pd-I catalyst is reversible and depends on partial pressure of hydrogen. The same experiment over parent Pd/ $\text{Al}_2\text{O}_3$  did not show any effect of hydrogen on the catalyst acidity (*Figure 3.14*). Thus, the remarkable catalytic behavior of the I-Pd/ $\text{Al}_2\text{O}_3$  catalysts could be explained by considering the electronic interactions between the Pd and iodine species. After dissociation of hydrogen on the surface of Pd, a strong electron withdrawing effect of the neighboring iodine species could cause polarization of hydrogen over the Pd-I pairs. Because of the high negative charge, the adsorbed iodine atoms would favor the stabilization of  $\text{H}^+$  produced during hydrogen dissociation resulting in the generation of Brønsted acidity. Hydrogen spillover over the Pd catalyst has been demonstrated previously [42-45]. Highly mobile hydrogen can generate Brønsted acid sites on the reducible supports such as  $\text{WO}_3$  and  $\text{CeO}_2$  [45]. Iglesia [46] et al in late nineties observed generation of Brønsted acidity in the presence of  $\text{H}_2$  on  $\text{WO}_x\text{-ZrO}_2$  catalysts with polytungstate domains. The exposure to hydrogen results in a slight reduction of tungsten and delocalization of an electron from an H atom resulting in  $\text{H}^{+\delta}$  (Brønsted acid site). The catalysts developed by Iglesia are obviously rather different from our Pd-I systems. The interest and advantage of the

catalytic system presented in this work is related to the generation of acidity in-situ during the reaction directly on the metal sites. This Pd-I catalyst results in the intimacy of metal and acid functions and thus, very efficient bifunctional catalysts.

**Table 3.4.** Model reactions of acetone to methylbutyl ketone (2 g acetone, 50 mg catalyst, 20 bar  $H_2$ , 200 °C, 3 h) and tert-amyl alcohol dehydration (TAA) (2 g TAA, 50 mg catalyst, 10 bar  $H_2$ , 200 °C, 3 h)

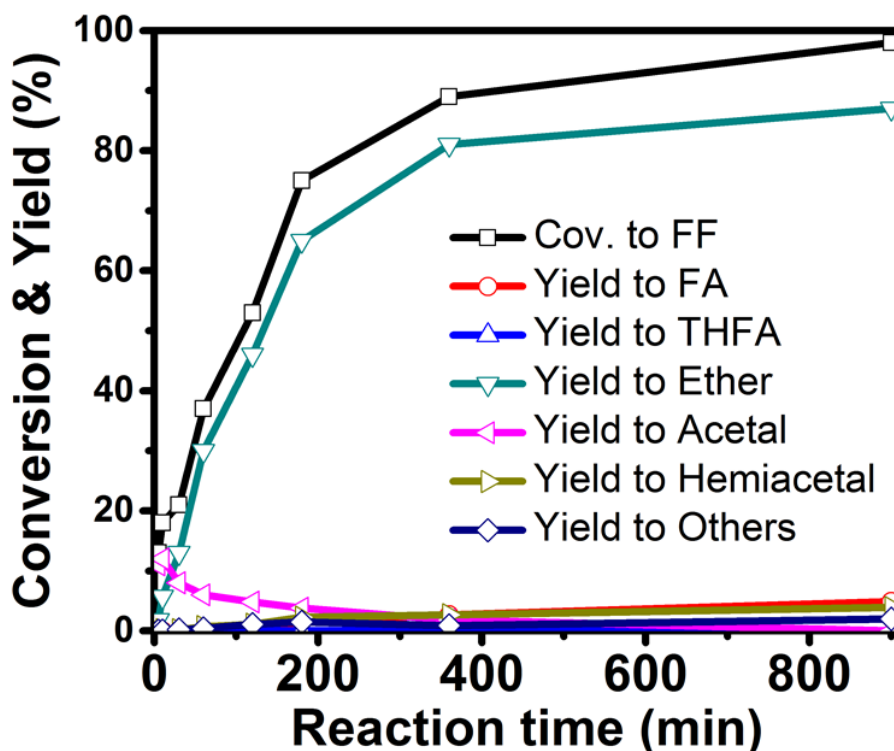
				
Catalyst	Conversion of acetone (%)	Selectivity (%)		
		Isopropanol	Mesityl oxide	MIBK
Pd/Al <sub>2</sub> O <sub>3</sub>	46.8	63.1	0	31.0
I-Pd/Al <sub>2</sub> O <sub>3</sub>	16.1	0	2.0	93.3

				
Catalyst	Conversion of TAA (%)	Selectivity (%)		
		Isopentane	Isoamylene	
Pd/Al <sub>2</sub> O <sub>3</sub>	7.1	99.9	0	
I-Pd/Al <sub>2</sub> O <sub>3</sub>	95.3	3.7	96.2	

In order to confirm generation of acidity over Pd in the presence of hydrogen, we have performed two model reactions: hydrogenation of acetone and dehydration of tert-amyl alcohol (TAA) over Pd/Al<sub>2</sub>O<sub>3</sub> before and after modification by EtI. **Table 3.4** shows that at 200 °C the non-promoted Pd/Al<sub>2</sub>O<sub>3</sub> produces isopropanol as the main product (63 %) with small amount of methyl isobutyl ketone (MIBK), which is a

product of aldol condensation of acetone. At the same time, I-Pd/Al<sub>2</sub>O<sub>3</sub> demonstrates totally different catalytic performance with high selectivity to MIBK (93 %). The aldol condensation of acetone proceeds over acid or basic sites. Dehydration of the product of condensation leads to mesityl oxide, which is hydrogenated to MIBK [47-48]. The presence of both Brønsted acid and metal sites in bifunctional catalysts such as Pd/Amberlyst-15 or Pd/zeolite is essential for this reaction. I-Pd/Al<sub>2</sub>O<sub>3</sub> provides both types of sites in close proximity to each other, which leads to the selective synthesis of MIBK.



**Figure 3.15.** Evolution of conversion of furfural and yield to various products with reaction time. Reaction conditions: 25 mg of I-Pd/Al<sub>2</sub>O<sub>3</sub>, 200 mg of furfural, 4 g of isopropanol, 60°C, 20 bar H<sub>2</sub>.

Dehydration of tert-amyl alcohol (TAA) was tested to confirm the generation of Brønsted acidity (Table 3.4). Notably, I-Pd/Al<sub>2</sub>O<sub>3</sub> exhibited high activity and selectivity

to isoamylene (Conv. 95.3% & Sel. 96.2%), while initial Pd/Al<sub>2</sub>O<sub>3</sub> has low activity with formation of isopentane as the main product. This significant difference could be ascribed to the in-situ generation of strong Brønsted acid over Pd-I active sites in the presence of hydrogen [49-50].

A feasible reaction pathway for the etherification of furfural and isopropanol on the bifunctional I-Pd/Al<sub>2</sub>O<sub>3</sub> catalyst is presented in [Figure 3.1](#). First, Brønsted acid sites (H<sup>+</sup>) are produced on the sites of adsorbed iodine atoms via hydrogen dissociation on Pd-I sites. Then, the acetal intermediates are produced via nucleophilic addition of alcohol to aldehyde catalyzed by the Brønsted acid sites.

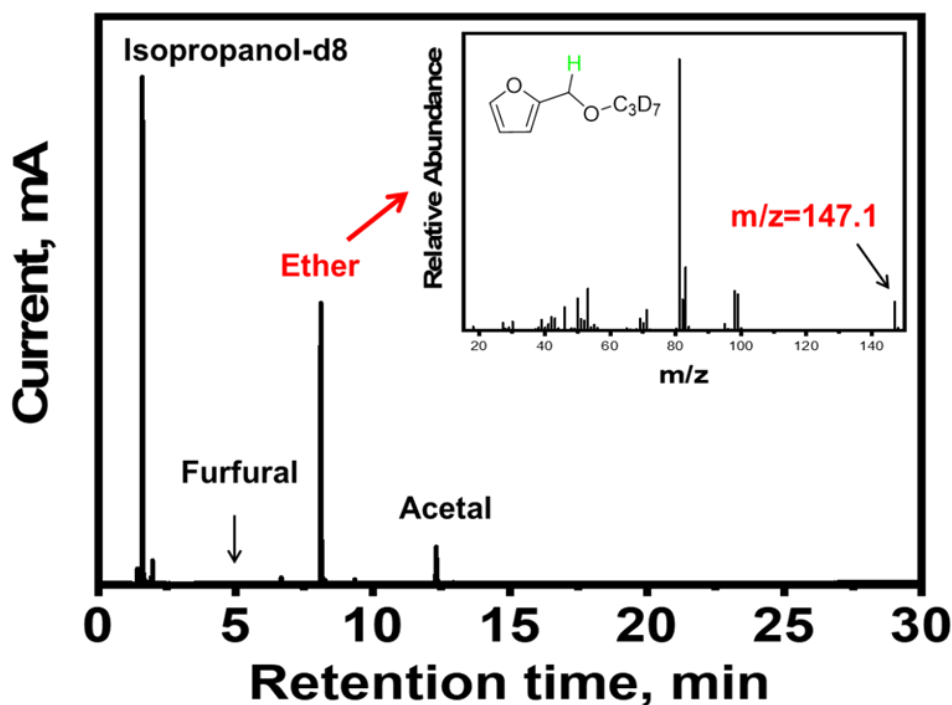


**Figure 3.16.** GC-MS analysis of isotope tracing experiment.

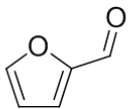
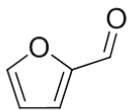
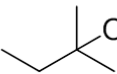
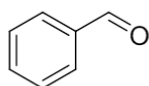
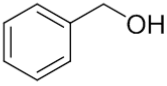
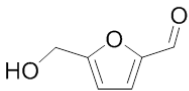
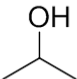
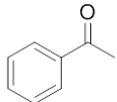
The highest selectivity to acetal is observed at the beginning of the reaction and decreases with the reaction time ([Figure 3.15](#)). Finally, the C-O bond dissociates with

formation of water and addition of H from Pd surface to form ether. This mechanism has been confirmed by isotope tracing experiment using deuterated isopropanol-d<sub>8</sub> as reagent (*Figure 3.16*). According to the literature, one of the possible routes for the reductive etherification could be catalyzed by acid sites via catalytic transfer hydrogenation of furfural by the MPV (Meerwein–Ponndorf–Verley) reduction with isopropanol as hydrogen donor with subsequent etherification of formed alcohol to the ether<sup>[10]</sup>. The presence of only <sup>1</sup>H hydrogen atom on the carbon atom in carbonyl group in furfural confirms the hydrogenolysis of grafted C-O bond and excludes the catalytic transfer hydrogenation involving deuterated isopropanol-d<sup>8</sup> and etherification pathway.

#### **3.2.4. Other substrates**

The I-Pd/Al<sub>2</sub>O<sub>3</sub> bifunctional heterogeneous catalyst was evaluated in the reductive etherification of different substrates. First, etherification of furfural with octanol also shows high selectivity to the relevant ether. This suggests that primary alcohols might be also used for the synthesis of surfactants and fuels (*Table 3.5*). Tertiary alcohol like tert-amyl alcohol has been also tested in reductive etherification of furfural. Although the catalytic activity is relatively low in comparison with other alcohols, we could observe selective formation of tert-amyl furfuryl ether. This low activity in the reaction with tertiary alcohols might be explained by difficulties in the formation of acetal-like intermediates due to steric hindrance. HMF is another valuable biomass-based product. It might be easily produced by dehydration of glucose and fructose. Reaction of HMF with isopropanol leads to the synthesis of the ethers with the selectivity close to 83 %.

**Table 3.5.** Reductive etherification of various substrates (0.1 g of aldehydes or ketones, 2 g alcohols, 50 mg Pd/Al<sub>2</sub>O<sub>3</sub> catalyst, 15 mg EtI were added in the reactor)

Aldehyde	Alcohol	Reaction conditions, T(°C)/t (h)/H <sub>2</sub> (bar)	Conv. <sup>a</sup> (%)	Sel. <sup>b</sup> (%)
	<chem>C7H15COH</chem>	60 / 15 / 20	95	95
		60/15/20	15	91
		60 / 15 / 20	52	80
		60 / 1 / 30	96	83 <sup>c</sup>
<chem>C7H15CHO</chem>	<chem>C7H15COH</chem>	60 / 15 / 20	96	92
	<chem>COH</chem>	80 / 3 / 30	61	90

<sup>a</sup> Conversion of the aldehydes or ketones

<sup>b</sup> Selectivity to corresponding ethers

<sup>c</sup> Summary selectivity of (5-(isopropoxymethyl)furan-2-yl)methanol and 2,5-bis(isopropoxymethyl)furan

The reductive etherification of an aromatic aldehyde might also be performed with an aromatic alcohol. Thus, reaction of benzyl aldehyde with benzyl alcohol leads to 80 % selectivity to benzyl ether. The possibility of self-etherification reaction has been verified by conducting the reaction without benzyl aldehyde. However, only traces of benzyl ether have been produced in this case. Substitution of an aromatic aldehyde by aliphatic 1-octanal also results in selective synthesis of ether (92 %). Acetophenone also selectively reacts with methanol. All these results demonstrate versatility of the Pd-I



catalyst, which can produce corresponding ethers from a variety of aldehydes and ketones.

### **3.3. Conclusion**

To conclude, modification of Pd catalysts by treatment with organic iodine compounds in hydrogen leads to surface modification of Pd. The resulting Pd-I bifunctional heterogeneous catalyst generates Brønsted acidity in-situ in the presence of hydrogen. The acid sites associated with adsorbed I species and Pd metal active sites are located in close proximity over the supported Pd nanoparticles. The newly designed bifunctional heterogeneous Pd-I catalysts showed high reductive etherification activity and selectivity even at ambient temperature. Numerous aldehydes and ketones reacted on the Pd-I bifunctional catalysts with alcohols at very mild reaction conditions yielding corresponding ethers with extremely high selectivity.

## Reference

1. Corma, A.; Iborra, S.; Velty, A. Chemical Routes for the Transformation of Biomass into Chemicals. *Chem. Rev.* **2007**, *107*, 2411-2502.
2. Chheda, J. N.; Huber, G. W.; Dumesic, J. A. Liquid-Phase Catalytic Processing of Biomass-Derived Oxygenated Hydrocarbons to Fuels and Chemicals. *Angew. Chem., Int. Ed. Engl.* **2007**, *46*, 7164-7183.
3. Chaffey, D. R.; Davies, T. E.; Taylor, S. H.; Graham, A. E. Etherification Reactions of Furfuryl Alcohol in the Presence of Orthoesters and Ketals: Application to the Synthesis of Furfuryl Ether Biofuels. *ACS Sustainable Chem. Eng.* **2018**, *6*, 4996-5002.
4. Feuer, H.; Hooz, J. Methods of Formation of the Ether Linkage. *In The Ether Linkage (1967)*, S. Patai ed.; **2010**.
5. Larmier, K.; Chizallet, C.; Maury, S.; Cadran, N.; Abboud, J.; Lamic-Humblot, A. F.; Marceau, E.; Lauron-Pernot, H. Isopropanol Dehydration on Amorphous Silica-Alumina: Synergy of Brønsted and Lewis Acidities at Pseudo-Bridging Silanols. *Angew. Chem., Int. Ed. Engl.* **2017**, *56*, 230-234.
6. Bringue, R.; Tejero, J.; Iborra, M.; Izquierdo, J.; Fite, C.; Cunill, F. Supported Nafion Catalyst for 1-Pentanol Dehydration Reaction in Liquid Phase. *Chem. Eng. J.* **2008**, *145*, 135-141.
7. Williamson, A. W., XXII.-On etherification. *Quarterly Journal of the Chemical Society of London* **1852**, *4*, 229-239.
8. Dermer, O. C. Metallic Salts of Alcohols and Alcohol Analogs. *Chem. Rev.* **1934**, *14*, 385-430.
9. Balakrishnan, M.; Sacia, E. R.; Bell, A. T. Etherification and Reductive Etherification of 5-(Hydroxymethyl)furfural: 5-(Alkoxymethyl)furfurals and 2,5-Bis(alkoxymethyl)furans as Potential Bio-diesel Candidates. *Green Chem.* **2012**, *14*, 1626-1634.
10. Shinde, S.; Rode, C. Cascade Reductive Etherification of Bioderived Aldehydes over Zr-Based Catalysts. *ChemSusChem* **2017**, *10*, 4090-4101.
11. Jadhav, D.; Grippo, A. M.; Shylesh, S.; Gokhale, A. A.; Redshaw, J.; Bell, A. T. Production of Biomass-Based Automotive Lubricants by Reductive Etherification. *ChemSusChem* **2017**, *10*, 2527-2533.
12. Zhao, C.; Sojda, C. A.; Myint, W.; Seidel, D. Reductive Etherification via Anion-Binding Catalysis. *J. Am. Chem. Soc.* **2017**, *139*, 10224-10227.
13. Nguyen, H.; Xiao, N.; Daniels, S.; Marcella, N.; Timoshenko, J.; Frenkel, A.; Vlachos, D. G. Role of Lewis and Brønsted Acidity in Metal Chloride Catalysis in Organic Media: Reductive Etherification of Furanics. *ACS Catal.* **2017**, *7*, 7363-7370.
14. Jennifer, D. L.; Stijn, V. V.; Anthony, J. C.; William, R. G.; Vladimir, K. M.; Robert, G. G.; Yuriy, R. L. A Continuous Flow Strategy for the Coupled Transfer Hydrogenation and Etherification of 5-(Hydroxymethyl)furfural using Lewis Acid

- Zeolites. *ChemSusChem* **2014**, *7*, 2255-2265.
15. Jungho, J.; Eyas, M.; Raul, F. L.; Dionisios; G. V. Cascade of Liquid-Phase Catalytic Transfer Hydrogenation and Etherification of 5-Hydroxymethylfurfural to Potential Biodiesel Components over Lewis Acid Zeolites. *ChemCatChem* **2014**, *6*, 508-513.
  16. Wang, Y.; Cui, Q.; Guan, Y.; Wu, P. Facile Synthesis of Furfuryl Ethyl Ether in High Yield via the Reductive Etherification of Furfural in Ethanol over Pd/C under Mild Conditions. *Green Chem.* **2018**, *20*, 2110-2117.
  17. Basu, M. K.; Samajdar, S.; Becker, F. F.; Banik, B. K. A New Molecular Iodine-Catalyzed Acetalization of Carbonyl Compounds. *Synlett.* **2002**, 319-321.
  18. Yoshimura, A.; Zhdankin, V. V. Advances in Synthetic Applications of Hypervalent Iodine Compounds. *Chem. Rev.* **2016**, *116*, 3328-435.
  19. Breugst, M.; von der Heiden, D. Mechanisms in Iodine Catalysis. *Chemistry* **2018**, *24*, 9187-9199.
  20. von der Heiden, D.; Bozkus, S.; Klusmann, M.; Breugst, M. Reaction Mechanism of Iodine-Catalyzed Michael Additions. *J. Org. Chem.* **2017**, *82*, 4037-4043.
  21. Kahsar, K. R.; Schwartz, D. K.; Medlin, J. W. Control of Metal Catalyst Selectivity through Specific Noncovalent Molecular Interactions. *J. Am. Chem. Soc.* **2014**, *136*, 520-526.
  22. Liu, P.; Qin, R.; Fu, G.; Zheng, N. Surface Coordination Chemistry of Metal Nanomaterials. *J. Am. Chem. Soc.* **2017**, *139*, 2122-2131.
  23. Zhang, J.; Ellis, L. D.; Wang, B.; Dzara, M. J.; Sievers, C.; Pylypenko, S.; Nikolla, E.; Medlin, J. W. Control of Interfacial Acid-Metal Catalysis with Organic Monolayers. *Nat. Catal.* **2018**, *1*, 148-155.
  24. Lange, J. P. Renewable Feedstocks: The Problem of Catalyst Deactivation and its Mitigation. *Angew. Chem., Int. Ed. Engl.* **2015**, *54*, 13186-13197.
  25. Liu, Q.; Bauer, J. C.; Schaak, R. E.; Lunsford, J. H. Supported Palladium Nanoparticles: An Efficient Catalyst for the Direct Formation of H<sub>2</sub>O<sub>2</sub> from H<sub>2</sub> and O<sub>2</sub>. *Angew. Chem., Int. Ed. Engl.* **2008**, *47*, 6221-6224.
  26. Zaera, F. Preparation and Reactivity of Alkyl Groups Adsorbed on Metal Surfaces. *Acc. Chem. Res.* **1992**, *25*, 260-265.
  27. Beatriz, C. Bravo.; Susan, L. M.; Manuel, P. S. Anodic Underpotential Deposition and Cathodic Stripping of Iodine at Polycrystalline and Single-crystal Gold Studies by LEED, AES, XPS, and Electrochemistry. *J. Phys. Chem.* **1991**, *95*, 5245-5249.
  28. Ayyoub, S.; Natalie, A. L.; Delphine, F.; Olivier, C.; Farid, C.; Mohamed, T. A Comparative Study of Solvent-Free and Highly Efficient Pinene Hydrogenation over Pd on Carbon, Alumina, and Silica Supports. *Org. Process Res. Dev.* **2017**, *21*, 60-64.
  29. Joyee, M.; Xiaoyuan, Z.; Thomas, R. Pd/C-Catalyzed Reactions of HMF: Decarbonylation, Hydrogenation and Hydrogenolysis. *Green Chem.* **2015**, *17*, 307-313.
  30. Richard, M. P.; George, W. K.; Richard, B.; Kevan, G.; Lyman, J. S.; Richard, C.;

- Christopher, D.; Donna, G.; Steven, L.; Teresa, L. Reactions of Unsaturated Compounds with Iodine and Bromine on  $\gamma$  Alumina. *J. Org. Chem.* **1988**, *53*, 4477-4482.
31. Md, R. R.; Mantu, R.; Badaker, M. L.; Priti, R. S.; Bekington, M. Iodine-Alumina as an Efficient and Useful Catalyst for the Regeneration of Carbonyl Functionality from the Corresponding 1,3-Oxathiolanes and. 1,3-Dithiolanes in Aqueous System. *Tetrahedron Lett.* **2010**, *51*, 2862-2864.
32. Nabajyoti, D.; Jadab, C. S. Highly Efficient Dithioacetalization of Carbonyl Compounds Catalyzed with Iodine Supported on Neutral Alumina. *Chem. Lett.* **2001**, *30*, 794-795.
33. Ira S.; Dilip C. B.; Jadab C. S. Three Component Condensations Catalyzed by Iodine-Alumina for the Synthesis of Substituted 3,4-Dihydropyrimidin-2(1H)-ones under Microwave Irradiation and Solvent-Free Conditions. *Tetrahedron Lett.* **2005**, *46*, 1150-1160.
34. Xiong, Y.; Cai, H.; Wiley, B. J.; Wang, J.; Kim, M. J.; Xia, Y. Synthesis and Mechanistic Study of Palladium Nanobars and Nanorods. *J. Am. Chem. Soc.* **2007**, *129*, 3665-3675.
35. M, Benkhalede.; S, Morin.; Ch, Pichon.; C, Thomazeau.; C, Verdon.; D, Uzio. Synthesis of Highly Dispersed Palladium Alumina Supported Particles: Influence of the Particle Surface Density on Physico-Chemical Properties. *Appl. Catal., A.* **2006**, *312*, 1-11.
36. Bhogeswararao, S.; Srinivas, D. Catalytic Conversion of Furfural to Industrial Chemicals over Supported Pt and Pd Catalysts. *J. Catal.* **2015**, *327*, 65-77.
37. Yong, W.; Jia, Yao.; Haoran, Li.; Dangsheng, Su.; Markus, A. Highly Selective Hydrogenation of Phenol and Derivatives over a Pd@Carbon Nitride Catalyst in Aqueous Media. *J. Am. Chem. Soc.* **2011**, *133*, 2362-2365.
38. Komanoya, T.; Kinemura, T.; Kita, Y.; Kamata, K.; Hara, M. Electronic Effect of Ruthenium Nanoparticles on Efficient Reductive Amination of Carbonyl Compounds. *J. Am. Chem. Soc.* **2017**, *139*, 11493-11499.
39. Nieminen, V.; Honkala, K.; Taskinen, A.; Murzin, D. Y. Intrinsic Metal Size Effect on Adsorption of Organic Molecules on Platinum. *J. Phys. Chem. C* **2008**, *112*, 6822-6831.
40. Kovh, I.; Solymosi, F. Thermal and Photoinduced Dissociation of C<sub>2</sub>H<sub>5</sub>I To Yield C<sub>2</sub>H<sub>5</sub> on a Pd(100) Surface. *J. Phys. Chem.* **1993**, *97*, 11056-11063.
41. An, J.; Wang, Y.; Lu, J.; Zhang, J.; Zhang, Z.; Xu, S.; Liu, X.; Zhang, T.; Gocyla, M.; Heggen, M.; Dunin-Borkowski, R. E.; Fornasiero, P.; Wang, F. Acid-Promoter-Free Ethylene Methoxycarbonylation over Ru-Clusters/Ceria: The Catalysis of Interfacial Lewis Acid-Base Pair. *J. Am. Chem. Soc.* **2018**, *140*, 4172-4181.
42. Yang, R. T.; Wang, Y. Catalyzed Hydrogen Spillover for Hydrogen Storage. *J. Am. Chem. Soc.* **2009**, *131*, 4224-4226.
43. Du, A. J.; Smith, S. C.; Yao, X. D.; Lu, G. Q. Hydrogen Spillover Mechanism on a Pd-Doped Mg Surface as Revealed by ab initio Density Functional Calculation. *J.*

- Am. Chem. Soc.* **2007**, *129*, 10201-10204.
44. Conner, W. C.; Falconer, J. L. Spillover in Heterogeneous Catalysis. *Chem. Rev.* **1995**, *95*, 759-788.
  45. Prins, R. Hydrogen Spillover. Facts and Fiction. *Chem. Rev.* **2012**, *112*, 2714-2738.
  46. David, G. B.; Max, S.; Ryan, D. W.; Stuart, L. S.; Enrique, I. Structure and Electronic Properties of Solid Acids Based on Tungsten Oxide Nanostructures. *J. Phys. Chem. B* **1999**, *103*, 630-640.
  47. Gamman, J. J.; Jackson, S. D.; Wigzell, F. A. Synthesis of Methyl Isobutyl Ketone over Pd/MgO/SiO<sub>2</sub>. *Ind. Eng. Chem. Res.* **2010**, *49*, 8439-8443.
  48. Wang, P.; Bai, S.; Zhao, J.; Su, P.; Yang, Q.; Li, C. Bifunctionalized Hollow Nanospheres for the One-Pot Synthesis of Methyl Isobutyl Ketone from Acetone. *ChemSusChem* **2012**, *5*, 2390-2396.
  49. Gates, B. C.; Wisnouskas J. S.; Heath, H. W. The Dehydration of t-Butyl Alcohol Catalyzed by Sulfonic Acid Resin. *J. Catal.* **1972**, *24*, 320-327.
  50. Josef, M.; Chelsey, D. B.; Marcos, M. L.; Stuart, L. S.; Yong, W.; Enrique, I. Support Effects on Brønsted Acid Site Densities and Alcohol Dehydration Turnover Rates on Tungsten Oxide Domains. *J. Catal.* **2004**, *227*, 479-491.



#### **4. Dual Metal-Acid Pd-Br Catalyst for Selective Hydrodeoxygenation of 5-Hydroxymethylfurfural (HMF) to 2, 5-Dimethylfuran at Ambient Temperature**

##### **ABSTRACT.**

Supported metal catalysts have found broad applications in heterogeneous catalysis. Traditionally, there have been two ways to the modify the catalytic performance of supported metal catalysts in multistage reactions. The first way is related to the modification of the intrinsic activity of the existing active metal sites by inorganic or organic promoters. The second way is relevant to the design of a bifunctional catalyst, containing two types of active sites. In the conventional bifunctional catalyst, the active metal sites are associated with the metal nanoparticles, while the acid sites are usually localized over the oxide support. Herein, we report a new type of supported metal bifunctional catalyst, which combined the advantages of the promotion and bifunctionality. The catalyst was designed by the pretreatment of supported palladium catalysts with bromobenzene compounds. The addition of bromine results in two simultaneous effects. First, the activity of metal sites has been tuned by the bromine promoter. Second, the promotion with bromine creates new Brønsted acid sites, which are localized directly on the surface of metal nanoparticles. An intimacy between metal and acid functions in this new bifunctional catalyst generates unique catalytic properties in hydrodeoxygenation of 5-hydroxymethylfurfural to dimethylfuran, occurring with

the yield up to 96 % at ambient temperature under 5 bar of H<sub>2</sub>. The catalyst exhibits stable catalytic performance.

**KEYWORDS.** Heterogeneous catalysis; Bifunctional catalysis; Biomass; Hydrodeoxygenation; Dimethylfuran.

Some content in chapter have been published in the following publications:

Dan Wu, Songwei Zhang, Willinton Y. Hernández, Walid Baaziz, Ovidiu Ersen, Maya Marinova, Andrei Y. Khodakov\*, and Vitaly V. Ordomsky\*. *ACS Catalysis*, under revision.



## 4.1. Introduction

Chemical reactions over heterogeneous catalysts usually involves multiple steps which may occur over different active sites. A rational combination of different active sites in one catalytic process for chemoselective transformation is highly desired [1-3]. While noble metal catalyst is active for hydrogenation, acid catalysts are effective for isomerization, dehydration and condensation [4-5]. Bifunctional metal-acid catalysts containing both metal and acid sites have been developed and widely applied for numerous important processes including conversion of biomass-derived platform molecules [6-9]. 5-hydroxymethylfurfural (HMF), which is produced from the abundant lignocellulosic biomass, has attracted intensive attention because of its conversion to value-added chemicals such as 2,5-bis(hydroxymethyl)furan (BHMF), 2,5-bis(hydroxymethyl)tetrahydrofuran (DHMTTHF) and 2,5-dimethylfuran (DMF) [10-14]. Among them, DMF has been proposed as a promising renewable transportation fuel due to its high boiling point, high energy density, high octane number and low water solubility [14]. Besides, DMF can be converted to *p*-xylene (PX) via Diels-Alder reactions, which is an important raw material in the production of polyethylene terephthalate (PET) [15-17].

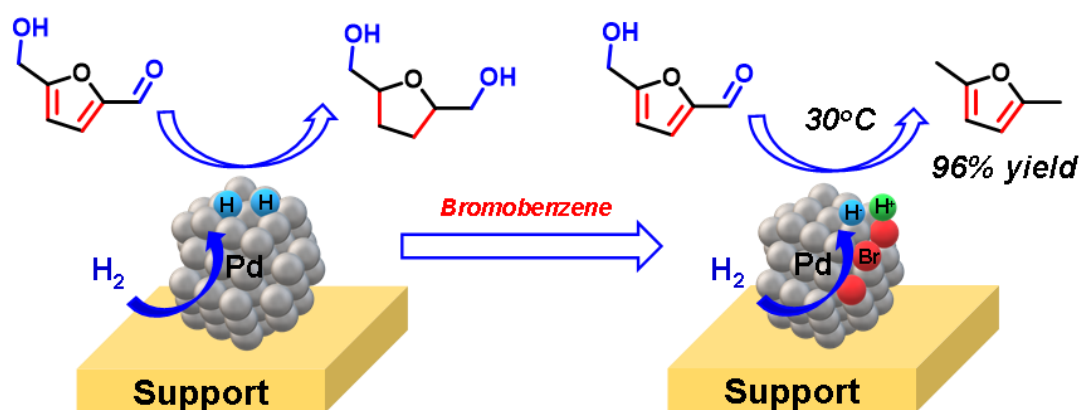
There are two groups of catalysts which have been proposed for conversion of HMF to DMF: 1) Pd, Pt, Ru, Ir, Co, Ni and Cu-based monometallic or bimetallic catalysts, which perform hydrogenolysis of C-O bond at the temperatures in the range of 150~250 °C. [14, 18-23] and 2) bifunctional metal-acid catalysts for hydrodeoxygenation through

protonation of the hydroxyl groups and dehydration at milder reaction conditions (60 ~ 130 °C) [24-32]. The disadvantage of the first route is that the high reaction temperature induces polymerization of highly reactive HMF to humins [33]. The best performance has been achieved so far over metal-based catalysts in the presence of homogeneous acids, however, this strategy induces environmental problems related to separation, recycling of acid solutions and corrosion of equipment [24-27].

Traditional heterogeneous bifunctional metal catalysts with acidic supports have been reported for production of DMF from HMF at mild conditions [28-32, 50]. Zu et al. have developed a heterogeneous Ru/Co<sub>3</sub>O<sub>4</sub> catalyst for hydrodeoxygenation of HMF to DMF and unveiled that Ru was responsible for hydrogenation of carbonyl groups to the hydroxyl groups, while CoO<sub>x</sub> species played an important role in the hydrogenolysis of hydroxyl groups to methyl groups [28]. A 93.4% yield was achieved at the temperature of 130 °C. Bifunctional Pd-Cs<sub>2.5</sub>H<sub>0.5</sub>PW<sub>12</sub>O<sub>40</sub>/K10 clay has been found as an efficient catalyst for HMF deoxygenation [29]. With the rapid hydrogenolysis rate facilitated by the acidic support, a yield up to 80 % could be obtained at 90 °C. Note that in the conventional catalysts, metal and acid functions are spatially separated. Metal sites are localized over metal nanoparticles, while acid sites are related to the zeolite phase. It has been shown that to the relative proximity of metal sites in the Pt/Al<sub>2</sub>O<sub>3</sub> catalysts modified by phosphonic acid could significantly improve the selectivity and activity towards hydrodeoxygenation (HDO) of alcohols [34]. Traditional bifunctional metal-acid catalysts such as metals supported over zeolites, cannot therefore provide a high

level of intimacy between metal and acid sites for deoxygenation and result in undesirable hydrogenation and polymerization reactions [28-32].

Combining metal and acid properties in a close proximity over the surface of metal nanoparticles could provide a breakthrough in development of highly efficient processes for deoxygenation reactions [35]. These sites would allow at the same time hydrogenation or carbonyl group, protonation, dehydration and hydride addition as the final step (*Scheme 4.1*). Our approach here relies on the deposition of electronegative Br atoms over Pd surface by bromobenzene hydrogenolysis, which induces generation of strong Brønsted acidity by hydrogen dissociation over Pd. These dual sites enable extremely selective hydrodeoxygenation of HMF to DMF at ambient temperature which has been achievable so far.



*Scheme 4.1.* HMF deoxygenation over Pd-Br catalyst via heterolytic dissociation of hydrogen.

## 4.2. Results and discussions

### 4.2.1. HMF deoxygenation over the Pd-Br catalyst at 60°C

**Table 4.1.** Conversion of HMF over palladium catalysts under different conditions. Unless stated otherwise, the reaction conditions were as follows: 50 mg catalyst, 10  $\mu$ l BrBen, 5 g THF, 100 mg HMF, 20 bar H<sub>2</sub>, 60 °C, 1h.

Reaction scheme showing the conversion of HMF (blue) to BHMF (blue), MFA (blue), and DMF (blue). BHMF is further converted to MTHFA (red) and DMTHF (red). BHMF is also converted to BHMTHF (red), which is then converted to HT (red).

Entry	Catalysts	Ad.	Conv.	Selectivity					
				HMF	BHMF	MFA	DMF	BHMTHF	HT
Pd catalysts with and without BrBen									
1	Pd/Al <sub>2</sub> O <sub>3</sub>	-	100	0	0	0	60.8	29.5	9.7
2	Pd/Al <sub>2</sub> O <sub>3</sub>	BrBen	100	0	1.2	96.7	0	0	2.1
3	Pd/Al <sub>2</sub> O <sub>3</sub> <sup>1</sup>		85.1	0	0	0	72.1	26.9	1.0
4	Pd/Al <sub>2</sub> O <sub>3</sub> <sup>1</sup>	BrBen	76.5	16.0	30.8	52.8	0	0	0.4
5	Pd/C	-	100	0	0	0	42.8	41.3	15.9
6	Pd/C	BrBen	100	0	1.4	94.9	0	0	3.7
7	Pd/SiO <sub>2</sub>	-	100	0	0	0	49.8	45.6	4.6
8	Pd/SiO <sub>2</sub>	BrBen	100	0	2.5	97.1	0	0	0.4
9	Pd black	-	94.2	0	0	0	81.3	18.6	0.1
10	Pd black	BrBen	85.6	4.4	12.5	82.1	0	0	1.0
11	-	BrBen	0.7	-	-	-	-	-	-
Heterogeneous Pd-Br catalysts									
12	Br-Pd/Al <sub>2</sub> O <sub>3</sub>	-	77.6	47.9	11.2	40.8	0	0	0.1
13	Br-Pd/C	-	66.9	63.6	8.5	26.8	0	0	1.1
14	Br-Pd/SiO <sub>2</sub>	-	86.5	19.0	34.3	46.5	0	0	0.2
15	Br-Pd black	-	34.7	57.4	18.6	23.1	0	0	0.9
Other Br sources <sup>2</sup>									
16	Pd/Al <sub>2</sub> O <sub>3</sub>	NH <sub>4</sub> Br	79.1	40.3	0.8	0	37.1	17.3	4.5
17	Pd/Al <sub>2</sub> O <sub>3</sub>	C <sub>16</sub> H <sub>33</sub> Br	61.9	12.7	0	0	62.2	21.2	3.9
Other halogens <sup>3</sup>									
18	Pd/Al <sub>2</sub> O <sub>3</sub>	ClBen	100	1.2	15.4	30.1	19.7	25.0	8.6
19	Pd/Al <sub>2</sub> O <sub>3</sub>	IBen	0.8	-	-	-	-	-	-
Ambient temperature <sup>4</sup>									
20	Pd/Al <sub>2</sub> O <sub>3</sub>		100	0	0	0	90.2	5.6	4.2
21	Pd/Al <sub>2</sub> O <sub>3</sub>	BrBen	100	0.6	1.5	95.3	0	0	2.6

22	Br-Pd/Al <sub>2</sub> O <sub>3</sub>	100	0	2.6	96.1	0	0	1.3
----	--------------------------------------	-----	---	-----	------	---	---	-----

1. The reactions were performed for 30 min.
2. NH<sub>4</sub>Br and C<sub>16</sub>H<sub>33</sub>Br were added for 15 mg in the reaction mixture, respectively.
3. ClBen and IBen were added for 10  $\mu$ l in the reaction mixture, respectively.
4. The reaction was performed at 30 °C with 5 bars of external H<sub>2</sub> pressure for 6 hours.

Hydrogenation of HMF has been conducted at 60 °C under 20 bar of H<sub>2</sub> pressure for 1 h both over promoted and unpromoted Pd catalysts. First of all, hydrogenation of HMF was performed over the non-promoted 5 wt% Pd/Al<sub>2</sub>O<sub>3</sub> catalyst. In agreement with previous reports, the main products were BHMTHF and 1,2,6-hexanetriol (HT), respectively, representing the strong hydrogenation and hydrogenolysis abilities of Pd (*Table 4.1, Entry 1*)<sup>[36]</sup>. The main reaction products are given in *Table 4.1*. Surprisingly, when 10  $\mu$ l of BrBen was added, the product distribution has changed to mainly DMF with 96.7% yield (*Table 4.1, Entry 2*). The promotion effect of BrBen could be observed as well for other Pd catalysts supported over SiO<sub>2</sub> (Pd/SiO<sub>2</sub>) and C (Pd/C) (*Table 4.1, Entry 5-10*). The non-supported Pd without promoter also provides BHMTHF as the main product (selectivity of 81.3%), while DMF was the dominant product in the presence of BrBen (selectivity of 82.1%). It is worth noting that without Pd, BrBen cannot catalyze the transformation of HMF (*Table 4.1, Entry 11*). These results confirm that BrBen totally changes the selectivity patterns during HMF hydrogenation over both supported and non-supported Pd catalysts. The effect seems to be not related to the catalytic support.

To clarify the effect of Br on the catalytic system, we have performed the pre-treatment of Pd catalysts by BrBen and hydrogen without HMF in the reactor. After the pretreatment, the Br-Pd/Al<sub>2</sub>O<sub>3</sub>, Br-Pd/C, Br-Pd/SiO<sub>2</sub> catalysts and Br-Pd black have

been separated from the liquid phase, thoroughly washed and tested in the conversion of HMF (*Table 4.1, Entry 12-15*). Interestingly, although the pre-treated catalyst showed a lower activity at the same reaction conditions in comparison to the non-modified catalyst in the presence of BrBen, the selectivity has totally changed. The main products of the reaction over the non-promoted Pd catalysts were BHMTHF and HT. Over the pre-modified Pd-Br catalysts, the product distribution has changed to BHMF, MFA and DMF. It is worth noting that BHMF and MFA can be considered as intermediates for hydrodeoxygenation of HMF to DMF [37]. They exhibit high selectivity over Pd/Al<sub>2</sub>O<sub>3</sub> at lower conversion in the presence of BrBen (*Table 4.1, Entry 3-4*).

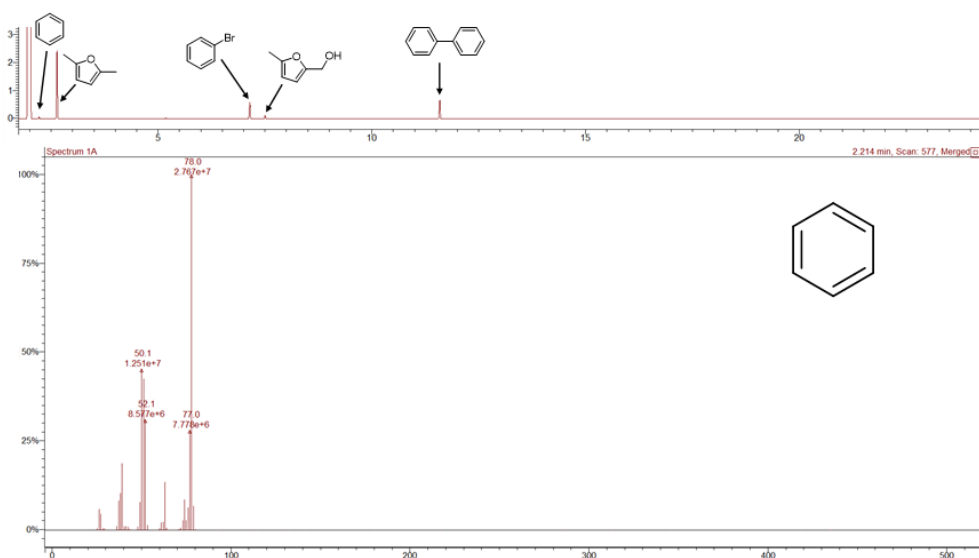


**Figure 4.1.** GC-MS analysis for the liquid-phase from HMF hydrodeoxygenation over Pd/Al<sub>2</sub>O<sub>3</sub> promoted with BrBen.

To investigate the mechanism of promotion of Pd/Al<sub>2</sub>O<sub>3</sub> using BrBen, the reaction mixture after catalysis has been analyzed by GC-MS. The presence of benzene in the reaction mixture indicates the dehalogenation of BrBen over the Pd surface (*Figure*

**4.1).** Therefore, it is rationally to suspect that the hydrogenolysis of BrBen over Pd surface leads to the modification of Pd surface with Br atoms and the newly formed Pd-Br sites could be responsible for the changes of selectivity during the conversion of HMF.

### **4.2.2. HMF deoxygenation at ambient temperature**

HMF is a complex biomass-based molecule, which is not stable during thermochemical reactions due to fast condensation reactions [38-39]. Thus, it would be highly desirable to perform hydrodeoxygenation at ambient reaction conditions where condensation does not take place. Hydrogenation of HMF at mild reaction conditions over Br-Pd/Al<sub>2</sub>O<sub>3</sub> catalyst has been performed at 30 °C and 5 bar of H<sub>2</sub> for 6 h. These are rather mild conditions in comparison with the 1 h tests performed at 60 °C and 20 bar of H<sub>2</sub>. Even at such mild conditions, HMF could be converted to DMF with yield of 95.3 % over the Br-Pd/Al<sub>2</sub>O<sub>3</sub> catalyst prepared by pre-treatment of the parent Pd/Al<sub>2</sub>O<sub>3</sub> with BrBen. A similar performance has been observed in the presence of BrBen added to the reactor. These results demonstrate that the hydrodeoxygenation of HMF could be carried out over Pd-Br catalyst with high selectivity and conversion at ambient temperature. To the best of our knowledge, this is the first ever reported heterogeneous catalyst for hydrodeoxygenation of HMF with H<sub>2</sub> at ambient temperature (*Table 4.3*).

### **4.2.3. Other promoting agents**

Other bromine sources such as 1-bromohexadecane and ammonium bromide have been tested for this reaction (*Table 4.1, Entry 16-17*). The resulting catalysts, however,

demonstrated the catalytic performance similar to the non-promoted Pd catalyst. This fact is due to higher stability and insignificant hydrogenolysis of these bromine compounds over the Pd surface. The absence of the products of decomposition of 1-bromohexadecane during these pretreatments was further confirmed by the GC-MS analysis (*Figure 4.2*).

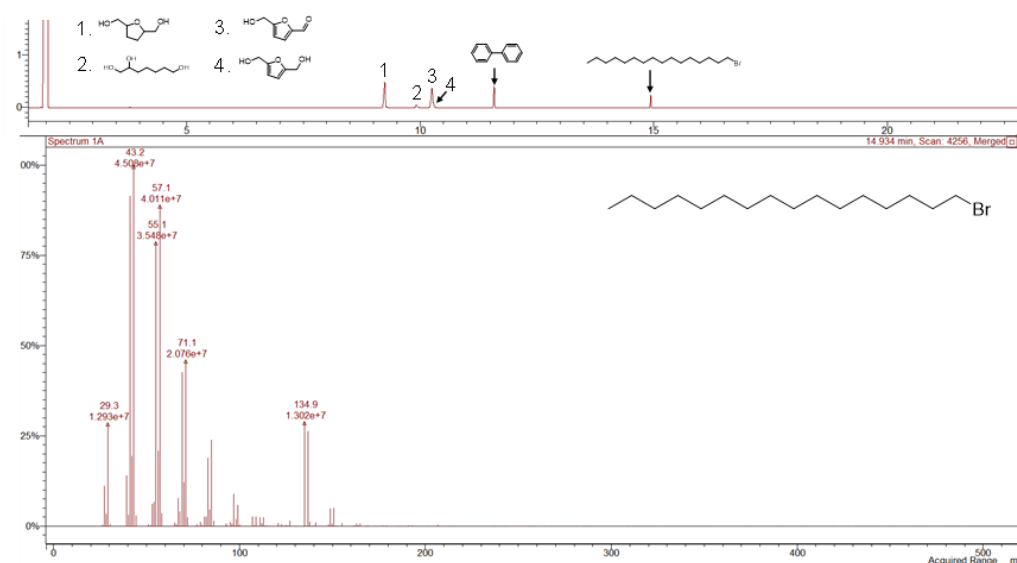


**Figure 4.2.** GC-MS analysis for the liquid-phase from HMF hydrodeoxygenation over Pd/Al<sub>2</sub>O<sub>3</sub> promoted with 1-bromohexadecane.

The effect of other halogens such as Cl and I has been also studied. The HMF conversion over Pd/Al<sub>2</sub>O<sub>3</sub> was investigated in the presence of ClBen and IBen (*Table 4.1, Entry 18-19*). The presence of iodine resulted in the complete deactivation of the catalyst. Our earlier studies have confirmed that the treatment of Pd by organic iodine leads to full coverage of surface Pd by I [35]. Addition of ClBen leads to low deoxygenation activity and noticeable hydrogenation of furan-rings. Thus, in the row of halogens, the activity of the catalysts in HMF hydrogenation increases in row I<Br<Cl with zero activity of the iodine-promoted catalysts, because of full coverage



of Pd by iodine and low effect of chlorine on the Pd catalyst. The increase in the electronegativity of the elements in this row should also lead to the increase in the polarity of the Pd-Hal bond. Bromine demonstrates intermediate activity with significant enhancement of selectivity toward deoxygenation instead of the aromatic ring hydrogenation.

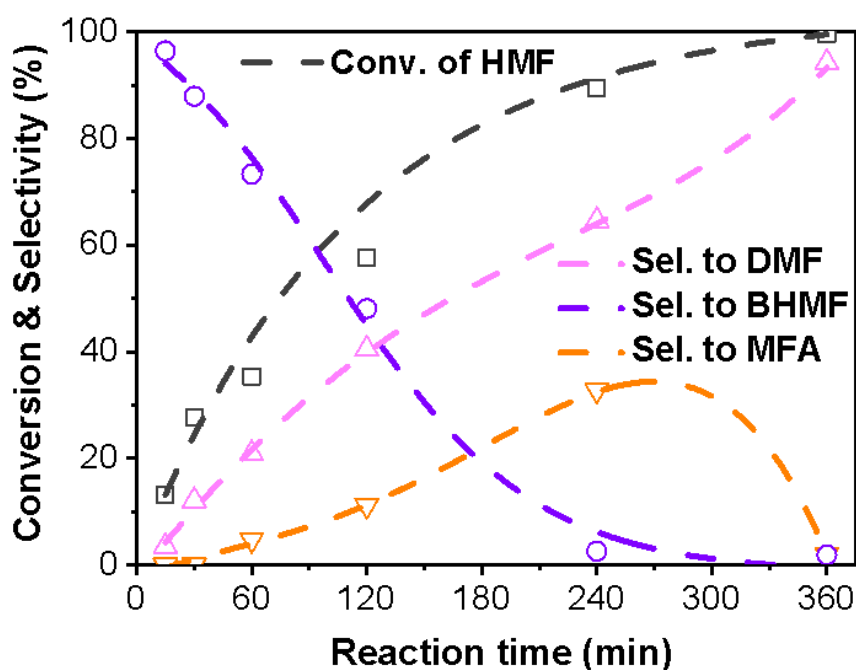


**Figure 4.3.** Kinetics of hydrogenation of HMF over Br-Pd/Al<sub>2</sub>O<sub>3</sub>. Reaction conditions: 50 mg of Br-Pd/Al<sub>2</sub>O<sub>3</sub>, 100 mg of HMF, 5 g of THF, 30 °C, 5 bar H<sub>2</sub>.

To provide more insights into the reaction pathway, the kinetic study of HMF hydrogenation over Br-Pd/Al<sub>2</sub>O<sub>3</sub> has been performed at ambient temperature (**Figure 4.3**). As expected, the conversion of HMF increases with the increase in the reaction time. The selectivity to BHMF is close to 100% at the initial reaction time. This suggests that BHMF is the primary product of the reaction over Br-Pd/Al<sub>2</sub>O<sub>3</sub> due to the fast hydrogenation of the carbonyl group in the HMF molecule. Afterward, this product

has been transformed into MFA and DMF which seem to be secondary products MFA is produced by deoxygenation of one of the hydroxyl groups of BHMF, while DMF is produced by simultaneous deoxygenation of both BHMF hydroxyl groups. Finally, MFA decreases at higher reaction time due to transformation to DMF. It is worth to note that when the reaction time progresses, the rapidly decrease of BHMF and the slow increase of MFA and DMF confirmed the high deoxygenation ability of Pd-Br catalyst, which can effectively deoxygenate hydroxyl groups. Thus, as indicated in [Table 4.1](#), the conversion of HMF molecules proceeds with intermediate hydrogenation of the carbonyl group and subsequent hydrodeoxygenation of hydroxyl groups to methyl groups.

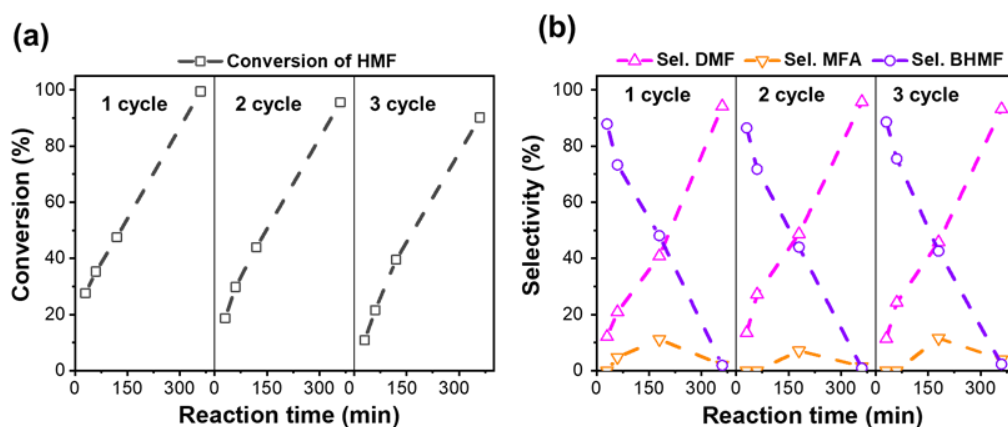


**Figure 4.4.** Evolution of conversion (a) and selectivity (b) for the first 3 cycles with reaction time. Reaction conditions: 50 mg Br-Pd/Al<sub>2</sub>O<sub>3</sub>, 100 mg HMF, 5 g THF, 30°C, 5 bar H<sub>2</sub>.

To confirm the recyclability of Pd-Br catalyst, the hydrodeoxygenation of HMF has been performed at 30 °C and 5 bar of H<sub>2</sub> over the Br-Pd/Al<sub>2</sub>O<sub>3</sub> catalyst in three consecutive cycles with intermediate separation of the catalyst ([Figure 4.4](#)). The catalyst demonstrates comparable activity in HMF transformation with a slight decrease

in the 2 and 3 cycles, which could be explained by the loss of catalysts during separation. The selectivity curves are very similar for all three cycles with the same distribution of the products and high selectivity to DMF (>90%) at high conversions. No catalyst deactivation was observed.

### 4.3. Characterization of the Pd-Br catalysts

**Table 4.2.** Summary of the results obtained from the characterizations of Pd/Al<sub>2</sub>O<sub>3</sub> and Br-Pd/Al<sub>2</sub>O<sub>3</sub>

Catalyst	Element analysis (wt. %)		Br amount (mmol/g)	CO amount (mmol/g)
	Pd	Br		
Pd/Al <sub>2</sub> O <sub>3</sub>	4.7	0	0	0.16
Br-Pd/Al <sub>2</sub> O <sub>3</sub>	5.1	0.11	0.014	0.059

The Pd-Br catalysts have been studied further to identify the nature of the interaction of Br with the catalyst and nature of active sites for HMF hydrodeoxygenation. First of all, the location of Br atoms was determined by TEM-EDS analysis. Due to the superposition of the main Br and Al edges in an EDS spectrum, Br-Pd/SiO<sub>2</sub> with a similar promotion effect was selected as a model catalyst for EDS mapping analysis. EDS mapping clearly shows the preferential localization of Br on the surface of palladium nanoparticles (**Figure 4.5**). The signal of Br atoms (in blue) is localized at the same places as Pd (in green) indicating spatial coexistence of both elements and a possible modification of Pd surface by the presence of Br atoms.

First of all, the location of Br atoms was determined by TEM-EDS analysis. Due to the superposition of the main Br and Al edges in an EDS spectrum, Br-Pd/SiO<sub>2</sub> with a similar promotion effect was selected as a model catalyst for EDS mapping analysis.

EDS mapping clearly shows the preferential localization of Br on the surface of palladium nanoparticles (*Figure 4.5*). The signal of Br atoms (in blue) is localized at the same places as Pd (in green) indicating spatial coexistence of both elements and a possible modification of Pd surface by the presence of Br atoms.

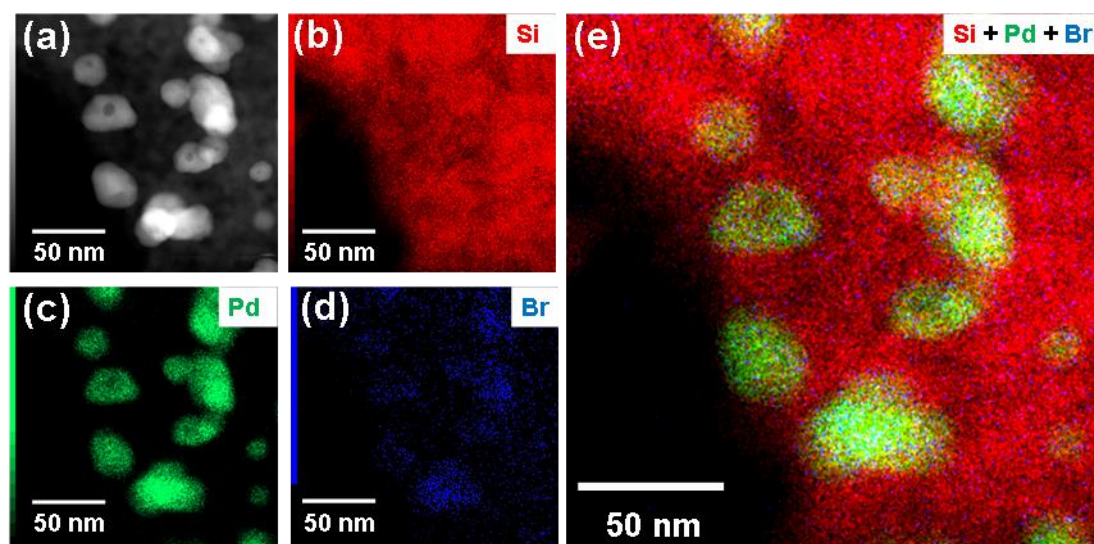


*Figure 4.5.* Characterization of Br-Pd/SiO<sub>2</sub> catalyst by TEM-EDS analysis (a) STEM image and (b-e) corresponding EDS elemental maps.

The amount of Br on the Pd/Al<sub>2</sub>O<sub>3</sub> and Br-Pd/Al<sub>2</sub>O<sub>3</sub> catalysts was measured by XRF analysis and the results are summarized in *Table 4.2*. The amount of Br in the catalyst (0.11 wt. %) is significantly lower in comparison with amount of Pd. CO-pulse chemisorption has been conducted to evaluate the amount of available surface Pd sites on the catalyst. *Table 4.2* shows that the amount of adsorbed CO over the initial Pd/Al<sub>2</sub>O<sub>3</sub> catalyst is 0.16 mmol/g, however, after pretreatment with BrBen, the CO adsorption amount decreases to 0.059 mmol/g. The dispersion of Pd (Pd<sub>CO</sub>/Pd) in the non-promoted catalyst corresponds to 33 % according to CO adsorption. This decline of the CO adsorption demonstrates the modification of Pd surface with the Br atoms,

which prevents the adsorption of CO on Pd. Considering the presence of Br over Pd surface, the ratio of Br/Pd<sub>CO</sub> corresponds to the coverage of Pd by Br close to 10 %.

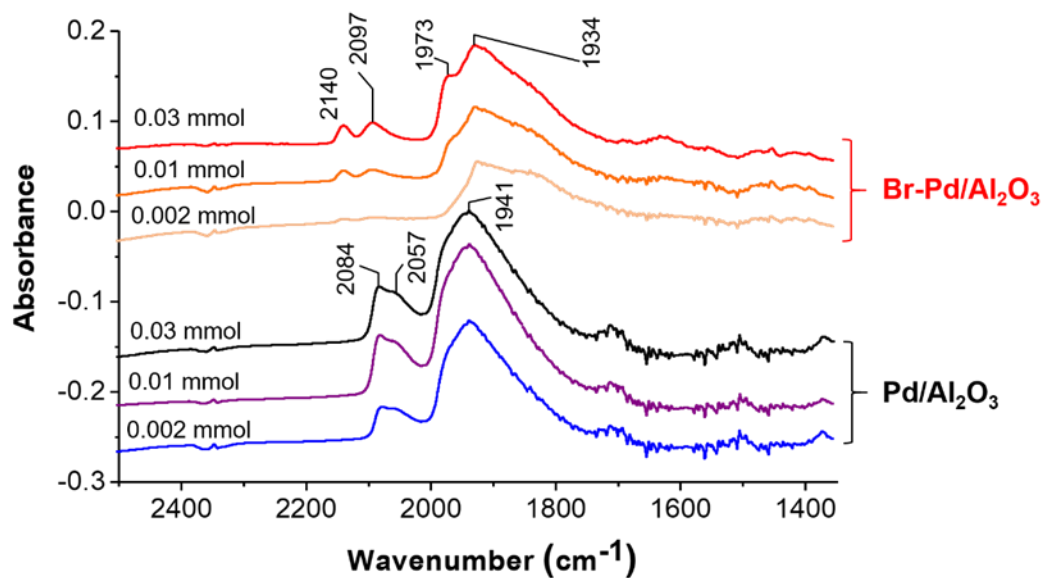


**Figure 4.6.** CO-FTIR for Pd/Al<sub>2</sub>O<sub>3</sub> and Br-Pd/Al<sub>2</sub>O<sub>3</sub>

FTIR spectroscopy of CO adsorption has been used to identify the localization of Br. A set of CO absorption bands have been observed on non-promoted Pd/Al<sub>2</sub>O<sub>3</sub>. The band at 2084 cm<sup>-1</sup> with a shoulder at 2057 cm<sup>-1</sup> is due to CO linearly adsorbed on defect sites of Pd nanoparticles presence at edges and corners. The intensive band at 1941 cm<sup>-1</sup> is related to CO adsorbed on the Pd nanoparticles planes with bridge-bonds (**Figure 4.6**) [42-43]. The modification of Pd by Br leads to the almost complete disappearance of the peak at 2084 cm<sup>-1</sup> with an obvious decrease in the intensity of the peaks attributed to CO adsorption over planes. Well-resolved peaks at 1973 cm<sup>-1</sup> and 1934 cm<sup>-1</sup> over Br-Pd/Al<sub>2</sub>O<sub>3</sub> could be assigned to CO adsorbed on Pd (100) and (111) facets, respectively [42]. The less adsorption of CO on (100) facets and the defect sites could be explained by simplified hydrogenolysis of BrBen and deposition of Br over these low-

coordination sites of Pd. Moreover, a small peak with higher frequency at  $2140\text{ cm}^{-1}$  is visible and assigned to CO bonded to Pd-Br sites, where electronic deficient Pd heightens the vibrational frequency of adsorbed CO [43].

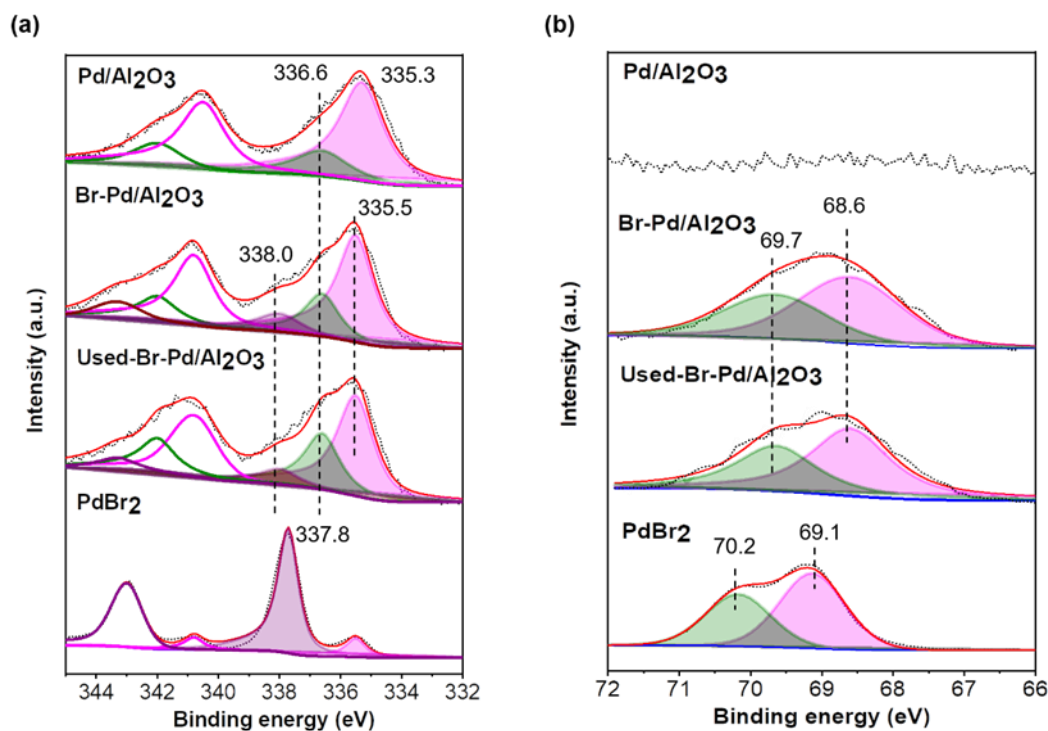


**Figure 4.7.** XPS (a) Pd 3d and (b) Br 3d core level spectra of Pd/Al<sub>2</sub>O<sub>3</sub>, Br-Pd/Al<sub>2</sub>O<sub>3</sub>, and Br-Pd/Al<sub>2</sub>O<sub>3</sub> after reaction.

The electronic state of Pd and Br in the Br-Pd/Al<sub>2</sub>O<sub>3</sub> catalyst has been studied by XPS.

**Figure 4.7** demonstrates the Pd 3d and Br 3d core-level spectra of Br-Pd/Al<sub>2</sub>O<sub>3</sub> before and after reaction in comparison with the parent Pd/Al<sub>2</sub>O<sub>3</sub>. The Pd 3d spectrum of Pd/Al<sub>2</sub>O<sub>3</sub> catalyst, as shown in **Figure 4.7a**, has two doublets with BE (Pd 3d<sub>5/2</sub>) at 335.3 eV and 336.6 eV attributed to metallic Pd<sup>0</sup> and Pd<sup>2+</sup> (PdO), respectively [40]. Both of these states coexist on the surface with the dominant metallic state. Interestingly, a shift (0.3 eV) of Pd 3d peaks to higher BE for the Br-Pd/Al<sub>2</sub>O<sub>3</sub> catalysts has been

observed after modification by Br. It can be attributed to the interaction of metallic Pd with Br adatoms with the electron withdrawal from Pd to electrophilic Br <sup>[41]</sup>.

Signal of oxidized Pd<sup>2+</sup> in PdO can be observed before and after modification by Br due to the partial oxidation of surface Pd atoms. Notably, an additional peak appears at much higher binding energy at 338.0 eV in the Pd 3d XPS spectrum after modification of the Br-Pd/Al<sub>2</sub>O<sub>3</sub> catalyst. PdBr<sub>2</sub> has a signal of Pd<sup>2+</sup> with binding energy at 337.8 eV. The peak at higher binding energy at 338.0 eV could be assigned to the presence of PdBr<sub>2</sub> species adsorbed over the surface of metal nanoparticles.

For the Br-Pd/Al<sub>2</sub>O<sub>3</sub> catalyst, the Br 3d<sub>5/2</sub> peak is located at 68.6 eV, which is lower than 69.1 eV for Br<sup>-</sup> in PdBr<sub>2</sub>. The red-shift (0.5 eV) indicates an increase in the electronic density in comparison with PdBr<sub>2</sub> due to the transfer of electronic density from Pd metallic nanoparticles to Br. The red shift of the Br 3d<sub>5/2</sub> XPS peak is consistent with the increase in the electron BE of Pd metal atoms due to the withdrawal of the electron density from palladium towards the bromine atoms. It has to be noted that the XPS spectra of Pd and Br of the Br-Pd/Al<sub>2</sub>O<sub>3</sub> catalyst are not affected by conducting the reaction.

Pyridine adsorption has been carried out on non-promoted Pd/Al<sub>2</sub>O<sub>3</sub> and Br-Pd/Al<sub>2</sub>O<sub>3</sub> to study the catalyst acidity in the absence and in the presence of H<sub>2</sub> (*Figure 4.8*). In the absence of hydrogen, the spectra of Py adsorption are very similar. Both non-promoted Pd/Al<sub>2</sub>O<sub>3</sub> and Br-Pd/Al<sub>2</sub>O<sub>3</sub> exhibit a peak at 1449 cm<sup>-1</sup> attributed to the Lewis acid sites, which are probably present on the Al<sub>2</sub>O<sub>3</sub> support <sup>[44]</sup>. Notably, there is no peak at 1540 cm<sup>-1</sup> for both catalysts, which is related to the adsorption of pyridine over the

Brønsted acid sites. In-situ pretreatment of Br-Pd/Al<sub>2</sub>O<sub>3</sub> in H<sub>2</sub> at 60°C at atmospheric pressure with subsequent adsorption of Py after hydrogen evacuation, leads to the appearance of a well-resolved peak at 1538 cm<sup>-1</sup> indicating the generation of Brønsted acidity in the presence of hydrogen.

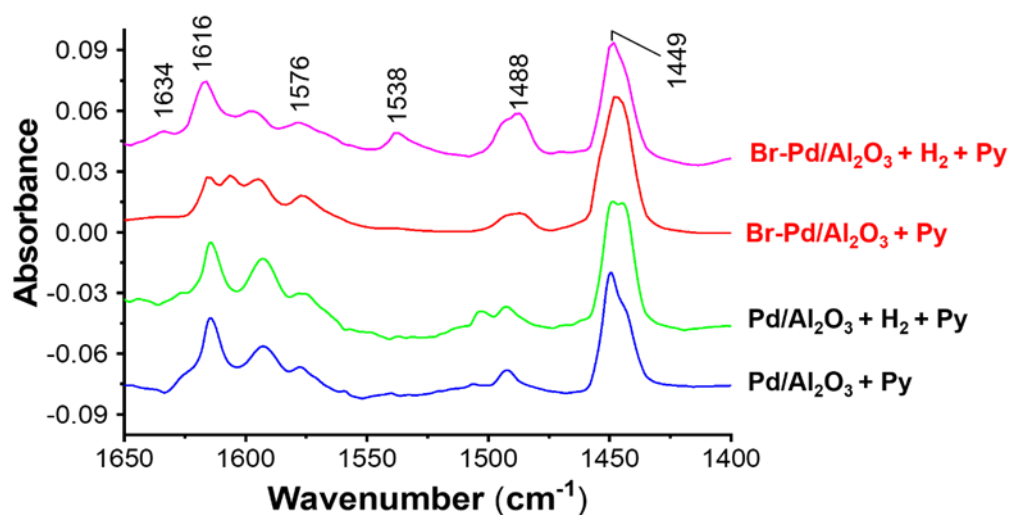


**Figure 4.8.** Pyridine-FTIR for Pd/Al<sub>2</sub>O<sub>3</sub> and Br-Pd/Al<sub>2</sub>O<sub>3</sub> with and without hydrogen pre-treatment.

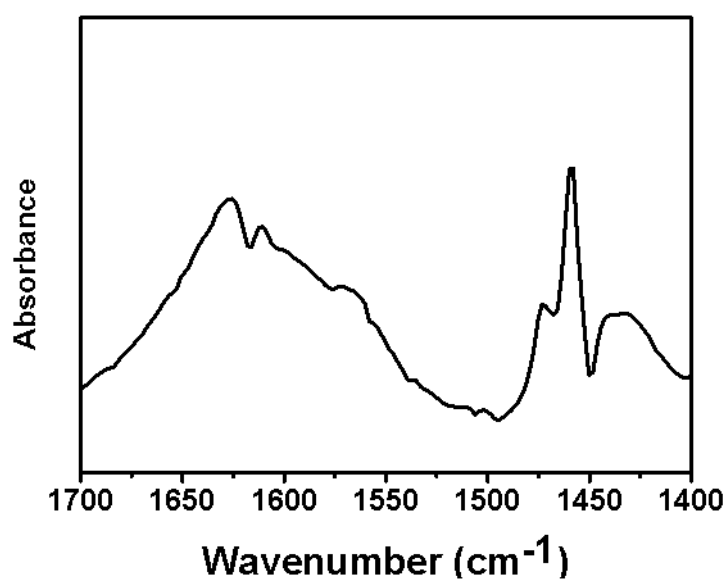


**Figure 4.9.** Pyridine-FTIR over Br-Pd/Al<sub>2</sub>O<sub>3</sub> in the co-presence of pyridine and H<sub>2</sub>.



It is worth mentioning that if hydrogen were still in the cell, Py has been hydrogenated leading to the complex spectrum (*Figure 4.9*). Thus, the exposure of the Br-Pd/Al<sub>2</sub>O<sub>3</sub> catalyst to hydrogen generates Brønsted acidity. This acidity is stable and does not disappear after the removal of hydrogen. The phenomenon is different from our previous data reported on the Pd catalyst treated by iodine, where the Brønsted acidity vanished after removing of H<sub>2</sub> [35]. This difference can be attributed to the higher electronegativity of bromine in comparison with iodine, which should result in the stronger stabilization of in-situ generated H<sup>+</sup> over the Br atoms. The same experiment over non-promoted Pd/Al<sub>2</sub>O<sub>3</sub> does not show any generation of the Brønsted acidity.

#### **4.4. Model reactions**

It is interesting to note that the presence of Br on the surface of Pd results in suppression of the hydrogenation of the aromatic ring in HMF. This effect can be explained by the electronic effect of Br over the Pd surface leading to a decrease in the electronic density over Pd and lower homolytic hydrogenation activity. In contrast, this catalyst provides high activity for heterolytic dissociation of H<sub>2</sub> towards hydride and proton on the Pd-Br sites. This results in the appearance of the Brønsted acidity and may favor the hydrogenation of polar functional groups [45-46].

To support these assumptions, additional model experiments over Pd/Al<sub>2</sub>O<sub>3</sub> and Br-Pd/Al<sub>2</sub>O<sub>3</sub> have been performed. These model experiments include hydrogenation of DMF, 3-phenylpropanal and benzyl alcohol. The goal was to demonstrate selectivity of

different sites over non-promoted and Br-promoted Pd nanoparticles for hydrogenation of furan ring, carbonyl group and hydrodeoxygenation of hydroxyl group, respectively.

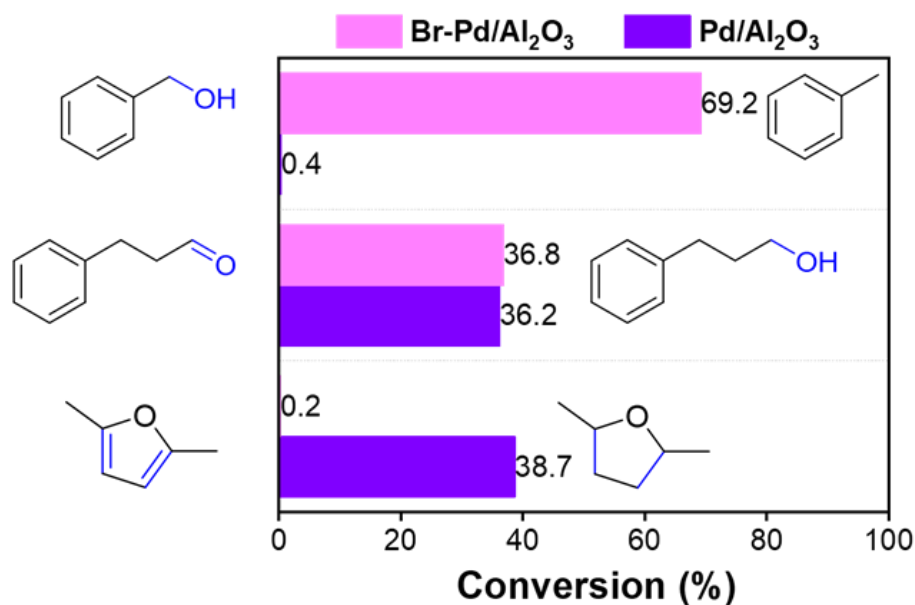


**Figure 4.10.** Model reactions of hydrogenation of DMF, 3-phenylpropanal, and benzyl alcohol over Pd/Al<sub>2</sub>O<sub>3</sub> and Br-Pd/Al<sub>2</sub>O<sub>3</sub>. Reaction conditions: 50 mg of catalyst, 100 mg reactant, 5 g of THF, DMF hydrogenation: 60°C, 20 bar H<sub>2</sub>, 1 h; 3-phenylpropanal hydrogenation: 30°C, 5 bar H<sub>2</sub>, 30 min; Benzyl alcohol deoxygenation: 30°C, 5 bar H<sub>2</sub>, 15 min.

**Figure 4.10** demonstrates higher activity the non-promoted Pd/Al<sub>2</sub>O<sub>3</sub> catalyst for hydrogenation of furan ring in DMF and carbonyl group in 3-phenylpropanal and almost zero activity for hydrodeoxygenation of benzyl alcohol to toluene. Modification by Br has changed dramatically the catalytic behavior with suppression of hydrogenation of aromatic ring in DMF. At the same time, the Br-Pd/Al<sub>2</sub>O<sub>3</sub> catalyst showed high activity for hydrogenation of 3-phenylpropanal to 3-phenyl-1-propanol and hydrodeoxygenation of benzyl alcohol to toluene. The Pd-Br catalyst seems to favor the hydrogenation of the polar carbonyl groups and deoxygenation. However, it exhibits extremely lower activity in the hydrogenation of low polarity aromatic rings.

## 4.5. Discussion

**Table 4.3.** Hydrodeoxygenation of HMF to DMF over various catalytic systems.

Entry	Catalyst	Conditions		Results		Ref.
		Solvent	T, °C	HMF Conv., %	DMF Yield, %	
1	Br-Pd/Al <sub>2</sub> O <sub>3</sub>	THF	30	100	96.1	This work
<b>Metal catalysts</b>						
2	CuRu/C	1-butanol	220	100	79	14
3	Ru/C	isopropanol	190	100	80	19
4	Ni/SBA-15	Dioxane	180	95	70.5	22
5	CoCu@C	Ethanol	180	100	99.4	23
6	PtCo/ MWCNTs	1-butanol	160	100	92.3	18
7	Ru/CNT	Dioxane	150	97	83.5	20
<b>Bifunctional metal-acid catalysts</b>						
8	Pd/C/Zn	THF	150	100	85	50
9	Ru/Co <sub>3</sub> O <sub>4</sub>	THF	130	100	93.4	28
10	NiSi-PS	Dioxane	130	100	72.9	30
11	Pd-C <sub>82.5</sub> H <sub>0.5</sub> PW <sub>12</sub> O <sub>40</sub> /K-10 clay	THF	90	98	79	29
12	Pd/C + Acetic acid	H <sub>2</sub> O-Dioxane	120	95	85	24
13	Pd/C + HCl	THF	60	99	99	25
14	PdAu/C + HCl	THF	60	99	99	25

Hydrogenation of HMF to DMF has been widely studied by different groups ([Table 4.3](#)). Almost for all catalysts the catalytic route for DMF synthesis passes through 3 steps: 1) Conversion of HMF to BHMF or methylfurfural (MFF), 2) hydrogenation of BHMF or MFF to MFA and finally 3) deoxygenation of MFA to DMF <sup>[47]</sup>. The scheme proposed during kinetic study of hydrodeoxygenation of HMF over Pd-Br catalyst in agreement with the literature reported by Alexis T. Bell et al. ([Table 4.1](#)) <sup>[48]</sup>.

However, this route is usually accompanied by different side reactions, which could be subdivided into two groups: hydrogenation of aromatic ring instead of the C=O and C-OH bonds and oligomerization of HMF at high temperature. Hydrogenation of the C=C bonds is thermodynamically preferable than hydrogenation of C=O, however, C=C is stabilized by aromatic conjugation [49-50]. It results in the formation of different by-products like MTHFA, BHMTF etc. The by-products formation can also lead to the catalyst deactivation. Indeed, even heating of HMF to 100°C in the presence of water leads to generation of humins [33].

The catalytic performance of Br-Pd/Al<sub>2</sub>O<sub>3</sub> has been compared with the most efficient catalytic systems in the literature (*Table 4.3*). *Table 4.3* shows two different types of catalysts that have been reported for the hydrogenation HMF to DMF. Metallic catalysts without acid promotions need high temperature for DMF production from HMF. For example, Román-Leshkov et al. integrated a CuRu/C catalyst in the process of production of DMF from fructose [14]. A yield up to 71% in the liquid phase hydrogenolysis of HMF was obtained at 220 °C and 6.8 bar H<sub>2</sub> pressure. The Pt-Co bimetallic on multi-walled carbon nanotubes (MWCNTs) catalyst needs a high temperature of up to 160 °C for this reaction (>90 %) [18].

While pure metallic catalysts need high temperature for DMF production and often exhibit fast deactivation, the usage of metal-acid bifunctional catalytic systems could significantly promote the deoxygenation rate of HMF to DMF (*Table 4.3, Entry 8-14*) [24-32, 50]. The conversion of HMF to DMF over metal-acid catalysts is performed by metallic sites responsible for hydrogenation of carbonyl groups, while the acid sites of

support are required for C-OH bond activation and simultaneous hydrogenolysis on metallic sites. The intimacy of metal and acid sites in the bifunctional catalysts seems to be primordial for deoxygenation. Insufficient contact between metal and acid sites limits the deoxygenation efficiency of HMF to DMF.

Up to date, the most active bifunctional metal-acid catalytic system for the HMF deoxygenation has been the combination of heterogeneous metal catalyst with homogeneous acid (*Table 4.3, Entry 12-14*)<sup>[24-27]</sup>. In the presence of acetic acid, the yield of DMF increased from 0 to 85% over Pd/C at 120 °C<sup>[24]</sup>. Bimetallic PdAu/C exhibited a significant yield of over 99% for selective hydrogenation of HMF toward DMF in the presence of homogeneous HCl at 60 °C<sup>[25]</sup>. The homogeneous acids provide intimacy of acid sites around the metal surface, which could protonate the substrate hydroxyl group and polarize the C-O bond and favor the cleavage of the C-O bond over Pd<sup>[49]</sup>. However, the addition of homogeneous organic or inorganic acid at the same time could result in the side self-condensation of HMF, which lowers the DMF productivity<sup>[33]</sup>. Besides, the presence of liquid acids in the reaction mixture leads to the corrosion of equipment.

Thus, the elaboration of efficient catalysts for deoxygenation of biomass-derived compounds faces the following dilemma. Heterogeneous metal catalysts with acidic support do not have require metal-acid intimacy, while the combination of the metal catalysts with homogeneous acid suffers from the side-reactions and corrosion issues. Our results demonstrate that the supported bifunctional metal catalysts promoted with bromine (*Table 4.3*) exhibit several advantages:

- Hydrogenation at ambient temperature;
- High-selectivity due to only hydrogenation of the C=O bonds;
- High-efficiency due to simultaneous activation and hydrogenolysis of C-OH bonds over metal and acid sites located in close proximity of metal palladium nanoparticles
- Heterogenization of the catalyst and easy separation of the catalyst and reaction products.

Indeed, heterolytic dissociation of hydrogen over the Pd-Br sites should favor hydrogenation of the polar C=O and C-OH groups and should hinder hydrogenation of non-polar C=C bonds as demonstrated in the model reactions (*Figure 4.10*). At the same time, generation of Brønsted acid sites over Pd-Br sites simplifies protonation and hydrogenolysis of the BHMF alcohol with direct generation of DMF. Thus, Pd-Br catalyst has dual metal-acidic properties and can be used for direct deoxygenation of biomass-derived alcohols and aldehydes. The conventional bifunctional catalysts such as metal-zeolite or metal oxide composites contain metal sites over metal nanoparticles and acid sites over the zeolite or oxide support. The metal and acid sites in these catalysts are often sterically separated and suffer from insufficient intimacy. Different to previously developed metal-acid bifunctional catalysts, the Pd-Br systems have both metal and acid sites located on the surface of the same metal nanoparticles. This results in the unique intimacy of metal and acid sites and in the spectacular enhancement of the catalytic performance and more particularly the reaction selectivity.

## 4.6. Conclusion

In this paper, an efficient Pd-Br bifunctional catalyst with intimate metal and acid sites, which are both localized over the same metal nanoparticles, was developed and exhibited extremely high yield (96 %) to DMF from HMF at ambient temperature. The promotion with bromine results in double effect on the catalytic performance. On the one hand, it tunes the hydrogenation activity of Pd active sites. On the other hand, the promotion bromine creates Brønsted acid sites, which are situated in extremely close proximity to the metal sites. The adsorbed Br atoms on the Pd surface can prevent the hydrogenation of furan-ring, while the hydrogenation of carbonyl groups is not affected. The formed Pd-Br sites on the Pd surface provide heterolytic dissociation of H<sub>2</sub> for deoxygenation of the hydroxyl groups to DMF. To summarize, this paper describes design of a new type of bifunctional catalysts with enhanced intimacy of metal and acid sites. It deepens the understanding of how halogens can be used for the modification of metal surface for the generation of new types of active sites for activation of hydrogen in a heterolytic way with generation of the Brønsted acidity.

## Reference

1. Wheeldon, I.; Minter, S. D.; Banta, S.; Barton, S. C.; Atanassov, P.; Sigman, M., Substrate Channelling as An Approach to Cascade Reactions. *Nat. Chem.* **2016**, *8* (4), 299-309.
2. Lohr, T. L.; Li, Z.; Marks, T. J., Thermodynamic Strategies for C-O Bond Formation and Cleavage via Tandem Catalysis. *Acc. Chem. Res.* **2016**, *49* (5), 824-858.
3. Wu, X.; Cruz, F. A.; Lu, A.; Dong, V. M., Tandem Catalysis: Transforming Alcohols to Alkenes by Oxidative Dehydroxylation. *J. Am. Chem. Soc.* **2018**, *140* (32), 10126-10130.
4. Liu, H.; Jiang, T.; Han, B.; Liang, S.; Zhou, Y., Selective Phenol Hydrogenation to Cyclohexanone over A Dual Supported Pd-Lewis Acid Catalyst. *Science* **2009**, *326* (5957), 1250-1252.
5. Konwar, L. J.; Maki-Arvela, P.; Mikkola, J. P., SO<sub>3</sub>H-Containing Functional Carbon Materials: Synthesis, Structure, and Acid Catalysis. *Chem. Rev.* **2019**, *119* (22), 11576-11630.
6. Cheng, K.; Zhou, W.; Kang, J.; He, S.; Shi, S.; Zhang, Q.; Pan, Y.; Wen, W.; Wang, Y., Bifunctional Catalysts for One-Step Conversion of Syngas into Aromatics with Excellent Selectivity and Stability. *Chem* **2017**, *3* (2), 334-347.
7. Chen, S.; Wojcieszak, R.; Dumeignil, F.; Marceau, E.; Royer, S., How Catalysts and Experimental Conditions Determine the Selective Hydroconversion of Furfural and 5-Hydroxymethylfurfural. *Chem. Rev.* **2018**, *118* (22), 11023-11117.
8. Xu, C.; Paone, E.; Rodriguez-Padron, D.; Luque, R.; Mauriello, F., Recent Catalytic Routes for The Preparation and The Upgrading of Biomass Derived Furfural and 5-Hydroxymethylfurfural. *Chem. Soc. Rev.* **2020**, *49* (13), 4273-4306.
9. Pang, J.; Sun, J.; Zheng, M.; Li, H.; Wang, Y.; Zhang, T., Transition Metal Carbide Catalysts for Biomass Conversion: A Review. *Appl. Catal. B* **2019**, *254*, 510-522.
10. Ordonsky, V. V.; Sushkevich, V. L.; Schouten, J. C.; van der Schaaf, J.; Nijhuis, T. A., Glucose Dehydration to 5-Hydroxymethylfurfural over Phosphate Catalysts. *J. Catal.* **2013**, *300*, 37-46.
11. Wang, J.; Wei, Q.; Ma, Q.; Guo, Z.; Qin, F.; Ismagilov, Z. R.; Shen, W., Constructing Co@N-doped Graphene Shell Catalyst via Mott-Schottky Effect for Selective Hydrogenation of 5-Hydroxymethylfurfural. *Appl. Catal. B* **2020**, *263*, 118339.
12. Ordonsky, V. V.; van der Schaaf, J.; Schouten, J. C.; Nijhuis, T. A., The Effect of Solvent Addition on Fructose Dehydration to 5-Hydroxymethylfurfural in Biphasic System over Zeolites. *J. Catal.* **2012**, *287*, 68-75.
13. Sudarsanam, P.; Peeters, E.; Makshina, E. V.; Parvulescu, V. I.; Sels, B. F., Advances in Porous and Nanoscale Catalysts for Viable Biomass Conversion. *Chem. Soc. Rev.* **2019**, *48* (8), 2366-2421.
14. Roman-Leshkov, Y.; Barrett, C. J.; Liu, Z. Y.; Dumesic, J. A., Production of Dimethylfuran for Liquid Fuels from Biomass-derived Carbohydrates. *Nature* **2007**, *447* (7147), 982-985.
15. Tao, L.; Yan, T.-H.; Li, W.; Zhao, Y.; Zhang, Q.; Liu, Y.-M.; Wright, M. M.; Li, Z.-H.; He, H.-Y.; Cao, Y., Toward an Integrated Conversion of 5-Hydroxymethylfurfural and Ethylene for the Production of Renewable *p*-Xylene. *Chem* **2018**, *4* (9), 2212-2227.
16. Rohling, R. Y.; Tranca, I. C.; Hensen, E. J. M.; Pidko, E. A., Mechanistic Insight into the [4 + 2] Diels-Alder Cycloaddition over First Row *d*-Block Cation-Exchanged Faujasites. *ACS Catal.* **2019**, *9* (1), 376-391.



17. Stadler, B. M.; Wulf, C.; Werner, T.; Tin, S.; de Vries, J. G., Catalytic Approaches to Monomers for Polymers Based on Renewables. *ACS Catal.* **2019**, *9* (9), 8012-8067.
18. Wang, X.; Liu, Y.; Liang, X., Hydrogenolysis of 5-Hydroxymethylfurfural to 2,5-Dimethylfuran over Supported Pt-Co Bimetallic Catalysts under Mild Conditions. *Green Chem.* **2018**, *20* (12), 2894-2902.
19. Jae, J.; Zheng, W.; Lobo, R. F.; Vlachos, D. G., Production of Dimethylfuran from Hydroxymethylfurfural Through Catalytic Transfer Hydrogenation with Ruthenium Supported on Carbon. *ChemSusChem* **2013**, *6* (7), 1158-1162.
20. Priecel, P.; Endot, N. A.; Carà, P. D.; Lopez-Sanchez, J. A., Fast Catalytic Hydrogenation of 2,5-Hydroxymethylfurfural to 2,5-Dimethylfuran with Ruthenium on Carbon Nanotubes. *Ind. Eng. Chem. Res.* **2018**, *57* (6), 1991-2002.
21. Jin, Z.; Yi, X.; Wang, L.; Xu, S.; Wang, C.; Wu, Q.; Wang, L.; Zheng, A.; Xiao, F.-S., Metal-Acid Interfaces Enveloped in Zeolite Crystals for Cascade Biomass Hydrodeoxygenation. *Appl. Catal. B* **2019**, *254*, 560-568.
22. Chen, S.; Ciotonea, C.; De Oliveira Vigier, K.; Jérôme, F.; Wojcieszak, R.; Dumeignil, F.; Marceau, E.; Royer, S., Hydroconversion of 5-Hydroxymethylfurfural to 2,5-Dimethylfuran and 2,5-Dimethyltetrahydrofuran over Non-Promoted Ni/SBA-15. *ChemCatChem* **2020**, *12* (7), 2050-2059.
23. Chen, B.; Li, F.; Huang, Z.; Yuan, G., Carbon-Coated Cu-Co Bimetallic Nanoparticles as Selective and Recyclable Catalysts for Production of Biofuel 2,5-Dimethylfuran. *Appl. Catal. B* **2017**, *200*, 192-199.
24. Mitra, J.; Zhou, X.; Rauchfuss, T., Pd/C-Catalyzed Reactions of HMF: Decarbonylation, Hydrogenation, and Hydrogenolysis. *Green Chem.* **2015**, *17* (1), 307-313.
25. Nishimura, S.; Ikeda, N.; Ebitani, K., Selective Hydrogenation of Biomass-Derived 5-Hydroxymethylfurfural (HMF) to 2,5-Dimethylfuran (DMF) under Atmospheric Hydrogen Pressure over Carbon Supported PdAu Bimetallic Catalyst. *Catal. Today* **2014**, *232*, 89-98.
26. Chatterjee, M.; Ishizaka, T.; Kawanami, H., Hydrogenation of 5-Hydroxymethylfurfural in Supercritical Carbon Dioxide-Water: A Tunable Approach to Dimethylfuran Selectivity. *Green Chem.* **2014**, *16* (3), 1543-1551.
27. Thananathanachon, T.; Rauchfuss, T. B., Efficient Production of The Liquid Fuel 2,5-Dimethylfuran from Fructose using Formic Acid as A Reagent. *Angew. Chem. Int. Ed.* **2010**, *49* (37), 6616-6618.
28. Zu, Y.; Yang, P.; Wang, J.; Liu, X.; Ren, J.; Lu, G.; Wang, Y., Efficient Production of The Liquid Fuel 2,5-Dimethylfuran from 5-Hydroxymethylfurfural over Ru/Co<sub>3</sub>O<sub>4</sub> Catalyst. *Appl. Catal. B* **2014**, *146*, 244-248.
29. Gawade, A. B.; Tiwari, M. S.; Yadav, G. D., Biobased Green Process: Selective Hydrogenation of 5-Hydroxymethylfurfural to 2,5-Dimethyl Furan under Mild Conditions Using Pd-C<sub>8</sub>S<sub>2.5</sub>H<sub>0.5</sub>PW<sub>12</sub>O<sub>40</sub>/K-10 Clay. *ACS Sustain. Chem. Eng.* **2016**, *4* (8), 4113-4123.
30. Kong, X.; Zhu, Y.; Zheng, H.; Li, X.; Zhu, Y.; Li, Y.-W., Ni Nanoparticles Inlaid Nickel Phyllosilicate as a Metal-Acid Bifunctional Catalyst for Low-Temperature Hydrogenolysis Reactions. *ACS Catal.* **2015**, *5* (10), 5914-5920.
31. Guo, D.; Liu, X.; Cheng, F.; Zhao, W.; Wen, S.; Xiang, Y.; Xu, Q.; Yu, N.; Yin, D., Selective Hydrogenolysis of 5-Hydroxymethylfurfural to Produce Biofuel 2, 5-Dimethylfuran over

- Ni/ZSM-5 Catalysts. *Fuel* **2020**, *274*, 117853.
32. Han, W.; Tang, M.; Li, J.; Li, X.; Wang, J.; Zhou, L.; Yang, Y.; Wang, Y.; Ge, H., Selective Hydrogenolysis of 5-Hydroxymethylfurfural to 2,5-Dimethylfuran Catalyzed by Ordered Mesoporous Alumina Supported Nickel-Molybdenum Sulfide Catalysts. *Appl. Catal. B* **2020**, *268*, 118748.
  33. Shen, H.; Shan, H.; Liu, L., Evolution Process and Controlled Synthesis of Humins with 5-Hydroxymethylfurfural (HMF) as Model Molecule. *ChemSusChem* **2020**, *13* (3), 513-519.
  34. Zhang, J.; Ellis, L. D.; Wang, B.; Dzara, M. J.; Sievers, C.; Pylypenko, S.; Nikolla, E.; Medlin, J. W., Control of Interfacial Acid-metal Catalysis with Organic Monolayers. *Nat. Catal.* **2018**, *1* (2), 148-155.
  35. Wu, D.; Hernández, W. Y.; Zhang, S.; Vovk, E. I.; Zhou, X.; Yang, Y.; Khodakov, A. Y.; Ordonsky, V. V., In Situ Generation of Brønsted Acidity in the Pd-I Bifunctional Catalysts for Selective Reductive Etherification of Carbonyl Compounds under Mild Conditions. *ACS Catal.* **2019**, *9* (4), 2940-2948.
  36. Chen, J.; Liu, R.; Guo, Y.; Chen, L.; Gao, H., Selective Hydrogenation of Biomass-Based 5-Hydroxymethylfurfural over Catalyst of Palladium Immobilized on Amine-Functionalized Metal-Organic Frameworks. *ACS Catal.* **2014**, *5* (2), 722-733.
  37. Goyal, R.; Sarkar, B.; Bag, A.; Siddiqui, N.; Dumbre, D.; Lucas, N.; Bhargava, S. K.; Bordoloi, A., Studies of Synergy Between Metal-Support Interfaces and Selective Hydrogenation of HMF to DMF in Water. *J. Catal.* **2016**, *340*, 248-260.
  38. Chimentão, R. J.; Oliva, H.; Belmar, J.; Morales, K.; Mäki-Arvela, P.; Wärnå, J.; Murzin, D. Y.; Fierro, J. L. G.; Llorca, J.; Ruiz, D., Selective Hydrodeoxygenation of Biomass Derived 5-Hydroxymethylfurfural over Silica Supported Iridium Catalysts. *Appl. Catal. B* **2019**, *241*, 270-283.
  39. Wang, H.; Zhu, C.; Li, D.; Liu, Q.; Tan, J.; Wang, C.; Cai, C.; Ma, L., Recent Advances in Catalytic Conversion of Biomass to 5-Hydroxymethylfurfural and 2, 5-Dimethylfuran. *Renew. Sust. Energ. Rev.* **2019**, *103*, 227-247.
  40. Bhogeswararao, S.; Srinivas, D., Catalytic Conversion of Furfural to Industrial Chemicals over Supported Pt and Pd Catalysts. *J. Catal.* **2015**, *327*, 65-77.
  41. Komanoya, T.; Kinemura, T.; Kita, Y.; Kamata, K.; Hara, M., Electronic Effect of Ruthenium Nanoparticles on Efficient Reductive Amination of Carbonyl Compounds. *J. Am. Chem. Soc.* **2017**, *139* (33), 11493-11499.
  42. Nieminen, V.; Honkala, K.; Taskinen, A.; Murzin, D. Y., Intrinsic Metal Size Effect on Adsorption of Organic Molecules on Platinum. *J. Phys. Chem. C* **2008**, *112* (17), 6822-6831.
  43. Ball, M. R.; Rivera-Dones, K. R.; Gilcher, E. B.; Ausman, S. F.; Hullfish, C. W.; Lebrón, E. A.; Dumesic, J. A., AgPd and CuPd Catalysts for Selective Hydrogenation of Acetylene. *ACS Catal.* **2020**, *10* (15), 8567-8581.
  44. An, J.; Wang, Y.; Lu, J.; Zhang, J.; Zhang, Z.; Xu, S.; Liu, X.; Zhang, T.; Gocyla, M.; Heggen, M.; Dunin-Borkowski, R. E.; Fornasiero, P.; Wang, F., Acid-Promoter-Free Ethylene Methoxycarbonylation over Ru-Clusters/Ceria: The Catalysis of Interfacial Lewis Acid-Base Pair. *J. Am. Chem. Soc.* **2018**, *140* (11), 4172-4181.
  45. Mitsui, T.; Rose, M. K.; Fomin, E.; Ogletree, D. F.; Salmeron, M., Dissociative Hydrogen Adsorption on Palladium Requires Aggregates of Three or More Vacancies. *Nature* **2003**, *422*

- (6933), 705-712.
46. Doudin, N.; Yuk, S. F.; Marcinkowski, M. D.; Nguyen, M.-T.; Liu, J.-C.; Wang, Y.; Novotny, Z.; Kay, B. D.; Li, J.; Glezakou, V.-A.; Parkinson, G.; Rousseau, R.; Dohnálek, Z., Understanding Heterolytic H<sub>2</sub> Cleavage and Water-Assisted Hydrogen Spillover on Fe<sub>3</sub>O<sub>4</sub>(001)-Supported Single Palladium Atoms. *ACS Catal.* **2019**, *9* (9), 7876-7887.
  47. Aellig, C.; Jenny, F.; Scholz, D.; Wolf, P.; Giovanazzo, I.; Kollhoff, F.; Hermans, I., Combined 1,4-Butanediol Lactonization and Transfer Hydrogenation/Hydrogenolysis of Furfural-Derivatives under Continuous Flow Conditions. *Catal. Sci. Technol.* **2014**, *4* (8), 2326-2331.
  48. Chidambaram, M.; Bell, A. T., A Two-Step Approach for the Catalytic Conversion of Glucose to 2,5-Dimethylfuran in Ionic Liquids. *Green Chem.* **2010**, *12* (7), 1253-1262.
  49. Volkov, A.; Gustafson, K. P. J.; Tai, C.-W.; Verho, O.; Bäckvall, J.-E.; Adolfsson, H., Mild Deoxygenation of Aromatic Ketones and Aldehydes over Pd/C Using Polymethylhydrosiloxane as the Reducing Agent. *Angew. Chem. Int. Ed.* **2015**, *127* (17), 5211-5215.
  50. Saha, B.; Bohn, C. M.; Abu-Omar, M. M., Zinc-Assisted Hydrodeoxygenation of Biomass-Derived 5-Hydroxymethylfurfural to 2,5-Dimethylfuran. *ChemSusChem* **2014**, *7* (11), 3095-3101.



## **5. Cleavage of Diphenyl Ether Lignin Model Compounds to Single-ring Aromatics over Ru-Br Catalyst**

### **ABSTRACT.**

The hydrogenolysis of C-O linkages in aromatic ethers in biomass-derived lignin compounds without hydrogenation of the aromatic-rings is a highly desirable route for the production of sustainable single-ring aromatics. Conventional strategies over the heterogeneous metal catalysts require the addition of homogeneous base additives causing purification and waste handling problems. Herein, we propose a heterogeneous Ru/C catalyst modified by Br atoms for the selective hydrogenolysis of C-O bonds in diphenyl ether without hydrogenation of aromatic-rings. Various model reactions and characterizations indicate that the terrace sites of Ru nanoparticles, which is responsible for aromatic rings hydrogenation are selectively poisoned by Br atoms. However, the edge and corner sites, which are responsible for C-O bonds hydrogenolysis are not affected. Moreover, electronegative Br atoms withdraw electrons from Ru enhancing the adsorption and cleavage of electron-rich C-O bonds on Ru. The Ru-Br catalyst is highly efficient for the production of phenol and benzene from diphenyl ether with an overall yield of single-ring aromatics up to 95% under mild reaction conditions. The Ru-Br catalyst is stable without obvious loss of activity and selectivity for consequent 3 cycles.

**Keywords:** Heterogeneous catalysis; Selective deactivation; Electronic effect; Surface modification; Lignin depolymerization.

## 5.1. Introduction

Renewable energy and chemicals produced from biomass is attracting more and more interest in both academic and industrial communities <sup>[1-3]</sup>. Lignocellulosic is the most abundant biomass in the world, while cellulose and hemicellulose are formed by highly oxygenated saturated hydrocarbons, lignin is a kind of highly branched and substituted aromatic polymers <sup>[4-6]</sup>. Production of single-ring aromatics from lignin is highly desirable due to the wide application of single-ring aromatics as solvent, polymers, dyes, pharmaceutical and so on <sup>[7, 8]</sup>. Most aromatic rings in lignin are linked by phenolic ether bonds, such as  $\beta$ -O-4,  $\alpha$ -O-4, and 4-O-5 linkages, in which 4-O-5 linkages are the most stable and robust <sup>[9-11]</sup>. Cleavage of these aryl ether bonds always need elevated temperature and high H<sub>2</sub> pressure, which causes the saturation and degradation of valuable single-ring aromatic products <sup>[12, 13]</sup>. Thus, selective cleavage of aryl ether bonds in lignin without saturation of the aromatic-rings is highly desirable for the production of sustainable single-ring aromatics from lignin.

On the other hand, due to the complexity and variability of real lignin biomass, model compounds such as diphenyl ether (DPE, 4-O-5 linkages) have been widely used as a lignin model compound for the investigation of C-O bonds cleavage in lignin <sup>[12, 14, 15]</sup>. Generally, catalytic hydrogenolysis of diphenyl ether produces equimolar concentrations of phenol (PhOH) and benzene (Bez) which are subsequently hydrogenated to cyclohexanone/cyclohexanol and cyclohexane, respectively (*Figure 5.1*). Wang et al. have systemically studied the cleavage of C-O bonds in diphenyl ether

over Ni, Pd, Ru and Pt catalysts<sup>[16-18]</sup>. And they found that both hydrogenation of phenyl rings and hydrogenolysis of C-O bonds proceed in parallel during the hydrogenation of DPE in an organic solvent. The main products of DPE hydrogenation at high conversion is cyclohexane and cyclohexanol with only trace amounts of single-ring aromatics at high conversion.

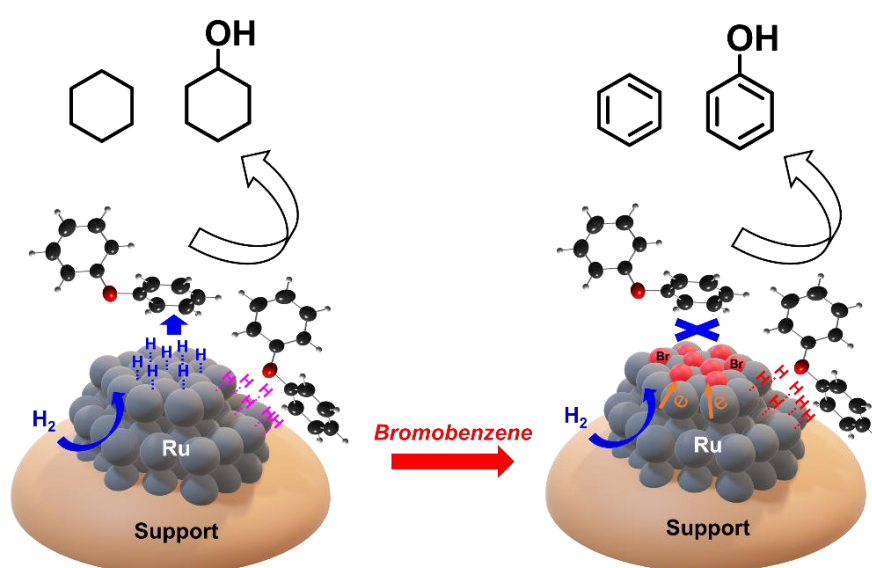
One of the main existing methods for preventing the hydrogenation of aromatic rings is the addition of homogeneous base additives<sup>[13, 19-21]</sup>. Hartwig et al reported a strategy for the hydrogenolysis of aromatic ethers using homogenous and heterogeneous nickel catalysts in the presence of NaOBu as base additive<sup>[19, 20]</sup>. Benzene and phenol are produced from DPE without further hydrogenation under mild conditions. However, regardless of the separation of homogeneous catalysts, the use of base additives suffers from the purification problem and base waste. Thus, it is still a challenge to selectively cleavage C-O bonds in DPE without hydrogenation of the aromatic rings over heterogeneous catalysts.

Indeed, hydrogenolysis and hydrogenation happen in parallel during the catalytic conversion of DPE over metal nanoparticle<sup>[12, 22, 23]</sup>. These two reactions take place on different active sites. Hydrogenolysis of C-O bonds is favored on the edge and corner sites<sup>[24-27]</sup>, while hydrogenation of aromatic rings proceed over terrace sites (As shown in *Schema 5.1*)<sup>[2, 25, 28, 29]</sup>. In order to prevent the hydrogenation of aromatic rings, selective deactivation of the terrace sites could be seen as a possible strategy<sup>[30-33]</sup>. Simon et al. reported that the reaction of furfural conversion could be directed by control of the availability of specific active sites over Pd nanoparticles<sup>[31]</sup>. Bulk organic



tail ligands restrict adsorption of furfural on terrace sites while edge and corner sites have been less affected. Although the selectivity to desired hydrogenation and hydrodeoxygenation products could be tuned, the strong poisoning effect of sulfur caused the loss of activity of the Pd catalysts. Therefore, up to now, selective deactivation of specific active sites without the loss of activity is still a challenge.

In this work, we present a Ru-Br catalyst prepared by hydrogenolysis of bromobenzene over Ru nanoparticles. Catalytic conversion of DPE over the Ru-Br catalyst under H<sub>2</sub> exhibited high selectivity to single-ring aromatics without deep hydrogenation of the aromatic rings. Characterizations and model reactions indicate that both selective poisoning effect and electronic effect contribute to the performance of the catalyst. The developed Ru-Br catalyst is highly efficient for the production of phenol (46% yield) and benzene (45% yield) from DPE with an overall yield of single-ring aromatics up to 91% under mild conditions (120°C & 5 bar of H<sub>2</sub>), and the activity and selectivity are stable for consequent 3 cycles.



**Schema 5.1.** Illustration of conversion of DPE over Ru and Ru-Br catalyst.

## 5.2. Results and discussions

### 5.2.1. Catalytic conversion of DPE

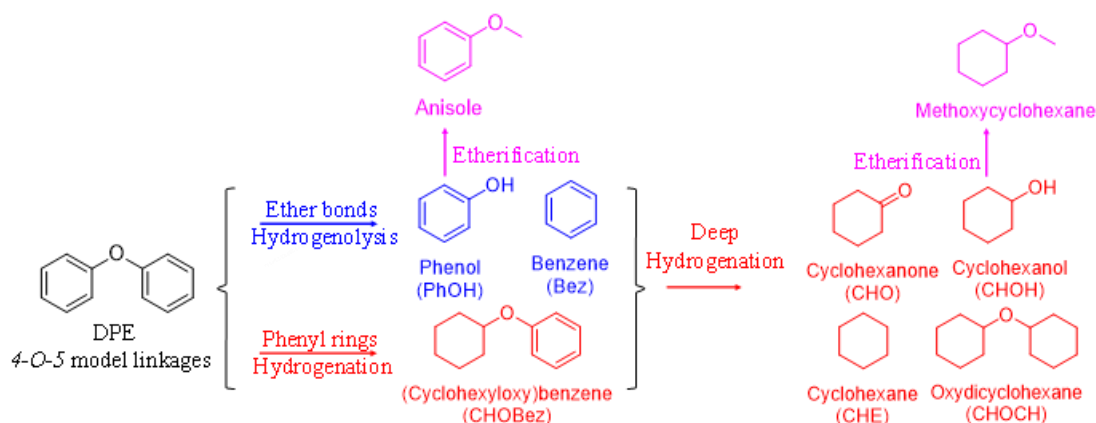


**Figure 5.1.** Illustration of the reaction pathway of DPE over Ru catalyst in methanol.

Generally, the conversion of DPE over Ru catalyst under reductive conditions involves several reaction pathways. As shown in **Figure 5.1**, in the absence of H<sub>2</sub>O there are two ways for DPE transformation. One is direct hydrogenolysis of the C-O ether bonds with the production of equivalent PhOH and Bez. Another way is the hydrogenation of one of the aromatic rings to cyclohexyloxybenzene (CHOBez). The following step includes the hydrogenolysis of CHOBez and deep hydrogenation of aromatic rings to cyclohexanone (CHO), cyclohexanol (CHOH), cyclohexane (CHE) and oxydicyclohexane (CHOCH) products. Although the direct hydrogenolysis of C-O bonds is thermodynamically more favorable than aromatic rings hydrogenation in the first step (-69.62 kJ/mol and -45.44 kJ/mol, respectively), the activation barrier for C-O bonds cleavage is very high (314 kJ/mol) [22]. Thus, the hydrogenation of aromatic rings is inevitable during the conversion of DPE under reductive conditions leading to the production of CHE, CHOH and CHOCH as the final products.

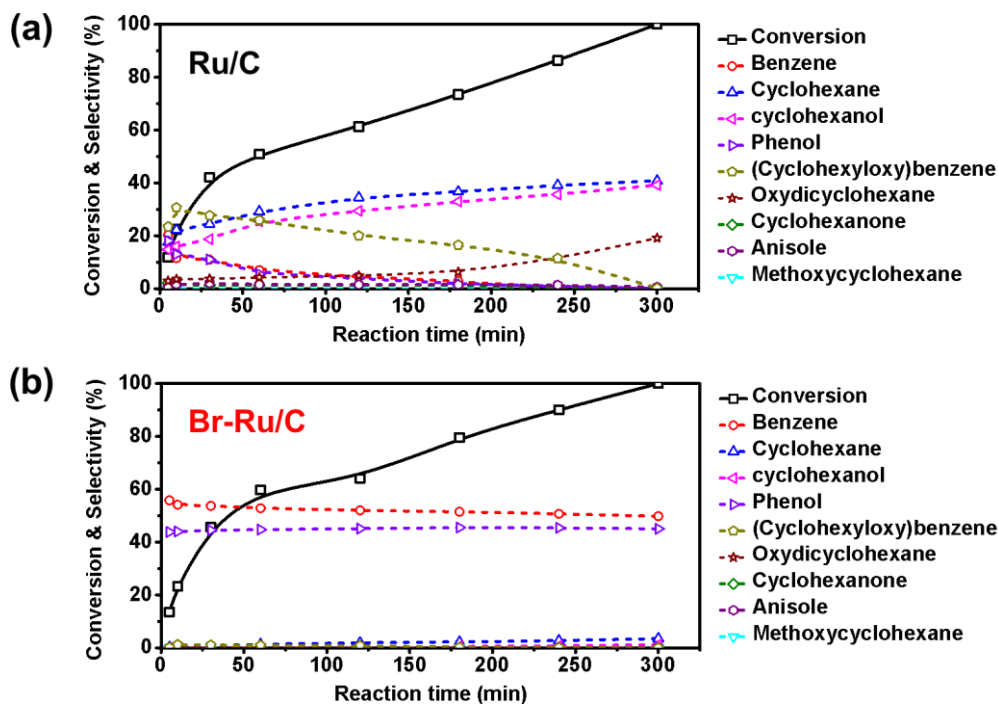


**Figure 5.2.** Conversion of DPE and selectivity to various products over (d) Ru/C, and (d) Br-Ru/C catalysts. Reaction conditions: 50 mg catalyst, 200 mg DPE, 5 g methanol, 120°C, 5 bar H<sub>2</sub>.

**Figure 5.2** shows the evolution of conversion and selectivity of DPE over Ru/C and Br-Ru/C catalysts in time. Performing the hydrogenation of DPE over the initial Ru/C catalyst yields Bez, PhOH and CHOBez as the main products at the initial time. Specifically, when the reaction time is 5 min, the conversion of DPE over the parent Ru/C was 11.8 % and the selectivity to Bez, PhOH and CHOBez were 20.3, 18.1, and 23.4 %, respectively. These results are in agreement with the literature [23, 34-37]. However, with the reaction time increase the selectivity to Bez and PhOH continuously decrease to 4.4 % and 4.0 %, respectively, at 120 min. At the same time, the selectivity to aromatic rings hydrogenation products such as CHE, CHOH, and CHOCH significantly increase. Notably, the selectivity to CHOBez increases from 23.4 % to 30.7 % at the beginning of the reaction with subsequent decrease to 20.0 % when the

reaction time was 120 min. This is due to further hydrogenation and hydrogenolysis of CHOBez. The main products of the reaction at full conversions of DPE are CHE (40.8%), CHO (39.8%) and CHOCH (19.1%).

Interestingly, after the modification of Ru by Br, the Br-Ru/C catalyst demonstrates different catalytic behavior. The reaction proceeds with the generation of Bez and PhOH as two main products reaching the selectivity to 49.8% and 45.0%, respectively. Thus, the hydrogenation of aromatic rings has been significantly suppressed during the whole reaction time. Notably, the total yield of single-ring aromatic products (Bez and PhOH) was 94.8 % over Br-Ru/C catalyst compared to 0% over initial Ru/C catalyst at full conversion. Although some etherification products such as methoxycyclohexane and anisole were observed over both Ru/C and Br-Ru/C catalyst due to the reaction with methanol as a solvent (*Figure 5.1*), the amount was quite low (< 2%). Usually this reaction requires acid sites and the low selectivity to ether products indicates the absence of acid sites over both Ru/C and Br-Ru/C catalysts [38].

The hydrogenolysis of DPE produces equivalent molar of Bez and PhOH. In the case of aromatic rings hydrogenation, the total selectivity to Bez and CHE ( $S_{\text{Bez+CHE}}$ ) should be equal to the total selectivity to oxygenated products such as PhOH, CHO and CHOCH ( $S_{\text{PhOH+CHO+CHOH}}$ ). However, regarding both Ru/C and Br-Ru/C catalysts, the  $S_{\text{Bez+CHE}}$  is always higher than  $S_{\text{PhOH+CHO+CHOH}}$ . Specifically, when the conversion is about 60 % over Ru/C catalyst%, the  $S_{\text{Bez+CHE}}$  is 38.9% in comparison with 34.7% of  $S_{\text{PhOH+CHO+CHOH}}$ . At the comparable conversion over Br-Ru/C catalyst, the  $S_{\text{bez+CHE}}$  is 53.9 %, which is higher than  $S_{\text{PhOH+CHO+CHOH}}$  of 45.3%. The higher amount of oxygen

free products could be ascribed to partial deoxygenation of PhOH and CHOH to Bez and CHE, respectively, which is reported by the literatures [39,40].

**Table 5.1.** TOF number of DPE over Ru/C and Br-Ru/C

Catalyst	Conversion (%) <sup>a</sup>	TOF (min <sup>-1</sup> ) <sup>b</sup>		
		DPE	Hydrogenolysis	Hydrogenation
Ru/C	11.8	5.4	3.8	3.3
Br-Ru/C	13.8	6.1	6.1	0.05

<sup>a</sup> Reaction conditions: 200 mg DPE, 50 mg catalyst, 5 g methanol, 120°C. 5 bar H<sub>2</sub>, 5 min.

<sup>b</sup> Turnover frequency (TOF) was calculated based on metal dispersion determined by O<sub>2</sub>-pulse chemistry (21%).

It is worth to note, although the hydrogenation of aromatic rings was suppressed, the activity of the catalysts did not decrease. The turnover frequency (TOF) numbers of DPE conversion over Ru/C and Br-Ru/C catalysts were calculated and summarized in **Table 5.1**. The TOF for DPE conversion over Br-Ru/C catalyst is comparable with initial Ru/C catalysts (5.4 min<sup>-1</sup> vs 6.1 min<sup>-1</sup>, **Table 5.1**). The TOF numbers for different reaction routes (hydrogenation of aromatic rings and hydrogenolysis of C-O ether bonds) were calculated based on the results obtained at low conversion (< 15 %). Notably, Br-Ru/C catalyst shows twice higher activity for hydrogenolysis of C-O ether bonds in comparison with Ru/C (3.8 min<sup>-1</sup> vs. 6.1 min<sup>-1</sup>), while the activity for hydrogenation of aromatic rings is totally suppressed (3.3 min<sup>-1</sup> vs. 0.05 min<sup>-1</sup>). These results indicate that after modification with Br, Br-Ru/C catalyst has enhanced hydrogenolysis ability for aryl ether bonds with almost no activity for aromatic rings hydrogenation.

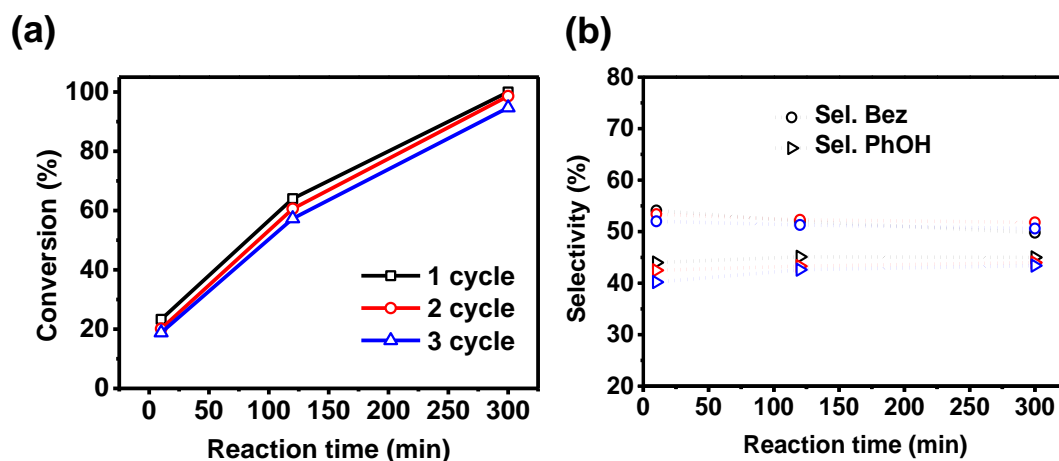


**Figure 5.3.** Stability test of Br-Ru/C catalyst (a) Conversion of DPE; (b) Selectivity to different products.

The stability of Br-Ru/C catalyst has been confirmed by the catalytic test of DPE conversion at 120 °C under 5 bar of H<sub>2</sub> in three consecutive cycles with intermediate separation of the catalyst (**Figure 5.3**). The catalyst demonstrates comparable activity and selectivity in DPE conversion for 3 cycles.

Other halogens such as Cl and I have been used to modify Ru/C catalyst. The prepared Cl-Ru/C and I-Ru/C catalysts were subjected to DPE conversion at 120 °C under 5 bar of H<sub>2</sub> for 300 min. As shown in **Table 5.2**, Cl-Ru/C catalyst showed the similar products distributions to initial Ru/C, with selectivity to CHE of 35.6 %, selectivity to CHOH of 31.9 % and selectivity to CHOCH to 12.5%. The selectivity to single ring aromatic products such Bez and PhOH was 8.9% and 9.7%, respectively. It means that Cl has some effect in deactivation of aromatic-rings hydrogenation but significantly lower in comparison with Br. I-Ru/C catalyst demonstrates almost no conversion for DPE, which means that Ru catalyst was totally deactivated by I. These catalytic results suggest that the changes of catalytic performance could be ascribed to the deactivation

effect of halogen atoms. While Cl has a weak deactivation effect for aromatic rings hydrogenation, I demonstrates strong poisoning effect for both hydrogenations and hydrogenolysis. Br demonstrates intermediate behavior with selectivity poisoning of Ru for aromatic rings hydrogenation.

**Table 5.2.** Catalytic DPE conversion over various catalysts.

Catalysts	Conversion <sup>a</sup> (%)	Selectivity <sup>b</sup> (%)							
		Bez	CHE	CHO	CHOH	PhOH	CHOCH	CHOBez	Ethers
Ru/C	100	0	40.8	0	39.2	0	19.1	0.2	0.4
Br-Ru/C	100	49.6	3.5	0.3	1.2	49.8	0	0	0.2
Cl-Ru/C	100	8.9	35.6	0.9	31.9	9.7	12.5	0.4	-
I-Ru/C	0.8	-	-	-	-	-	-	-	-
Ru/SiO <sub>2</sub>	47.4	5.1	23.5	1.8	20.8	4.6	4.2	39.5	0.3
Br-Ru/SiO <sub>2</sub>	18.6	48.4	1.0	0.3	1.4	47.6	0.0	0.9	0.2

<sup>a</sup> Reaction conditions: 200 mg DPE, 50 mg catalyst, 5 g methanol, 120°C, 5 bar H<sub>2</sub>, 300 min.

<sup>b</sup> A trace amount of acetalization products such as (dimethoxymethyl)cyclohexane and (dimethoxymethyl)benzene were also observed.

Ru catalyst over other support such as SiO<sub>2</sub> at the same loadings has been also studied in DPE conversion. Although the initial Ru/SiO<sub>2</sub> catalyst showed lower activity in comparison to Ru/C, the products distributions are similar. The main products over Ru/SiO<sub>2</sub> catalyst were CHE (23.5%), CHOH (20.8%) and CHOBez (40.9%), providing high efficiency for hydrogenation of aromatic rings. Similarly, after modification with Br, although the conversion of DPE decreased from 47.4% to 18.6%, Br-Ru/SiO<sub>2</sub> showed high selectivity to Bez (48.4%) and PhOH (47.6%) with full suppression of aromatic rings hydrogenation. The same trend of product distribution after modification

of Ru by Br indicates that the key role in the changes of the selectivity is due to interaction between Ru nanoparticles and Br.

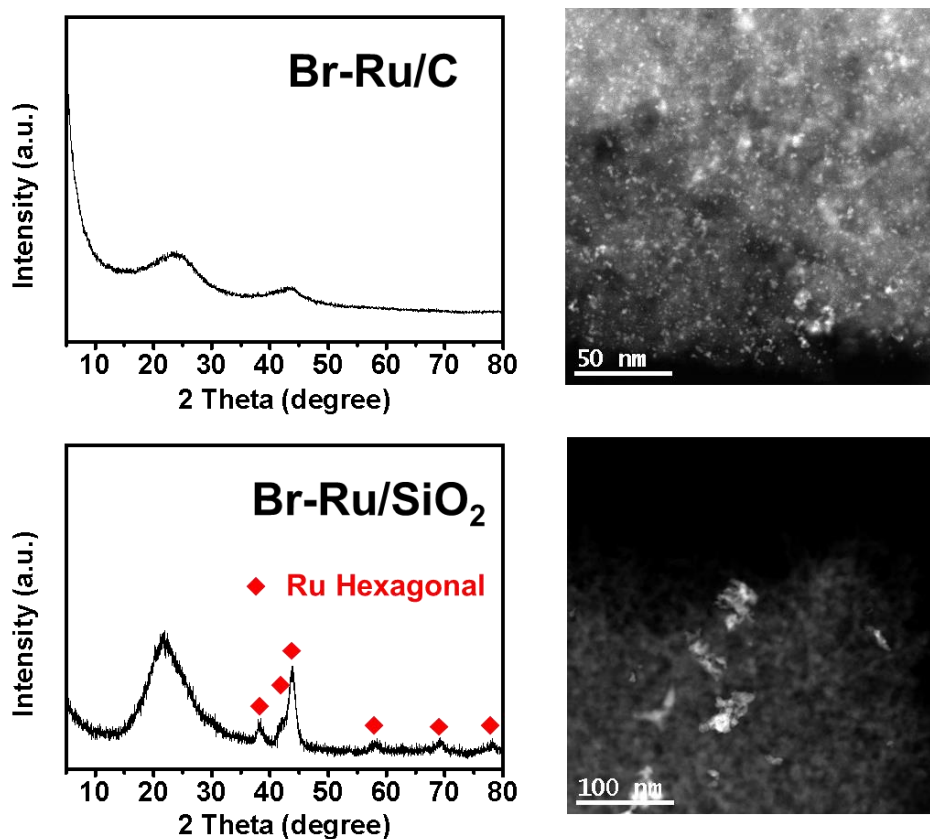


**Figure 5.4.** XRD and TEM analysis of Br-Ru/C and Br-Ru/SiO<sub>2</sub> catalysts.

The decrease of DPE conversion over Br-Ru/SiO<sub>2</sub> compared to Br-Ru/C could be possibly explained by the particle size effect<sup>[41]</sup>. As indicated in **Figure 5.4**, the XRD and TEM analysis suggest that Ru has a much larger particle size on SiO<sub>2</sub> than on C. The contribution of edges and corners over Ru nanoparticles increase with decrease of the particle sizes. It has been reported that hydrogenation of aromatic rings is a mild structure sensitive reaction<sup>[28]</sup>, while hydrogenation of C-O is a strong structure sensitive reaction<sup>[27]</sup>. Hydrogenation of aromatic rings usually proceeds on the terrace sites, while the hydrogenolysis of C-O bonds proceeds on the edge and corner sites.



Thus, it is reasonable to suspect that the decrease of the activity of Br-Ru/SiO<sub>2</sub> in comparison with Br-Ru/C catalyst could be assigned to deactivation of terrace sites on Ru nanoparticles.

### 5.2.2. Characterizations

The role of Br in the modification of the catalytic performance has been studied using different characterization tools. First of all, the Ru-Br catalyst was subjected to STEM-EDS analysis to determine to localization of Br. Obviously, the Br signals come from the same position with Ru, confirming the treatment of BrBen leads to the modification of Ru nanoparticles with Br atoms (*Figure 5.5*).

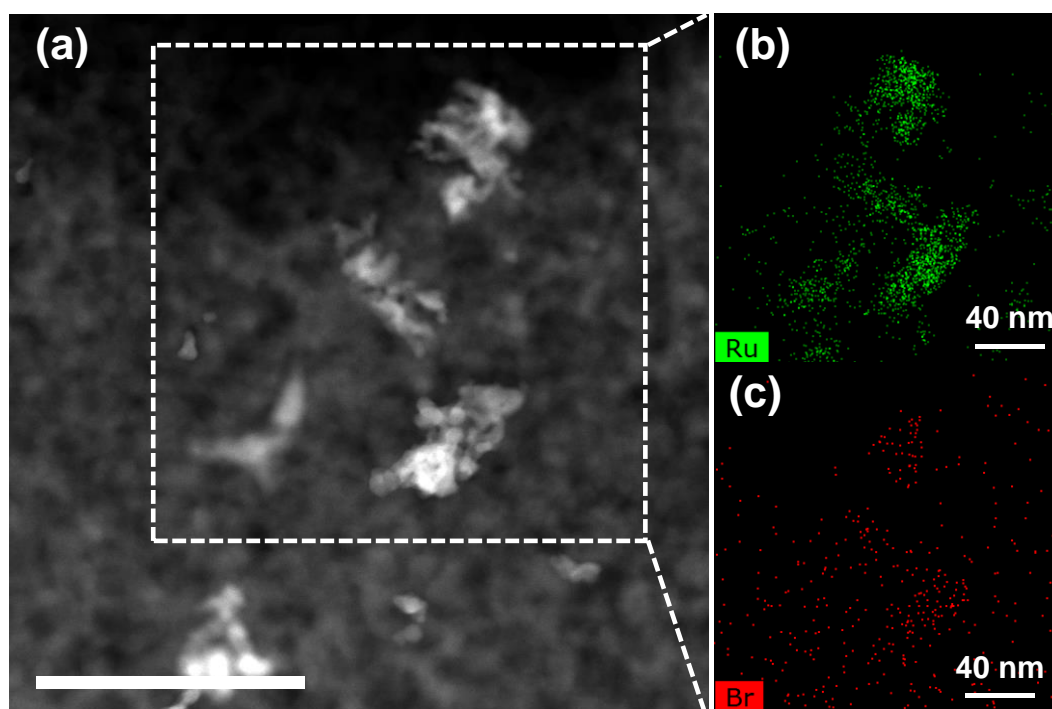


*Figure 5.5.* TEM-EDS analysis (a) STEM image, (b - c) corresponding EDS elemental maps of Br-Ru/SiO<sub>2</sub> catalyst.

XPS analysis was carried out to determine the electronic effect of Br and Ru in Br-Ru/C catalyst. *Figure 5.6* shows Ru 3p and Br 3d core level spectra of Br-Ru/C catalyst

before and after reaction compared with spectra of initial Ru/C. A Ru 3p spectrum has 3p<sub>3/2</sub> and 3p<sub>1/2</sub> components with 22.2 eV spin-orbit splitting<sup>[42]</sup>. As shown in *Figure 5.6a*, initial Ru/C has two doublets with BE (Ru 3p<sub>3/2</sub>) 462.3 eV and 465.1 eV attributed to metallic Ru<sup>0</sup> and Ru<sup>3+</sup>, respectively. Both of these states co-exist on the surface with domination of the metallic state. A minor shift of Ru 3p peaks to higher BE for Br-Ru/C catalysts (both before and after reaction) can be attributed to interaction of Ru with Br. This interaction leads to the electron withdrawal effect from Ru to Br. In Br-Ru/C catalyst, Br withdraws electrons from Ru nanoparticles resulting in lower electron density and positive charge of the Ru nanoparticles. It is interesting that the Ru<sup>3+</sup> also exist in Br-Ru/C sample (both before and after reaction), indicating the presence of oxidized Ru over Ru-Br nanoparticles.

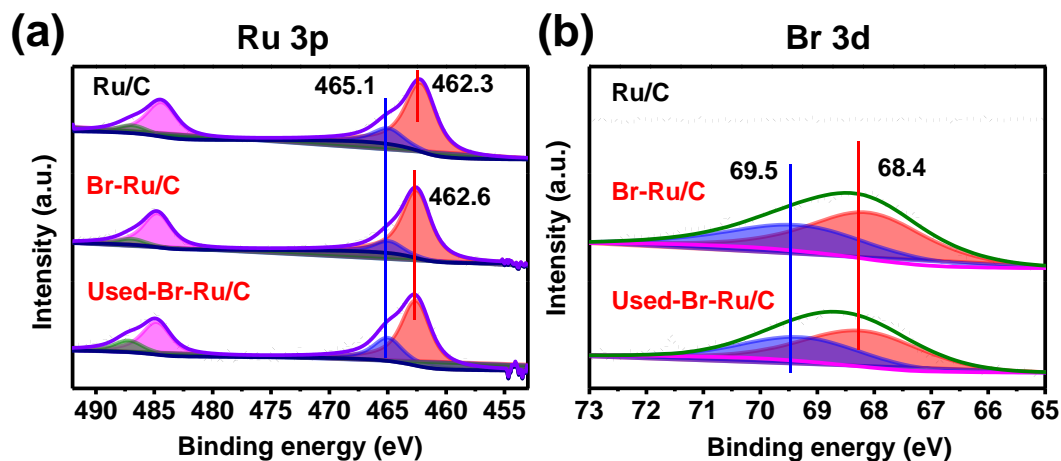


*Figure 5.6.* XPS Ru 3p (a) and Br 3d (b) core level spectra of Ru/C, Br-Ru/C and Br-Ru/C after reaction.

Br 3d spectra of the considered samples are shown in *Figure 5.6b*, demonstrating 3d<sub>5/2</sub> and 3d<sub>3/2</sub> spin-orbit doublets with 1.04 eV splitting<sup>[43]</sup>. For Br-Ru/C catalyst (both before and after reaction), the Br 3d<sub>5/2</sub> peak has BE at 68.4 eV confirming the presence

of Br on these catalysts. It is worth to note that Br-Ru/C after reaction shows similar Ru 3p and Br 3d spectra suggesting high stability of the Ru-Br catalyst.

XPS indicates the electronic withdrawal of electrons from Ru to Br. It has been reported earlier that the electronic properties of metal nanoparticles affect its reactivity for different groups. For example, the negative charged Pd nanoparticles modified with phosphine ligands showed higher activity for electronic deficiency groups such as nitrobenzene but lower activity for electronic rich groups such as benzyl aldehydes, comparing with the non-modified counterpart <sup>[44, 45]</sup>. Thus, the increased activity for hydrogenolysis of C-O bond from 3.8 min<sup>-1</sup> to 6.1 min<sup>-1</sup> (*Table 5.1*) could be ascribed to the electropositive state of Ru in comparison with the parent Ru catalyst.

FTIR spectroscopy of CO adsorption has been used to identify the state of the active sites on Ru. The band at 1998 cm<sup>-1</sup> is due to CO linearly adsorbed on defect sites at edges and corners of Ru nanoparticle. The intensive band at 1877 cm<sup>-1</sup> is related to CO adsorbed on the Ru nanoparticles planes with bridge-bonds (*Figure 5.7*) <sup>[33, 46]</sup>. The modification of Ru by Br leads to the complete disappearance of the peak at 1877 cm<sup>-1</sup> with a shift of the peaks attributed to CO adsorption over edges and corners. The disappearance of the adsorption of CO on terrace sites could be explained by the simplified hydrogenolysis of BrBen and selective deposition of Br over the planes of Ru nanoparticles. And the red-shift of the peak at 1998 cm<sup>-1</sup> to 2006 cm<sup>-1</sup> was due to the electronic withdraw effect of Br on Ru nanoparticles. Moreover, a small peak with frequency at 2072 cm<sup>-1</sup> is visible and could be assigned to CO adsorbed over unsaturated Ru-Br sites with electron deficient Ru sites. Thus, the role of Br on the

deactivation of aromatic rings hydrogenation over Ru nanoparticles could be assigned to the selective deactivation of terrace sites.

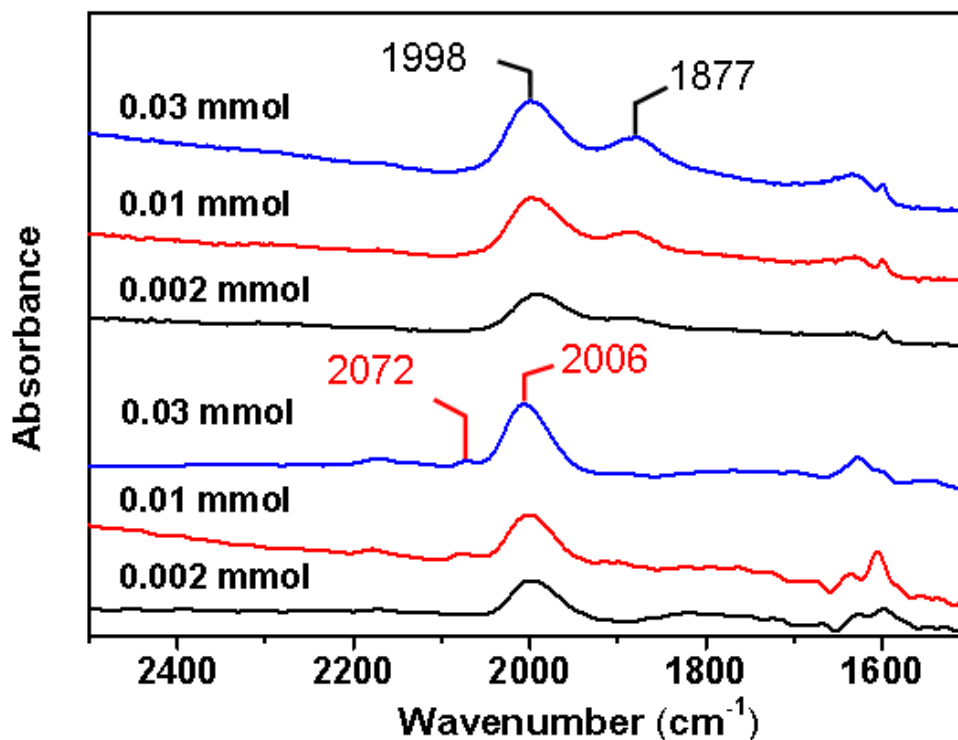


**Figure 5.7.** CO-FTIR for Ru/SiO<sub>2</sub> and Br-Ru/SiO<sub>2</sub>

According to the STEM-EDS, XPS, and CO-FTIR, we can conclude that the modification of Ru nanoparticles with BrBen leads to the selective deposition of Br atoms on the terrace sites of Ru nanoparticles with electronic withdraw effect from Ru to Br. The combination of selective poisoning of terrace sites and electronic withdrawal effects result in the efficient production of single-ring aromatic products from DPE. While the selective poisoning of terrace sites deactivates the most active sites for aromatic rings hydrogenation, the electron withdrawing effect of Br over Ru surface further leads to an increased activity for C-O bond hydrogenolysis. Thus, an increase of the TOF numbers for hydrogenolysis of C-O bonds over Br-Ru/C catalyst could be

explained the electron withdrawing effect from Ru to Br and the significant decrease of the TOF number for aromatic rings hydrogenation could be explained by the selective deactivation of terrace sites.

### 5.2.3. Model reactions

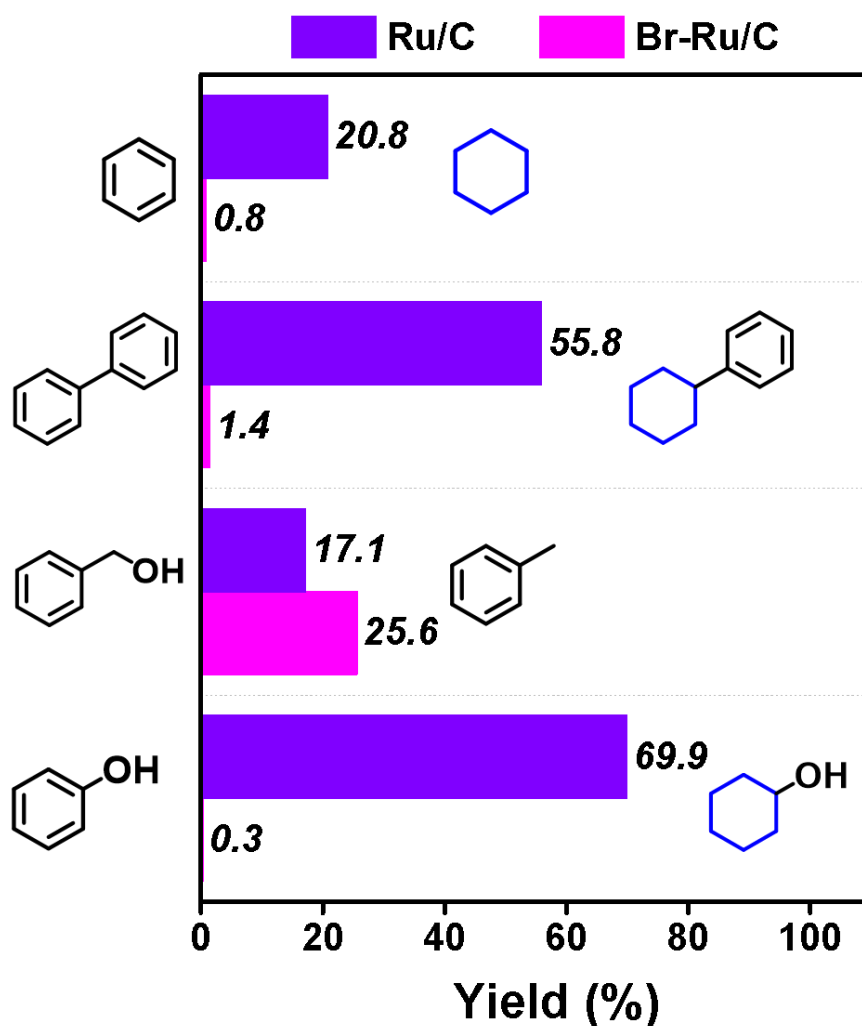


**Figure 5.8.** Model reactions of hydrogenation of Bez, biphenyl, benzyl alcohol, and PhOH over Ru/C and Br-Ru/C catalysts, respectively. Reaction conditions: Benzyl alcohol hydrogenolysis: 15 mg catalyst, 200 mg benzyl alcohol, 5 g methanol, 80°C, 5 bar H<sub>2</sub>, 30 min; Biphenyl hydrogenation: 50 mg catalyst, 200 mg biphenyl, 5 g methanol, 120°C, 5 bar H<sub>2</sub>, 1 h; Bez hydrogenation: 50 mg catalyst, 200 mg biphenyl, 5 g methanol, 120°C, 5 bar H<sub>2</sub>, 1 h; PhOH hydrogenation: 50 mg catalyst, 200 mg benzyl alcohol, 5 g methanol, 80°C, 5 bar H<sub>2</sub>, 30 min.

To support these conclusions, additional model reactions were performed over Ru/C and Br-Ru/C catalysts. These model experiments include hydrogenation of Bez, biphenyl, PhOH and hydrogenolysis of benzyl alcohol. The aim of these model reactions was to demonstrate activity for aromatic rings hydrogenation and C-O bonds hydrogenolysis over Ru and Br- Ru catalysts.

*Figure 5.8* confirmed high activity of the Ru/C catalyst for hydrogenation of aromatic rings in Bez, PhOH and biphenyl, while a significant decrease of activity for the same reactant was observed over Br-Ru/C catalyst. It confirms that modification by Br has dramatically suppressed the hydrogenation of aromatic rings. At the same time, a higher activity for C-O bonds hydrogenolysis of benzyl alcohol conversion to toluene has been observed over Br-Ru/C catalyst. Model reactions confirmed the deactivation of aromatic rings hydrogenation and increase of hydrogenolysis of C-O bonds over Ru-Br catalysts. This effect is derived from the synergy of selective poisoning effect and electron withdrawal effect of Br <sup>[47-49]</sup>.

### **5.3. Conclusion**

In this work, Ru-Br catalyst prepared by simple hydrogenolysis of bromobenzene over supported Ru nanoparticles has been used for the directly hydrogenolysis of diphenyl ether to benzene and phenol with high activity and selectivity in comparison with the synthesis of hydrogenated products over Ru catalyst. The two roles of Br in modification of the properties of Ru has been identified. First of all, Br provides selective poisoning of terrace sites of Ru nanoparticles active in aromatic rings

hydrogenation with no effect on edges and corners effective in hydrogenolysis of C-O bonds. The selective poisoning effect of Br is responsible for the high selectivity to Bez and PhOH. Another effect is related to electron withdrawing induced by Br which makes the Ru nanoparticle positively charged with increase of the activity for hydrogenolysis of electron-rich C-O bonds. This work describes a synergy of selective poisoning and electronic effects in surface modification of metal nanoparticles with halogens, which provides a powerful tool for design of metal catalysts for selective processes.

## Reference

1. Gerardy, R.; Debecker, D. P.; Estager, J.; Luis, P.; Monbaliu, J. M., Continuous Flow Upgrading of Selected C<sub>2</sub>-C<sub>6</sub> Platform Chemicals Derived from Biomass. *Chem. Rev.* **2020**, *120* (15), 7219-7347.
2. Mondelli, C.; Gozaydin, G.; Yan, N.; Perez-Ramirez, J., Biomass valorisation over metal-based solid catalysts from nanoparticles to single atoms. *Chem. Soc. Rev.* **2020**, *49* (12), 3764-3782.
3. Wu, X.; Luo, N.; Xie, S.; Zhang, H.; Zhang, Q.; Wang, F.; Wang, Y., Photocatalytic transformations of lignocellulosic biomass into chemicals. *Chem. Soc. Rev.* **2020**, *49* (17), 6198-6223.
4. Gao, F.; Webb, J. D.; Sorek, H.; Wemmer, D. E.; Hartwig, J. F., Fragmentation of Lignin Samples with Commercial Pd/C under Ambient Pressure of Hydrogen. *ACS Catal.* **2016**, *6* (11), 7385-7392.
5. Gazi, S., Valorization of wood biomass-lignin via selective bond scission: A minireview. *Appl. Catal. B* **2019**, *257*, 117936.
6. Lahive, C. W.; Deuss, P. J.; Lancefield, C. S.; Sun, Z.; Cordes, D. B.; Young, C. M.; Tran, F.; Slawin, A. M.; de Vries, J. G.; Kamer, P. C.; Westwood, N. J.; Barta, K., Advanced Model Compounds for Understanding Acid-Catalyzed Lignin Depolymerization: Identification of Renewable Aromatics and a Lignin-Derived Solvent. *J. Am. Chem. Soc.* **2016**, *138* (28), 8900-8911.
7. Lin, J.; Wu, X.; Xie, S.; Chen, L.; Zhang, Q.; Deng, W.; Wang, Y., Visible-Light-Driven Cleavage of C-O Linkage for Lignin Valorization to Functionalized Aromatics. *ChemSusChem* **2019**, *12* (22), 5023-5031.
8. Zhou, C.; Shi, J.; Zhou, W.; Cheng, K.; Zhang, Q.; Kang, J.; Wang, Y., Highly Active ZnO-ZrO<sub>2</sub> Aerogels Integrated with H-ZSM-5 for Aromatics Synthesis from Carbon Dioxide. *ACS Catal.* **2019**, *10* (1), 302-310.
9. Mahajan, J. S.; O'Dea, R. M.; Norris, J. B.; Korley, L. T. J.; Epps, T. H., Aromatics from Lignocellulosic Biomass: A Platform for High-Performance Thermosets. *ACS Sustainable Chem. Eng.* **2020**, *8*, 40, 15072-15096.
10. Nguyen, S. T.; Murray, P. R. D.; Knowles, R. R., Light-Driven Depolymerization of Native Lignin Enabled by Proton-Coupled Electron Transfer. *ACS Catal.* **2019**, *10* (1), 800-805.
11. Wong, S. S.; Shu, R.; Zhang, J.; Liu, H.; Yan, N., Downstream processing of lignin derived feedstock into end products. *Chem. Soc. Rev.* **2020**, *49* (15), 5510-5560.



12. Jiang, L.; Guo, H.; Li, C.; Zhou, P.; Zhang, Z., Selective cleavage of lignin and lignin model compounds without external hydrogen, catalyzed by heterogeneous nickel catalysts. *Chem. Sci.* **2019**, *10* (16), 4458-4468.
13. Li, H.; Song, G., Ru-Catalyzed Hydrogenolysis of Lignin: Base-Dependent Tunability of Monomeric Phenols and Mechanistic Study. *ACS Catal.* **2019**, *9* (5), 4054-4064.
14. Mauriello, F.; Paone, E.; Pietropaolo, R.; Balu, A. M.; Luque, R., Catalytic Transfer Hydrogenolysis of Lignin-Derived Aromatic Ethers Promoted by Bimetallic Pd/Ni Systems. *ACS Sustainable Chem. Eng.* **2018**, *6* (7), 9269-9276.
15. Xu, G.-Y.; Guo, J.-H.; Qu, Y.-C.; Zhang, Y.; Fu, Y.; Guo, Q.-X., Selective hydrodeoxygenation of lignin-derived phenols to alkyl cyclohexanols over a Ru-solid base bifunctional catalyst. *Green Chem.* **2016**, *18* (20), 5510-5517.
16. Wang, M.; Shi, H.; Camaioni, D. M.; Lercher, J. A., Palladium-Catalyzed Hydrolytic Cleavage of Aromatic C–O Bonds. *Angew. Chem. Int. Ed.* **2017**, *56* (8), 2110-2114.
17. Wang, M.; Zhao, Y.; Mei, D.; Bullock, R. M.; Gutiérrez, O. Y.; Camaioni, D. M.; Lercher, J. A., The Critical Role of Reductive Steps in the Nickel-Catalyzed Hydrogenolysis and Hydrolysis of Aryl Ether C–O Bonds. *Angew. Chem. Int. Ed.* **2020**, *59* (4), 1445-1449.
18. Wang, M.; Gutiérrez, O. Y.; Camaioni, D. M.; Lercher, J. A., Palladium-Catalyzed Reductive Insertion of Alcohols into Aryl Ether Bonds. *Angew. Chem. Int. Ed.* **2018**, *57* (14), 3747-3751.
19. Sergeev, A. G.; Hartwig, J. F., Selective, nickel-catalyzed hydrogenolysis of aryl ethers. *Science* **2011**, *332* (6028), 439-443.
20. Sergeev, A. G.; Webb, J. D.; Hartwig, J. F., A heterogeneous nickel catalyst for the hydrogenolysis of aryl ethers without arene hydrogenation. *J. Am. Chem. Soc.* **2012**, *134* (50), 20226-20229.
21. Zhao, W.; Li, X.; Li, H.; Zheng, X.; Ma, H.; Long, J.; Li, X., Selective Hydrogenolysis of Lignin Catalyzed by the Cost-Effective Ni Metal Supported on Alkaline MgO. *ACS Sustainable Chem. Eng.* **2019**, *7* (24), 19750-19760.
22. Bulut, S.; Siankevich, S.; van Muyden, A. P.; Alexander, D. T. L.; Savoglidis, G.; Zhang, J.; Hatzimanikatis, V.; Yan, N.; Dyson, P. J., Efficient cleavage of aryl ether C–O linkages by Rh-Ni and Ru-Ni nanoscale catalysts operating in water. *Chem. Sci.* **2018**, *9* (25), 5530-5535.
23. Guo, M.; Peng, J.; Yang, Q.; Li, C., Highly Active and Selective RuPd Bimetallic NPs for the Cleavage of the Diphenyl Ether C–O Bond. *ACS Catal.* **2018**, *8* (12), 11174-11183.

24. Dong, L.; Yin, L.-L.; Xia, Q.; Liu, X.; Gong, X.-Q.; Wang, Y., Size-dependent catalytic performance of ruthenium nanoparticles in the hydrogenolysis of a  $\beta$ -O-4 lignin model compound. *Catal. Sci. Technol.* **2018**, *8* (3), 735-745.
25. Yang, F.; Liu, D.; Zhao, Y.; Wang, H.; Han, J.; Ge, Q.; Zhu, X., Size Dependence of Vapor Phase Hydrodeoxygenation of m-Cresol on Ni/SiO<sub>2</sub> Catalysts. *ACS Catal.* **2018**, *8* (3), 1672-1682.
26. Zhang, L.; Zhou, M.; Wang, A.; Zhang, T., Selective Hydrogenation over Supported Metal Catalysts: From Nanoparticles to Single Atoms. *Chem. Rev.* **2020**, *120* (2), 683-733.
27. Chiu, C. C.; Genest, A.; Borgna, A.; Rosch, N., C-O cleavage of aromatic oxygenates over ruthenium catalysts. A computational study of reactions at step sites. *Phys. Chem. Chem. Phys.* **2015**, *17* (23), 15324-15330.
28. Pushkarev, V. V.; An, K.; Alayoglu, S.; Beaumont, S. K.; Somorjai, G. A., Hydrogenation of benzene and toluene over size controlled Pt/SBA-15 catalysts: Elucidation of the Pt particle size effect on reaction kinetics. *J. Catal.* **2012**, *292*, 64-72.
29. Chacón, G.; Dupont, J., Arene Hydrogenation by Metal Nanoparticles in Ionic Liquids. *ChemCatChem* **2018**, *11* (1), 333-341.
30. Legras, B.; Ordonsky, V. V.; Dujardin, C.; Virginie, M.; Khodakov, A. Y., Impact and Detailed Action of Sulfur in Syngas on Methane Synthesis on Ni/ $\gamma$ -Al<sub>2</sub>O<sub>3</sub> Catalyst. *ACS Catal.* **2014**, *4* (8), 2785-2791.
31. Pang, S. H.; Schoenbaum, C. A.; Schwartz, D. K.; Medlin, J. W., Directing reaction pathways by catalyst active-site selection using self-assembled monolayers. *Nat. Commun.* **2013**, *4*, 2448.
32. Snelders, D. J. M.; Yan, N.; Gan, W.; Laurencyzy, G.; Dyson, P. J., Tuning the Chemoselectivity of Rh Nanoparticle Catalysts by Site-Selective Poisoning with Phosphine Ligands: The Hydrogenation of Functionalized Aromatic Compounds. *ACS Catal.* **2012**, *2* (2), 201-207.
33. Zhang, F.; Fang, J.; Huang, L.; Sun, W.; Lin, Z.; Shi, Z.; Kang, X.; Chen, S., Alkyne-Functionalized Ruthenium Nanoparticles: Impact of Metal-Ligand Interfacial Bonding Interactions on the Selective Hydrogenation of Styrene. *ACS Catal.* **2018**, *9* (1), 98-104.
34. Hua, M.; Song, J.; Xie, C.; Wu, H.; Hu, Y.; Huang, X.; Han, B., Ru/hydroxyapatite as a dual-functional catalyst for efficient transfer hydrogenolytic cleavage of aromatic ether bonds without additional bases. *Green Chem.* **2019**, *21* (18), 5073-5079.

35. Luo, Z.; Zheng, Z.; Wang, Y.; Sun, G.; Jiang, H.; Zhao, C., Hydrothermally stable Ru/HZSM-5-catalyzed selective hydrogenolysis of lignin-derived substituted phenols to bio-arenes in water. *Green Chem.* **2016**, *18* (21), 5845-5858.
36. Wu, H.; Song, J.; Xie, C.; Wu, C.; Chen, C.; Han, B., Efficient and Mild Transfer Hydrogenolytic Cleavage of Aromatic Ether Bonds in Lignin-Derived Compounds over Ru/C. *ACS Sustainable Chem. Eng.* **2018**, *6* (3), 2872-2877.
37. Zhang, L.; Wang, Y.; Yang, Y.; Zhang, B.; Wang, S.; Lin, J.; Wan, S.; Wang, Y., Selective hydrogenolysis of aryl ether bond over Ru-Fe bimetallic catalyst. *Catal. Today* **2020**.
38. Wu, D.; Hernández, W. Y.; Zhang, S.; Vovk, E. I.; Zhou, X.; Yang, Y.; Khodakov, A. Y.; Ordonsky, V. V., In Situ Generation of Brønsted Acidity in the Pd-I Bifunctional Catalysts for Selective Reductive Etherification of Carbonyl Compounds under Mild Conditions. *ACS Catal.* **2019**, *9* (4), 2940-2948.
39. Liu, S.; Wang, H.; Smith, K. J.; Kim, C. S., Hydrodeoxygenation of 2-Methoxyphenol over Ru, Pd, and Mo<sub>2</sub>C Catalysts Supported on Carbon. *Energy Fuels* **2017**, *31* (6), 6378-6388.
40. Nelson, R. C.; Baek, B.; Ruiz, P.; Goundie, B.; Brooks, A.; Wheeler, M. C.; Frederick, B. G.; Grabow, L. C.; Austin, R. N., Experimental and Theoretical Insights into the Hydrogen-Efficient Direct Hydrodeoxygenation Mechanism of Phenol over Ru/TiO<sub>2</sub>. *ACS Catal.* **2015**, *5* (11), 6509-6523.
41. Cao, S.; Monnier, J. R.; Williams, C. T.; Diao, W.; Regalbuto, J. R., Rational nanoparticle synthesis to determine the effects of size, support, and K dopant on Ru activity for levulinic acid hydrogenation to  $\gamma$ -valerolactone. *J. Catal.* **2015**, *326*, 69-81.
42. Martínez-Prieto, L. M.; Puche, M.; Cerezo-Navarrete, C.; Chaudret, B., Uniform Ru nanoparticles on N-doped graphene for selective hydrogenation of fatty acids to alcohols. *J. Catal.* **2019**, *377*, 429-437.
43. Smykalla, L.; Shukryna, P.; Korb, M.; Lang, H.; Hietschold, M., Surface-confined 2D polymerization of a brominated copper-tetraphenylporphyrin on Au(111). *Nanoscale* **2015**, *7* (9), 4234-4241.
44. Komanoya, T.; Kinemura, T.; Kita, Y.; Kamata, K.; Hara, M., Electronic Effect of Ruthenium Nanoparticles on Efficient Reductive Amination of Carbonyl Compounds. *J. Am. Chem. Soc.* **2017**, *139* (33), 11493-11499.
45. Guo, M.; Li, H.; Ren, Y.; Ren, X.; Yang, Q.; Li, C., Improving Catalytic Hydrogenation Performance of Pd Nanoparticles by Electronic Modulation Using Phosphine Ligands. *ACS Catal.* **2018**, *8* (7), 6476-6485.

46. Campisi, S.; Ferri, D.; Villa, A.; Wang, W.; Wang, D.; Kröcher, O.; Prati, L., Selectivity Control in Palladium-Catalyzed Alcohol Oxidation through Selective Blocking of Active Sites. *J. Phys. Chem. C* **2016**, *120* (26), 14027-14033.
47. Sá, J.; Medlin, J. W., On-the-fly Catalyst Modification: Strategy to Improve Catalytic Processes Selectivity and Understanding. *ChemCatChem* **2019**, *11* (15), 3355-3365.
48. Liu, P.; Qin, R.; Fu, G.; Zheng, N., Surface Coordination Chemistry of Metal Nanomaterials. *J. Am. Chem. Soc.* **2017**, *139* (6), 2122-2131.
49. Yang, F.; Deng, D.; Pan, X.; Fu, Q.; Bao, X., Understanding nano effects in catalysis. *Natl. Sci. Rev.* **2015**, *2* (2), 183-201.

## **6. Molecular Imprinting on the Supported Metal Catalysts for Size-dependent Selective Hydrogenation Reactions**

### **ABSTRACT.**

The confinement of enzymatic active sites inside a protein matrix provides a specificity for reagents during the interaction with the active site. To mimic enzymatic system, molecularly imprinted polymers complementary to the template molecules in shape, size, and functional groups have been developed for adsorbents, sensors, and catalysts. However, this concept cannot be applied for metallic catalysts traditionally used in industry. The strategy for the preparation of imprinted catalyst involves adsorption of a template molecule, deactivation with poisoners with reservation of non-poisoned active islands with pre-determined shape and size for selective transformation of the molecules corresponding to templates. We demonstrate this strategy for selective hydrogenation of aromatic molecules with different alkyl radicals by preliminary deposition of these molecules as template over Pd catalyst and deactivation using dimethylaminopropylamine (DMAPA).

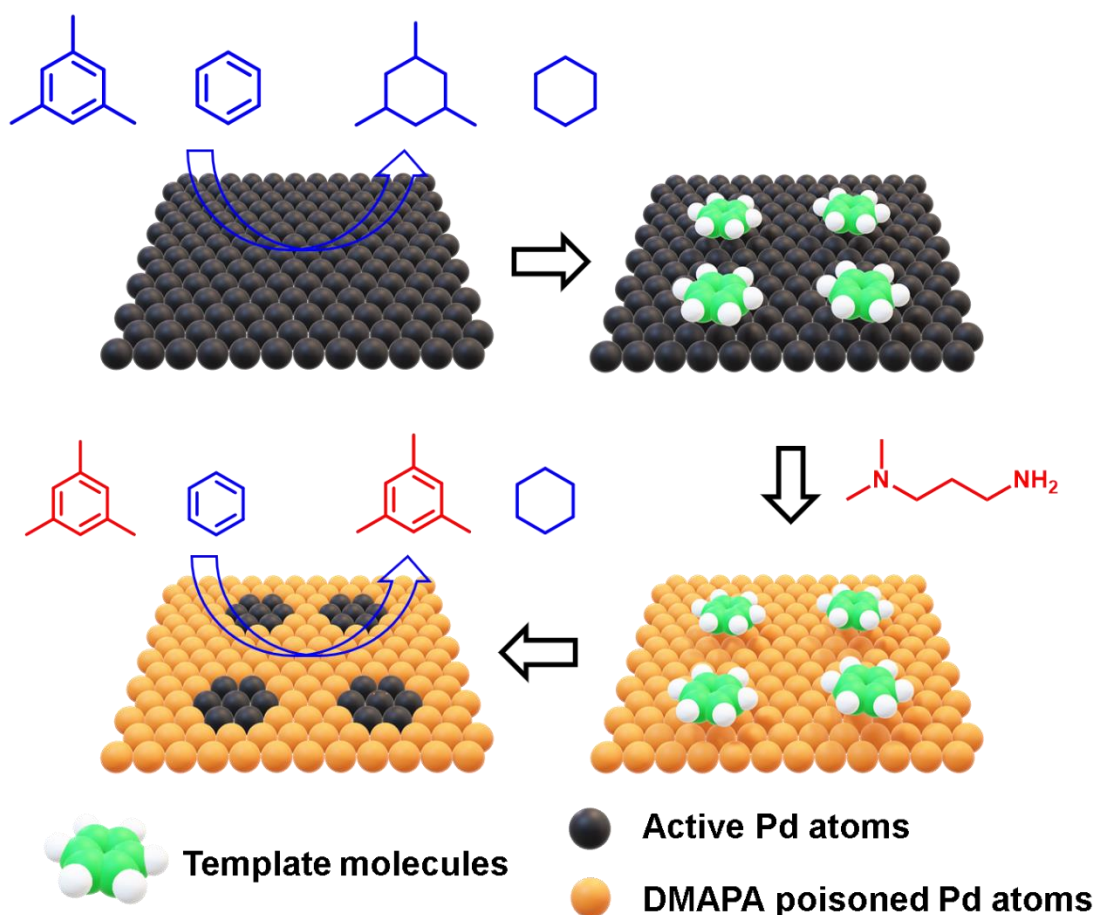
**Keyword:** Molecular imprinting; Heterogeneous catalysis; Surface modification; Molecular recognition; Selective reactions

## 6.1. Introductions

Specific reactivity to particular molecules is one of the main characteristics of enzymatic catalysis, which ensures the enzyme catalysts simultaneously high activity and selectivity in a complex reaction condition <sup>[1, 2]</sup>. Generally, enzymatic catalysis occurs at a localized active site within a protein matrix. The protein matrix provides a specific reaction cave which is compatible with the reactant molecules in shape, size, and functional groups <sup>[3, 4]</sup>. The high selectivity of enzymes attracts lots of research interests in the development of sensors, adsorbents, and new catalysts <sup>[5-7]</sup>.

One of the techniques to mimic enzyme catalysts is the so-called molecular imprinting <sup>[8-11]</sup>. Molecularly imprinted polymers (MIPs) have been developed by using template molecules and functional monomers that can polymerize around them <sup>[12, 13]</sup>. After removing of template molecules, the resultant MIPs have pre-determined cavities in a polymer matrix with specific sizes and shapes corresponding to template molecules <sup>[14, 15]</sup>. However, molecularly imprinted polymeric catalysts with organic or inorganic matrix are limited to low temperature reactions over acid, base of metal ions localized in the cavities. The metal supported heterogeneous catalysts are the most popular materials in chemical industry for the reactions of hydrogenation, dehydrogenation, oxidation and amination due to high catalytic activity, easy separation and low cost. Molecular imprinting over the surface of metal based heterogeneous catalysts could be seen as a breakthrough to enhance the performance of catalysts in terms of specificity to reaction <sup>[16-19]</sup>.

Recently, TiO<sub>2</sub> has been reported as a matrix for the production of molecularly imprinted sieve-layers on the surface by atomic layer deposition (ALD). This kind of imprinted TiO<sub>2</sub> catalyst showed a size-dependent reactivity towards less hindered reactants during the photocatalytic oxidations and transfer hydrogenations [20]. Regardless of molecular imprinting over the metal oxide surface, however, up to now, it is still challenging to apply molecular imprinting over the metal surface for selective reactions [18]. The key challenge for adapting molecular imprinting strategy over the metal surface is the uncontrolled distribution of blocking agents on metal sites, which normally indiscriminately block the entire metal surface [21-26]. Simon H. Pang et al. have reported to modify the Pd metal surface with different organic thiols (1-octadecanethiol and 1-adamantanethiol). The density of self-assembled thiols monolayer could be controlled by changing the steric bulk of the organic tail ligands [27]. The modified catalysts showed a different reaction pathway during furfural hydrogenation reactions. Xiao Liu et al. have modified the Pt nanoparticles with Co<sub>3</sub>O<sub>4</sub> by area-selective atomic layer deposition [28]. By using 1-octadecanethiol as the sacrificial block agents, Co<sub>3</sub>O<sub>4</sub> nanotraps were produced on the surface of the catalyst and strongly fix the Pt nanoparticle on support, which shows high activity and sintering resistance during CO oxidation. Although there are several methods to selective deposit blocking agents on the metal surface with some pre-determined distributions, the modification process is still difficult to control precisely, and a general and simple method is still desired.



**Scheme 6.1.** Illustration of the molecular imprinting strategy over Pd surface

Herein, we propose a novel and general molecular imprinting strategy over supported Pd catalysts for specific size-dependent hydrogenation reactions. The proposed concept is shown in *Scheme 6.1*, after a first step of cleaning and reduction, the surface of the Pd catalyst was subjected to adsorption of a template molecule (e.g. benzene). Further on, the free surrounding active sites of Pd were deactivated by interaction with dimethylaminopropylamine (DMAPA), which could strongly coordinate on the Pd surface. During this step, the Pd sites under the template will be protected by the template and are therefore not expected to be poisoned. After deactivation, the adsorbed templates will be removed from the surface by hydrogenation whereas the poisoner



DMAPA remains on the surface. Finally, an imprinted Pd catalyst with reserved active islands has been produced. Confirming by the catalytic results, these active islands are reactive for the transformation of molecules displaying similar structures with the template molecules in comparison with the parent catalysts. The further application of this kind of imprinted Pd catalyst was examined by the selective hydrogenation of carcinogenic benzene in mixed aromatics. The imprinted Pd catalysts with benzene as a template show a preference for benzene hydrogenation compared with other aromatics. The developed molecular imprinting strategy on the metal surface opens a way for the preparation of a smart catalytic surface for the selective processes.

## **6.2. Results and discussion**

### **6.2.1. Poisoning of supported Pd/SiO<sub>2</sub> catalysts by DMAPA**

The key step of molecular imprinting over the Pd surface is the selective poisoning process. A good poisoner should have strong coordination with Pd and provide steric hindrance to prevent the adsorption of reactant molecules on the poisoning surface. Additionally, the poisoner should have less effect on the electronic properties of Pd nanoparticles and should not infiltrate into the Pd lattice. Although non-metallic poisoners such as iodine and sulfur have strong interaction with Pd, they significantly change the electronic properties of Pd nanoparticles [29-31, 22]. Also, sulfur has been reported to migrate and infiltrate in the Pd nanoparticles with the generation of Pd sulfide [29, 30]. In this work, we propose an organic poisoner DMAPA with high basicity and ability to coordinate with Pd nanoparticles via nitrogen [32-34]. The carbon chain of

DMAPA can create steric hindrances on the poisoning surface to suppress the interaction of the molecules with metal surface [35].

To investigate the poisoning effect of DMAPA, the Pd/SiO<sub>2</sub> (10 wt.% Pd loading) catalyst has been reduced at 200 °C with subsequent treatment by DMAPA vapors at 80°C in a fix-bed reactor (**Figure 2.1**). The catalytic property of the poisoned Pd catalyst has been examined by performing liquid-phase hydrogenation of toluene in a bath-reactor. The high activity over the parent Pd/SiO<sub>2</sub> catalyst in toluene hydrogenation decreases to almost 0 over D-Pd/SiO<sub>2</sub> after poisoning by DMAPA (**Figure 6.1a**) [36].

**Figure 6.1b** shows the H<sub>2</sub>-chemisorption on the initial Pd/SiO<sub>2</sub> and poisoned D-Pd/SiO<sub>2</sub> catalysts. The uptake of H<sub>2</sub> over Pd/SiO<sub>2</sub> is 0.077 mmol/g corresponding to the surface of Pd 0.154 mmol/g using the ratio of H to Pd equal to 1 (**Table 6.1 & Figure 6.5**). However, after poisoning with DMAPA, the D-Pd/SiO<sub>2</sub> has almost no H<sub>2</sub> uptake (0.0016 mmol/g) indicating total poisoning of Pd by DMAPA following catalytic results.

**Table 6.1.** Summary of the chemisorption on various Pd/SiO<sub>2</sub> catalysts.

Catalyst	Amount of DMAPA (mmol/g) (Determined by TG analysis)	Bared Pd sites (mmol/g) (Determined by H <sub>2</sub> adsorption)
Pd/SiO <sub>2</sub>	-	0.154
D-Pd/SiO <sub>2</sub>	0.159	0.0032
Partial-D-Pd/SiO <sub>2</sub>	0.11	0.096
TL-Print-Pd/SiO <sub>2</sub>	0.096	0.12
ML-Print-Pd/SiO <sub>2</sub>	0.1	0.102
TPB-Print-Pd/SiO <sub>2</sub>	0.14	0.07
Ben-Print-Pd/SiO <sub>2</sub>	0.145	0.054

N1s XPS analysis of D-Pd/SiO<sub>2</sub> confirmed the presence of DMAPA on the Pd surface (**Figure 6.1c**). The peaks located at 400.2 and 401.4 eV correspond to the N=C and N-C species, respectively, which are attributed to the adsorbed DMAPA species on the Pd surface. The presence of C=N on D-Pd/SiO<sub>2</sub> indicates the dehydrogenation of C-N to C=N group on Pd surface [37-39]. The dehydrogenation of DMAPA on Pd surface has been further demonstrated by FTIR analysis (**Figure 6.1d**). The adsorption peak at 1695 cm<sup>-1</sup> corresponds to imine groups on the surface of D-Pd/SiO<sub>2</sub> catalyst [40]. The other adsorption peaks at 2800 ~ 3000 and 1500 cm<sup>-1</sup> were assigned to the stretching and bending vibration of C-H bonds in DMAPA [41]. It is worth to note that the spontaneous dehydrogenation of amines on the Pd surface has been reported by the literature [38].

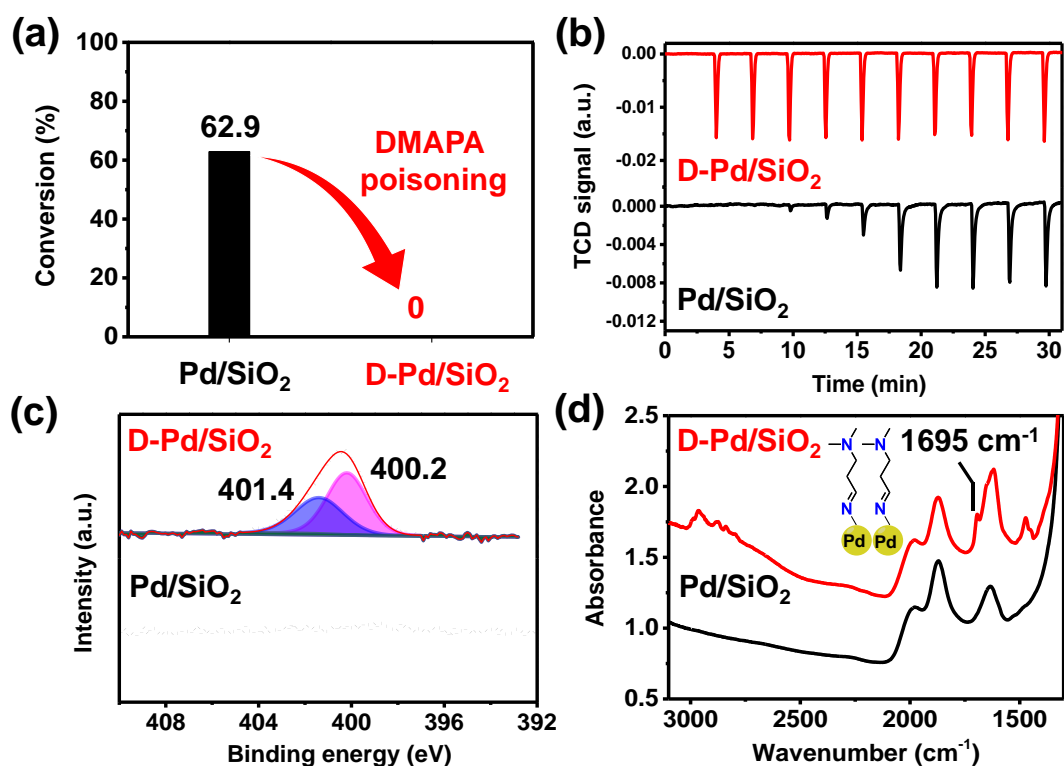


**Figure 6.1.** Catalytic performance and characterizations of Pd/SiO<sub>2</sub> and DMAPA poisoned Pd/SiO<sub>2</sub> catalysts. Reaction conditions: 50 mg Pd/SiO<sub>2</sub> catalyst, 100 mg toluene, 5 g n-decane, 20 bar H<sub>2</sub>, 120 °C, 1 h.

The concept of imprinting implies preservation of the morphology and electronic properties of Pd nanoparticles after poisoning by DMAPA. **Figure 6.2** summarized the XRD, TEM and Pd 3d XPS analysis of Pd/SiO<sub>2</sub> and D-Pd/SiO<sub>2</sub> catalysts. Three well resolved XRD peaks observed on both D-Pd/SiO<sub>2</sub> and Pd/SiO<sub>2</sub> catalysts correspond to Pd (111), Pd (200), and Pd (220) planes, respectively <sup>[42]</sup>. D-Pd/SiO<sub>2</sub> catalyst has the same XRD patterns as parent Pd/SiO<sub>2</sub> indicating the same shape and particle size about 16 nm before and after poisoning <sup>[43]</sup>. The same morphology and particle size were further confirmed by TEM analysis (**Figure 6.2c & d**). XPS analysis of Pd 3d core-level spectra in Pd/SiO<sub>2</sub> and D-Pd/SiO<sub>2</sub> show a dominate binding energy located at 335.3 eV corresponding to metallic Pd phase in both samples (**Figure 6.2b**). A small peak at 337.1 eV in Pd/SiO<sub>2</sub> catalyst can be assigned to Pd<sup>2+</sup> indicating the partial oxidation of the Pd surface under air conditions <sup>[44]</sup>. However, D-Pd/SiO<sub>2</sub> has Pd<sup>2+</sup> binding energy shifted to 336.6 eV which could be attributed to the interaction between surface Pd and DMAPA. The electronic rich nitrogen with lone pair of electrons will donate electrons to Pd with an increase of electronic density of surface Pd atoms and lower binding energy <sup>[21]</sup>. Although the electronic properties of surface Pd has been changed because of interaction with DMAPA, the main phase of Pd nanoparticles were still in the same electronic state as the parent Pd/SiO<sub>2</sub> catalyst.

The stability of DMAPA on Pd/SiO<sub>2</sub> has been studied by TGA analysis (**Figure 6.3**). The surface DMAPA start to desorb at 165°C with full removal at 350°C. The weight loss corresponds to 0.157 mmol of DMAPA adsorbed over 1 g of Pd/SiO<sub>2</sub> catalyst (**Table 6.1 & Figure 6.5**). According to the amount of surface Pd according to hydrogen

adsorption and the amount of DMAPA on D-Pd/SiO<sub>2</sub> catalyst, the mole ratio between surface Pd atoms and DMAPA molecules is about 1.

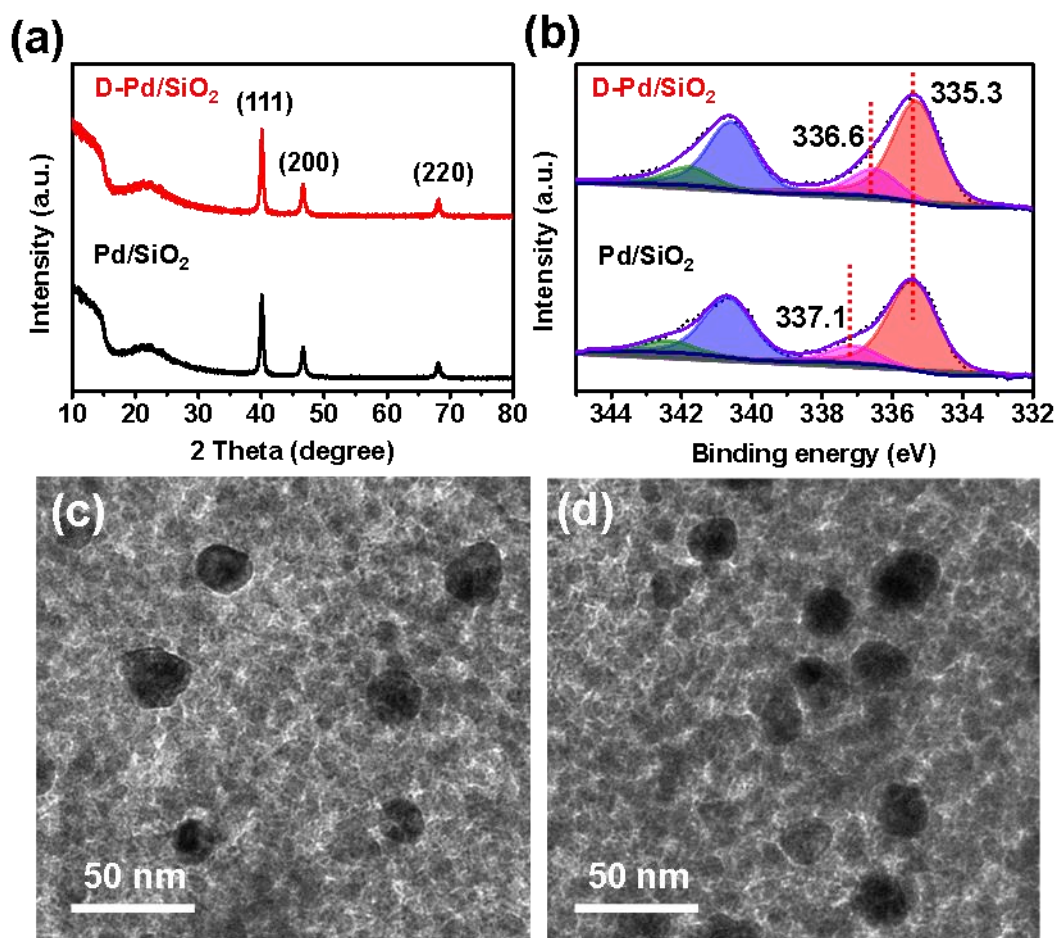


**Figure 6.2.** Characterizations of Pd/SiO<sub>2</sub> and D-Pd/SiO<sub>2</sub> (a) XRD patterns; (b) Pd 3d XPS spectrums; (c-d) TEM images.

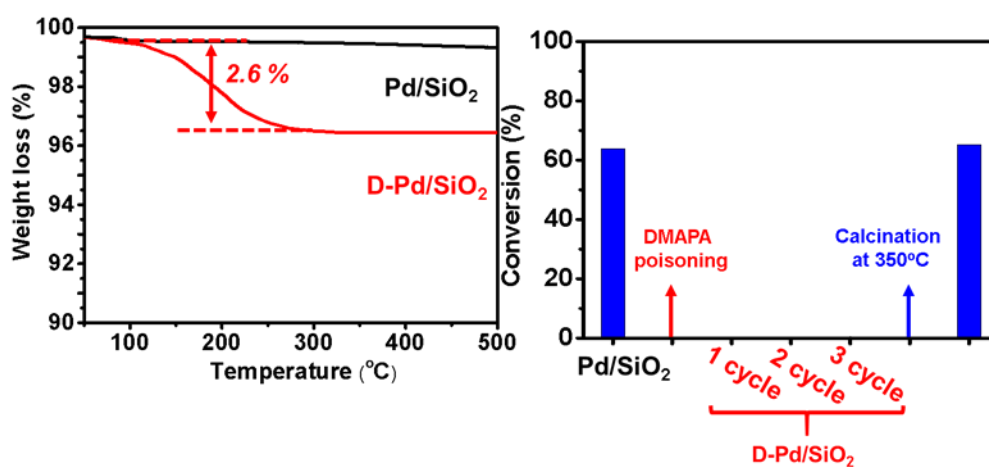


**Figure 6.3.** TGA analysis and stability test of D-Pd/SiO<sub>2</sub> catalyst.

Hydrogenation of toluene over D-Pd/SiO<sub>2</sub> has been conducted in a consequence three cycles and showed no activity demonstrating the high stability of DMAPA on Pd surface (*Figure 6.3*). However, calcination at 350°C for 3 h recovers the activity of the catalyst. The easy regeneration of DMAPA poisoned Pd/SiO<sub>2</sub> catalyst can be used for multiple imprinting of the same industrial catalyst without its loss.

Thus, characterization and catalytic tests of Pd/SiO<sub>2</sub> and D-Pd/SiO<sub>2</sub> catalysts suggest that DMAPA could effectively poison the Pd/SiO<sub>2</sub> catalyst and can be used for further imprinting of the catalyst

### 6.2.2. Investigations for imprinting process

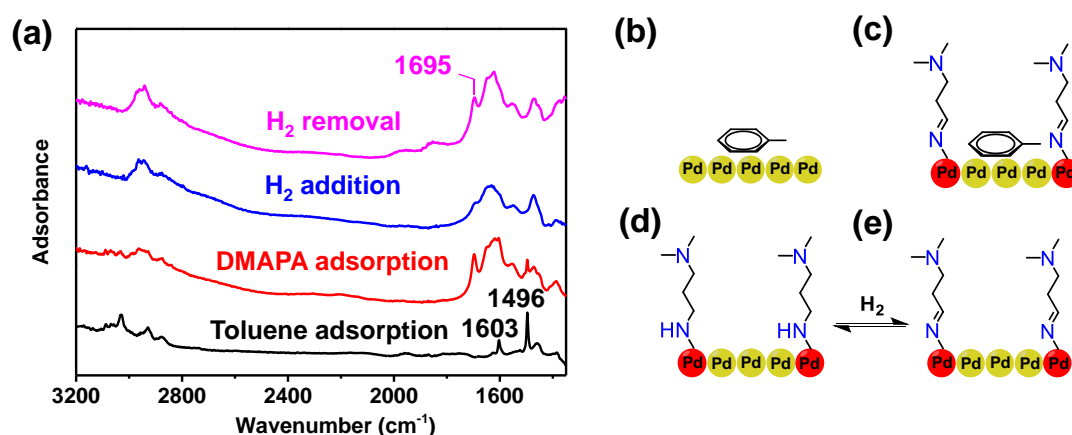


**Figure 6.4.** In-situ FTIR studies of the preparation of the molecularly imprinted Pd/SiO<sub>2</sub> catalyst.

To investigate the possibility of a molecular imprinting process, toluene has been selected as a template for the preliminary studies on the Pd/SiO<sub>2</sub> with DMAPA as a poisoner. In-situ FTIR analysis has been used to monitor the imprinting process (*Figure 6.4*). The adsorption of toluene over Pd/SiO<sub>2</sub> (*Figure 6.4 b*) demonstrates a set of obvious adsorption peaks at 1603 cm<sup>-1</sup> and 1496 cm<sup>-1</sup> corresponding to the phenyl ring

of breathing vibrations [45, 46]. According to the literature, toluene can be horizontally adsorbed over Pd surface via the interaction between conjugated phenyl ring and Pd planes [47, 48, 49, 50].

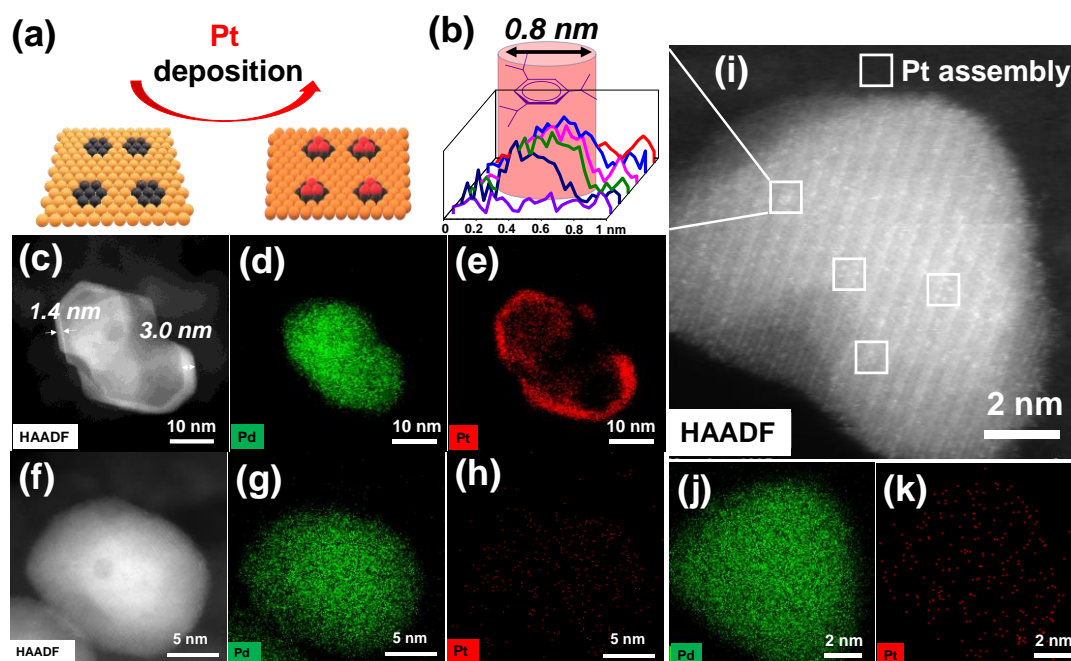


**Figure 6.5.** Scheme of highlighting of imprinted zones using Pt deposition (a, b), HAADF STEM images and corresponding EDS elemental analysis of TPB-Print-Pd/SiO<sub>2</sub> (i, j, k), parent Pd/SiO<sub>2</sub> catalyst (c, d, e) and D-Pd/SiO<sub>2</sub> (f, g, h).

Next, the sample has been subjected to the adsorption of DMAPA. Similar to D-Pd/SiO<sub>2</sub> catalyst, a new peak at 1695 cm<sup>-1</sup> appeared immediately after adding DMAPA due to C=N stretch in imine compounds. However, the peaks of toluene (1603 cm<sup>-1</sup> and 1496 cm<sup>-1</sup>) were still visible, confirming the co-presence of DMAPA and toluene on the Pd surface. The co-presence of toluene and DMAPA on the Pd surface demonstrates that toluene can protect active sites during DMAPA poisoning, leading to reservations of active islands as illustrated in [Figure 6.4c](#) [51]. It is worth to note that during the heating of the sample at 120 °C in the presence of hydrogen the peak at 1695 cm<sup>-1</sup> decreased a

lot while the peaks at  $1500\text{ cm}^{-1}$  and  $2800 \sim 3000\text{ cm}^{-1}$  have not been affected. It suggests that the imine groups were hydrogenated back to amine still adsorbed on the Pd surface (*Figure 6.4d*). Hydrogen evacuation leads to the re-appearance of the peak at  $1695\text{ cm}^{-1}$  due to dehydrogenation back to imine groups on Pd surface (*Figure 6.4e*). Notably, heating at  $120\text{ }^{\circ}\text{C}$  in the presence of  $\text{H}_2$  results in the disappearance of the peaks at  $1603\text{ cm}^{-1}$  and  $1496\text{ cm}^{-1}$  indicating the desorption of the template molecules.

HAADF-STEM has been used for further analysis of imprinted Pd/SiO<sub>2</sub> catalyst. In order to identify the active islands, Pt atoms with much heavier atomic weight than Pd has been deposited on the imprinting areas. The different contrast of Pt and Pd atoms in STEM-HAADF images makes it possible to highlight the imprinting areas [52, 53]. 1,3,5-triisopropyl benzene (TPB) with a size of about 0.85 nm has been selected as the template for the preparation of molecularly imprinted Pd/SiO<sub>2</sub> catalyst for the STEM analysis [54-56]. The deposition of Pt atoms has been performed by mild reduction of Pt(acac)<sub>2</sub> solution on the initial Pd/SiO<sub>2</sub>, TPB-Print-Pd/SiO<sub>2</sub>, and D-Pd/SiO<sub>2</sub> catalysts, respectively, in the presence of H<sub>2</sub>. Due to the high activity of the bared Pd surface, the Pt atoms should be selectively reduced on the imprinting area without reduction on the DMAPA poisoned Pd surface (*Figure 6.5a*). As shown in *Figure 6.5c*, without molecular imprinting, the initial Pd/SiO<sub>2</sub> exhibited a thick Pt layer 1.4 ~ 3 nm around Pd nanoparticles. The STEM-EDS mapping images of initial Pd/SiO<sub>2</sub> indicated the formation of a core-shell structure with Pd core and Pt shell (*Figure 6.5d ~ e*). The well-distributed Pt shell around Pd nanoparticles demonstrated the high activity of the Pd surface toward Pt reduction. However, totally deactivated Pd/SiO<sub>2</sub> has a very low



amount of Pt atoms on the Pd surface (*Figure 6.5f ~ h*), confirming that the Pd surface has been poisoned by DMAPA. Interestingly, molecular imprinting with TPB as the template shows no Pt shell on the surface of Pd (*Figure 6.5i ~ k*). Instead of a Pt shell, a scattered distributed Pt atoms assembly of 4 ~ 8 atoms have been observed on the imprinted Pd catalyst (*Figure 6.5i*). The HAADF intensity of the imprinted areas has been plotted in *Figure 6.5b*. The size of Pt atoms is around 0.8 nm, which is in agreement with the size of the template molecule TPB. The formation of Pt atoms assembly on the imprinted Pd surface confirms the successful preparation of the imprinting zones on Pd surface with pre-determined size.

### **6.2.3. Model reactions over imprinted Pd/SiO<sub>2</sub> catalyst**

To check the catalytic activity of the imprinted Pd catalysts, a series of imprinted Pd/SiO<sub>2</sub> catalyst have been prepared by using toluene (TL), mesitylene (ML), and 1,3,5-triisopropyl benzene (TPB) as template, respectively, and DMAPA as a poisoner (named as TL-Print-Pd/SiO<sub>2</sub>, ML-Print-Pd/SiO<sub>2</sub> and TPB-Print-Pd/SiO<sub>2</sub>). The molecular size of these templates decreases in the row TPB > ML > TL and the size of resultant imprinted areas should decrease TPB-Print-Pd/SiO<sub>2</sub> > ML-Print-Pd/SiO<sub>2</sub> > TL-Print-Pd/SiO<sub>2</sub>. Hydrogenation of aromatic rings in TL, ML and TPB were performed over these imprinted Pd/SiO<sub>2</sub> catalysts. As it has been reported earlier, the hydrogenation of aromatic rings requires flat adsorption of the molecules over the metal surface <sup>[57, 58]</sup>. If the size of the molecule is larger than the size of the imprinted area it cannot be hydrogenated over the catalyst because of the steric hindrance during

adsorption. Additionally, a reference catalyst (Partial-D-Pd/SiO<sub>2</sub>) has been prepared by partial deactivation without pre-adsorption of template molecules to demonstrate the role of template molecule for the creation of imprinting area.

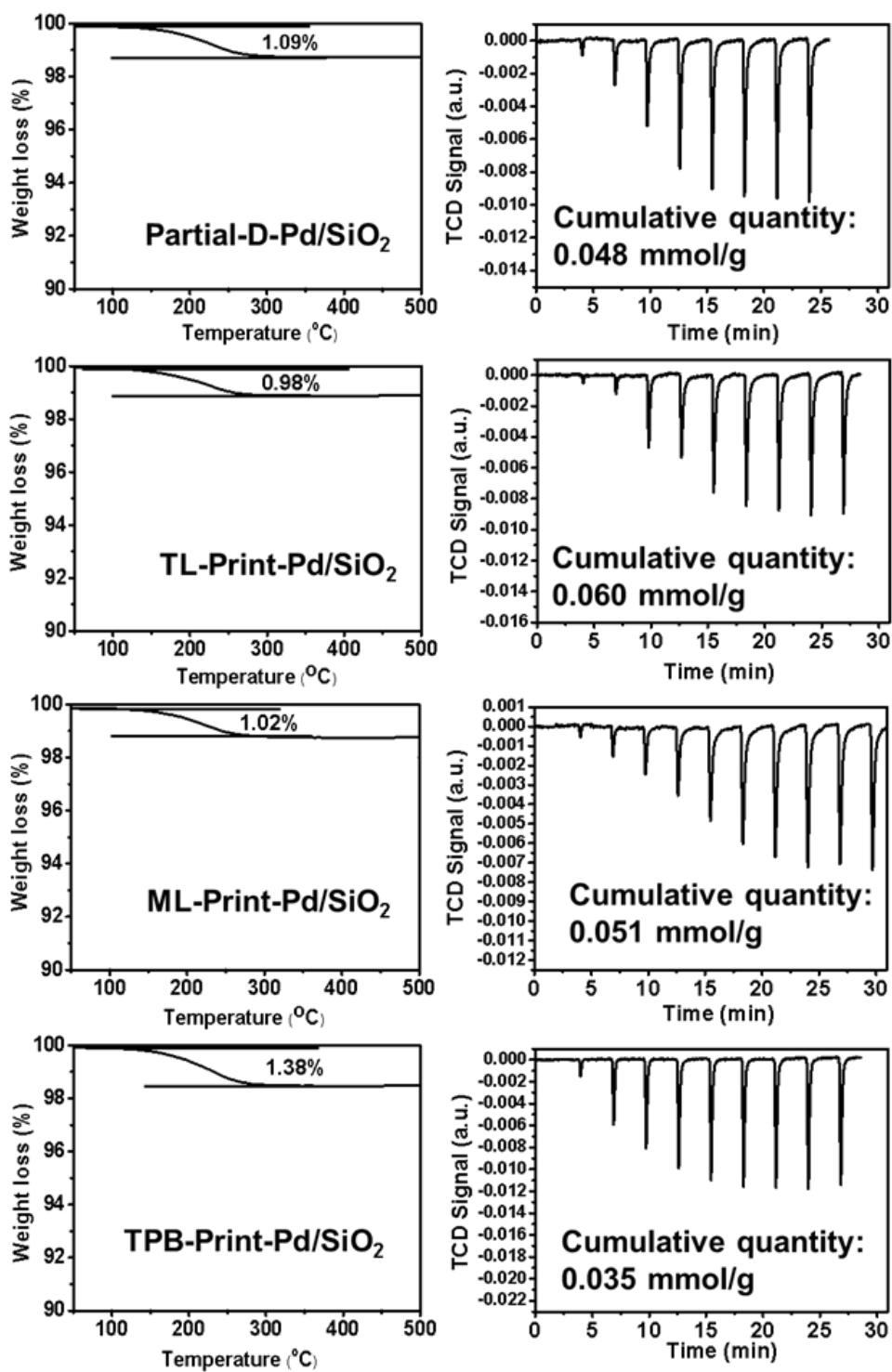


**Figure 6.6.** TGA and H<sub>2</sub>-pulse chemisorption over various catalysts.

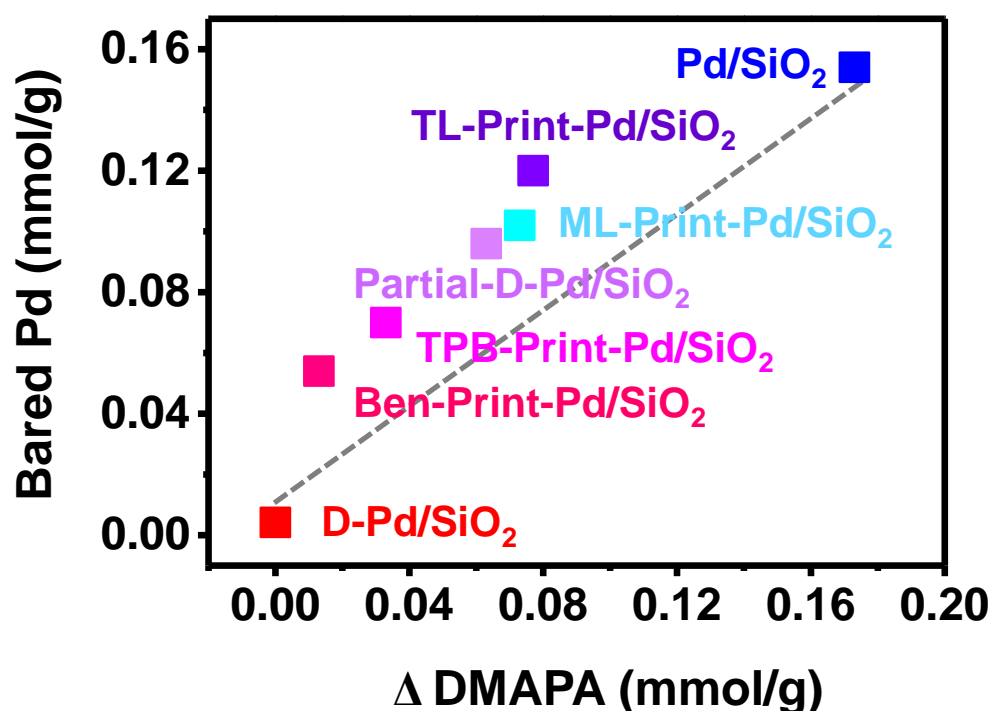


**Figure 6.7.** Correlation between hydrogen adsorption and difference between DMAPA over parent Pd/SiO<sub>2</sub> and imprinted catalysts

The amount of DMAPA over various catalysts was determined by TGA analysis. As shown in **Figure 6.6**, the weight loss over Partial-D-Pd/SiO<sub>2</sub>, TL-Print-Pd/SiO<sub>2</sub>, ML-Print-Pd/SiO<sub>2</sub>, and TPB-Print-Pd/SiO<sub>2</sub> catalysts were 1.09, 0.98, 1.02 and 1.38 % which corresponds to 0.11, 0.096, 0.10, and 0.14 mmol/g of DMAPA, respectively. The reserved active sites have been measured by H<sub>2</sub>-pulse chemisorption. As summarized in **Table 6.1**, the cumulative quantity of H<sub>2</sub> uptakes were 0.048, 0.06, 0.051 and 0.035 mmol/g over Partial-D-Pd/SiO<sub>2</sub>, TL-Print-Pd/SiO<sub>2</sub>, ML-Print-Pd/SiO<sub>2</sub> and TPB-Print-Pd/SiO<sub>2</sub> catalysts, respectively. The H<sub>2</sub>-pulse chemisorption correlates well with the TGA analysis, where the low amount of DMAPA corresponds to a higher quantity of

H<sub>2</sub> uptake (*Figure 6.7*). The slightly higher amount of bared Pd atoms calculated from H<sub>2</sub> chemisorption over the imprinted catalyst could be explained by the electronic effect of DMAPA on the Pd increasing the stoichiometric ratio of H to Pd.

The TOF numbers over various catalysts were measured and calculated based on the H<sub>2</sub>-pulse chemisorption results (*Figure 6.8*). The TOF numbers of hydrogenation of toluene, mesitylene, and TPB over the parent Pd/SiO<sub>2</sub> were 220, 110 and 306 h<sup>-1</sup>, respectively, which decreases to zero after poisoning with DMAPA. Surprisingly, the toluene imprinted Pd/SiO<sub>2</sub> (TL-Print-Pd/SiO<sub>2</sub>) catalyst shows still high TOF for toluene (3.9 h<sup>-1</sup>) but low TOF numbers for hydrogenation of mesitylene (0.21 h<sup>-1</sup>) and TPB (0.13 h<sup>-1</sup>). This phenomenon can be explained by the protection of active islands over Pd surface by pre-adsorbed toluene during poisoning. In this case, active islands on the Pd surface with a similar shape and size to the toluene molecule could be produced. Thus, after imprinting with toluene, the imprinted active island can only adsorb toluene but unable to adsorb mesitylene and TPB with a larger molecule size. This explanation has been further supported by using mesitylene as a template. ML-Print-Pd/SiO<sub>2</sub> exhibited higher TOF numbers for both toluene and mesitylene (5.04 and 0.83 h<sup>-1</sup>) but a low TOF for TPB (0.14 h<sup>-1</sup>). Further, Pd/SiO<sub>2</sub> imprinted by TPB has demonstrated a high TOFs for hydrogenation of toluene (8.47 h<sup>-1</sup>), mesitylene (2.14 h<sup>-1</sup>) and TPB (3.2 h<sup>-1</sup>). Increase of the size of template molecules results in expanding of the size of active islands for hydrogenation of larger molecules. It is worth to note that the partial deactivated Pd/SiO<sub>2</sub> catalyst (Partial-D-Pd/SiO<sub>2</sub>) exhibits different catalytic behavior compared with imprinted catalysts. The TOF numbers for toluene, mesitylene and TPB

over Partial-D-Pd/SiO<sub>2</sub> catalyst are 1.58, 0.68 1.43 h<sup>-1</sup>, respectively. In comparison with imprinted counterparts, the activity is comparable for all molecules over Partial-D-Pd/SiO<sub>2</sub> indicating the indiscriminate distribution of DMAPA on the Pd surface without the generation of specific islands for the adsorption of aromatic rings. The catalytic results over Partial-D-Pd/SiO<sub>2</sub> catalyst show that the size-dependent reactivity could be introduced by the imprinting process and not the electronic or poisoning effect of adsorbed DMAPA.

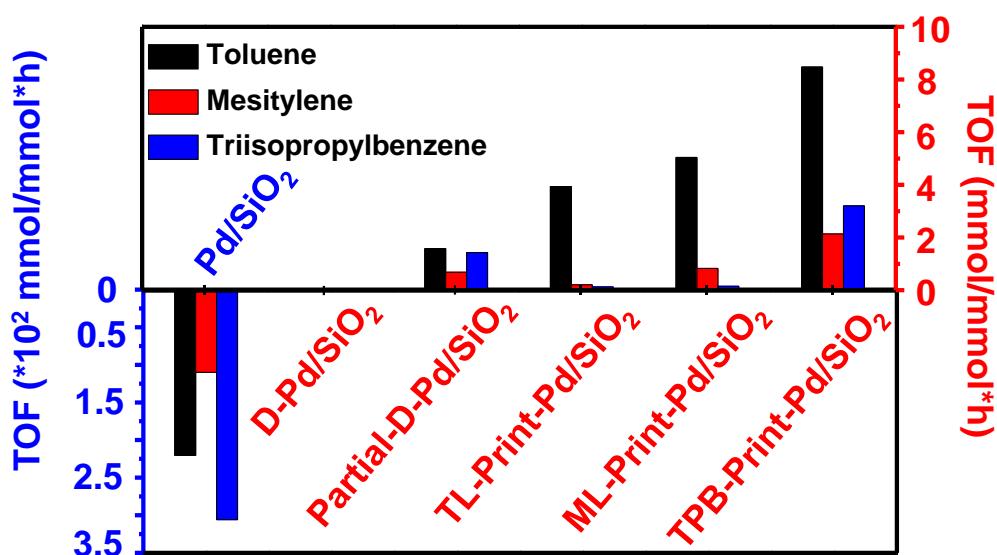


**Figure 6.8.** Hydrogenation of toluene, mesitylene and TPB over various imprinted Pd/SiO<sub>2</sub>. Reaction conditions: 50 mg catalyst, 100 mg aromatics, 5 g n-decane, 120°C, 20 bar H<sub>2</sub>, 0.5 h for Pd/SiO<sub>2</sub> and 6 h for poisoned Pd/SiO<sub>2</sub>.

The significant decrease of the intrinsic activity after imprinting could be explained by the electronic effects of DMAPA over surface Pd sites. It has been reported earlier that the electronic effect of modifiers is less significant over large metal particles. In order to support this assumption Pd sponge with low surface area and dispersion (0.58 %) has been used for imprinting similar to Pd/SiO<sub>2</sub> catalyst (**Figure 6.9**). The TOF numbers of

TL, ML and TPB hydrogenation over the parent sponge were 25.6, 14 and 9.7 h<sup>-1</sup>, respectively, which is about an order lower in comparison with Pd/SiO<sub>2</sub> catalyst and could be explained by the high activity of defect Pd sites in hydrogenation.

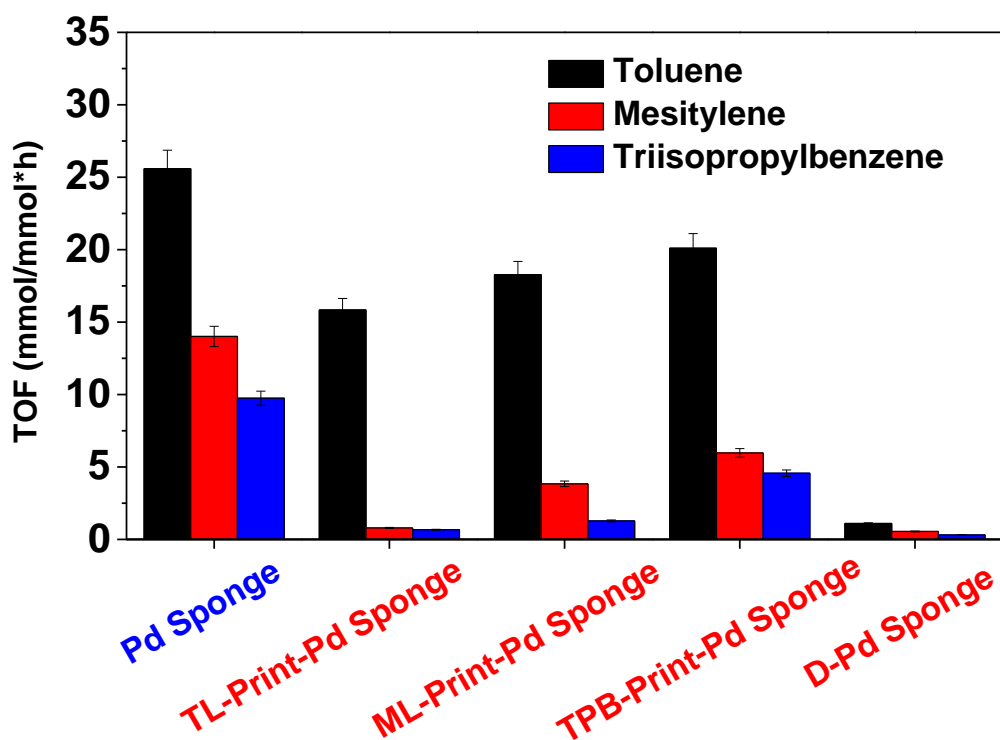


**Figure 6.9.** Hydrogenation of toluene, mesitylene and TPB over various imprinted Pd sponge. Reaction conditions: 30 mg catalyst, 0.1 mmol/h feed rate, 5 ml (STP)/min N<sub>2</sub>, 5 ml (STP)/min H<sub>2</sub>, 120°C, atmosphere pressure, WHSV = 0.3 ~ 0.68 h<sup>-1</sup>.

Treatment by DMAPA results in almost total deactivation of the surface. Imprinting of Pd sponge by TL leads to still high TOF of toluene hydrogenation (15.8 h<sup>-1</sup>), however, negligibly low activity for mesitylene and TPB hydrogenation. The same effect has been observed over ML-Print-Pd sponge providing high activity for hydrogenation of TL (18.3 h<sup>-1</sup>), ML (3.8 h<sup>-1</sup>) at low TOF for hydrogenation of TPB (1.2 h<sup>-1</sup>). Imprinting by TPB demonstrates high activity such as 20, 6 and 4.6 h<sup>-1</sup> for TL, ML and TPB,

respectively. Thus, it provides the catalytic effect similar to those over imprinted Pd/SiO<sub>2</sub>, however, it is interesting to note that the catalytic activity is comparable to the parent catalyst. This effect can be explained by the significantly lower electronic effect of DMAPA over continuous Pd sites in comparison with highly dispersed supported Pd catalysts.

#### **6.2.4. Selective removal of benzene from the mixture**

The developed molecular imprinting methodology can be used for the selective transformation of imprinted molecules for their transformation in the reaction mixture. This concept has been demonstrated for the selective removal of benzene from the mixture of aromatics. Benzene is a carcinogenic compound and its content has to be limited to less than 1% in gasoline <sup>[59]</sup>. The traditional route for selective benzene removal includes adsorption, catalytic hydrogenation, and catalytic alkylation <sup>[60-62]</sup>. While adsorption has a low capacity for benzene removal and catalytic alkylation consumed a large number of expensive olefins, catalytic hydrogenation could be considered as a promising method <sup>[63, 64-66]</sup>. However, the hydrogenation of benzene in mixed-aromatics will not only hydrogenate benzene but also hydrogenate other aromatic molecules. Therefore, a smart catalyst that could selectively hydrogenate benzene in the mixed-aromatics without hydrogenation of other aromatics would be highly desirable.

The imprinted Pd/SiO<sub>2</sub> catalyst was prepared by using benzene as a template and named Ben-Print-Pd/SiO<sub>2</sub>. The amount of DMAPA over Ben-Print-Pd/SiO<sub>2</sub> catalyst was 0.16

mmol/g determined by TG analysis at the amount of bared Pd site determined by H<sub>2</sub> adsorption 0.027 mmol/g. The TOF numbers of various aromatics such as benzene, toluene, *p*-xylene, and mesitylene were measured for the initial Pd/SiO<sub>2</sub> and Ben-Print-Pd/SiO<sub>2</sub>. As shown in **Figure 6.10a**, after imprinting with benzene, the TOF numbers for benzene hydrogenation decreased from 311 to 16 h<sup>-1</sup>. However, the TOF numbers for hydrogenation of toluene, *p*-xylene and mesitylene decreased significantly more. These results show that Ben-Print-Pd/SiO<sub>2</sub> demonstrates preferential behavior for hydrogenation of benzene in comparison with other aromatic molecules.

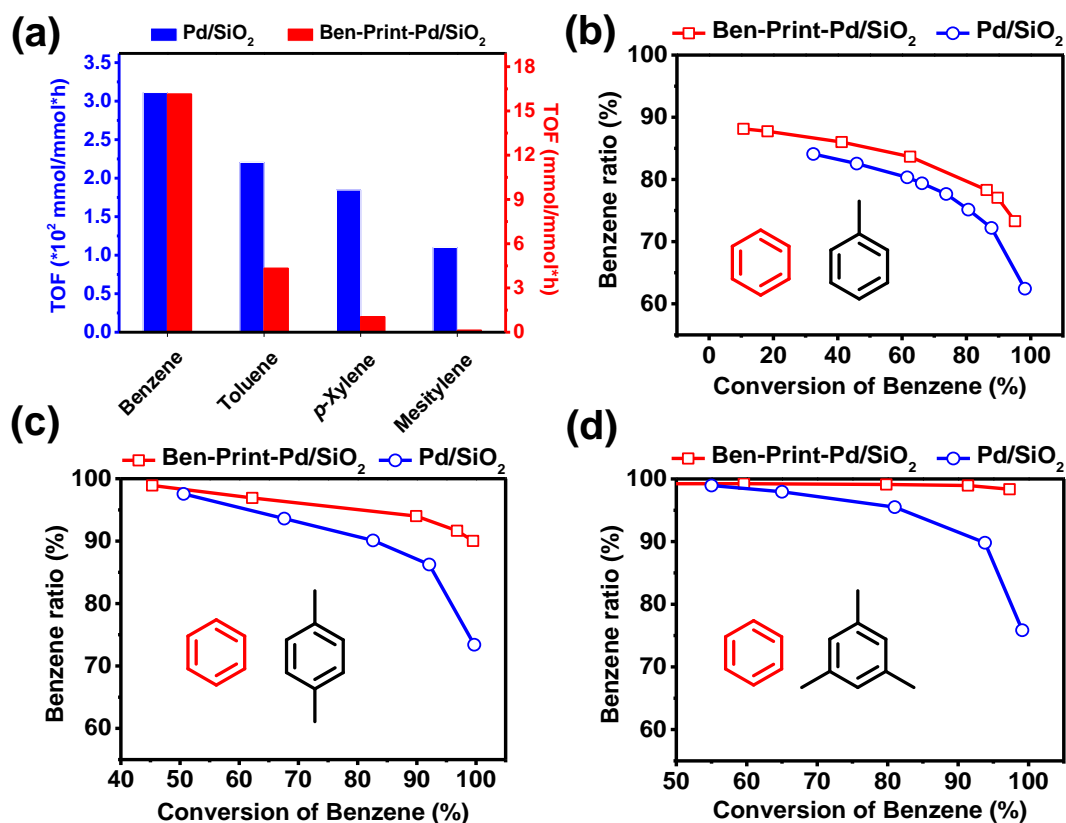


**Figure 6.10.** Selective hydrogenation of benzene in mixed-aromatics. Reaction conditions: 50 mg initial Pd/SiO<sub>2</sub> catalyst or 100 mg imprinted catalyst, 100 mg benzene mixed with 100 mg toluene, or *p*-xylene, or mesitylene, 5 g *n*-decane, 120°C, 20 bar H<sub>2</sub>, 0.5 ~ 48 h.



Subsequently, we performed hydrogenation of benzene in the mixture with other aromatic molecules (benzene/toluene, benzene/*p*-xylene, and benzene/mesitylene). As shown in *Figure 6.10b ~ d*, the selectivity of benzene hydrogenation over Ben-Print-Pd/SiO<sub>2</sub> catalyst was always higher in comparison with Pd/SiO<sub>2</sub>. However, the selectivity of benzene hydrogenation demonstrates only about 5 % difference in the mixture with toluene which could be explained by comparable sizes of benzene and toluene. At the same time, in the presence of *p*-xylene, the selectivity of benzene hydrogenation already increases from 73.4 % for Pd/Al<sub>2</sub>O<sub>3</sub> to 90.0 % for Ben-Print-Pd/SiO<sub>2</sub> at full benzene conversion. The difference increases further for benzene/mesitylene mixture) from 75.9% for Pd/Al<sub>2</sub>O<sub>3</sub> to 98.4 % for Ben-Print-Pd/SiO<sub>2</sub>. These results demonstrate the potential application of molecularly imprinted Pd catalysts for selective benzene removal.

### 6.3. Conclusions

In this chapter, we firstly proposed and demonstrated the molecular imprinting strategy over Pd surface for selective hydrogenation reactions. Using DMAPA as a poisoner and various aromatic molecules like toluene, mesitylene and 1,3,5-triisopropylbenzene with different molecular sizes as a template, we have successfully prepared a series of imprinted Pd catalysts. The catalytic results demonstrate that the imprinted Pd catalyst has a size-dependent hydrogenation reactivity with hydrogenation of similar and smaller size aromatic molecules in comparison with template and no activity for hydrogenation of larger molecules. Finally, we could apply imprinted Pd catalysts for

selective hydrogenation of benzene in a mixed-aromatics for potential application in selective removal of benzene in reformat gasoline. The molecular imprinting strategy not only provides a powerful way to design a selective catalytic surface but also gains an understanding of interfacial catalysis on the metal surface.

## Reference

1. Wu, J.; Wang, X.; Wang, Q.; Lou, Z.; Li, S.; Zhu, Y.; Qin, L.; Wei, H., Nanomaterials with enzyme-like characteristics (nanozymes): next-generation artificial enzymes (II). *Chem. Soc. Rev.* **2019**, *48* (4), 1004-1076.
2. Wu, W.; Huang, L.; Wang, E.; Dong, S., Atomic engineering of single-atom nanozymes for enzyme-like catalysis. *Chem. Sci.* **2020**, *11*, 9741-9756
3. Zhao, X.; Zang, S. Q.; Chen, X., Stereospecific interactions between chiral inorganic nanomaterials and biological systems. *Chem. Soc. Rev.* **2020**, *49* (8), 2481-2503.
4. Callender, R.; Dyer, R. B., The dynamical nature of enzymatic catalysis. *Acc. Chem. Res.* **2015**, *48* (2), 407-413.
5. Jo, B. H.; Moon, H.; Cha, H. J., Engineering the genetic components of a whole-cell catalyst for improved enzymatic CO<sub>2</sub> capture and utilization. *Biotechnol. Bioeng.* **2020**, *117* (1), 39-48.
6. Yang, Y.; Cho, I.; Qi, X.; Liu, P.; Arnold, F. H., An enzymatic platform for the asymmetric amination of primary, secondary and tertiary C(sp<sup>3</sup>)-H bonds. *Nat. Chem.* **2019**, *11* (11), 987-993.
7. Lee, W. C.; Kim, K. B.; Gurudatt, N. G.; Hussain, K. K.; Choi, C. S.; Park, D. S.; Shim, Y. B., Comparison of enzymatic and non-enzymatic glucose sensors based on hierarchical Au-Ni alloy with conductive polymer. *Biosens. Bioelectron.* **2019**, *130*, 48-54.
8. Chen, L.; Wang, X.; Lu, W.; Wu, X.; Li, J., Molecular imprinting: perspectives and applications. *Chem. Soc. Rev.* **2016**, *45* (8), 2137-2211.
9. Katz, A.; Davis, M. E., Molecular imprinting of bulk, microporous silica. *Nature* **2000**, *403* (6767), 286-289.
10. Liu, J. Q.; Wulff, G., Functional mimicry of the active site of carboxypeptidase a by a molecular imprinting strategy: cooperativity of an amidinium and a copper ion in a transition-state imprinted cavity giving rise to high catalytic activity. *J. Am. Chem. Soc.* **2004**, *126* (24), 7452-7453.
11. Brunkan, N. M.; Gagné, M. R., Effect of Chiral Cavities Associated with Molecularly Imprinted Platinum Centers on the Selectivity of Ligand-Exchange Reactions at Platinum. *J. Am. Chem. Soc.* **2000**, *122* (26), 6217-6225.
12. BelBruno, J. J., Molecularly Imprinted Polymers. *Chem. Rev.* **2019**, *119* (1), 94-119.
13. Wulff, G., Enzyme-like catalysis by molecularly imprinted polymers. *Chem. Rev.* **2002**, *102* (1), 1-27.

14. Cowen, T.; Stefanucci, E.; Piletska, E.; Marrazza, G.; Canfarotta, F.; Piletsky, S. A., Synthetic Mechanism of Molecular Imprinting at the Solid Phase. *Macromolecules* **2020**, *53* (4), 1435-1442.
15. Zhou, Z.; Ying, H.; Liu, Y.; Xu, W.; Yang, Y.; Luan, Y.; Lu, Y.; Liu, T.; Yu, S.; Yang, W., Synthesis of surface molecular imprinting polymer on SiO<sub>2</sub>-coated CdTe quantum dots as sensor for selective detection of sulfadimidine. *Appl. Surf. Sci.* **2017**, *404*, 188-196.
16. Vladimir M. Mirsky, T. H., Sergey A. Piletsky, Otto S. Wolfbeis, A Spreader-Bar Approach to Molecular Architecture: Formation of Stable Artificial Chemoreceptors. *Angew. Chem. Int. Ed.* **1999**, *38* (8), 3. 1108-1110.
17. Zhang, Z.; Zhang, X.; Liu, B.; Liu, J., Molecular Imprinting on Inorganic Nanozymes for Hundred-fold Enzyme Specificity. *J. Am. Chem. Soc.* **2017**, *139* (15), 5412-5419.
18. Canlas, C. P.; Lu, J.; Ray, N. A.; Grosso-Giordano, N. A.; Lee, S.; Elam, J. W.; Winans, R. E.; Van Duyne, R. P.; Stair, P. C.; Notestein, J. M., Shape-selective sieving layers on an oxide catalyst surface. *Nat. Chem.* **2012**, *4* (12), 1030-1036.
19. Chen, G.; Xu, C.; Huang, X.; Ye, J.; Gu, L.; Li, G.; Tang, Z.; Wu, B.; Yang, H.; Zhao, Z.; Zhou, Z.; Fu, G.; Zheng, N., Interfacial electronic effects control the reaction selectivity of platinum catalysts. *Nat. Mater.* **2016**, *15* (5), 564-569.
20. Wu, D.; Hernández, W. Y.; Zhang, S.; Vovk, E. I.; Zhou, X.; Yang, Y.; Khodakov, A. Y.; Ordonsky, V. V., In Situ Generation of Brønsted Acidity in the Pd-I Bifunctional Catalysts for Selective Reductive Etherification of Carbonyl Compounds under Mild Conditions. *ACS Catal.* **2019**, *9* (4), 2940-2948.
21. Marshall, S. T.; O'Brien, M.; Oetter, B.; Corpuz, A.; Richards, R. M.; Schwartz, D. K.; Medlin, J. W., Controlled selectivity for palladium catalysts using self-assembled monolayers. *Nat. Mater.* **2010**, *9* (10), 853-858.
22. Kahsar, K. R.; Schwartz, D. K.; Medlin, J. W., Control of metal catalyst selectivity through specific noncovalent molecular interactions. *J. Am. Chem. Soc.* **2014**, *136* (1), 520-526.
23. Duran Pachon, L.; Yosef, I.; Markus, T. Z.; Naaman, R.; Avnir, D.; Rothenberg, G., Chiral imprinting of palladium with cinchona alkaloids. *Nat. Chem.* **2009**, *1* (2), 160-164.
24. Niu, F.; Xie, S.; Bahri, M.; Ersen, O.; Yan, Z.; Kusema, B. T.; Pera-Titus, M.; Khodakov, A. Y.; Ordonsky, V. V., Catalyst Deactivation for Enhancement of Selectivity in Alcohols Amination to Primary Amines. *ACS Catal.* **2019**, *9* (7), 5986-5997.

25. Pang, S. H.; Schoenbaum, C. A.; Schwartz, D. K.; Medlin, J. W., Directing reaction pathways by catalyst active-site selection using self-assembled monolayers. *Nat. Commun.* **2013**, *4*, 2448.
26. Liu, X.; Zhu, Q.; Lang, Y.; Cao, K.; Chu, S.; Shan, B.; Chen, R., Oxide-Nanotrap-Anchored Platinum Nanoparticles with High Activity and Sintering Resistance by Area-Selective Atomic Layer Deposition. *Angew. Chem. Int. Ed.* **2017**, *56* (6), 1648-1652.
27. Zhao, X.; Zhou, L.; Zhang, W.; Hu, C.; Dai, L.; Ren, L.; Wu, B.; Fu, G.; Zheng, N., Thiol Treatment Creates Selective Palladium Catalysts for Semihydrogenation of Internal Alkynes. *Chem* **2018**, *4* (5), 1080-1091.
28. Albani, D.; Shahrokhi, M.; Chen, Z.; Mitchell, S.; Hauert, R.; Lopez, N.; Perez-Ramirez, J., Selective ensembles in supported palladium sulfide nanoparticles for alkyne semi-hydrogenation. *Nat. Commun.* **2018**, *9* (1), 2634.
29. Mori, A.; Mizusaki, T.; Kawase, M.; Maegawa, T.; Monguchi, Y.; Takao, S.; Takagi, Y.; Sajiki, H., Novel Palladium-on-Carbon/Diphenyl Sulfide Complex for Chemoselective Hydrogenation: Preparation, Characterization, and Application. *Adv. Synth. Catal.* **2008**, *350* (3), 406-410.
30. Xian, J.; Hua, Q.; Jiang, Z.; Ma, Y.; Huang, W., Size-dependent interaction of the poly(N-vinyl-2-pyrrolidone) capping ligand with Pd nanocrystals. *Langmuir* **2012**, *28* (17), 6736-6741.
31. Shanahan, R. M.; Hickey, A.; Bateman, L. M.; Light, M. E.; McGlacken, G. P., One-Pot Cross-Coupling/C-H Functionalization Reactions: Quinoline as a Substrate and Ligand through N-Pd Interaction. *J. Org. Chem.* **2020**, *85* (4), 2585-2596.
32. Arrigo, R.; Schuster, M. E.; Xie, Z.; Yi, Y.; Wowsnick, G.; Sun, L. L.; Hermann, K. E.; Friedrich, M.; Kast, P.; Hävecker, M.; Knop-Gericke, A.; Schlögl, R., Nature of the N-Pd Interaction in Nitrogen-Doped Carbon Nanotube Catalysts. *ACS Catal.* **2015**, *5* (5), 2740-2753.
33. Cure, J.; Coppel, Y.; Dammak, T.; Fazzini, P. F.; Mlayah, A.; Chaudret, B.; Fau, P., Monitoring the coordination of amine ligands on silver nanoparticles using NMR and SERS. *Langmuir* **2015**, *31* (4), 1362-1367.
34. Chen, J. J.; Winograd, N., The adsorption and decomposition of methylamine on Pd(111). *Surf. Sci.* **1995**, *326* (3), 285-300.
35. Gong, J.; Mullins, C. B., Surface science investigations of oxidative chemistry on gold. *Acc. Chem. Res.* **2009**, *42* (8), 1063-1073.

36. Ding, S. Y.; Gao, J.; Wang, Q.; Zhang, Y.; Song, W. G.; Su, C. Y.; Wang, W., Construction of covalent organic framework for catalysis: Pd/COF-LZU1 in Suzuki-Miyaura coupling reaction. *J. Am. Chem. Soc.* **2011**, *133* (49), 19816-19822.
37. Vogt, L.; Schulte, E.; Collins, S.; Quaino, P., Theoretical and FTIR Investigations of the Acetonitrile Hydrogenation Pathways on Platinum. *Top. Catal.* **2019**, *62* (12-16), 1076-1085.
38. Rahaman, M.; Dutta, A.; Broekmann, P., Size-Dependent Activity of Palladium Nanoparticles: Efficient Conversion of CO<sub>2</sub> into Formate at Low Overpotentials. *ChemSusChem* **2017**, *10* (8), 1733-1741.
39. Bachiller-Baeza, B.; Anderson, J. A., FTIR and Reaction Studies of Styrene and Toluene over Silica–Zirconia-Supported Heteropoly Acid Catalysts. *J. Catal.* **2002**, *212* (2), 231-239.
40. Safronov, A. P.; Kurlyandskaya, G. V.; Chlenova, A. A.; Kuznetsov, M. V.; Bazhin, D. N.; Beketov, I. V.; Sanchez-Ilarduya, M. B.; Martinez-Amesti, A., Carbon deposition from aromatic solvents onto active intact 3d metal surface at ambient conditions. *Langmuir* **2014**, *30* (11), 3243-3253.
41. Ohtani, H.; Bent, B. E.; Mate, C. M.; Van Hove, M. A.; Somorjai, G. A., Structure determination with HREELS and LEED: The molecular structure of chemisorbed benzene on Pd (111). *Appl. Surf. Sci.* **1988**, *33-34*, 254-260.
42. Zou, S.; Williams, C. T.; Chen, E. K. Y.; Weaver, M. J., Probing Molecular Vibrations at Catalytically Significant Interfaces: A New Ubiquity of Surface-Enhanced Raman Scattering. *J. Am. Chem. Soc.* **1998**, *120* (15), 3811-3812.
43. Ioannides, T.; Verykios, X. E., The Interaction of Benzene and Toluene with Rh Dispersed on SiO<sub>2</sub>, Al<sub>2</sub>O<sub>3</sub>, and TiO<sub>2</sub> Carriers. *J. Catal.* **1993**, *143* (1), 175-186.
44. Vasiurrahman, M., The hydrogenation of toluene and o-, m-, and p-xylene over palladium II. Reaction model. *J. Catal.* **1991**, *127* (1), 267-275.
45. Poondi, D.; Albert Vannice, M., Competitive Hydrogenation of Benzene and Toluene on Palladium and Platinum Catalysts. *J. Catal.* **1996**, *161* (2), 742-751.
46. Verma, D. K.; des Tombe, K., Benzene in gasoline and crude oil: occupational and environmental implications. *AIHA J (Fairfax, Va)* **2002**, *63* (2), 225-30.
47. Galadima, A.; Muraza, O., Role of zeolite catalysts for benzene removal from gasoline via alkylation: A review. *Microporous Mesoporous Mater.* **2015**, *213*, 169-180.
48. Laredo, G. C.; Castillo, J.; Cano, J. L., Benzene reduction in gasoline range streams by adsorption processes using a PVDC–PVC carbon molecular sieve. *Fuel* **2014**, *135*, 459-467.

49. Savva, P. G.; Goundani, K.; Vakros, J.; Bourikas, K.; Fountzoula, C.; Vattis, D.; Lycourghiotis, A.; Kordulis, C., Benzene hydrogenation over Ni/Al<sub>2</sub>O<sub>3</sub> catalysts prepared by conventional and sol–gel techniques. *Appl. Catal. B* **2008**, *79* (3), 199-207.
50. Gu, W.; Stalzer, M. M.; Nicholas, C. P.; Bhattacharyya, A.; Motta, A.; Gallagher, J. R.; Zhang, G.; Miller, J. T.; Kobayashi, T.; Pruski, M.; Delferro, M.; Marks, T. J., Benzene selectivity in competitive arene hydrogenation: effects of single-site catalyst...acidic oxide surface binding geometry. *J. Am. Chem. Soc.* **2015**, *137* (21), 6770-6780.





## **7. General Conclusions and Perspectives**

### **7.1. General Conclusion**

The interaction between the reactant and surface of the heterogeneous catalyst plays a major role in the catalytic process. Modification of electronic structure and environment of metal nanoparticles by promoters as well as the construction of bifunctional sites by functional promoters are efficient strategies for enhancement of the activity and selectivity. Catalytic selectivity is the primary consideration for an industrial process, especially for the conversion of biomass-derived molecules for the production of sustainable chemicals and fuels. Biomass-derived molecules with various functional groups and unsaturated bonds suffer from low selectivity over metal nanoparticles. Considering that one of my Ph.D. sponsor Solvay is dedicated to the development of eco-efficient products and processes, my Ph.D. study was especially focused on the selective conversion of biomass-based molecules via surface modification of metal catalysts.

#### **7.1.1. In-situ generation of acid sites over metal nanoparticles**

The first invention in this thesis is the development of bifunctional Pd-I and Pd-Br catalyst. We found that iodine and bromine atoms can be grafted strongly on the Pd surface. It results in significant changes of the catalytic properties. Further characterization such as XPS, CO-FTIR and in-situ Pyridine FTIR demonstrated that iodine and bromine atoms can withdraw electrons from Pd. The highly charged iodine and bromine ad-atoms promote the heterolytic dissociation of H<sub>2</sub> with in-situ generation

of Brønsted acidity directly on the metal surface. The spatial proximity of metal-acid bifunctional sites efficiently promotes the activity and selectivity of the catalyst. As shown in *Figure 7.1*, the Pd catalyst promoted with iodine was applied for the reductive etherification of carbonyl compounds (e.g. furfural) and various alcohols (e.g. isopropanol) with high selectivity (>90%) to ether product at very mild conditions. The Pd-Br catalyst was found to be extremely efficient for the hydrodeoxygenation of HMF to dimethylfuran at ambient temperature with a selectivity of up to 96%. The development of novel Pd-I and Pd-Br bifunctional catalysts would contribute to the sustainable production of chemicals and fuels from biomass.

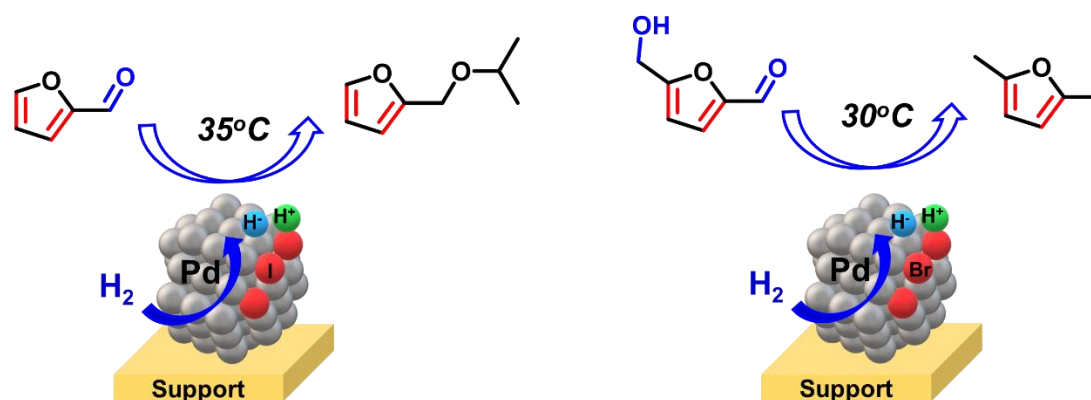


*Figure 7.1.* Catalytic conversion of biomass-based furans over Pd-I and Pd-Br bifunctional catalysts.

### 7.1.2. Selective blocking active sites

The second development is related to the selective poisoning of Ru catalyst by Br atoms (*Figure 7.2*). We found that the hydrogenolysis of bromobenzene over Ru nanoparticles resulted in the modification of Ru nanoparticles with Br atoms. The Ru-Br catalysts were found to be highly selective for the production of benzene and phenol by the cleavage of diphenyl ether, which was used as lignin model compounds. In-situ CO-

FTIR indicated that after modification with Br, the terrace sites on Ru nanoparticles were selectively blocked by Br ad-atoms, while the edge and corner sites are not affected. The selective blocking of continuous terrace sites results in a significant decrease in the selectivity to cyclohexane and cyclohexanol, where the hydrogenation of the aromatic ring takes place. Moreover, the electron withdrawal effect of Br makes the Ru nanoparticles positively charged, which further enhances the reactivity with electron-rich C-O ether bonds. This selective poisoning and electron modulation strategy opens a way for the design of catalyst for the selective cleavage of C-O bonds.

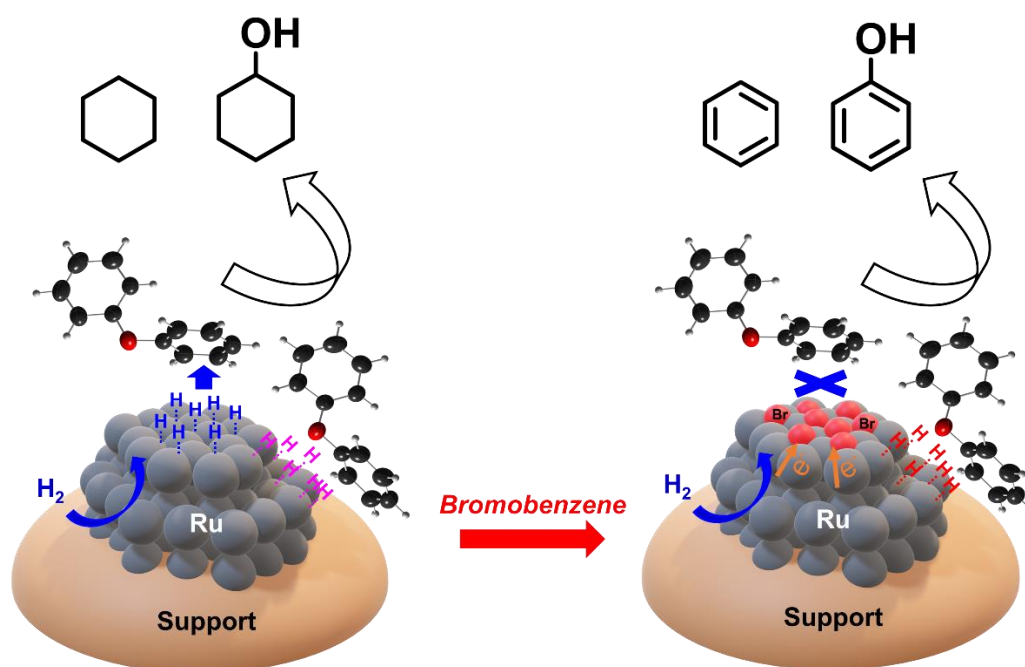


**Figure 7.2.** Selective poisoning effect of Br on Ru nanoparticle for the conversion of diphenyl ether.

### 7.1.3. Molecular imprinting over heterogeneous catalyst

The third development is demonstration of molecular imprinting strategy over the metal surface for selective processes (**Figure 7.3**). By the first adsorption of an aromatic template molecule on the Pd surface and then poisoning the Pd surface with amines, we

found that the adsorbed template molecules could protect the Pd sites during poisoning with generation of an active imprinting area after desorption of the template. The imprinted area over Pd surface was observed by HAADF-STEM analysis. The imprinted Pd catalysts that have reserved active islands with predetermined shape and size could selectively convert the molecules displaying similar to template structures. The imprinted Pd catalyst with benzene as a template has shown a potential application for the selective removal of carcinogenic benzene from industrial aromatics. The development of molecular imprinting strategy could be a powerful tool for the manipulation of the metal surface with controllable reactivity.

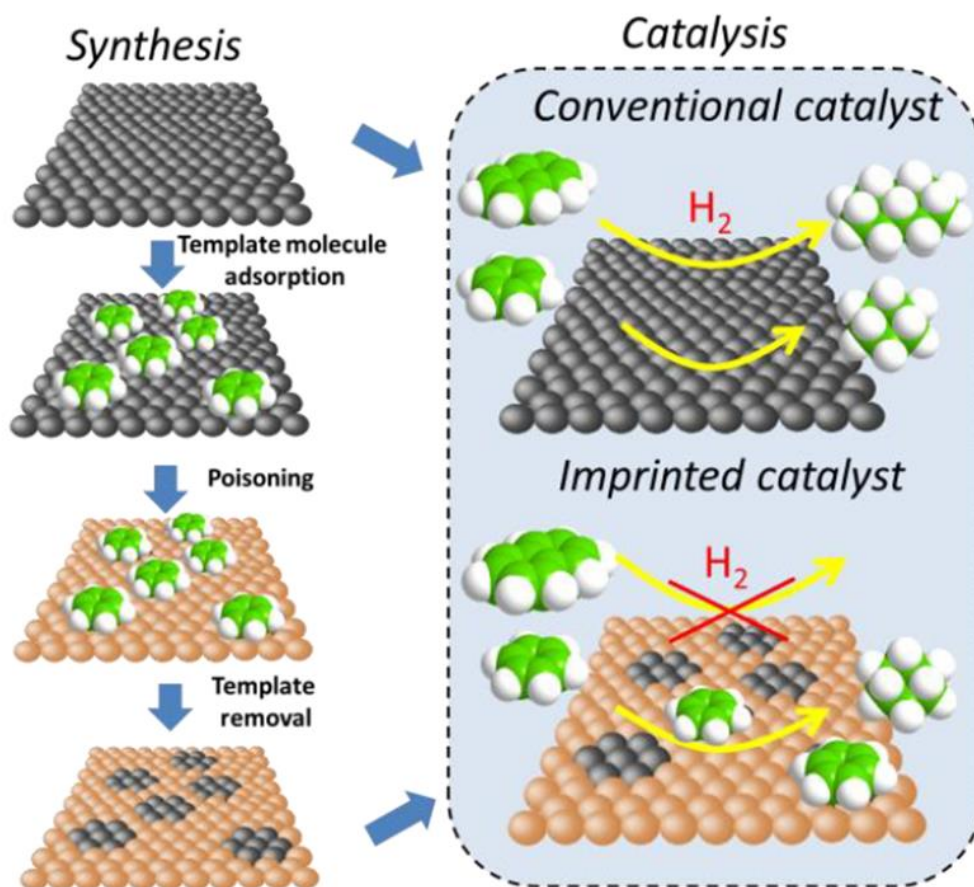


**Figure 7.3.** Molecular imprinting over metal surface for selective reactions.

## 7.2. Perspective

Although we have developed several new strategies to control the selectivity of metal catalysts via non-metallic promotion, there are still a lot of problems that have to be solved:

1. Pd-I and Pd-Br bifunctional catalysts with spatial intimate metal-acid active sites would be a robust catalyst for cascade reactions. Besides hydrogenation-etherification and hydrogenation-deoxygenation, other types of reactions could be studied over these materials like hydrogenation-esterification, hydrogenation-dehydration and hydrogenation-isomerization.
2. Selective blocking of Ru sites by Br should be extended to other metals such as Pt, Rh and Ir. Non-noble transition metals like Co and Ni could be investigated in different catalytic reactions after modification of halogens.
3. Molecular imprinting over the metal surface is a powerful strategy for the design of a smart catalyst surface. However, we have observed significant decrease in activity caused by the inevitable electronic effect of amines as poisoners which could be an obstacle for application of this concept. Thus, the optimization and development of new templates and poisoners should be further studied. For example, metallic and inert poisoner such as Au could be a possible option.